FILTRATION OF REDISPERSED POWER-STATION FLY ASH BY A PANEL BED FILTER WITH PUFFBACK

by

Kun-chieh Lee

A dissertation submitted to the Graduate Faculty in Chemical Engineering in partial fulfillment for the degree of Doctor of Philosophy, The City University of New York

1975

This manuscript has been read and accepted for the Graduate Faculty in Engineering in satisfaction of the dissertation requirement for the degree of Doctor of Philosophy.

April 16, 1975
Date

Arthur M. Squires
Chairman of Examining Committee

4/16/75
Date

Jacques E. Beneniste
Executive Officer

Prof. A.M.Squires (Chairman & Mentor)

Prof. R.Pfeffer (Co-Mentor)

Prof. C.J.Costantino

Prof. C.Miller

Supervisory Committee

The City University of New York

ABSTRACT

A method for removing fly ash from power station stack gas at high efficiency is presented. This entails the use of a gas-solids contacting device called a panel bed filter, in which gases flow across a tall, narrow bed of a granular solid retained between two parallel, vertical perforated walls. Construction permits the fly ash in the entering gas to be deposited upon a free surface of the granular solid to form a filter cake. The filter cake is removed periodically by "puffback" (a sudden burst of high pressure air through the back of the bed) along with a small amount of granular solid, allowing a new free surface to form.

This research aims to determine the operating features of a panel bed filter, and includes both panel bed filtration studies and puffback studies. We have shown that under suitable conditions, the panel bed filter with puffback is capable of removing redispersed power station fly ash from air at efficiencies beyond 99.99% and can be operated for many cycles with no permanent increase in pressure drop.

From the filtration studies we conclude that adhesion and autohesion properties of the dust and granules are important variables in respect to filtration efficiency. The panel bed filter takes advantage of the filter cake of dust to filter the dust-laden air. We found that dirty sand filters better than clean sand because dirty sand

provides condensation nuclei for the formation of the filter cake.

From the puffback study we conclude that puffback sand spill is a transient soil mechanics failure phenomenon caused by transient aerodynamic drag forces. The sand spill is a result of a body movement of the entire sand bed. A steady blowback of air cannot remove sand from the louver surfaces uniformly and cannot produce the desired body movement, but will cause only undesired local surface failure of the sand. The reverse surge of air flow (puffback) has to rise very rapidly to build a pressure on the clean side of the panel bed filter which exceeds a critical minimum pressure to produce a body failure of the sand, leading to the desired body movement and a uniform sand spill.

High speed movies were used for visual analysis of the puffback phenomena. High resolution quartz transducers were used to study the transient aerodynamic pressure changes. Empirical correlations were obtained connecting the puffback sand spill and puffback intensity expressed in terms of the "active time", ie., the time during which the pressure on the clean side of the filter exceeds the critical minimum to cause sand to spill.

ACKNOWLEDGEMENTS

The author wishes to thank Professor Arthur M. Squires and Professor Robert Pfeffer for their guidance throughout the entire investigation.

I am grateful to The City University of New York for an appointment as University Research Assistant for 2-½ years during my studies.

Thanks are also due to Mr. John Bodnaruk and the Chemical Engineering Shop personnel for their assistance in constructing the experimental apparatus.

The author also wishes to thank Dr. D. DeCoursin and Mr. R. Davini of Fluidyne Engineering Corp., Minneapolis, for their help in the initial CEC transducer measurements and Dr. J.D. Plunkett and Mr. R. Marchese of Materials Consultants, Inc., Denver, for their help in taking the high speed motion pictures. Dr. Plunkett also built the transparent unit.

Professor Squires furnished much-appreciated financial support during the studies.

Dedicated to my wife, Shiow.

TABLE OF CONTENTS

LIST OF TABLES

LIST OF FIGURES

Figures

NOMENCLATURE

a	= a constant
A	= projected panel bed louver area
b	= thickness of the bed
c	= a constant
C	= a constant, particle concentration
d	= particle diameter
D	= diameter of the conduit
f	= force
f_p	= drag force around the particle
F_{ad}	= adhesive force
F_{aut}	= autohesive force
g	= acceleration of gravity
h	= height
i	= characteristic constant of granular material
k	= permeability
K	= particle deposition velocity
m	= mass of the body, puffback pressure parameter
m_T	= mass of air in the puffback tank
m_c	= mass of air in the clean side chamber
M	= Much number
n	= number of particles adhesion to the surface
n_o	= initial number of particles adhesion to the surface
N	= normal force
P	= pressure, bottom pressure
P_c	= clean side pressure

P_L = lateral pressure

P_T = puffback tank pressure

$P_{T,o}$ = initial puffback tank pressure

ΔP = pressure drop

ΔP_f = steady blowback failure pressure drop

$\Delta P_{min.}$ = minimum failure pressure drop for puffback

ΔP_{peak} = peak pressure drop

R = gas constant, hydraulic radius

Re_k = permeability Reynold number

Re_p = particle Reynold number

t = time

t_a = active time

t_r = rise time

t_f = failure time

T absolute temperature, duration time

u = local velocity

U = circumference of the bin

v = superficial velocity

v_e = superficial escape velocity

V_c = volume of the clean side chamber

V_T = volume of the puffback tank

w = sand spill per unit area

W = bulk density of granular material

x = displacement

α = a coefficient

β = shape factor, angle of repose, a coefficient

γ = adhesion number, ratio of specific heats

δ = puffback tank pressure decay constant

ϵ = porosity

ϵ_o = initial porosity

θ = angle of failure plane

λ = a coefficient

μ = viscosity, soil friction coefficient

μ' = friction coefficient due to sliding

φ = angle of incidence, approaching angle

ρ = density

τ = shear stress

τ_f = shear stress at failure

ϕ = angle of internal friction of granular material

ϕ' = friction angle due to sliding

ϕ_{cv} = angle of internal friction at ultimate condition or at critical volume

Chapter 1: Introduction

The problem of removing fly ash from the stack gas of a power station has received considerable attention. Conventional dust collecting systems can be classified in four main groups (6).

(1) Centrifugal dust collectors.

(2) Dust filters, either fibrous or granular bed.

(3) Wet scrubber.

(4) Electrostatic precipitators.

A major opportunity for obtaining clean power from sulfurous fuels such as coal or residual oil embraces the combustion of the fuel at high pressure in the presence of a desulfurizing agent, and the generation of power by a combination of gas and steam turbine cycles. For example, a large scale experiment to obtain cheaper power using fluidized bed combustion of coal at 800°C and 8 atmospheres power is under way at BCURA industrial laboratories at Leatherhead, England (24). However, the presence of alkali fume in the gases reaching the gas turbine would injure the turbine blading and soon render them inoperative. BCURA's temperature, 800°C was chosen to minimize evolution of alkali fume from the combustion bed.

A higher efficiency could be obtained if the coal were gasified, rather than burned completely, so that a fuel gas could be burned ahead of the gas turbine, thereby providing a gas at a higher temperature to the turbine.

A coal gasifier must operate at a temperature considerably above 800°C, and the resulting fuel gas inevitably will contain a large amount of volatilized alkali salts as well as other fine particulates. The gas could be cooled and scrubbed to remove alkali fume, but a better arrangement would be to remove the fume and dust by filtration, preferably at a temperature of 800°C or a little below. Filtration at such a high temperature would lead to a higher thermal efficiency of power generation than cooling and scrubbing.

Thus, there is a need for a high efficiency filter operating at high temperatures and pressure which is capable of reducing alkali fume and particulates to a level meeting the gas turbine designer's requirement for gas cleanliness. The successful implementation of such a filter would be an important step in the development of some of the new schemes available for obtaining cheaper clean power from the combustion of coal and fuel oil as described in reference (43).

An objective of this research is to contribute to the development of a panel bed filter to clean dust-laden gases at high pressure and at high temperature to a degree sufficient for the gases to be fed to an expansion turbine generating power. The device would also be useful for removing fly ash from conventional coal-fired power stations, as well as for cleaning other dusty gases in industry.

An old idea, probably invented in 1876 to provide a reactor for the Deacon chlorine process, is to treat a gas by causing it to flow in the horizontal direction across a bed of granular solid disposed in a tall, narrow "panel"(31). The bed may be held in place, for example, by inclined louvers that form walls that resemble venetian blinds (Figure1-1).

We have been working at The City College on a technique to remove solid from a panel bed (42,44). We term our technique "puffback". Figure 1-2 shows our first test set-up. We used the bed with sand to filter fly ash from air. The pressure drop across the panel bed builds up as a run proceeds, and when the pressure drop is too high, we stop the flow of dirty air. We then open a valve that releases air from the puffback bottle. This causes a surge flow of air across the panel in the direction opposite to the normal flow of dirty air. We found that this surge flow removes sand and the fly ash deposit from the dirty face of the panel. A steady backflow of gas does not accomplish a useful purpose, merely leading to a spill of solid from the top gas-entry surface of the panel. Puffback restores the pressure drop to the pressure drop to the initial figure, and the panel bed is ready for another filtration cycle. With a crude arrangement we measured a filtration efficiency of 99.7%.

With some modification, the present research indicates that the panel bed filter with puffback might be capable of removing redispersed power station fly ash from air at

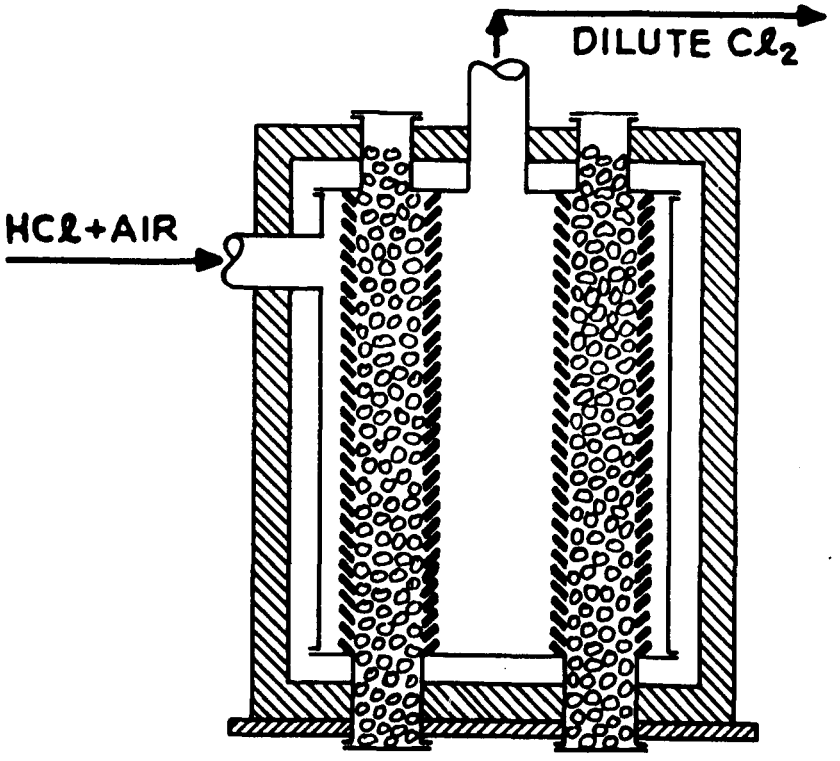

DEACON PROCESS REACTOR

Figure 1-1: Panel Bed Reactor for Deacon Process
NB. The twelve-sided, nearly circular panel was housed in a circular steel shell within a brick furnace. The catalyst space was 3 ft across, and both outer diameter and height were about 15 ft. The catalyst space was divided by partitions into six segments, one of which was dumped and renewed each fortnight.

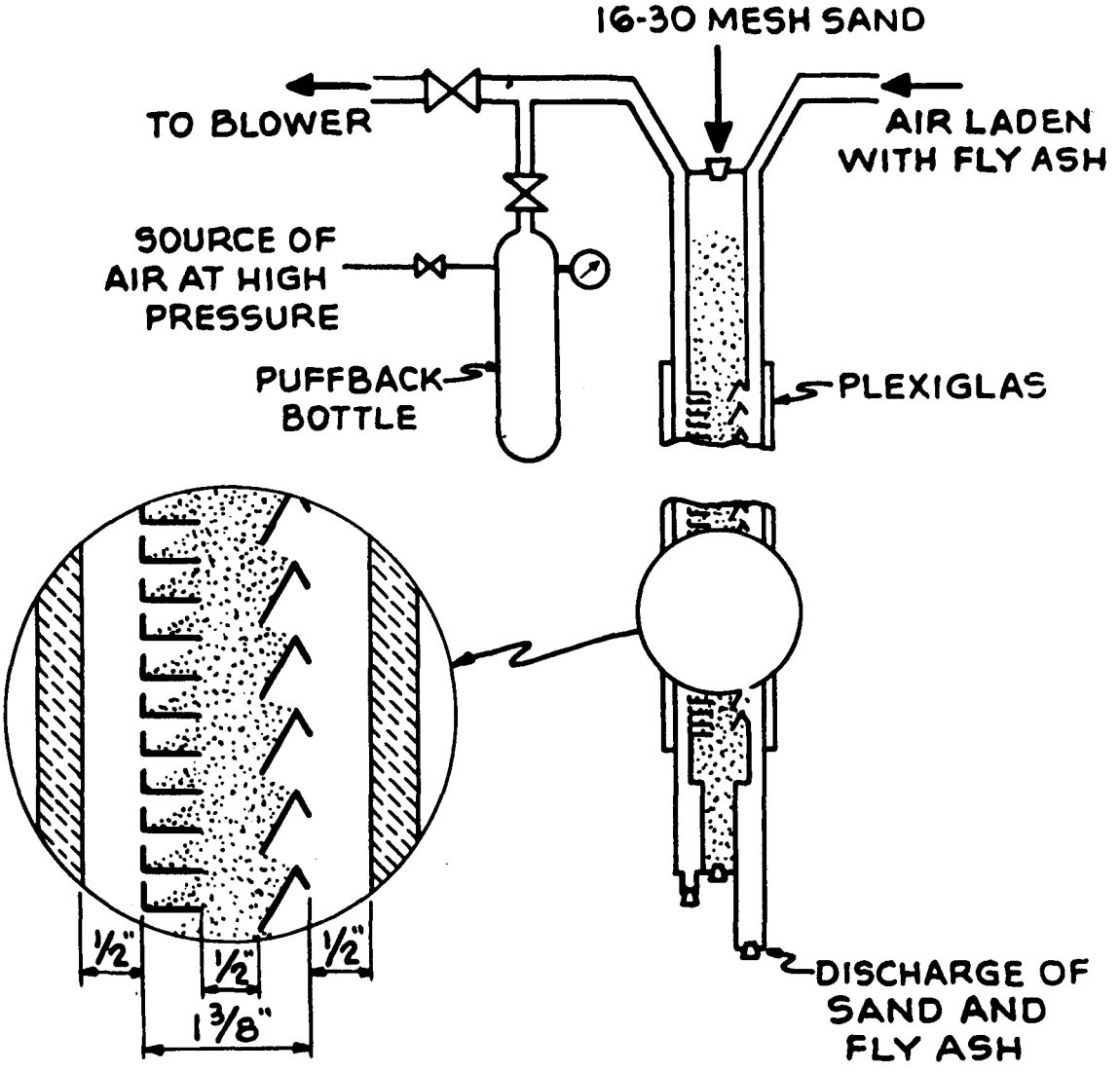

Figure 1-2: Arrangement of Unit LS-1

efficiencies beyond 99.99%.

Chapter 2: Literature Review

2.1 Filtration.

In order to study the panel bed filtration we will have to review basic filtration theory. Special attention will be given to the role of adhesion and autohesion of dust in the filtration process. The adhesion and autohesion properties of dust are believed to be extremely important in the success of panel bed filtration.

2.1.1 Aerosol Filtration Theory.

Mechanisms involved in the filtration of aerosols are diffusion, direct interception, inertial impaction, and gravity settling. Electrical and thermal effects may also appear, but generally these effects are induced external to the filtration process.

Deposition by diffusion is caused by the Brownian motion of the aerosol particle which results in a deviation from the fluid stream lines and subsequent deposition and adherence to the filter media. This effect is prevalent at low velocities and for small particles.

Deposition by direct interception occurs when particles moving along streamlines of a fluid approach the filter object within a distance equal to the radius of the impinging particle. This mechanism is independent of the velocity, but increases with the size of the aerosol particle.

The mechanism of removal by inertial impaction occurs when the size or velocity of the particle is so large that

it does not follow the streamlines of the fluid but resists the directional change imposed by the filter media and strikes it. Increase in velocity and size of the impinging particle increases the effect of this mechanism.

Deposition by gravity settling can be considered as a mechanism superimposed on any of the above. It is more prevalent at lower velocities and for larger particles.

The general effect of velocity and particle size on penetration is illustrated in Figure 2.1-1. A more complete description of aerosol filtration theory can be found in Chen (8), Fuchs (17), Paretsky (35), or Green and Lane (20).

These four mechanism act simultaneously but with differing relative significance, depending upon the specific case. It is a basic premise of classical filtration theory that is a particle strikes a filter, no matter what the cause, it sticks. Analysis of the influence of the various mechanisms only defines the path of the particles in relation to the fibers it might encounter. Recently, studies of filtration theory indicated many anomalous results such as:

(1) there is an increase filtration efficiency with increasing electrophoretic mobility of the particles (25),

(2) a heavy spherical particle or drop is more difficult to be filtered than a lighter one of the same size (37),

(3) there is a decline in efficiency of a high velocity filter (50) which may be interpreted as being due to the non-adherence of some of the aerosol particles and drops

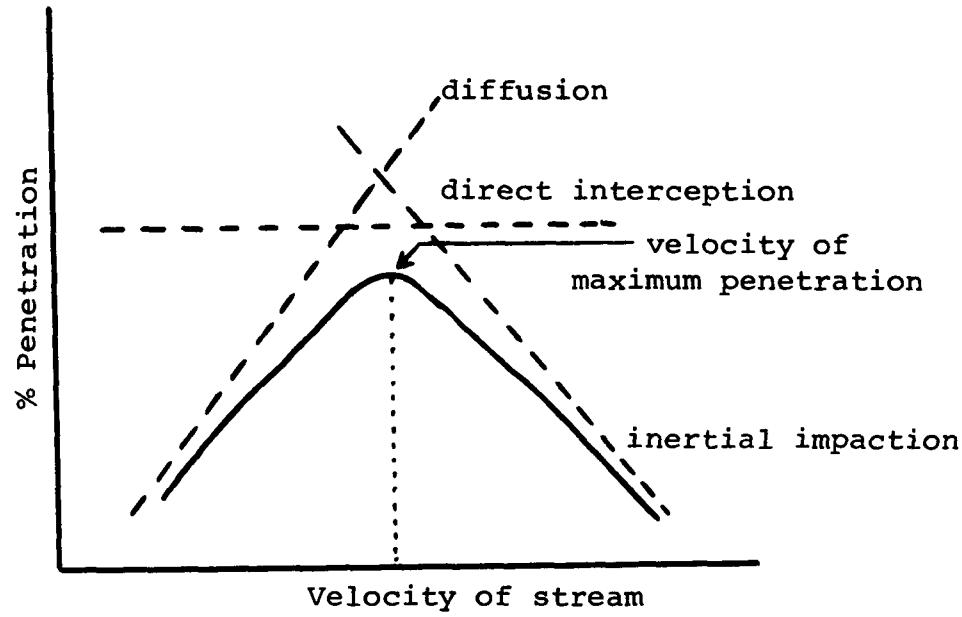

Figure 2.1-1-a: Effect of Velocity on % Penetration at Constant Particle Diameter

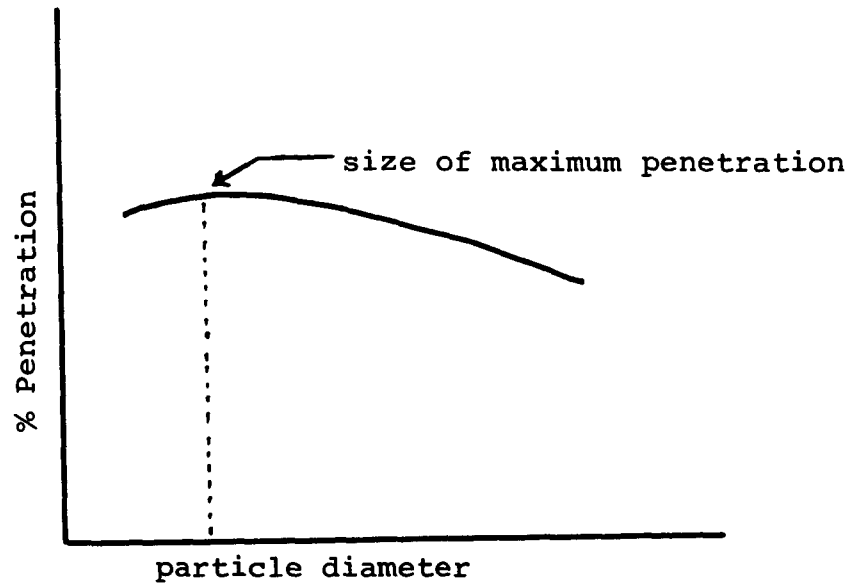

Figure 2.1-1-b: Effect of Particle Diameter on % Penetration at Constant Velocity

which come in contact with the fiber filter.

Annis (1), and Gillespie (18,19) observed there is a certain range of velocity where particles bouncing or re-entrainment will occur. At low velocity, the aerodynamic force is not strong enough to carry away the particles. At high velocity, due to the elastic properties of the particle and surface the contact area at impaction is so large that the attraction force is larger than the aerodynamic force. Also, there is more intimate contact at high velocity impaction. In our own experience with fly ash powder, it was observed that a layer of fly ash deposited on a flat surface at high velocity cannot be detached by a lower velocity air stream while a layer of fly ash deposited on a flat surface at lower velocity was easy to be detached by a higher velocity air stream.

Preliminary data using Teflon, perlite and fly ash as a filter aid showed evidence of the importance of the role of adhesive force and/or autohesive force. The data will be given in Section 7.3.

2.1.2. Adhesion and Autohesion of Particles.

Adhesion is defined as the interaction of particles with a solid surface and autohesion is defined as the interaction of particles among themselves. Adhesion and autohesion are due to analogous causes. Cohesion is defined as the attraction between the molecules within the bounds of a single body. In discussion of filtration phenomena, we are just interested in adhesive forces of

the powders.

2.1.2.1. Causes of Adhesion.

1. Van der Waals' attraction forces: When the gap between contiguous bodies is not greater than a few molecular diameters and the particles are not electrically charged, the Van der Waals force is the major cause for adhesion. The energy and the force of molecular interaction depend greatly on the particle dimensions and the true contact area. Small particles have a better contact area and smaller gap, hence have stronger adhesive forces.

2. Coulomb forces: The Coulomb forces appear when the particles are charged in advance. The forces exceed molecular forces in value and determine the adhesion in particles. The conductivity of the particle material, as well as moisture, causes charge leakage and lead to a reduction in the Coulomb forces. Hence, the Coulomb force is a function of contact time.

3. Capillary forces: This arises in the presence of a liquid meniscus in the space between the particle and the surface. The surface tension force of the liquid will hold contiguous bodies together. For fine particles, the capillary condensation starts to appear at a relative humidity over 65% (11). Better wettability of the surface, greater particle size, and greater surface tension of the liquid will lead to greater adhesive force. Under the condition of capillary condensation, the adhesive forces are determined entirely by capillary force.

4. Others: Presence of oil film will cause adhesion as a result of surface tackiness.

2.1.2.2. Factors which will affect Adhesion.

The following factors will affect adhesion:

1. Particle size: Generally speaking, the adhesive force is inversely proportional to particle size. Small particles have stronger adhesive force.

2. The gap between the contiguous bodies and the real contact area. More intimate contact will lead to stronger adhesive force.

3. Properties of the contiguous bodies and medium.

4. Surface contamination.

5. Surface roughness: The adhesive force of a macroscopic rough surface is stronger than a perfect smooth surface which is in turn stronger than microscopic rough surface due to the difference in contact area and gap.

6. Modification of surfaces: Using a surfactant to condition the surface to make it either hydrophilic or hydrophobic will change the adhesive forces.

7. Particle shape: Oblong particles have stronger adhesive forces than spherical particles. Particles of irregular shape will have a greater spread of adhesive forces.

Since there are so many variables which effect the adhesive force, not all the particles, even of the same size, have the same adhesive or autohesive forces. In discussing adhesion, we must use the adhesion number to

characterize it. The adhesion number γ is defined as:

$$\gamma = \frac{n}{n_o} \quad 100 \qquad (2.1\text{-}1)$$

n = number of particles remaining after the application of a given force to the particles.

n_o = number of particles originally attached to the surface.

2.1.2.3. Adhesion of Dust by Free Settling and Striking.

The adhesion of dust is largely determined by the conditions of contact between the dust particles and the surface and by the elastic properties of the surface. First, we consider the simple case of free particle settling. The particle velocity can be easily calculated from Stokes' law. Also, the deformation of the contact zone is negligible, since the particles situated in air are acted upon the force of gravity which causes them to settle. When dust particles settle and come into contact with an inclined surface, the dust might be held on the surface by adhesion and friction forces if the kinetic energy of particles is not too large. Or, they will slide down if the kinetic energy of particles is too big.

2.1.2.4. Detachment of Dust.

The detachment of dust from a surface depends on air velocity, the turbulence of the flow, the thickness of the boundary layer, the adhesive force of particles and the particle size. Generally speaking, small particles are much harder to be removed due to the decrease in frontal pressure and increase in adhesive force.

In the detachment of an adhering dust layer by an air

flow, the following processes may occur (55):

Erosion (Autohesive type detachment) - the removal of the top particles, i.e., the overcoming of autohesion. This is possible when $F_{ad} > F_{aut}$ In this case, the dust is raised to a comparatively short distance above the original surface. The removing process will take quite a long time.

Denudation (Adhesive type detachment) - the detachment of a layer of dust, i.e., the overcoming of the adhesive forces in the layer, and the detachment of individual particles remaining after the removal of the layer. This is possible when $F_{aut} > F_{ad}$. In denudation, detachment of the dust starts at the leading edge of the dust deposit and a dust cloud rapidly fills the whole channel. In denudation, all dust deposits are removed in about 0.5 sec. Hence, the denudation velocity is the main parameter determining this process.

In erosion, a considerable amount of adhering dust remains even 18 sec. after the start of an air flow at a velocity of 25 m./sec. Hence, erosion depends not only on the velocity of the air flow but also on the period for which it acts on the adhering dust.

We should pay attention to the fact that in erosion, a longer time will be required to detach the dust. If the deposition rate is the same, this might explain the filter cake formation phenomena discussed later (Section 2.1.3 and Section 2.1.4).

2.1.2.5. The Adhesion and Detachment of Dust to Cylindrical and Spherical Surfaces.

The deposition and adhesion of dust particles on cylindrical and spherical surfaces take place in a nonuniform manner. The number of deposited loess dust particles (55) is presented as a function of the angle of incidence φ on a cylindrical surface for various flow velocities in Figure 2.1-2. The number of the deposited particles falls as the angle rises from 0 to 90°. For a φ close to zero, the flow velocity is minimal, so that the detachment of particles as a result of aerodynamic forces will be negligible. For φ close 90°, the number of adhering particles falls sharply since the oblique impact communicates a rotatory motion to the particles. Also, there is an increasing flow velocity around the side surfaces. At the back of the obstacle adhesion increases as a result of eddies, particularly for smallish particles. The mechanism underlying the deposition of particles on the front and back surfaces of the obstacle in the flow differs, depending on the dimensions of the particles and the direction of the flow.

The detachment of particles from a cylinder is shown in Figure 2.1-3. It follows from Figure 2.1-3 that the detachment of the particles depends not only on the air flow velocity, but also on the position of the surface relative to the axis of the flow, i.e., the angle at which the flow meets the surface. Maximum detachment occurs for φ values of 90° and 270°, only a small number of particles

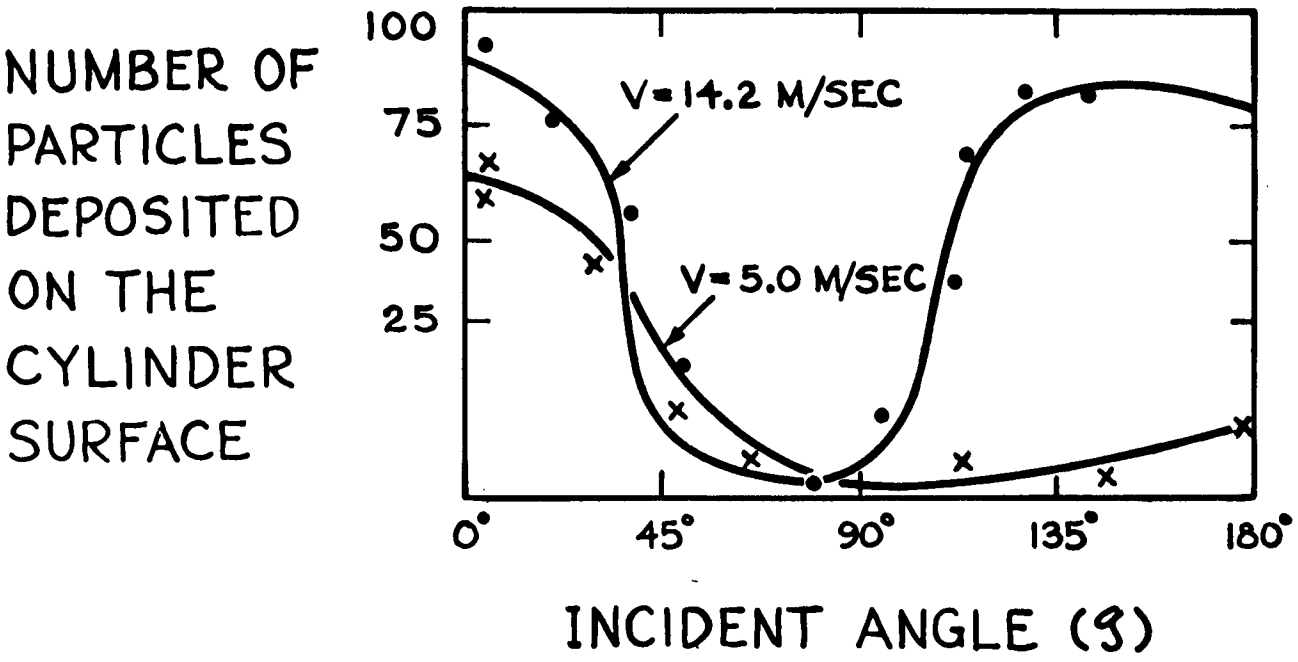

Figure 2.1-2: Numbers of the Particles Deposited on a Cylinder as Functions of the Incident Angle.

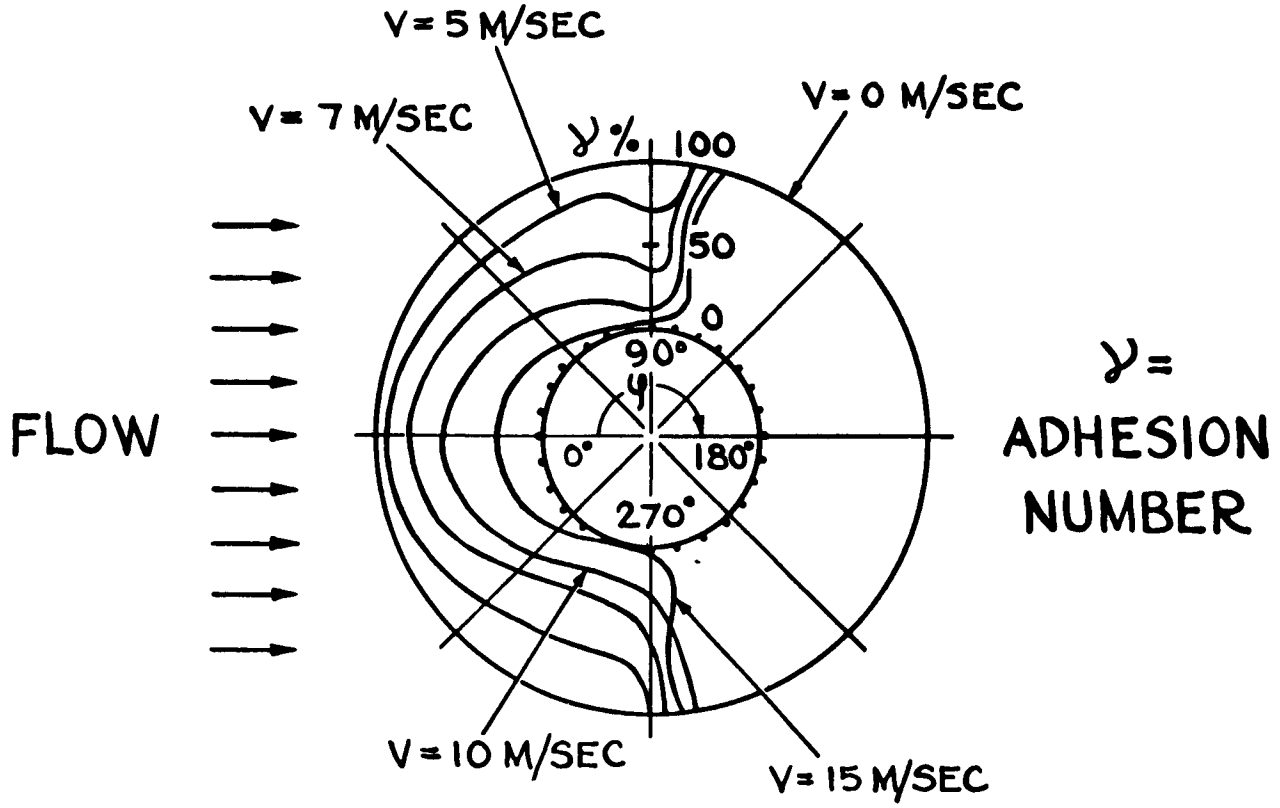

Figure 2.1-3: Detachment of Particles from a Cylindrical Surface.

are detached from the front and none at all from the back at the velocities in question. With increasing velocity, the adhesion number diminishes. However, even under these conditions more particles come away from surfaces placed parallel to the flow than frontally. This fact is of particular importance in the filtration of aerosols (See Section 2.1.3.). Flow around spherical surfaces resembles that around cylindrical surfaces.

2.1.3. Fibrous Filtration Phenomena.

The buildup of a filter cake of solid particles such as fly ash on a filter media is described by First and Silverman (15). Initially, the larger particles are strained by the filter media and start to form a filter cake. The smaller particles (a few microns and less) penetrate into the media, are collected in the conventional manner by attachment to the media, and begin to act as secondary collectors. As the fly ash is deposited the initial filter cake begins to strain the smaller particles causing the porosity of the filter media surface to decrease and the efficiency as well as the pressure drop to increase rapidly.

These authors emphasized that filtration efficiency in bag filtration art is often very poor until the fabric is loaded with a permanent filter cake which is not removed by cleaning. First and Silverman reported, for example, that flocking a bag filter with asbestos floats, to the extent of 194 grains per square foot, raised collection efficiency for 1.2 micron oil smoke from 20.3 to 99.9%.

Fuchs (17) reviewed work by Eliseev on formation of deposits of fine powders on metal gauze. The deposits were said to have had a solid volume fraction of only 6%, yet were impervious to the lead and zinc oxide smokes from which the deposits had been made.

Thus adhesion appears at two stages of the filtration process: in holding the particles when these touch the filtering element, and preventing them from being carried away on subsequent passage of the gas, and also in connection with the regeneration of a spent filter.

In order to discover the part played by adhesion in the filtration process, let us consider the depostion of particles on a single cylindrical filament placed in a flow of aerosol (See Section 2.1.2.5.). The way in which the dust deposit is formed on individual cylindrical filaments of a filtering barrier for a rate of flow rate of 1 m./sec. is shown in Figure 2.1-4 (55). The clearly visible local side are directed at an angle of 110-120° to the axis of the flow. As more aerosol passes the growths come together forming a continuous layer which plays the part of a secondary filtering medium. The sticking of dust to the sides started after the formation of the frontal layer. It should be noted that the buildup of dust on the side surface took place in a nonuniform manner.

We must emphasize the difference in the character of the adhesion to a dust-free (fresh) filter and to a dust-laden filter, particularly for highly dispersed dusts. The

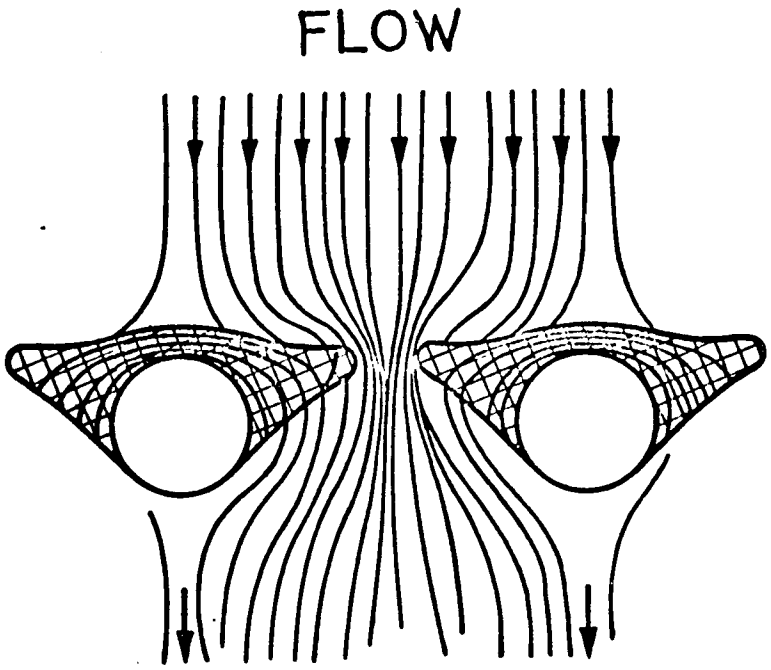

Figure 2.1-4: Formation of Filter Cake on Individual Filaments.

dust-holding capacity of filters improves sharply as they gather dust; the secondary porous barrier formed by the particles of dust deposited in the pores between the fibers or grains of the filter are more efficient in trapping partilces as a result of diffusion and straining and contact. The deposition of particles on single filaments and wires depends on the flow conditions around the obstacle and the elastic properties of the surface as well as the adhesion force. This is the case for a clean filter. In the filtration process on a dust-laden filter, the whole volume of the pores in the filter ultimately becomes filled with particles and clogging takes place.

We should notice also that when a dust-laden surface is subjected to a dust-laden air flow, two processes - the detachment of previously adhering particles, and the deposition of particles carried alongby the flow, may take place simultaneously.

2.1.4. Granular Bed Filtration Phenomena.

Due to the much bigger pore size and much lower porosity in granular beds, granular bed filtration phenomena are believed to be somewhat different from a fibrous filtration. Adhesion and autohesion of powders and turbulent deposition of powders are believed to play a very important role in granular bed filtration. In panel bed filtration of the kind that interests us in the present research, the secondary filtration process or filter cake filtration will be much more important than the primary filtration process or clean bed filtration.

2.1.4.1. Light Aerosol Penetration Studies.

Previous experimental results of granular bed filtration of dilute aerosols had been reported by Thomas and Yoder (46,47), whose work established the existence of a size of maximum penetration (at a constant face velocity of about 0.5 cm./sec.) of about 0.6 micron diameter, which increased with decreasing face velocity. Paretsky (34,35) performed experiments using 1.1 micron polystyene aerosol and confirmed the existence of a velocity of maximum penetration.

2.1.4.2. Fly Ash Penetration Studies.

Taub (45) studied the penetration of fly ash through a granular bed filter. His experiments were performed with filter beds composed of smooth glass spheres, 6 mm., 4 mm., and o.47 mm. in diameter, and with limestone 0.6 mm. or 1.49 mm. average diameter. Maximum operating time was 240 minutes. The depth of bed was varied from 6 mm. to 4 inches and test air velocity ranged from 30 to 120 cm./sec. The inlet concentration of fly ash was varied from 1.0 to 10.5 grains per standard cubic foot of gas. The bulk of experiments were performed with 4 inch beds of 6mm. glass shperes, weighing 1200 grams with porosity of 0.40.

His data at a velocity of 60 cm./sec. are shown in Figure 2.1-5. He observed a saturation phenomenon in the granular bed filtration. The filtration efficiency decreased with time and finally reached a point where the bed was saturated with fly ash and the efficiency dropped to zero. But this saturation phenomena was not observed

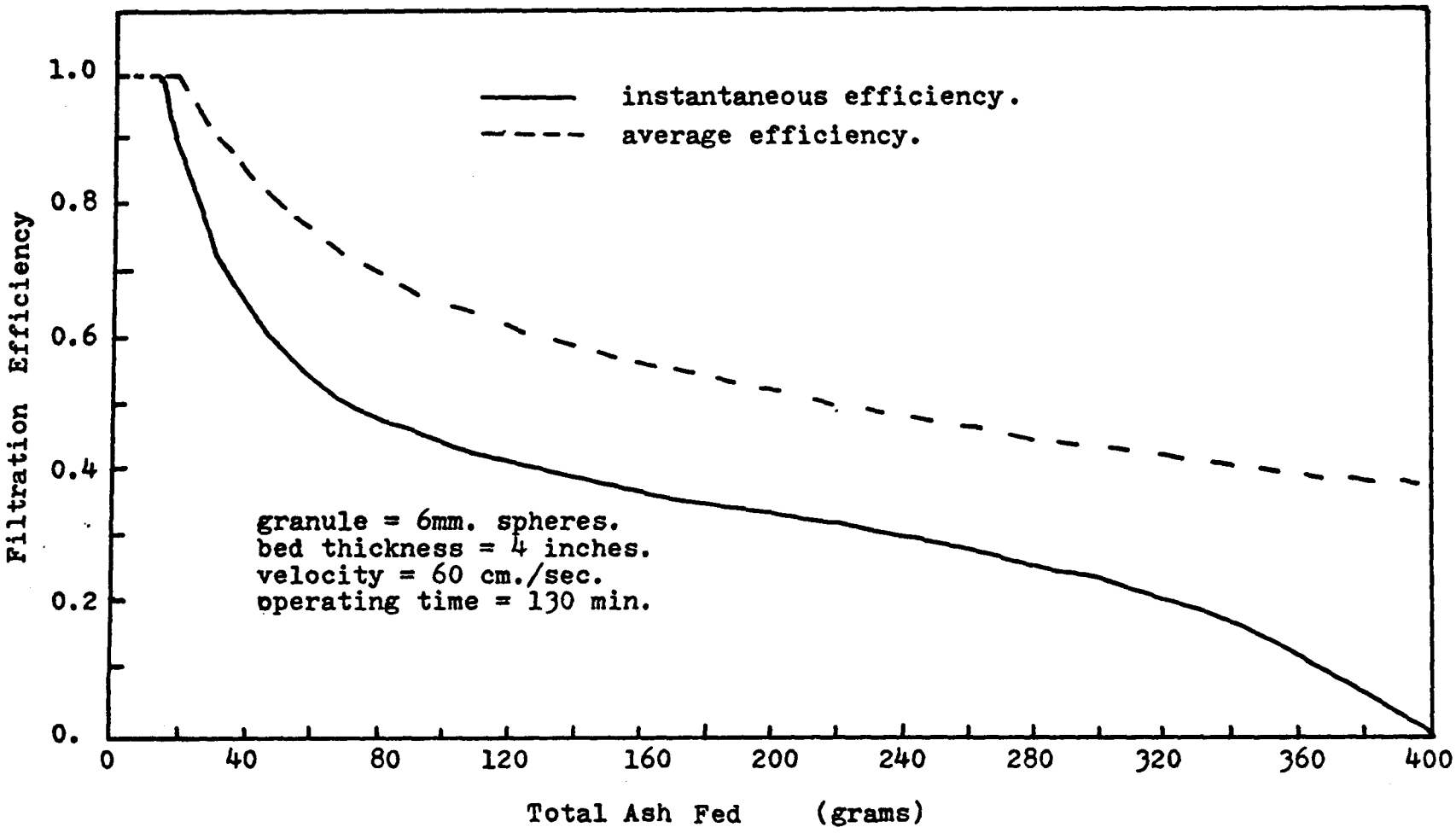

Figure 2.1-5 : Taub's Filtration Efficiency Data Which Shows Saturation Phenomenon.

for his 30 cm./sec. data. He also observed there is no size distribution change in the ash which was fed in, the ash retained in the bed and the ash which passed through the bed.

This saturation phenomena was not observed in our panel bed filtration study (Chapter 4). The difference might be due to the finer granular material which we used and the lower operating velocities. The difference in adhesive forces which results in a difference in denudation or erosion detachment of dust layers around the granules is also a possibility. The fact that the air flow turned a 90^0 angle before entering the sand in the panel bed might also help to build up the filter cake which results in a increase in efficiency with time on 20-30 mesh sand.

2.1.5. Turbulent Deposition in a Tube.

Relatively small dust capable of changing its motion as a result of turbulent pulsations directed to the surface of the wall tends to stick to the wall of the air conduit due to its inertial motion. The net rate of deposition depends both on the rate of transport of the particles to the wall and on the rate of re-entrainment.

Schwendiman and Postama (40), and Friedlander and Johnstone's (16) work on turbulent deposition observed that deposition is extremely sensitive to particle size and sampling velocity. Small particles were much easy to deposit on the wall due to stronger adhesive forces. Also, larger particles projected farther into the gas stream

and are acted on by stronger frontal forces from the stream.

Schwendian and Postama derived an equation for turbulent deposition in a tube as given below with negligible particle re-entrainment.

$$\frac{C}{C_o} = \text{Exp}\left(\frac{-4KL}{vD}\right) \qquad (2.1\text{-}2)$$

C_o = entrance concentration

C = concentration at a point L cm. downstream

v = average velocity in cm./sec.

D = diameter of the conduit in cm.

K = depostion velocity (cm./sec.) which is the quotient of the number particles deposited per unit time per unit area of the wall divided by the number of particles per unit volume in the gas stream.

From the above equation, it is clear that the deposition rate is very sensitive to velocity.

2.2. Fluid Dynamics.

We believe that the puffback sand spill is caused by aerodynamical drag forces on the sand grains. A review of flow through porous material is necessary for an understanding of panel bed puffback operation.

2.2.1. Shock Wave and Its Wave Propagation Properties.

A shock wave is a relatively thin region of rapid variation of state properties across which there is a flow of matter. Because the region of variation is thin, it can almost always be idealized as a surface of discontinuity in space. This surface propagates into the fluid and the compressible fluid immediately behind the shock front

traveling in the same direction with the shock is referred to a shock induced motion. In general, all fluid properties - pressure, velocity, density, etc. - are discontinuous across the surface. In puffback the shock propagates into a stationary fluid (Figure 2.2-1-a). Alternative names for the surface are shock, shock wave, and shock front. The treatment of shock waves as discontinuities or surfaces of zero thickness, is an idealization of inviscid gas dynamics. Physically, shocks are found to have a finite and measurable thickness, commonly of the order of 10^{-6}m.(48).

When a plane shock wave hit a porous material, a portion of the shock will bounce back and a portion of it will transmit into the porous medium (5,48). A weak shock has all the basic properties of wave propagation - reflection when it bounces back and refraction when it is transmitted into a second medium (Figure 2.2.-1-b).

2.2.2. Nature of Resistance to Flow Through Porous Material.

The resistance offered by any stationary object immersed in a flowing fluid is compoased of both the shear stress acting tangentially to the surface of the object (shear drag) and the normal stress or pressure acting perpendicularly to the surface of the object (form drag). The total resistance offered by the object in any given direction becomes the sum total of the corresponding components of the shear stress and pressure acting over the entire surface of the object.

Because of the complex geometry of a pore system, an

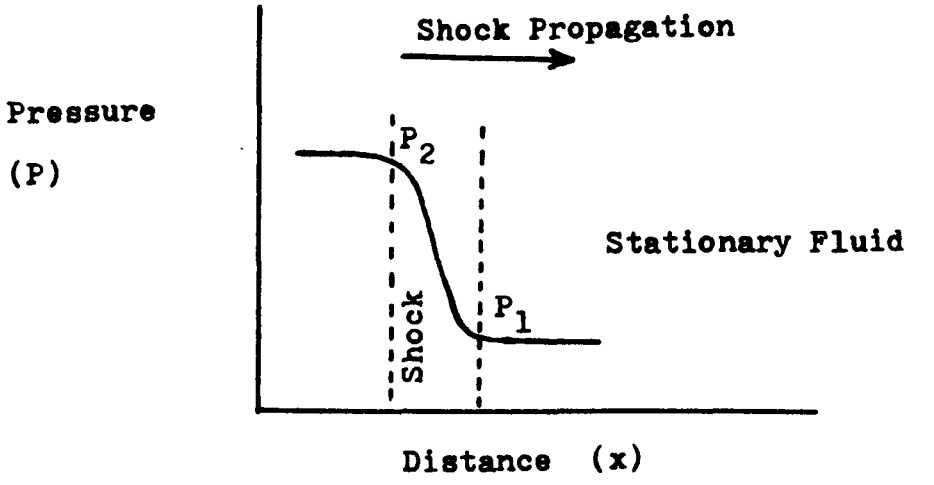

(a)

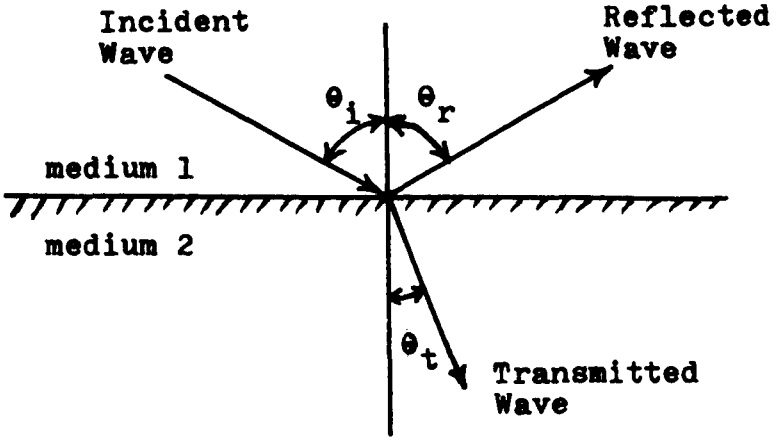

(b)

Figure 2.2-1: Shock Wave and Its Wave Propagation Properties.

exact solution of the Navier-Stokes equations for this problem is impossible. A simplified yet extremely useful picture is obtained by considering the fluid motion on a macroscopic scale and the use of macroscopic properties (9,13).

2.2.3. Linear Laminar Flow Regime or Darcy's Law

The resisting force offered by a single sphere for the special case of slow viscous flow of a Newtonian fluid is given by Stokes' law. This law can be expressed in a generalized form as

$$f_p = \lambda \mu d u \qquad (2.2\text{-}1)$$

in which f_p is the resistance or drag on a single particle, μ represents the dynamic viscosity of the fluid, d represents the characteristic dimension of the particle, u denotes the local velocity of the flow around the particle or the pore velocity and λ represents a coefficient that takes into account the effects of neighboring particles. For a single sphere in a infinite fluid, $\lambda = 3\pi$. For a packed bed, λ will depend upon the porosity, the shape of the particles and the size distribution of the particles.

By considering the total resistance across the porous bed as the summation of the resistance of each individual particles from Stokes's law, we can obtain the familiar Darcy's law (13),

$$v = -\frac{k}{\mu}\frac{dP}{dx} \qquad (2.2\text{-}2)$$

where k is the permeability and has the units of length squared and v is the superficial velocity.

A useful relationship (13) between the permeability and media parameters that can be used for design purpose is

$$k = \frac{\beta \ \epsilon^2}{\lambda(1 - \epsilon)} d^2 \qquad (2.2\text{-}3)$$

For a media composed of spheres, the coefficient β is equal to $\pi/6$. From experimental results, an average value of $\lambda = 174$ was obtained (13). If the porosity is $\epsilon = 0.37$, Equation 2.2- 3 becomes

$$k=(6.54 \times 10^{-4}) \ d^2 \quad (cm.^2) \qquad (2.2\text{-}4)$$

Another way to approach this problem is based on estimating the total drag of the fluid on the solid boundaries of the tortuous channels through the bed of particles (32). This is called the capillary tube model and gives similar results.

2.2.4. Turbulent Flow Regime.

At high flow rate the inertial forces neglected in the deriviation of Stokes' law are no longer small. These inertia terms are derived from the convective acceleration resulting from the constantly varying cross-sectional area exposed to the flow, and also from the centrifugal acceleration resulting from the curvature of the flow path. For these reasons, equation 2.2-2 ceases to be valid when the resistance function can no longer be given by a generalization of Stokes' law. This occurs when the permeability Rynolds number Re_k is larger than 0.5 to 1. The permeability Reynolds number is defined as

$$Re_k = \frac{v \ k^{\frac{1}{2}} \ \rho}{\mu} \qquad (2.2\text{-}5)$$

and is better able to characterize the flow through porous materials than the particle diameter Reynolds number Re_p (3,49).

The inertial effects can be accounted for by a second term containing the square of the velocity. It was first suggested by Reynolds (38) and later by Muskat (33) that the axial pressure gradient might be represented in the form

$$-\frac{dP}{dx} = \frac{\mu v}{k} + \frac{c\rho}{k^{\frac{1}{2}}} v^2 \qquad (2.2\text{-}6)$$

which is a modified Darcy's equation. Here c is a constant for a given medium and μ is the viscosity of the flowing fluid. Beavers and Sparrow's (3) work on fibrous porous media and Ward's (49) work on water through different granular media verified this equation.

At low velocities, the second term is negligible and the equation reduces to Darcy's law. At high velocities the first term will be negligible.

2.2.5. Compressible Flow Through a Porous Material.

Several theoretical studies have been done on compressible flow through a porous material (4,2,14). Consider one-dimensional flow of a perfect gas through a plate of uniform porosity ϵ (Figure 2.2-3). The cross-sectional area of the plate is taken to be unity; consequently the area available to the flow within the plate is ϵ.

Air is treated as a perfect gas (γ=1.4) and the

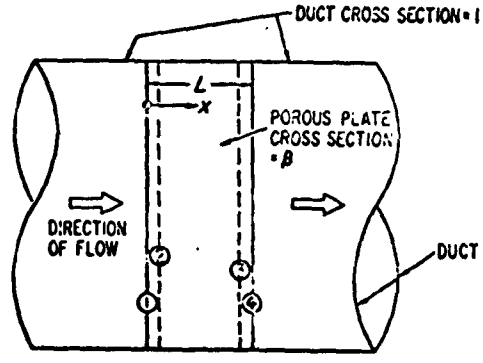

Figure 2.2-2: Flow Schematic for a Porous Plate Inside a Duct.

variation of viscosity with temperature is neglected. It has been pointed out (4,14) that a complete description of this flow must include a description of the flow entering and leaving the material, where the flow experiences sudden changes in area. To do this the flow region is divided into three parts, as shown in Figure 2.2-2. Positions 1 and 4 correspond, respectively, to locations immediately upstream and downstream of the permeable plug.. Position 2 describes the gas within the plug just downstream of the front face, and position 3 describes the gas just within the plug at the down stream end. The gas adjusts from position 1 to position 2 and from position 3 to position 4 in a distance of a few pore diameter. The Mach number of the gas is defined as:

$$M^2 = \frac{u^2}{\gamma(P/\rho)} = \frac{R\,T\,(\rho\,u)^2}{\gamma\,p^2} \qquad (2.2\text{-}7)$$

where γ is the ratio of specific heats, P is pressure, R is the gas constant, T is temperature and u is velocity.

Let us consider the flow in the entry and exit regions of the plug. Emanuel and Jones (14) argued that the flow between positions 1 and 2 is analogous to that in converging nozzle, with the gas undergoing an isentropic expansion. In describing the flow out ot the plug, Emanuel and Jones suggested that the flow experiences a sudden area change, from an area ϵ to unit area, which is an adiabatic but nonisentropic process due to viscous energy dissipation. When $M_3 < 1$, this is a compression, $P_3 < P_4$, which results in

$M_4 < M_3$. They derived several theoretical results to relate the Mach numbers and pressure changes for these end effects. For the panel bed filter the situation is much more complicated because of the additional effects of the louvers.

Emanuel and Jones' (14) work showed that when the Mach number is small, there will be a simple relation

$$M_1 = \epsilon M_2 = \epsilon \left(\frac{P_4}{P_1}\right) M_3 = \left(\frac{P_4}{P_1}\right) M_4 \qquad (2.2\text{-}8)$$

They also showed, when $M_3 < 0.239$, the gas can be practically assumed to be incompressible. In this case, we can simply neglect the convective term and use the modified Darcy's equation (Equation 2.2-6).

2.3. Soil Mechanics.

Sand is one kind of cohesionless soil; hence, its motion during puffback is governed by the principles of soil mechanics. A study of Casagrande's paper (7) about the stability of sand leads us to believe puffback is actually a soil failure phenomenon. Hence, a review of soil mechanics is necessary, especially the shearing strength of the soil.

2.3.1. Generalized Stress-Strain Diagram and Failure.

Figure 2.3-1 shows generalized stress-strain diagram of soil. The stress τ represented in these diagrams is usually the average shearing stress on the plane of shear, calcuated as the shearing force divided by shear plane area. There is no sharp break in the stress-strain diagram which

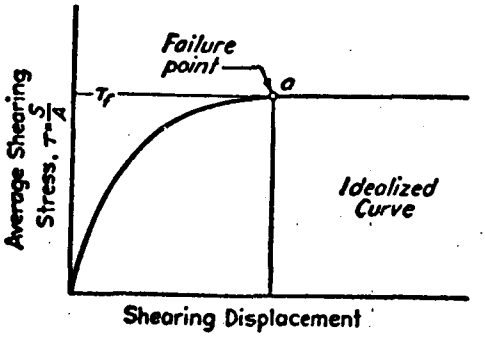

Figure 2.3-1: Shearing Stress Displacement Diagram for Test Specimen.

can be recognized as evidence of failure. Failure in test specimens of soil may be said to occur when continuous shearing displacement takes place at relatively constant shearing stress, as at point 'a' in Figure 2.3-1. After this point has been reached the shearing stress cannot be increased except through an acceleration of shearing displacement.

2.3.2. Nature of Soil Strain.

When an applied force is transmitted through the soil or contact forces are developed between adjacent particles, the forces can be resolved into components normal N and tangential T to the contact surfaces (Figure 2.3-2) (30). The individual particles deform as the result of these contact forces. There are two major types of strain for sand. First is elastic or plastic strain in the immediate vicinity of the contact points where particle crushing can occur, especially at high stress (Figure 2.3-3-a). These deformations will lead to relative movements between the adjacent particles. In addition, once the shear force at a contact becomes larger than the shear resistance at the contact, there will be a relative sliding or rolling between the particles (Figure 2.3-3-b). This leads to the second type of strain. The overall strain of a soil mass will be partly the result of deformation of individual particles and partly the result of relative sliding and rolling between particles with the second type of strain

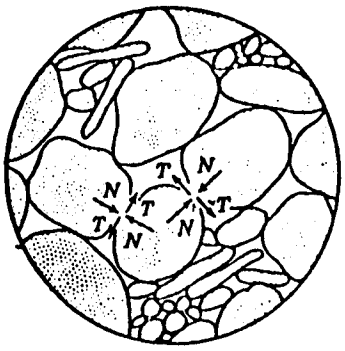

Figure 2.3-2: Schematic Representation Showing Forces at Two of the Contact Points.

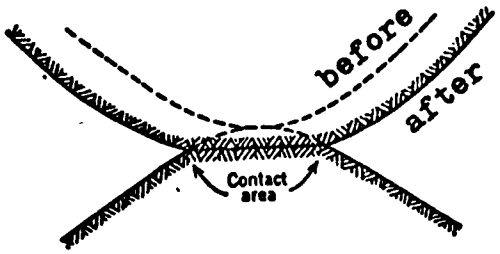

(a) deformation of contact.

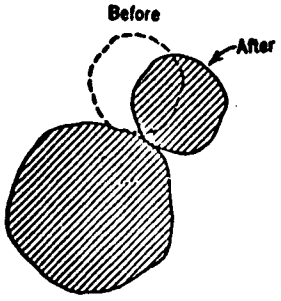

(b) interparticle sliding.

Figure 2.3-3: Causes of Relative Motions Among Soil Particles.

dominating. At each of the contacts between particles the local strain may be very large, much larger than the overall strain. As Lambe (28,29) said, the motions within an actual soil are too complex to be analyzed by any simple model. At any instant during the deformation process different mechanisms may be acting in different parts of an element of soil. At any one spot within the element, the relative importance of the different mechanisms may change as the deformation process continues. This indicates that the puffback failure is a very complex process if considered from the microscopic point of view.

2.3.3. Source of Soil Strength.

Soil shear strength is based on the shear resistance between contact surfaces, the interlocking of granular particles, and the true cohesion in the soil. The shear strength for sand comes from the shear resistance between mineral surfaces and the interlocking of particles. True cohesion can develop between particle surfaces which contribute some of the strength. But usually this is not important after the sand bed is penetrated by dust. Also, at high temperature operation, sintering of dust might cause strong cohesion.

The shear resistance can be described by Amonton's law of friction - the shear resistance between two bodies is proportional to the normal force between the bodies.

$$F = \mu' N = \tan (\phi') N \qquad (2.3\text{-}1)$$

where F is the shear resistance or friction force, μ' is the friction coefficient, N is the normal force and ϕ' is the friction angle.

Rowe's (39) work on shear resistance between granular material and a smooth mineral surface showed that the friction angle ϕ' is affected by the size of the particles involved in the test (Figure 2.3-4). Larger particles showed smaller friction angles, possibly because the larger particles are able to roll more easily than the smaller particles as a result of their center of gravity being further away from the plane of shear. Hence the measured friction angle for larger particles involves both rolling and sliding components.

Strength due to interlocking can be best illustrated by Figure 2.3-5. When a granular material undergoes a shearing force along plane a-b, there is an upward component, as sliding occurs on the inclined faces of adjacent particles. Hence, the particles must move up and over one another and this causes more energy to be consumed and results in a greater shear strength.

2.3.4. Shearing Strength of Sand.

The value of the shearing strength of a given soil may vary over a wide range with changes in conditions of saturation, normal loading, and other factors (23). In the panel bed filter we use dry sand, hence we will not consider the effect of saturation.

2.3.4.1. Effect of Normal Pressure.

The effect of variation in normal loading is usually observed by performing tests on a number of specimens with

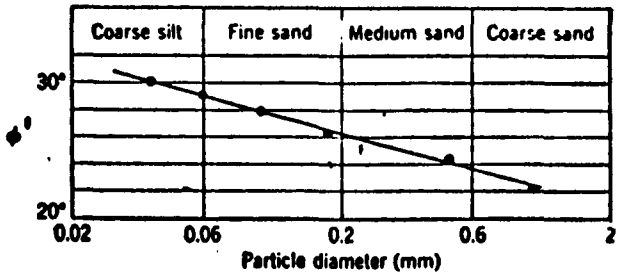

Figure 2.3-4: Friction Angle of Quartz Sand as Function of Grain Size, Measured for Displacement of the Sand on a Smooth Mineral Surface.

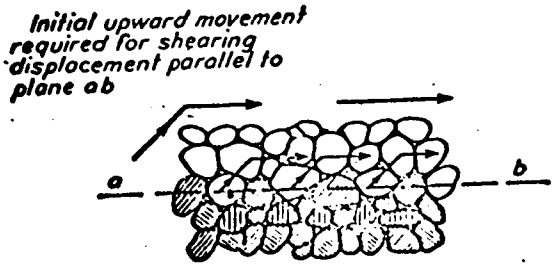

Figure 2.3-5: Particle Interlocking in Dense, Granular Material.

a different normal loading being applied in each test. Figure 2.3-6 presents a group of stress-strain diagrams representing data obtained from a series of such tests on specimens of cohesionless soil.

While it is evident from inspection of Figure 2.3-6-a that the unit shearing strength of cohesionless soil increases with effective normal pressure, this relationship can be represented more clearly in what is termed a shearing-strength diagram as shown in Figure 2.3-6-b. The general slop of the diagram is usually indicated by the angle ϕ which is referred to as the angle of internal friction or simply the friction angle of soil. This relation is similar ot Equation 2.3-1 and can be described by

$$\tau_f = N \tan \phi$$
$$= N \mu \qquad (2.3\text{-}2)$$

where μ is soil friction coefficient, N, the normal force.

2.3.4.2. Effect of Initial Porosity.

The effect of soil porosity as observed during triaxial shear tests may be described as in Figure 2.3-7 (29). Curve A in Figure 2.3-7 shows data for cohesionless soil which was initially at or near its maximum density. The resistance in the specimen develops to a maximum at point 'a' with increasing shearing displacement. The shearing strength of the dense speciment at point 'a' is termed peak strength. After the peak strength, dense sand will lose strength. Point c is called the ultimate strength of the sand which is independent of the initial porosity. If the specimen was initially at

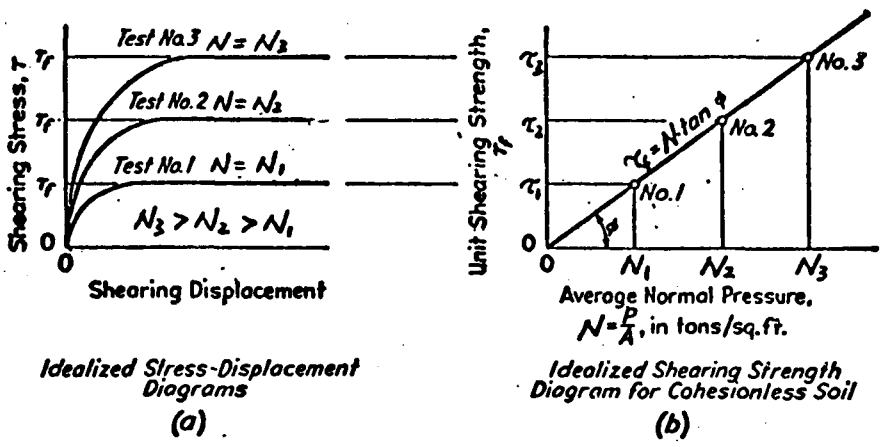

Figure 2.3-6: Effect of Normal Pressure on Shearing Resistance in Granular Soil.

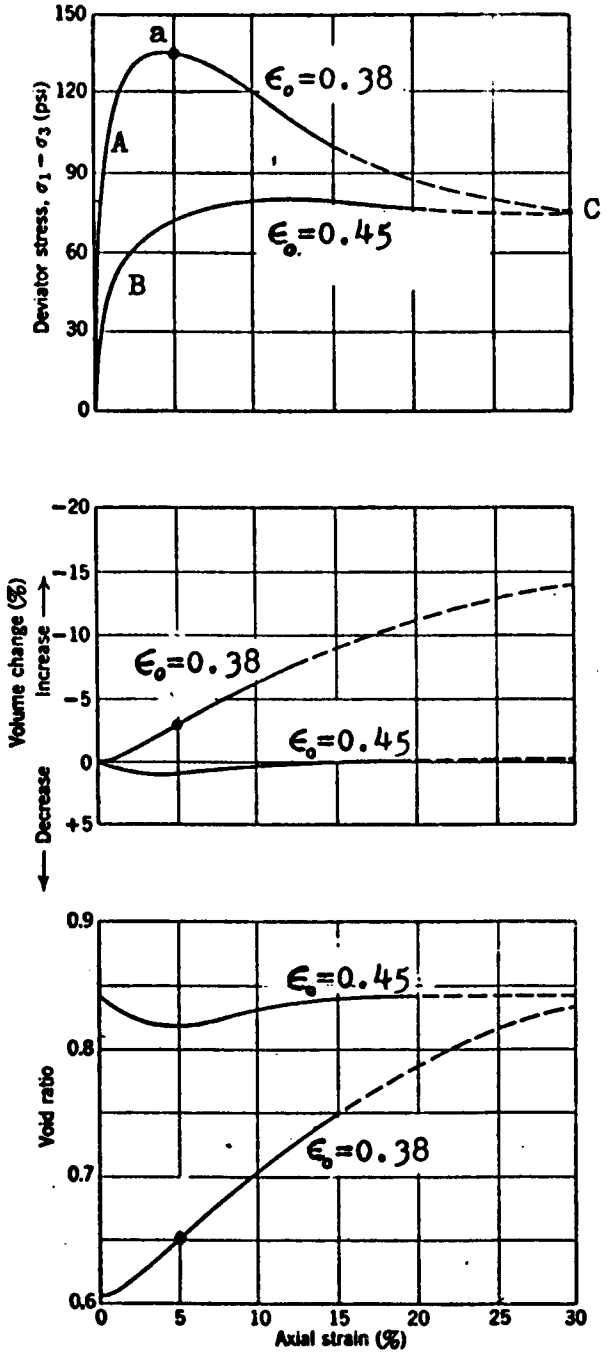

Figure 2.3-7: Stress-strain Curves for Loose and Dense Specimens, Medium-fine Sand.

an extremely loose condition, development of strength, as indicated by curve B in Figure 2.3-7, would be observed. The ultimate strength will also be the same as the initial dense specimen.

The reason for this phenomenon is because the denser the sand, the greater the interlocking, hence the greater the friction angle. Figure 2.3-8 shows Rowe's (39) result of the relationship between friction angle $\emptyset$ and the initial porosity for medium fine sand. It shows the general trend of higher friction angle for denser sand. $\emptyset_{cv}$ is the friction angle at the ultimate condition or at the critical volume.

It may be noted that $\emptyset'$ for the medium fine sand of Figure 2.3-8 is 26^{o}, in contrast to $\emptyset_{cv} = 32^{o}$. The difference between $\emptyset'$, the friction angle for the sand sliding on a smooth surface and $\emptyset_{cv}$, the ultimate friction angle that expresses the ultimate strength, is caused by particle interlocking.

2.3.4.3. Volume Change During Straining.

It is unusual when shearing action in soil does not produce some change in soil volume aside from changes due to simple compression under normal loading.

Figure 2.3-7 (29) shows the volume change for a triaxial test for both initially dense and initially loose specimens. When a dense specimen undergoes shear, its volume decreases a little bit at the very beginning and then expands a lot. On the other hand the loose specimen

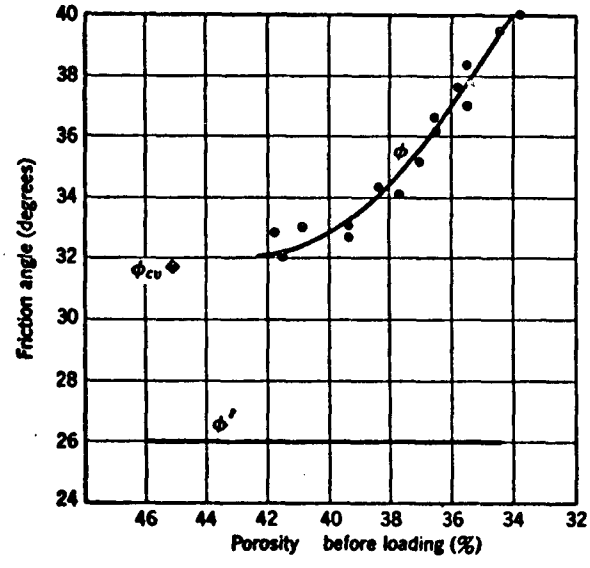

Figure 2.3-8: Friction Angle Versus Initial Porosity for Medium Fine Sand.

first decreases in volume, then expands once again and finally ends up at a constant volume.

In order to have a shear failure between particles, it is not only necessary to overcome the surface frictional resistance, it is also necessary to make particles move up and over one another. The volume will either decrease or increase depending on the inital porosity. It will decrease first to a more dense and hence more stable state. But additional shear strain will force particles to move up and over one another to overcome the interlocking which causes a volume increase to make the shear strain possible. For initially dense specimens, as the shear motion continues, the degree of interlocking must decrease, and consequently the shear force necessary to continue the motion must also decrease to an ultimate condition. The volume at the ultimate strength is called the critical volume which is independent of the initial void ratio.

The interlocking of particles explains why the initially dense specimens and initially loose specimens have the same ultimate shearing strength, since by shearing distortion they are brought to approximately the same condition of density. In the ultimate condition, the interlocking between the soil particles has decreased to the point where continuous shear deformation can continue without further net volume change.

2.3.4.4. Effect of Rate of Shear.

The development of shearing resistance in a direct

shear test specimen of cohesionless soil has been found to be relatively independent of the rate of shearing displacement. For given test conditions, approximately the same strength will be developed whether the increase in shearing stress is gradual or rapid.

Whitman and Healy (51) studied shear strength of sands during rapid loadings by triaxial tests. This transient failure phenomena is similar to our puffback failure. They found the friction angle of sand is substantially the same whether the sand is loaded to failure in five milliseconds or in five minutes. The creation of excess pore pressure and the dissipation of excess pore pressure by drainage are time dependent and hence will change the strength of sand by changing the shear rate. In dry sand the change in excess pressure is usually negligible. The dissipation of excess pore pressure by drainage depends upon the boundary conditions for each individual problem. For dry sand, the increase in friction angle from the slower to the faster loading rate is at most 10% and probably is only 1-2% by considering the effect of the boundary conditions for the test.

Whitman, Miller and Moore's work (52) on small increments of stress superimposed on an initial stress showed the importance of elastic or plastic deformation for rapid loadings. Their results (Figure 2.3-9) showed an "S" shaped stress-strain curve for dry sand so that the modulus for small stress changes is greater than the

secant modulus for larger stress changes. As the load is first applied, strain results primarily from deformation of the individual grains. With further loading, grains start to slide relative to one another and resistance to straining decreases. The effect of increasing the rate of stressing was thus to increase the elastic or plastic deformation. Hence putting all of the stress on suddenly apparently made it more difficult for the soil to strain. The behavior due to a small stress increment superimposed on an initial stress is shown in Figure 2.3-10 (29). Sliding between particles does not begin until the stress increment exceeds some critical level. The critical stress increases with increasing initial stress and decreasing porosity and is larger for rapid loadings than for slow loadings. This behavior is similar to what we observed in puffback sand failure, which will be discussed later (Section 9.1).

2.3.4.5. Effect of Confining Stress.

There are two effects of confining stress. First, the resistance to sliding at each contact point is proportional to the normal force at that contact, and hence the overall resistance increases as the confining stress increases. Second, interlocking decreases as the confining stress increases, because the particles become flattened at contact point, sharp corners are crushed and particles break. Even though these actions result in a denser specimen, they make it easier for shear deformation to occur.

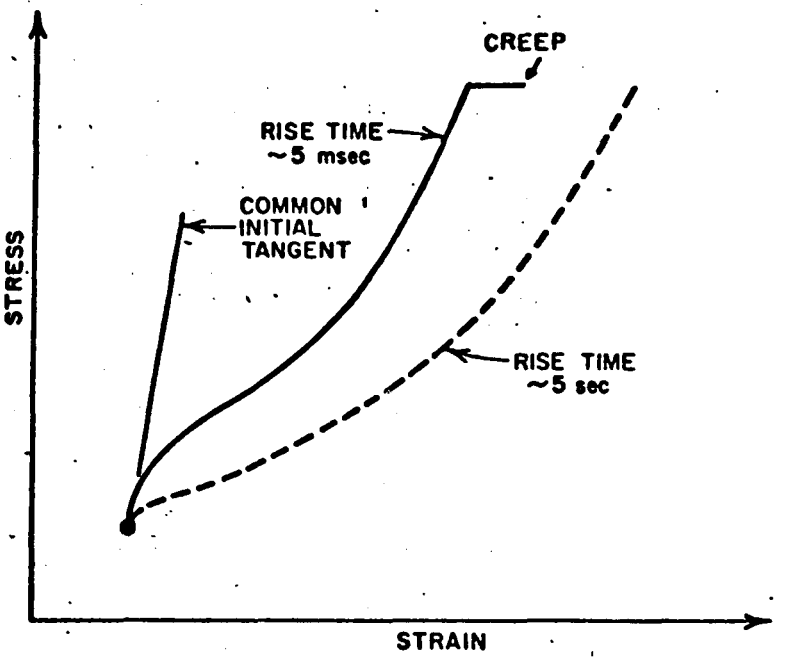

Figure 2.3-9 : Typical Observed Stress-strain Behavior at Different Loading Rate.

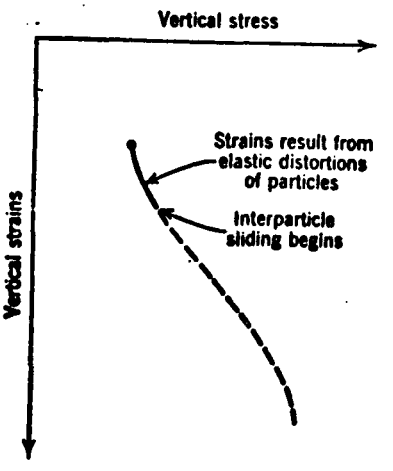

Figure 2.3-10: Behavior During Small Stress Increment Superimposed upon an Initial Stress.

2.3.4.6. Effect of Particle Size, Grading, and Angularity.

Experimental data(30) showed particles of different sands have almost the same friction angle. The effect of the greater initial interlocking in sand with bigger particles is compensated by the greater degree of grain crushing and fracturing that occurs with the larger particles because of the greater force per contact. Also larger particles are able to roll more easily than the smaller particles as a result of their centers of gravity being further away from the plane of shear.

Well graded sand (sand which has a wide range in grain size and has almost equal percentage of each size) has both a smaller porosity and a larger friction angle because the better distribution of particles sizes produces a better interlocking. Well graded sand also experiences less breakdown than a uniform soil of the same particle size, since in a well graded soil there are many interparticle contacts and the load per contact is thus less than in the uniform soil. Hence well graded sand has a higher soil strength.

Particle shape affects its performance in particle interlocking. Flat or angular particles can be fitted together in a very dense condition which results in the development of very effective interlocking and hence higher soil strength. Table 2.3-1 (22) shows the general effect of grading and shape on soil strength.

Table 2.3-1: Effect of Angularity and Grading on Peak Friction Angle.

Shape and Grading	Loose	Dense
Rounded, uniform	30°	37°
Rounded, well graded	34°	40°
Angular, uniform	35°	43°
Angular, well graded	39°	45°

2.3.5. Rupture of Soil.

The stresses which can be developed at given point are limited by the strength of the material. There are a number of different theories as to the nature and extent of this limitation. For materials like cohesionless soil, which derive strength from solid friction the Mohr rupture theory is considered most satisfactory.

It is shown in mechanics (23,26) that when a body is subject to loading, along any plane through a point within the body, the stress can be resolved into two components. One is the normal stress or pressure normal to the plane and the other is the shear stress tangential to the plane. If stress on all possible planes through the point are evaluated, it will be found that there are two mutually perpendicular planes on which the tangential shear stresses are zero. The normal stress on one of these planes has a maximum value among all the possible normal stress through this point and that plane is termed the plane of major principal stress. On the other plane the normal stress has its minimum value and that plane is termed plane of minor principal stress.

According to Mohr's theory, in cohesionlesss soil, failure will occur when the ratio of the shear stress and the normal stress at a certain plane becomes equal to the tangent of the internal friction angle of the material. The location of the failure plane with reference to the plane of major principal stress in granular soil is illustrated by the following equation:

$$\theta = 45^{o} + \frac{\phi}{2} \qquad (2.3\text{-}3)$$

where θ is the angle of failure plane with the plane of major principal stress and ϕ is the angle of internal friction or angle of friction.

2.3.6. The Angle of Repose.

There are two different types of angle of repose. One is obtained when a pile of solids is formed, and the other when it is drained. The difference between the two angles is a function of the particle size distribution. Figure 2.3-11 (54) illustrates these two versions of the angle of repose. The picture represents flow of powder from a rectangular experimental bin. The line of demarcation between stationary and flowing solids is usually quite definite and the angle θ is the angle of failure plane. The top angle of repose β was formed by draining of particles and the botton angle of repose β was formed by piling up of particles.

2.3.7. Stress Analysis for Granular Materials Confined Between Walls or Bin.

Because of the existence of the failure plane within

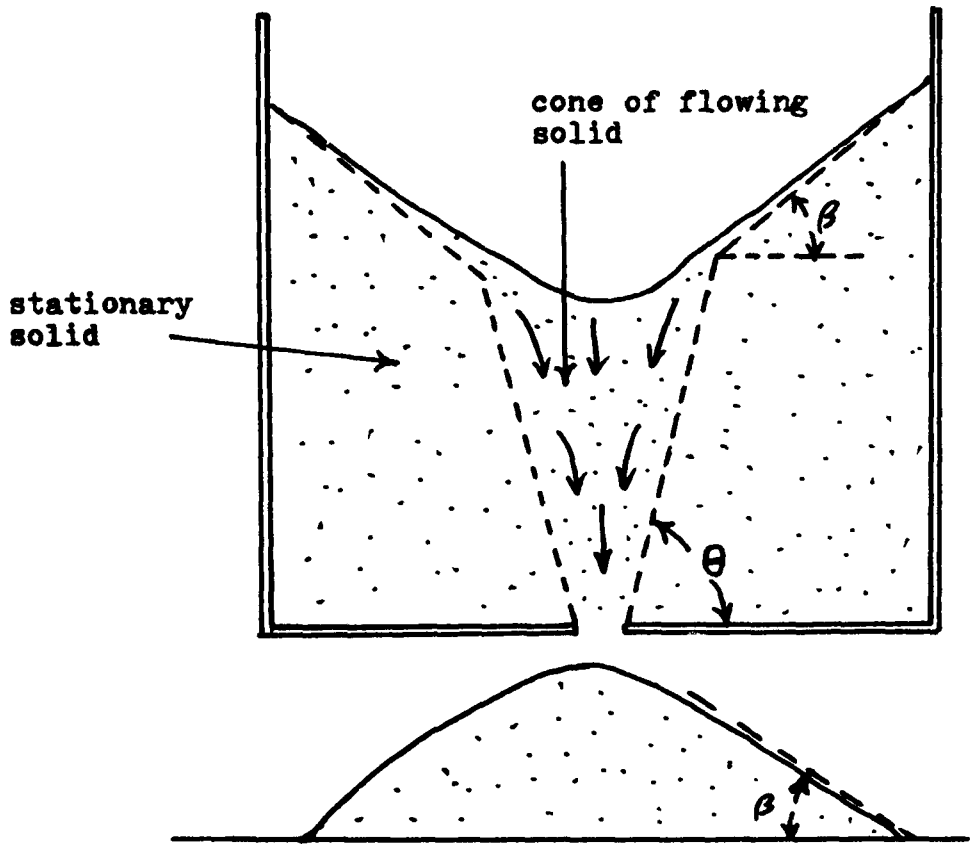

Figure 2.3-11: Bin Flow Test Illustrating Angle of Repose β and Angle of Failure Plane θ.

the granular material and the particle to bounding surface friction force, there are many peculiar internal and surface phenomena for particulate systems. The rheology for particulate flow is entirely different from the usual fluid dynamics. The bin flow test illustrated in Figure 2.3-11 showed there will be a stationary portion below the plane of failure. This stationary portion will stay stationary until the surface of the particles cuts the plane of failure and then the particles will flow down along the angle of repose.

According to hydrostatics, the vertical pressure P at any point within the fluid is proportional to the height of the fluid h;

$$P = \rho h \qquad (2.3\text{-}4)$$

and the lateral pressure P_L at any point is equal to the vertical pressure P at that point;

$$P_L = P \qquad (2.3\text{-}5)$$

This is not the case for particulate systems.

Experiments (27) have shown that the pressure at the base of a bed of granular materials in a bin increases proportionally with the bed depth up to a certain height, about twice the width of the bed, at which the incremental pressure build-up begins to decrease and finally, about at a height three times more than the width of the bed, approaches a constant value independent of further increase in bed height. Also, the lateral pressure at any point is less than the vertical pressure.

The following shows Janssen's result (27) for the analysis of the stresses in grain bins which agree very closely with the experimental data. Janssen assumed a bin with a uniform area A, a constant circumference U, the bin is filled with granule weighing W per unit of volume. Let P be the vertical pressure, and P_L be the lateral pressure at any point, both P and P_L being assumed as constant for all points on the same horizontal plane. μ' is the friction coefficient between the bin wall and the granular material. Let R be the hydraulic radius of the bin, R = A/U. Also, experimental results showed that in a granular mass, the lateral pressure P_L at any point is equal to the vertical pressure times i, a constant for the particular granule, and

$$P_L = i P \qquad (2.3\text{-}6)$$

If h be taken as the depth of the granule at any point, his analysis result,

$$P = \frac{W R}{i \mu'} \left(1 - e^{\frac{-i \mu' h}{R}} \right) \qquad (2.3\text{-}7)$$

From Equation 2.3-6 we get,

$$P_L = \frac{W R}{\mu'} \left(1 - e^{\frac{-i \mu' h}{R}} \right)$$

Both μ' and i can only be determined by experiment on the particular granule and kind of bin. Jamieson's (27) data on dry sand is shown in Figure 2.3-12 and gives i = 0.33.

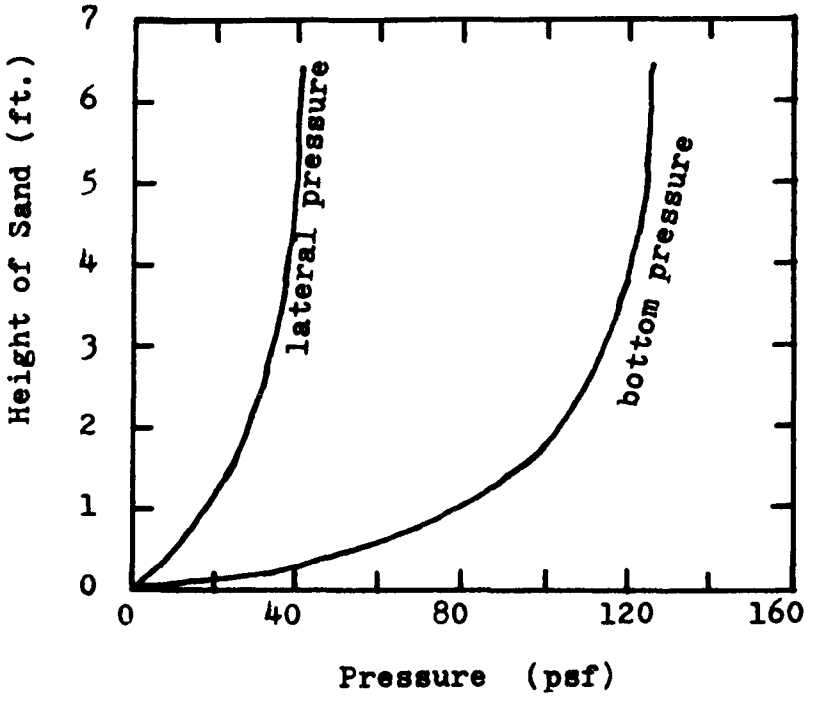

Figure 2.3-12: Experiments on Pressure of Sand in a Model Smooth Steel Bin 12 Inches Diameter.

Chapter 3. Experimental Arrangement for Study of Panel Bed Filtration and Puffback.

In this chapter we will discuss the development of the panel bed filter test unit and the louver design. We will also discuss the equipment and procedures for all of the tests related to the panel bed filtration study and puffback study. Some additional miscellaneous tests and equipment will be discussed in Chapter 7.

3.1 Design of the Fly Ash Feeder.

Figure 3.1-1 shows our feeder for fly ash. It is based on a modification of a feeder used by the Bureau of Mines at Morgantown, West Virginia. The design has two objectives. The first objective is to supply fly ash at a slow, steady flow. This is done with a screw feed that is driven by a motor with variable speed control. The fly ash is supplied to the screw from a cylinder that is stirred by paddles on a shaft driven by a second motor. The purpose of the paddles is to prevent bridging and consolidation of fly ash particles in the cylinder.

The second objective is to redisperse the fly ash into a cloud of individual particles. We do not want to have any agglomerates of fly ash particles. Each particle should be individual. This is accomplished by feeding the fly ash into a chamber supplied with air at about 2 atmospheres. The fly ash and air then flow across a critical orifice, and the fly ash appears to be well

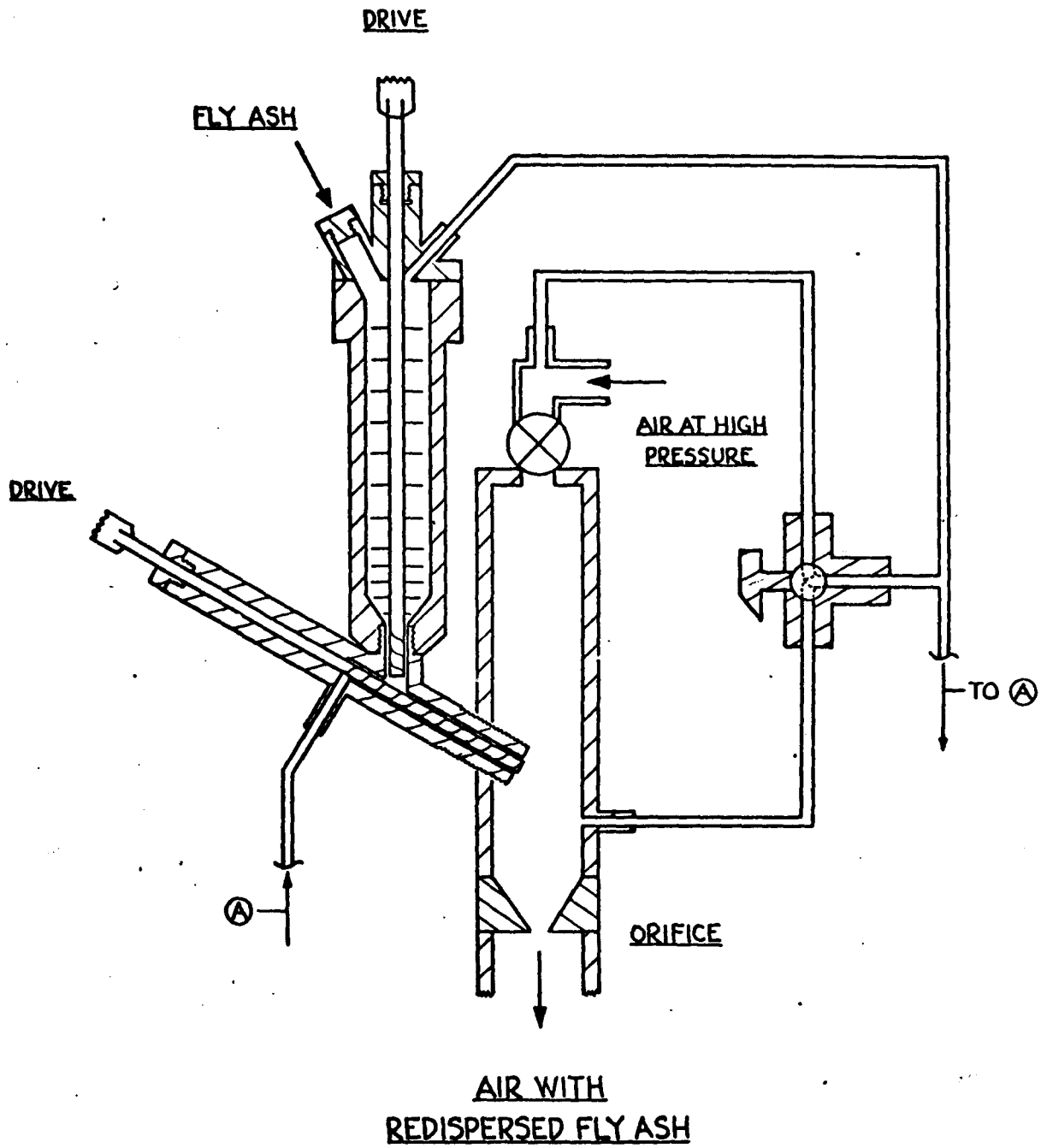

Figure 3.1-1: Feeder for Redispersal of Fly Ash in Air at Atmospheric Conditions

dispersed downstream of the orifice. We have collected samples and looked at them through a microscope, and we believe that the fly ash is well dispersed. A series of different size orifices were used for different test air velocities.

Because we feed the ash into a high pressure (about two atmospheres) air stream, we have to be very careful to balance the pressure within the system. When the air velocity was low the pressure inside the fly ash supply cylinder and screw feeder were connected to the air chamber through the three-way valve. When the air velocity was high the pressure of the cylinder and the screw feeder were kept slightly higher than the pressure in the air chamber by turning the three-way valve to the air inlet tube where the pressure was kept slightly higher than the air in the chamber by a gate valve. This slightly higher pressure in the fly ash cylinder helped push the fly ash into the air chamber.

We obtained fly ash from Consolidated Edison Company of New York. It was collected by an electrostatic precipitator working at beyond 99 per cent collection efficiency, and is typical power station fly ash. Figure 3.1-2 (35) shows the size distribution of Con Edison fly ash.

3.2. Development of the Panel Bed Filter Test Unit.

Figure 3.2-1 shows a schematic of the panel bed filter experimental apparatus. Two dryers using molecular sieves which can dry the air to a dew point below $-100^{0}F$,

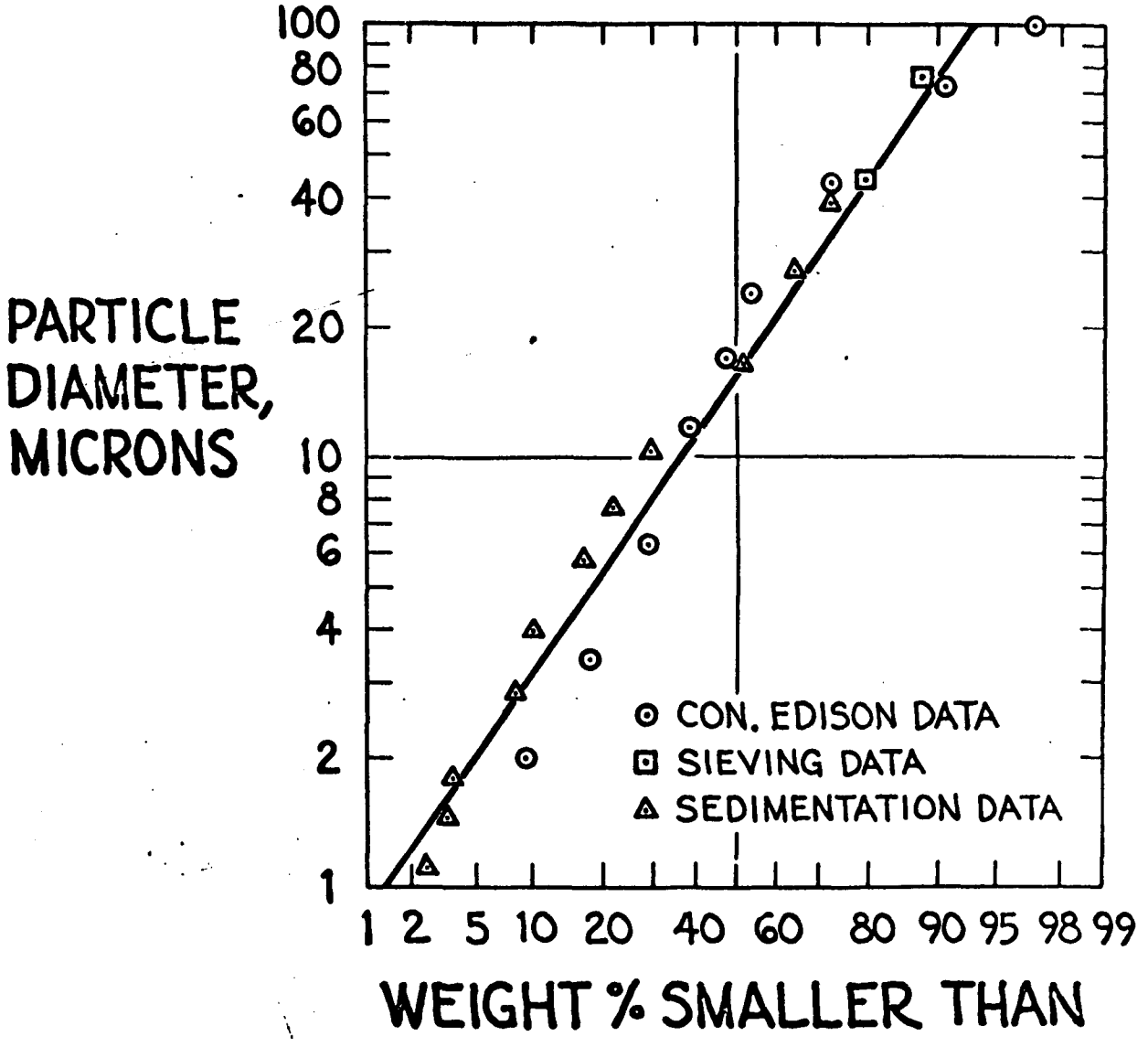

Figure 3.1-2: Particle Size Distribution of Fly Ash Collected by an Electrostatic Precipitator at High Efficiency and Used in Tests of Panel Bed Filter

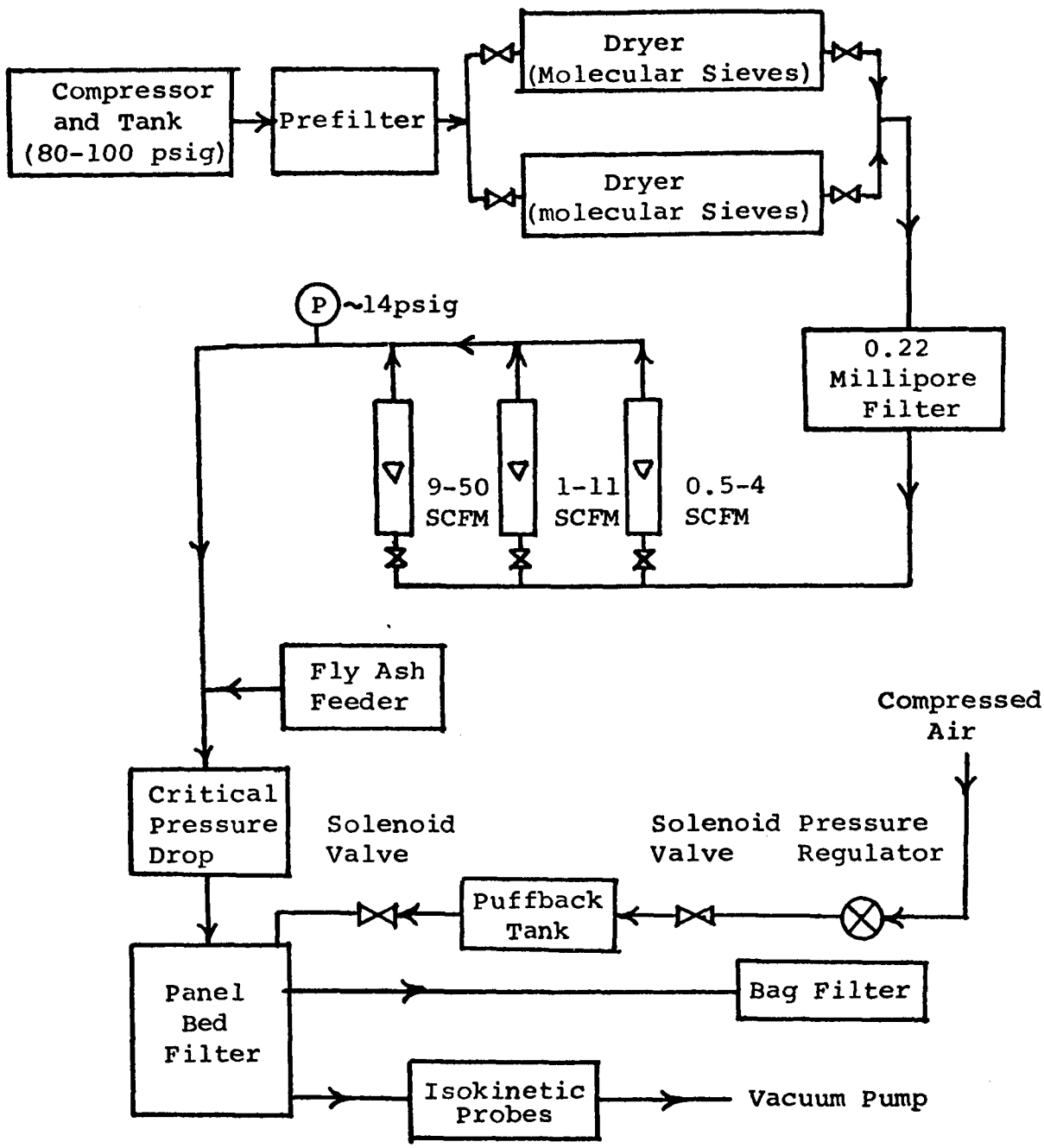

Figure 3.2-1: Schematic of Panel Bed Experimental Apparatus.

were used alternately to dry the air. The molecular sieves were regenerated by 700°F air for one day after running for two days. One of the three rotameters was used for different velocity ranges as shown in the figure.

The panel bed filter test unit has been subject to many modifications and we will discuss some of the more important modifications which we made.

3.2.1. Vertical Back Test Unit - Preliminary Unit.

Our first test unit for this work is shown in Figure 3.2-2. This unit has a vertical back plate facing the back louvers. Redispersed power station fly ash in air entered at the top of a vertical passage for dirty air, and the air entered the panel bed through gas-entry surfaces disposed upon louvers resembling venetian blinds, and across the panel from left to right as shown in the figure. The louver area is 3 inches wide and 12 inches high. The sand bed thickness is 1 inch. Clean air came out from the lower end of the clean side chamber and went out through a one inch plastic tube and a ball valve.

The pressure drop across the panel bed built up as a run proceeded, and when the pressure drop reached a certain level we stopped the flow of dirty air and closed the ball valve. We then opened the solenoid valve that released air from the puffback tank. This caused a surge flow of air across the panel in the direction opposite to the normal flow of dirty air and removed the surface filter cake and a few layers of sand.

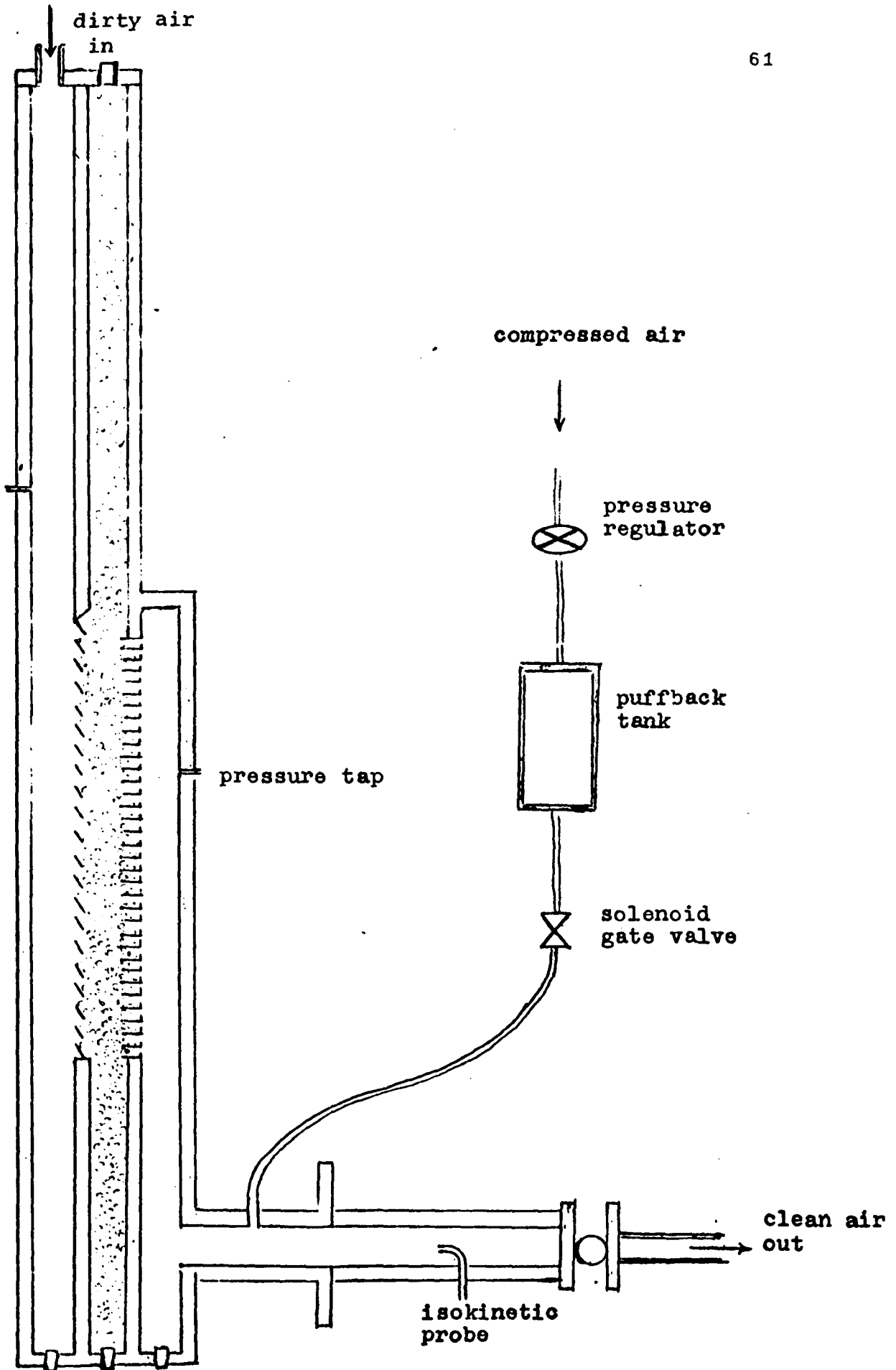

Figure 3.2-2: Schematic Cross-Sectional View of Apparatus for Test of Panel Bed Filter- Preliminary Unit.

The pressure drop restored to the initial level and the unit was ready for another filtration cycle.

The filtration efficiency was determined from the dust collected isokinetically on a 0.45 micron Millipore filter paper and the fly ash collected from the puffback sand spill. After some preliminary tests, we were surprised to observe that the panel bed filter with puffback can achieve filtration efficiencies beyond 99.9% on 20-30 mesh sand and the filtration efficiencies increased with increasing air velocities.

We examined our equipment and found that the vertical back plate facing the back louver acted as a secondary dust collector or as an impinger collector because of the inertia of the unfiltered dust particles as the air turned 90^{o} and went downward. There was some additional dust lost when the air turned another 90^{o} near the bottom of the filter and went out. In order to get more accurate filtration data we modified our test unit to avoid any loss of dust before the air reaches the sampling filter paper.

In increasing the air velocity to 15 cm./sec. or higher, we found some other problems. At higher velocities the fine sand grains will be entrained by the air flow. Also, when the pressure drop across the sand bed was too high the sand bed collapsed. This high pressure drop could be caused either by a high flow rate or by the building up of filter cake. The maximum

pressure drop before the sand bed collapsed for this particular louver arrangement was about 14 inches water. Since this filter tends to work better at higher velocities we had to modify the apparatus in order to be able to operate at higher pressure drops and higher velocities.

3.2.2. Tapered Outlet Test Unit - The First Unit.

We call this the first unit because this is the first unit which we were able to take reliable data.

Figure 3.2-3 is a schematic cross-sectional diagram of the tapered outlet unit. Redispersed power station fly ash in air entered at the top of a 8^{o} tapered vertical inlet passage for dirty air and the air entered the panel bed through gas-entry surfaces disposed upon louvers resembling a chevron. The development of these louvers will be discussed in Section 3.2.4. The louver area was 3 inches wide and 12 inches high. There were three columns of louvers. The gas flowed from left to right across the panel as seen in the figure. The first column presented sand surfaces for filtering the dirty gas. A set of closely spaced louvers separated the fine filter sand from the coarse sand. Both the fine sand and the coarse sand beds were one inch wide. We provided the coarse sand so that the air can disengage from the downstream face of the panel at high velocity without danger of spilling sand. We showed that this arrangement can stand at least 45 inches of water pressure drop without collapsing. Air left the bed of coarser sand across gas

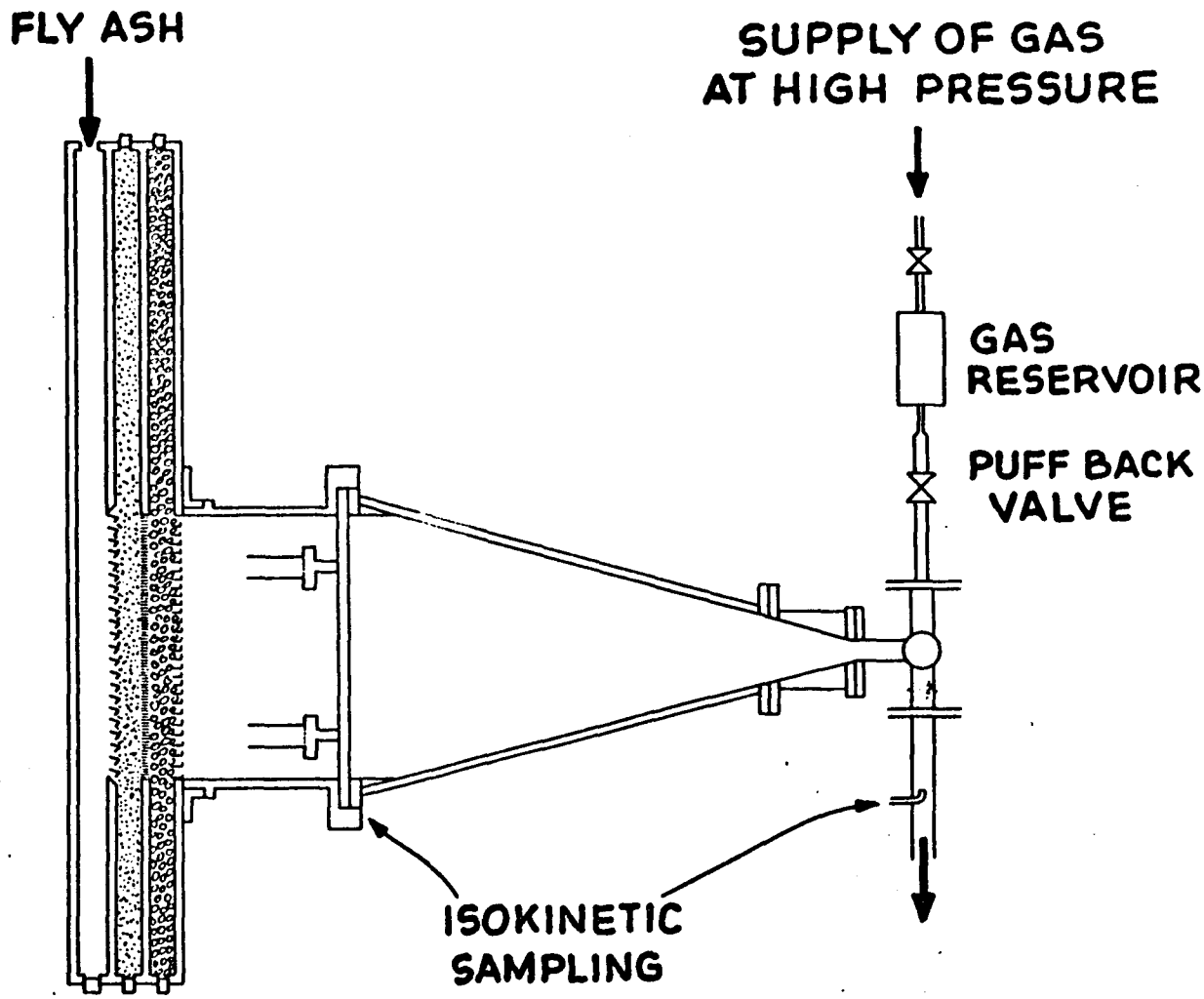

Figure 3.2-3: Schematic Cross-Sectional View of Apparatus for Test of Panel Bed Filter - The First Unit.

exit surfaces that rest upon horizontal louvers fitted with up-turned "tabs" that retain the coarse sand.

Without change in velocity, the filtered air flowed horizontally through a tapered chamber that housed two stations for isokinetic sampling at the relatively low velocity of air flowing from the filter. Each sampling station comprised a holder for a filter paper, a duct to draw air through the filter paper (not seen in Figure 3.2-3), and a gas-collecting "chimney" facing the gas stream. The rate at which gas was pulled through the filter paper was governed so that a sample of gas entered the chimney at the same velocity as the main gas flow past the chimney (isokinetic sampling). Dust particles in the air were collected directly on the sampling filter paper without changing either in direction or in velocity. Two sets of dust collecting chimneys were used. One set, 1-1/4 inches ID and 2-3/4 inches long was used for low velocity isokinetic sampling. The other set, 13/16 inch ID and 2-3/4 inches long, was used for high velocity isokinetic sampling.

Following the chamber that housed the two low-velocity isokinetic sampling stations, the air entered a region of contracting section for air flow. This region terminated in an outlet for air that led to a three-way valve. The distance between the three-way valve and the clean side of the sand bed was 34 inches. During the normal filtration testing, the air flowed downward from the three-way valve

and past a conventional isokinetic sampling station. At the end of a filtration cycle, the flow of air was interrupted, and the position of the three-way valve was changed so that the exit of the contracting region communicated to a puffback valve and gas reservoir filled with air at a pre-determined high pressure. The puffback valve was opened suddenly, allowing air to dump from the reservoir into the clean side of the panel bed through one piece of 1/2 inche brass pipe about 4 inches long, and the three-way valve. With proper adjustment of reservoir volume and puffback valve area, a small amount of the finer sand was dislodged from each gas-entry surface of the panel along with a filter cake that had formed on each surface. The resistance of the panel bed to air flow was restored substantially to its initial level, and the panel was ready for a succeeding filtration cycle.

The spent solid was collected from the bottom of the collection bin in the dirty side of the panel bed through a one inch ID hole. The spent solid was sieved to separate the ash from the sand, and weighed. The separated sand was recycled and used as fresh solid.

The overall fly ash collection efficiency (weight percent) was calculated from the dust collected on the isokinetic sampling filter paper and the fly ash separated from the spent solid.

The front plate on the dirty side was mounted with a glass window for visual observation of puffback and

filtration from the front. The front plate can be removed in order to get access to the front louvers.

3.2.3. Transparent Test Unit - The Second Unit.

Although the first unit had a front glass window for visual observation of the panel bed filter, we could not see what is happening inside the sand bed during either the filtration cycle or the puffback cycle. Hence, we decided to build a unit with transparent side wall so that we could see what is happening inside.

We built our first unit with a large tapered outlet chamber in order to obtain reliable filtration data. In a commercial unit, we would not need this large tapered box and we would prefer to introduce puffback from the top of the panel bed. Hence, we wanted to build a test unit so that we can apply puffback from the top also. With these objectives in mind, we built our second unit - the transparent unit.

The transparent panel bed filter was of the same scale as the first test set-up. Figure 3.2-4 shows an isometric of the transparent unit. The side plate of the first test set-up was replaced by a piece of glass. The louvers were so designed that one end of the louver will rest against the glass with no interference of any kind at this end. The motion of the sand can be studied from the glass side both by visual inspection and by high speed motion pictures.

This unit was designed in such a manner that it can be used to study sideshot puffback by removing the rear

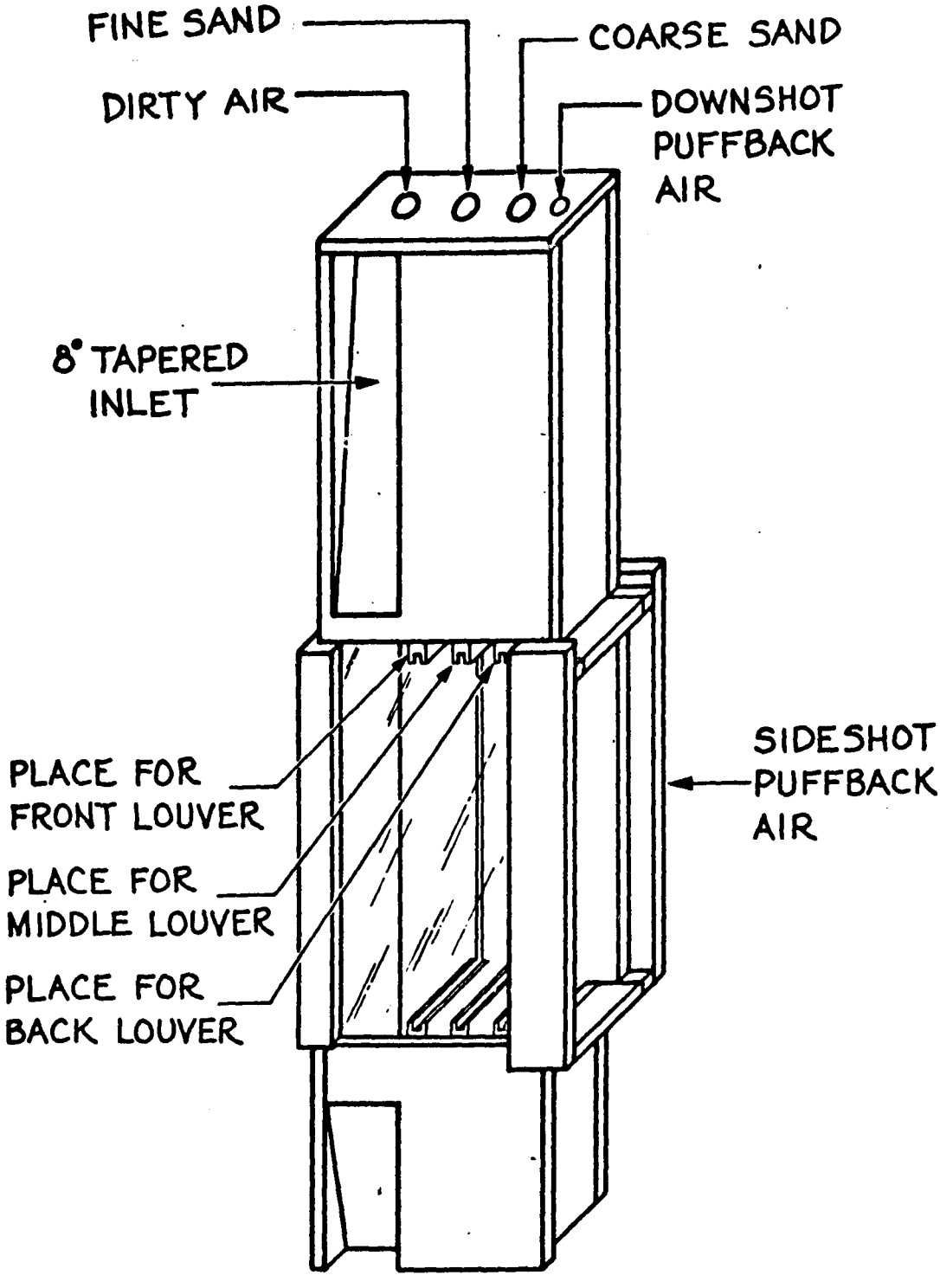

Figure 3.2-4: Isometric of the Second Unit with Glass Wall for Visual Observation of Puffback.

plate facing the back louver and attaching the tapered outlet section of the first unit to the back. By putting back the rear plate facing the back louver, we can study downshot puffback by introducing puffback air from the top of the unit through a 1/4 inch pipe hole. The puffback valve was connected to the top of the unit by one pice of 1/4 inche brass pipe, about 3 inches long.

3.2.4. Louver Design and Construction.

We have tested a series of dirty-face louvers (front louvers) in the panel bed filter. The louvers tested are shown in Figure 3.2-5. The louvers are designed so that the angle of the louver opening for the sand free surface with the horizontal (the louver surface angle) should be less than the angle of repose of sand. The louver surface angle was designed at 27° (see Figure 3.2-5). The angle of repose for sand ranges from 30° to 35° depends on the sand properties.

Design A Louver is a louver inclined at 60° and was the first louver used in studying the panel bed filter (42,44). Design B louver is the "chevron" shape louver which we found to be the best. It has two benefits. First, there is a converging section to concentrate the puffback air flow. Second, the upper part of the louver plate can hold the dirty sand near the surface without letting the dirty sand fall down to fill up the vacancy below, left by the sand spilling during puffback. The amount of sand holdup is controlled by the angle of

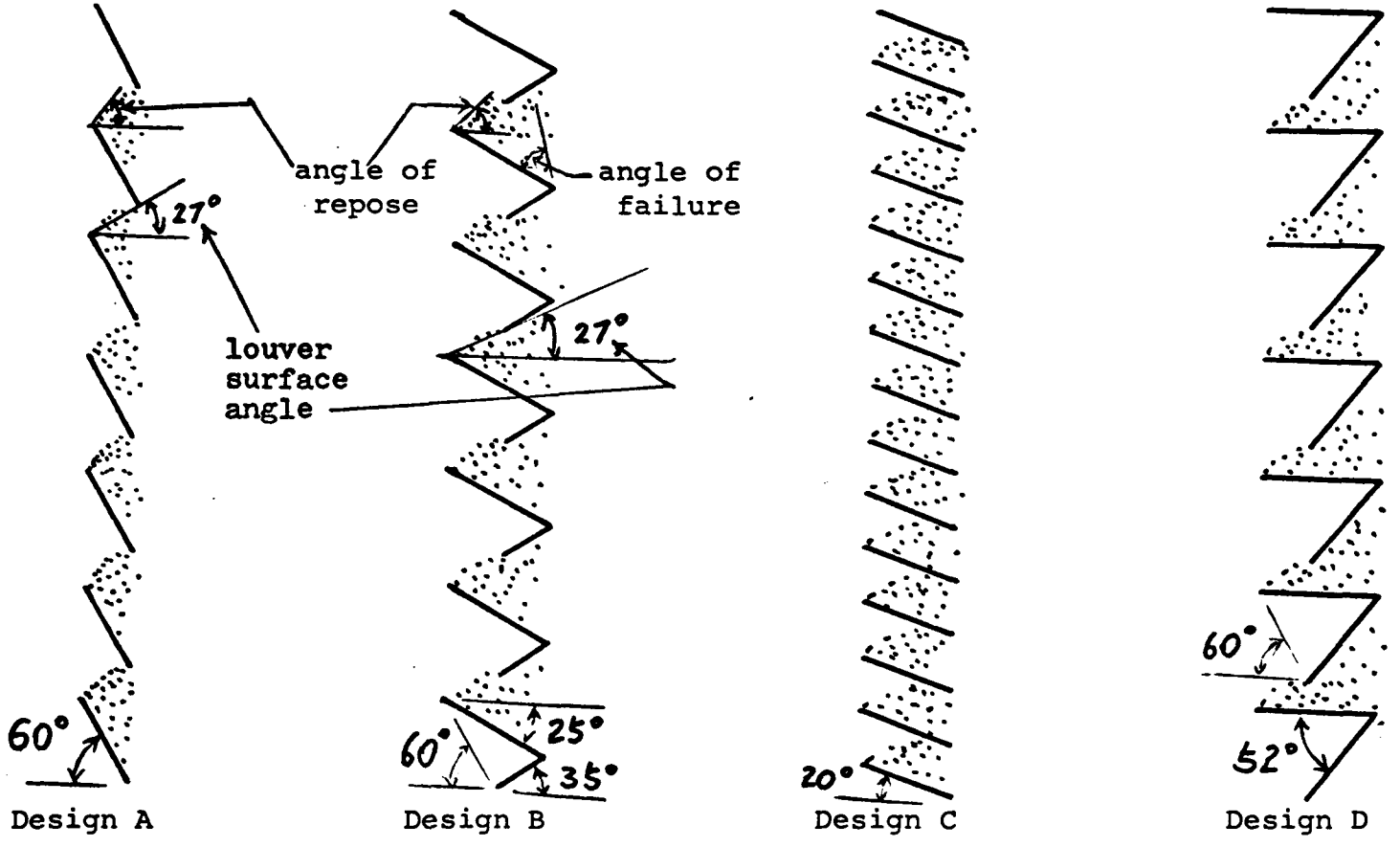

Figure 3.2-5: Louver Designs Used at the Dirty Face in Panel Bed Experimentation

N.B. Dirty gas flows from left to right

failure plane. The angle of failure plane was discussed in Section 2.3.5.

Design C louver is a 20° inclined louver which gave poor results. The reason for trying this design was to get more free sand surface and a higher capacity. It failed because it gives poor puffback results.

Design D louver is also poor probably because the convergence of the opening space is too sharp. The sand appeared to jam at the opening during the puffback.

Two different sets of louvers were built. One set was used in the first test unit and the other was used in the second test unit. When we first fuilt the chevron louver (Design B) for the first uint, we were not able to control the spaces between louver plates. We were forced to open the louver spaces by cutting out the edges of each louver plate.and the actual louver surface angle was larger than 27°. The actual angle was close to 30°. The spaces between louver plates were carefully controlled for the louvers used in the second unit. The actual surface angle was at about 26°.

Figure 3.2-6 shows the details of the preferred arrangement of louvers for the panel bed filter.

3.3. High Speed Motion Picture Study.

We took high speed motion pictures of puffback at 3000 frames per second with a Hycam high speed movie camera and the transparent unit (the second unit). From the high speed movies, we were able to find out

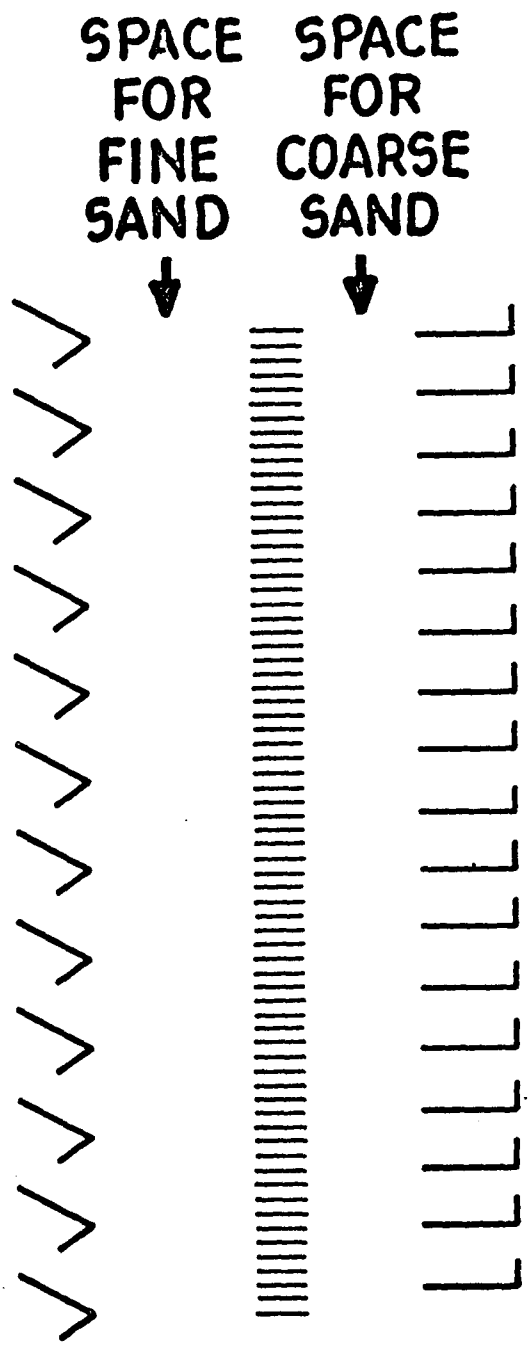

Figure 3.2-6: Details of Preferred Arrangement of Louvers for Panel Bed Filter

what was happening during puffback and the time period of each individual event of puffback with the help of a Lafayette movie analyzer.

3.4. Equipments Used in Puffback Tests.

Broadly speaking, five variables determine the intensity of puffback:

(1) Size of puffback gas reservoir.

(2) Area of puffback valve.

(3) Speed of opening of valve.

(4) Puffback gas pressure.

(5) Geometry of passage between valve and the clean face of the panel.

In order to determine the dependence of sand spill upon these variables, we used five different puffback bottles, three solenoid valves, and two puffback configurations, as follows:

Puffback bottles: (1) 2" ID by 2" length or 1.03×10^2 cm.^{3}

(2) 2" ID by 4" or 2.06×10^2 cm.^{3}

(3) 2" ID by 8" or 4.12×10^2 cm.^{3}

(4) 3-3/4" ID by 7" or 1.27×10^3 cm.^{3}

(5) 6" ID by 5-1/2" or 2.55×10^3 cm.^{3}

Solenoid Valves: Two solenoid gate valves manufactured by Valcor Engineering Corp., Kenilworth, N.J. were used. One has a 3/16 inch orifice diameter and C_v = 1.8. Another has a 5/16 inch orifice diameter and C_v = 3.4. One 1" solenoid globe valve manufactured by Atkomatic Valve Co., Indianapolis, Indiana was used. This globe valve has a one inch orifice diameter and C_v = 9.9. The valve opening time for all three valves is about 15 to 20 milliseconds.

Puffback configurations: Two configurations, downshot puffback and sideshot puffback, were tested on the second test unit. The volume between puffback valve and the clean side of the panel for downshot puffback tests was 7.13×10^2 cm.^{3} and the volume for sideshot tests was 1.19×10^4 cm.^{3}.

3.4.1. Use of Transducers to Study the Fluid Mechanics.

We began the transducers measurements with two type 4-312 diaphragm transducers manufactured by Consolidated Engineering Corp. (CEC), Pasadena, California. We had no information on the resolution and rise time of these transducers. But, we had no idea what would be the pressure range we were going to measure and how fast the response time should be either. From these first CEC transducers measurements we knew roughly what kind of transducers we should use, and we bought two better transducers in order to get better data.

We used two high sensitivity and fast response transducers to study the puffback fluid mechanics. The

transducers chosen were quartz transducers manufactured by Kistler Instrument Co., Redmond, Washington. These transducers have a resolution of 0.0008 psi or 0.056 cm. of water and a response time of 3 microseconds. The two transducers were hooked to a two channel oscilloscope equipped with a Polaroid camera. In this way, we were able to study the time delay between two test points and the pressure change between these two points. Several points were tested as follows:

(1) The transducer was installed at the exit of the puffback bottle before the valve so that we could study the pressure decay of puffback bottle.

(2) The transducer was installed near the back surface of the panel so that we could study the aerodynamic force acting on the sand bed on the clean side.

(3) The transducer was installed in the dirty side of the panel. From the difference of this curve and the curve taken on the clean side we were able to study the pressure drop change across the sand bed.

(4) The transducer was installed near the middle louvers to study the sand motion.

3.4.2. Sand Spill Uniformity Test.

We collected sand dislodged from each individual louver space to find the sand spill distribution as a function of louver design and other possible factors, such as geometry of back space, puffback intensity, and louver arrangement. Thus,we obtained some information about the mechanism of sand spill and how to get a

uniform sand spill. All the tests were performed on the first unit with the front plate removed.

3.4.3. Puffback Code to Specify the Puffback Test Conditions.

Because there are so many puffback variables which we investigated, we will use the following code system to specify the puffback test arrangement for each individual set of data. The puffback code will include five groups of alphabeticals and numerals as in the following:

A-3-B-3-60-D

The first alphabet indicates sand grade tested,

A: 20-30 mesh sand.

C: 40-50 mesh sand.

D: 10-14 mesh sand.

The second numeral indicates louver shape,

1: 60^{o} louver, Design A.

2: 20^{o} louver, Design C.

3: Chevron louver, Design B.

The third alphabet indicates puffback valve size,

S: 3/16 inch orifice diameter solenoid gate valve.

B: 5/16 inch orifice diameter solenoid gate valve.

G: One inch orifice diameter solenoid globe valve.

The fourth numeral indicates puffback bottle number,

Volume	Volume Ratio
1: 1.03×10^{2} cm.^{3}	1
2: 2.06×10^{2} cm.^{3}	2
3: 4.12×10^{2} cm.^{3}	4
4: 1.27×10^{3} cm.^{3}	12
5: 2.55×10^{3} cm.^{3}	24

The fifth numeral indicates puffback pressure in psig. The sixth alphabet indicates test unit configuration.

D: Downshot puffback.

H: Sideshot or horizontal shot puffback.

For example, A-3-B-3-60-D means 20-30 mesh sand, chevron louver, 5/16 inch orifice valve, number 3 puffback bottle, 60 psig puffback bottle pressure, and downshot puffback.

Chapter 4: Panel Bed Filtration Data

Filtration results are expressed here in terms of "penetration" rather than "efficiency", because the penetration numbers give a more meaningful measure of filtration performance. For example, a percentage penetration of 0.01% is a filtration efficiency of 99.99%; a penetration of 0.3% is an efficiency of 99.7%. The former provides a gas that is 30 times cleaner than the latter, something that the efficiency values do not immediately convey.

4.1. Dirty Sand is Better than Clean Sand.

There is a synergism between the puffback cleaning techniques and filtration efficiency. Penetrations always decline during the first three to five filtration cycles, the later values often being some 5 to 10 times smaller than the penetration during the first filtration cycle.

This effect has been confirmed by comparing a filtration test for a panel charged with washed, clean sand and a filtration test for a panel charged with "dirty" sand. The dirty sand gave a penetration some 5 times smaller than the clean sand.

We believe that dirty sand filters better than clean sand because particles of fly ash adhering to the dirty sand act as "condensation nuclei" for growth of a fly ash deposit. Fly ash may stick to itself better

than to sand, and presence of some fly ash already stuck to the sand helps in the collection of additional fly ash. In other words, the autohesivity of fly ash is important, as well as its adhesivity to sand, in promoting good cleaning of the gas.

Although our puffback technique for "cleaning" the sand at the conclusion of a filtration cycle generally restores the flow resistance of the sand bed to substantially its initial resistance, nevertheless, it is clear that puffback does not remove each and every particle of fly ash that has been filtered by the bed. Hence, penetrations decline during successive filtration cycles until a substantially steady performance level is reached.

These views tend to be confirmed by our observations that the first filtration cycle after the filter has been left standing overnight usually gives a higher penetration than the steady performance level reached the afternoon before. We believe that some of the fly ash adhering to the sand at the end of the afternoon's operation falls away from the sand. This might be caused by the small vibrations to which our set-up is subjected in its City environment. Such fly ash then lies in pockets away from the mainstream of the gas flow through the granular bed. We have sometimes noticed a small deterioration in performance even when the unit is left standing idle for merely one-half to one hour.

4.2. High Efficiencies at Higher Velocities.

In the summer of 1972, we obtained the result,

surprising to us, that filtration efficiency rose sharply with approach velocity up to the maximum then attainable, about 33 ft/min. This is illustrated by the following penetration data:

Velocity, ft/min.	Penetration, per cent
6.8	0.4
12	0.7
22	0.2
33	0.03

This was for 20-30 mesh sand and louvers inclined at 60° from the horizontal (See Section 2.2). Only a single grade of sand was present in the panel. Notice the seven-fold decline in penetration between 22 and 33 ft/min. The penetration of .03% at 33 ft/min. was particularly surprising at the time, for nothing in our work before the Summer of 1972 had hinted at the potential of the panel bed filter for achieving such a low penetration (i.e., such a high efficiency as 99.97%).

The serviceability of the filter at velocities higher than 15 ft/min. was a surprise in light of our earlier attitude toward the filter. We believed that good filtration needed the development of sound filter cake. We beleived that the device inherently needed to operate at a relatively low velocity in order to achieve such a filter cake, without risk that fly ash would be carried deep into the bed. What we did not realize was that fly ash within the bed also serves to assist the filtration

process, by the mechanism alluded to in Section 2.4.1. above, when such fly ash is brought forward to the gas-entry surface by action of puffback.

However, penetration of fly ash deep into the bed may not always be a good thing. (See Chapter 8.)

The above data revealed existence of a velocity of maximum penetration in the vicinity of 12 ft/min. The effect of velocity on filtration efficiency is a complex problem, and we have to consider both the change in the approach of the dust particles to the filter medium and the change in the performance of the filter cake.

Later work with other louvers has generally confirmed the low penetrations achieved in the summer of 1972, but has not reproduced the dramatic seven-fold decline in penetration between 21 and 33 ft/min. of the above data. For example, a survey of velocity for 20-30 mesh sand for Louvers B and C gave penetrations as follows:

	Penetration, percent	
Velocity, ft/min.	Louver B	Louver C
11		0.02
19		0.06
31	0.02	0.05
42	0.02	0.02
60		0.05
80		0.03

The data for Louver C display a two-fold occurrence of a rise and fall in penetration with increase in velocity.

When we learned of the opportunity for better performance

as well as higher capacity at higher air flows, we modified our set-up to place a coarser sand behind the fine sand that actually performs the task of filtration. Presence of the coarser sand allows for a higher throughout without the risk that fine sand will be blown away from the clean side of the panel bed.

We have now conducted many filtration tests using 20-30 mesh sand backed by 10-14 mesh sand. Much of the testing was to explore variations in louver design and in puffback conditions, and was not extended to runs comprising a large number of filtration cycles. Table 4.2-1 shows a series that was extended to 42 cycles of filtration. The pressure drop varied somewhat during the series of cycles, but did not climb steadily upward. So far as we can tell, we could have operated for many more cycles with no permanent increase in pressure drop. In other words, puffback seemed to be doing a good job. The penetration on the first cycle is higher than the second and the third. After the third cycle, the penetration settled down at values between about 0.02% and 0.05%.

Data in Table 4.2-1 illustrate also the invariable tendency for the first cycle after the filter is idle overnight to display a poorer result. Data in the table also illustrate the variation in size of the spill of sand with variation in puffback pressure, and the accompanying variation in pressure drop across the "cleaned" filter.

We have conducted a number of filtration tests at

Table 4.2-1

Series of Filtration Cycles on Panel Bed Filter
Charged with 20-30 Mesh Sand Backed by 10-14 Mesh Sand

Face velocity = 31 feet per minute

Fly ash loading = about 3.6 grams per cubic meter

Duration of one cycle = about 17 minutes

Filter paper used to filter isokinetic sample stated to be capable of filtering to 0.45 micron

Cycle Number	Puffback Pressure, psig	Initial Pressure Drop, inches water	Final Pressure Drop, inches water	Weight Ratio of Ash to Sand from Puffback	Percentage Penetration
1	20	0.99	2.30	0.12	0.33
2	20	1.09	2.36	0.17	0.07
3	20	1.14	2.30	0.18	0.02
4	20	1.26	2.36	0.16	0.02
5	25	1.26	2.36	0.16	0.02
6	25	1.26	2.36	0.16	0.02
7	25	1.26	2.36	0.15	0.02
8	25	1.29	2.36	0.15	0.02
9	25	1.27	2.37	0.14	0.02
10	25	1.27	2.39	0.15	0.02
overnight					
11	25	1.24	2.36	0.15	0.07
12	25	1.37	2.37	0.15	0.02
13	25	1.35	2.37	0.14	0.02
14	25	1.38	2.37	0.15	0.02
15	25	1.40	2.52	0.14	0.02
16	25	1.45	2.52	0.16	0.02

(continued on next page)

Table 4.2-1 (continued)

Cycle Number	Puffback Pressure, psig	Initial Pressure Drop, inches water	Final Pressure Drop, inches water	Weight Ratio of Ash to Sand from Puffback	Percentage Penetration
17	25	1.45	2.52	0.15	0.04
18	25	1.45	2.55	0.15	0.02
19	25	1.46	2.58	0.15	0.02
20	25	1.48	2.58	0.14	0.02
overnight					
21	25	1.45	2.78	0.15	0.05
22	25	1.51	2.59	0.14	0.02
two puffbacks applied					
23	25	1.35	2.61	0.12	0.06
24	25	1.48	2.59	0.15	0.02
25	25	1.51	2.59	0.16	0.02
overnight					
26	35	1.41	2.64	0.16	0.03
27	35	1.41	2.59	0.12	0.02
28	35	1.35	2.59	0.11	0.02
29	35	1.37	2.67	0.11	0.02
30	35	1.35	2.64	0.10	0.04
31	35	1.35	2.59	0.09	0.03
32	35	1.34	2.61	0.09	0.05
overnight					
33	35	1.23	2.52	0.10	0.08
34	35	1.30	2.52	0.09	0.05
35	35	1.29	2.52	0.09	0.03
36	35	1.29	2.53	0.10	0.05

(continued on next page)

Table 4.2-1 (continued)

Cycle Number	Puffback Pressure, psig	Initial Pressure Drop, inches water	Final Pressure Drop, inches water	Weight Ratio of Ash to Sand from Puffback	Percentage Penetration
37	35	1.30	2.52	0.13	0.06
38	25	1.40	2.61	0.16	0.06
39	25	1.50	2.61	0.15	0.03
40	25	1.50	2.59	0.16	0.03
41	25	1.50	2.59	0.15	0.03
42	25	1.51	2.59	0.15	0.03
43		1.51			

60 and 100 ft/min. This work revealed the necessity of avoiding vorticity in the flow of gas past the dirty face of the panel. Any scouring action of this flow will continuously remove fly ash from portions of the dirty face, with bad effects upon filtration efficiency and operability of the panel. When vorticity was avoided, filtration efficiencies were comparable to these seen at 30 ft/min. Pressure drops were appreciably higher, however, and cycle durations were appreciably shorter. Our impression is that 30 ft/min. may be not far from an economic optimum. It should be pointed our that the panel bed filter operating at 30 ft/min. will occupy ground area amounting to approximately one-quarter the ground area required for an electrostatic precipitator that affords 99% removal of fly ash (See Appendix 1).

We believe that our efficiencies mean that fly ash is being filtered by a fly ash filter cake. The sand simply supports the filter cake. Dirty sand filters better than fresh, clean sand. We think that fly ash particles on dirty sand act as "condensation nuclei" to promote establishing a new filter cake at the start of a cycle.

4.3. Superhigh Efficiencies for 40-50 Mesh Sand and Royco Data.

In operations with 40-50 mesh sand backed by 14-20 mesh sand, we have generally achieved penetrations smaller than 0.01%. Table 4.3-1 gives typical data for a series of 95 cycles with 40-50 mesh sand. The pressure drop was steady during these cycles. There was no evidence of any

Table 4.3-1

Summation of Data for Series of 95 Cycles on Panel Bed Filter Charged with 40-50 Mesh Sand Backed by 14-20 Mesh Sand

Face velocity = 31 feet per minute

Fly ash loading = about 4.3 grams per cubic meter

Duration of one cycle = about 5.3 minutes

Increase of pressure drop due to filter cake = 1.3 inches water

Average Ash/Sand Ratio = 0.20

Filter paper used to filter isokinetic sample stated to be capable of filtering to 0.1 micron

Puffback pressure = 15 to 20 psig

Cycle Number	Penetration	Pressure Drop (inches of water)	
		initial	final
1 through 5	0.03%	2.8	4.1
6 through 95	0.007%	3.5	4.8

permanent increase in pressure drop. Puffback seemed to be doing a good job of keeping the interior of the panel bed clean of fly ash. Several times we scraped away the dirty sand from one of the surfaces of the dirty face of the panel bed. We checked this again at the end of the run. Fly ash penetrates only about 0.1 inch into the sand bed. Beyond this distance, the sand looks clean.

The penetration from cycle 6 through 95 was 0.007%. This is a collection efficiency of 99.993%. The penetration is just about at the limit of our ability to measure it. The weight gain on the filter paper from cycle 6 through 95 was only one-half milligram. Obviously, the penetration of 0.03% for cycles 1 through 5 is only a crude estimate. We believe, however, that the penetration as higher during these first cycles on fresh sand.

The penetration in our work on 40-50 mesh sand are so low that we have found it possible to obtain useful information by passing the filtered air through a Royco particle counter having channels for four nominal particle sizes: 0.3 to 0.5 microns; 0.5 to 1.0 microns; 1.0 to 2.0 microns; and over 2.0 microns. It should be emphasized that the Royco's discrimination of particle size is rough and has only relative value, particularly for an irregular, non-uniform particle such as fly ash. The data ought to have some value, however, in a relative sense.

Figure 4.3-1 shows how the particle count per liter of air appearing on a Royco channel for particles "over 2 microns" declines versus time during a filtration cycle.

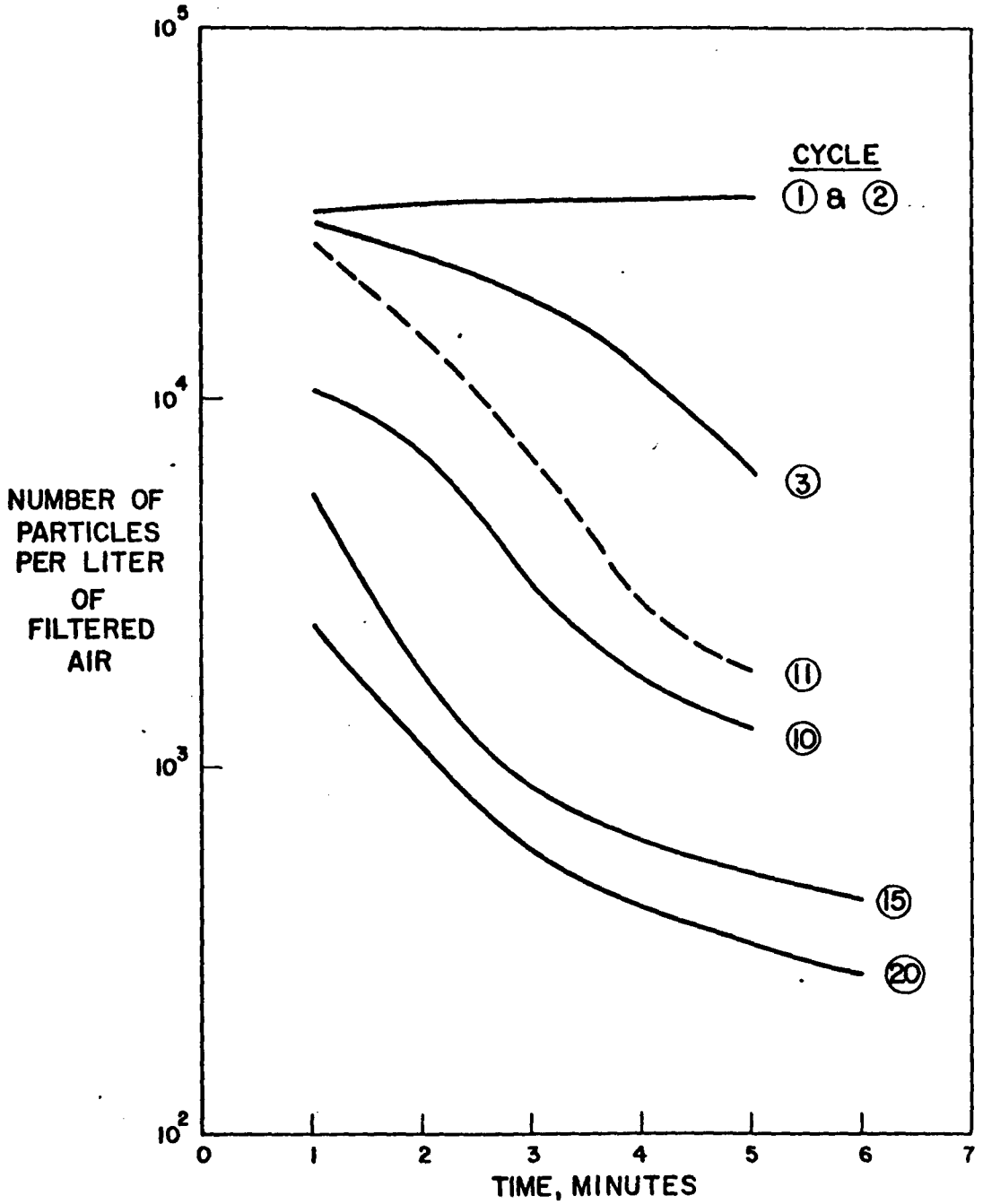

Figure 4.3-1: Number of Particle Counts per Liter of Air Appearing on a Royco Channel for Particles of Nominal Size "Larger than 2 Microns" versus Elapsed Time During a Filtration Cycle for Operation with 40-50 Mesh Sand at 31 Feet per Minute

NB. The numbers alongside the curves indicate the ordering of the filtration cycles.

The data are for a series of 20 cycles conducted at a puffback pressure of 10 psig. The "initial" pressure drop climbed slowly during this series of runs, an indication that the puffback pressure was too low. The data of Figure 4.3-1, however, are plausible in the way in which they show how the filtration efficiency improves versus time during later cycles of the series. The number of particles in the clean gas is steady in the first and second cycles. In the third cycle, the number drops as the cycle proceeds. The improvement from the third to the tenth cycle is striking. Notice, too, how the 11th cycle gave slightly poorer results than the 10th. The unit was shut down overnight between the 10th and the 11th cycles.

During this same series of cycles, as can be seen in Figure 4.3-2 particle counts on channels for 0.3 to 0.5 microns, for 0.5 to 1.0 microns, and for 1.0 to 2.0 microns remained approximately steady at approximately 30 to 40,000 particles per liter on each channel.

It is of passing interest to note that an air sample drawn from outside the window of our filtration laboratory typically shows comparable counts of 0.5 to 1.0 micron particles. Our Royco channel for 0.3 to 0.5 microns is not operating properly just now, and so no comparison can be made for this nominal size. Our filtered air typically registers particle counts on channels for the 1.0 to 2.0 micron and over 2.0 micron that are several times, but never ten times, greater than the counts

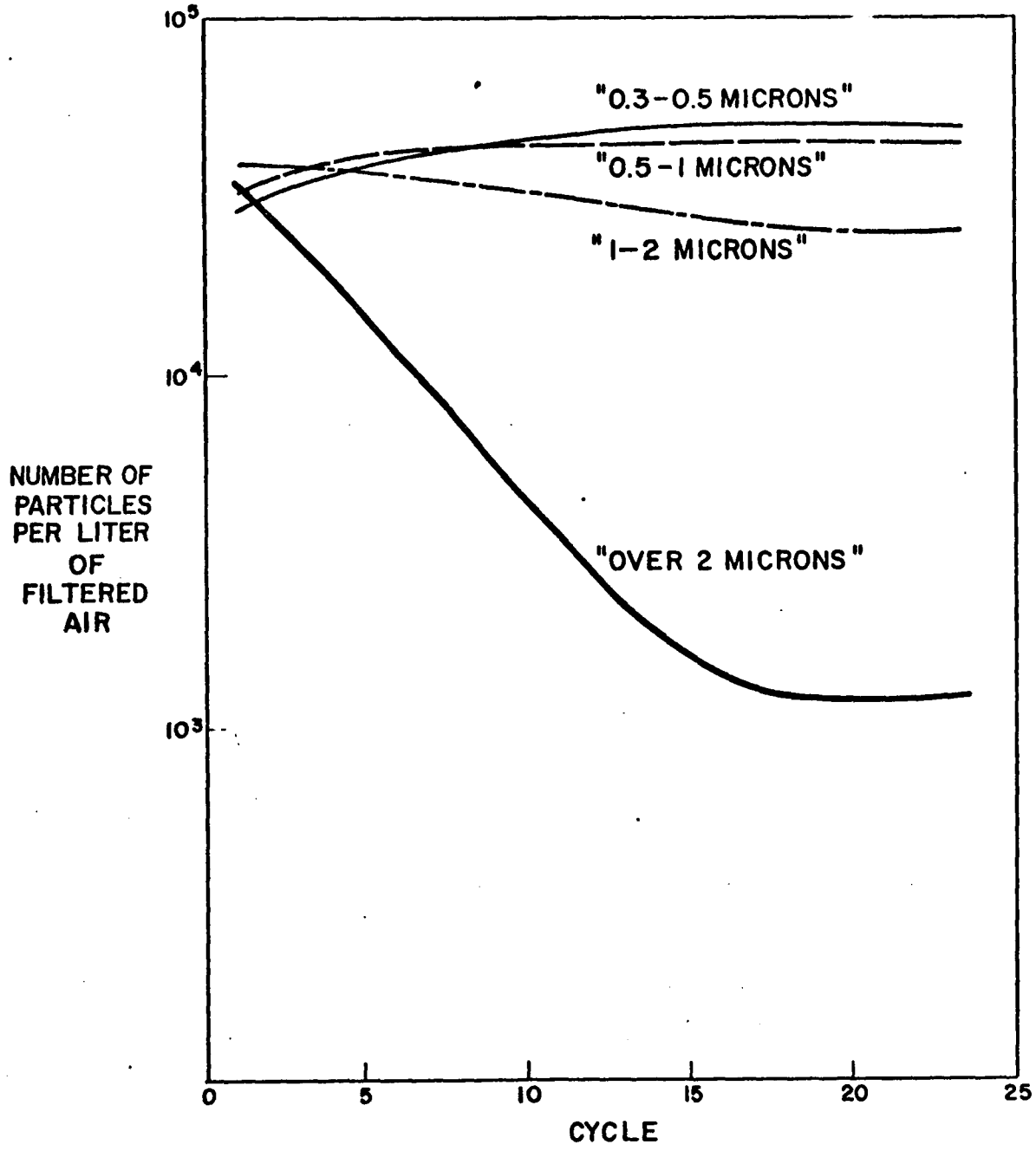

Figure 4.3-2: Number of Average Particle Counts per Liter of Air Appearing on Royco Channels for Several Nominal Sizes versus Filtration Cycle for Operation with 40-50 Mesh Sand at 31 Feet per Minute

NB. The numbers alongside the curves indicate the nominal particle sizes in microns.

registered by samples of New York City air.

By extrapolating the distribution of particle sizes given in Figure 3.1-2 and by assuming a weight of particle corresponding to one of the Royco channels and by taking the nominal sizes of the Royco channels literally, it is possible to estimate (very roughly!) a filtration efficiency for particles corresponding to each of the Royco channels. With the following assumed weights for fly ash particles registered by the respective Royco channels, we estimate the following penetrations in the respective size ranges after a number of filtration cycles:

Channel	Particle Weight, grams	Percentage Penetration
0.3 to 0.5 microns	6.97×10^{-13}	0.3
0.5 to 1.0 microns	4.6×10^{-12}	0.4
1.0 to 2.0 microns	36.8×10^{-12}	0.5

The assumed particle weights are probably on the high side, and so the percentage penetrations may also be too high. These values are not to be taken too seriously, but they are roughly consistent with overall penetrations judged by increase in weight of a filter paper in place throughout the series of cycles. It is reasonable that the penetration should be smaller for the smaller size of maximum penetration through a filtration device.

It should be remarked that visual observation of the filter paper under a microscope discloses only particles smaller than about 2 microns. This points up the nominality

of the channel ranges on the Royco when this instrument looks at fly ash.

A series of filtration cycles conducted on 40-50 mesh sand at a face velocity of 9 feet per minute give an average penetration of 0.013%. We cannot be certain that this value is significantly larger than the penetration of about 0.005% generally observed in tests on this sand at 31 feet per minute. The trend with velocity is the same as for work on 20-30 mesh sand, and we are inclined to believe that the penetration was indeed somewhat higher at the lower face velocity.

4.4. Filtration Data on 10-14 Mesh Sand.

At high velocities, such as 30 ft./min., no uniform filter cake formed over the surface of 10-14 mesh sand. This was because of the large pore in the 10-14 mesh sand bed. Most of the fly ash penetrated onto the sand bed. We have run a series of tests of over 45 cycles on 10-14 mesh sand at 30 ft./min. The pressure drop through the sand bed kept on increasing as the cycles went on indicating the fly ash penetrated deeper and deeper into the bed. The penetration decreased for the first few cycles in the manner observed for 20-30 mesh sand and 40-50 mesh sand. However, as the cycles went on the penetration would increase as a result of the continuous penetration of fly ash. This is similar to the saturation phenomenon observed by Taub (45) (also see Section 2.1.4.2.).

Table 4.4-1 shows operating data for a series of five cycles on 10-14 mesh sand at 11 feet per minute face velocity.

Table 4.4-1

Summation of Data for Series of 5 Cycles with 10-14 Mesh

Face velocity = 11 feet per minute

Fly ash loading = about 3.6 grams per cubic meter

Duration of one cycle = about 45 minutes

Increase of pressure drop due to filter cake = about 0.15 inches water

Average Ash/Sand Ratio = 0.30

Filter paper used to filter isokinetic sample stated to be capable of filtering to 0.1 micron

Puffback pressure = 50 psig

Cycle Number	Penetration	Pressure Drop (inches of water)	
		initial	final
1	1.2%	0.1	0.26
2	0.6%		
3	0.4%		
4 and 5	0.3%		

The back up sand was also 10-14 mesh. At least for these five cycles, there was no change in pressure drop and the pressure drop was negligible.We could have run much longer than the 45 minutes per cycle to obtain a higher final pressure drop. The table shows no change in penetration for the fourth and fifth cycle; the penetration was 0.3% and the filtration efficiency 99.7%. This may be high enough for commercial power plant application, but operation at a velocity as low as 11 ft./min. may not be commercially attractive.

Chapter 5: High Speed Movies Data.

We were puzzled by how puffback works. Two models were proposed. The first model assumed the sand spill was caused by a shock wave. As a shock front hits the sand surface on the clean side of the panel, sand would be removed from the dirty side by the shock force. In other words, puffback would be a result of a shock phenomenon. The second model assumed the sand spill was created by the aerodynamic force or the drag force on sand grains due to the air flow. We resolved this question by analyzing high speed movies of puffback. We could see from the high speed movies that puffback is caused by the surge of gas flow as it leaves the sand surfaces at the dirty face of the panel. Thus, the second model appears to be correct.

5.1. Local Failure and Body Failure.

From the high speed movies, we could see three stages of failure for each puffback, no matter whether it was a downshot puffback or a sideshot puffback. First, the sand jumped up from the inner side of the sand surface (Figure 5.1.-1b). A few milliseconds later, the bulk of the sand started to move forward (Figure 5.1.-1-c). While the bulk of the sand was moving, the sand stopped jumping up from the inner sand surface. When the puffback intensity was high, we could see a clear separation (free space) of the fine sand from the middle louvers indicating that the whole bed of fine sand moved forward. At the same time

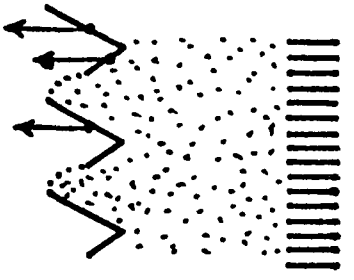

(a) sand grains thrown out. $t = t_1 = 0$

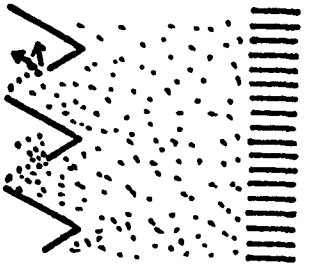

(b) first stage; sand grains jump up, local failure.

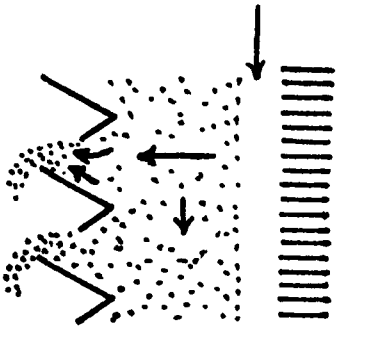

(c) second stage; body failure and separation.

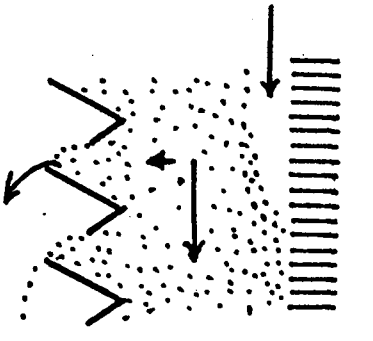

(d) third stage; local failure and de-separation.

Figure 5.1-1: Stages of Puffback Failure.

the sand bed moved downward to fill up the empty space produced by the puffback sand spill. The downward motion was due to gravity setting and was relatively small compared to the big forward motion at this stage. The second stage lasts from about 10 milliseconds to 100 milliseconds, depending on the puffback intensity. Almost all of the sand was removed at this stage.

Then came the third stage (Figure 5.1.-1-d) which is several times longer than the second stage. During the third stage, only a few grains of sand fall from the outer-most edges of the louvers. This stage lasts a long time, In the body of the sand bed, there was almost no forward motion with most of the sand moving down to fill up the vacant space produced by sand spill. Separation between the fine sand and the middle louvers would close up gradually at this stage. During the third stage, the major motion of sand was downward, in contrast to the second stage where the major motion was forward. The transition from the second stage to the third stage was gradual, because of the inertia of the sand which will make the second stage last longer and mix with the third stage. Thus, it is very hard to tell exactly when the third stage begins in the high speed movies. The existence of the second stage and the third stage was also observed in the transducer data, which will be discussed in Section 7.6.

The failure phenomenon which occurred during these three stages can be divided into two categories--local failure and body failure. During the first stage and the

third stage, the sand failure only occurred at the surface of the sand and this is referred to as local failure. At the second stage, the whole sand bed failed, and this is referred to as body failure. Body failure is the important mechanism in the puffback phenomenon.

Local failure occurred at the first stage in a way to cause sand to jump up from the inner side of sand surface. We believed this failure to be due to the shock front deflection. As will be discussed in Section 6.1., the transducer data showed that the initial portion of the puffback surge flow was basically a shock wave. A portion of this shock front bounces back (reflection) when it hits the sand bed and a portion of the shock front is transmitted through the porous sand bed. When this transmitted shock left the sand bed and went into the dirty side air, there is a change of medium causing the shock front to deflect. This deflected shock front will carry some of the surface sand grains with it and causes the first stage local failure, the jumping up of sand grains at the inner edge of each sand surface. The shock intensity required to cause the sand to jump up perhaps corresponds to the minimum fluidization velocity.

The body failure which occurred at the second stage was believed to be due to the aerodynamic forces acting on the sand bed. This is a soil mechanics failure phenomenon.

Local failure occurred at the third stage: the removal of surface sand grains only was believed to be due to the declining tail of the surge flow. At least part of the

final spill of surface sand may be a result of an adjustment of the new sand surface to a position that is stable. As we know from Section 2.3.4.1., the sand strength is proportional to the normal force acting on the sand. At the surface of the sand the only normal force acting on the sand grains is the weight of the sand grains. These surface sand grains have a very weak soil resistance. The tail of the surge flow which was not strong enough to cause body failure, is nevertheless, enough to remove the surface sand.

From the above discussion we conclude that when the puffback intensity is low, only the first stage local failure will occur. For this case, only a few grains of sand are removed from the sand surfaces. At still lower puffback intensity, no sand spill will occur.

5.2. Elapsed Time for Each Stage From High Speed Movies.

The movies were taken in a unit with a glass window pressing against the ends of the louvers. The ends of the louvers do not fit the glass perfectly. Actually, as we fill up the unit with sand, some grains of sand will fall out from the clearance between the louvers edge and the glass window. However, some of the sand grains appear to be held there in a meta-stable position, and can be easily removed with very little disturbance. We can see a few grains of sand thrown from the inside edge of a louver just before the surge flow of puffback air reaches the sand surfaces (Figure 5.1.-1-a). We can take this point as the starting point when the first puffback shock front reaches the sand surfaces. We will count the elapsed time in the

movies from theis point. In some cases, there was no sand thrown from the inside edge of a louver and we will take the starting of jumping up as the zero time.

Five events were identified in high speed movies. They are:

1. A few grains of sand thrown from the inside edge of the louvers indicating arrival of the puffback surge flow. We take this point as the starting point. This time was taken as $t = t_1 = 0$.

2. Sand grains jumped up from the inner side of the sand surfaces indicating the shock strength is high enough to fluidize the surface sand grains. This time was taken as $t = t_2$.

3. Sand grains start falling over the end of the louvers indicating the start of body failure. This time was taken as $t = t_3$.

4. Sand grains cease jumping up from the inner side of the sand surfaces and all the jumping sand has stopped indicating the end of the first stage local failure. This time was taken as $t = t_4$.

5. Sand grains stop falling over the end of the louvers indicating the puffback is over. The time was taken as $t = t_5$.

Data are shown in Table 5.2.-1 for 20-30 mesh sand and Table 5.2.-2 for 40-50 mesh sand. The movies were taken at 3,000 frames per second. All five events were indentified by eye. The elapsed time was obtained by counting the number of frames of film. The data given

Table 5.2-1: Puffback Elapsed Time for 20-30 Mesh Sand

Puffback Code Number*	Elapsed Time in Milliseconds				
	t_1	t_2	t_3	t_4	t_5
A-3-B-2-60	0.0	6.3	18.8	40.0	218.8
A-3-B-2-50	0.0	5.5	16.8	39.3	180.0
A-3-B-4-30	0.0	12.3	22.7	23.8	111.3
A-3-B-4-30	0.0	11.7	15.7	64.0	208.3
A-3-S-2-30	0.0	2.2	19.7	47.0	259.9

Table 5.2-2: Puffback Elapsed Time for 40-50 Mesh Sand

Puffback Code Number*	Elapsed Time in Milliseconds				
	t_1	t_2	t_3	t_4	t_5
C-3-B-1-15	-	0.0	10.0	-	172.3
C-3-B-3-30	0.0	5.0	10.0	33.5	221.7
C-3-B-3-10	-	0.0	5.0	-	198.8

* Refer to Section 3.4.3. for the definition of these codes.

in Table 5.2.-1 and Table 5.2.-2 can be used only for a qualitative analysis since the eye cannot judge each event accurately. Another thing that should be mentioned is that the movies were taken before we knew that there was some leakage around the glass window and the junction between the filter and the tapered back portion. This slight leakage will decrease the effective puffback pressure and explains why the sand spills were much less than the sand spills shown in transducer dataat corresponding puffback conditions. We will discuss this in more detail in Section 9.3.

Chapter 6: Puffback Experimental Data.

This chapter presents basic data on the puffback study. Some more miscellaneous data will be presented in Chapter 7. Section 6.1 will discuss the pressure change at different locations of the panel bed filter during the puffback process. Scetion 6.2. will talk about the sand spill uniformity test under different puffback conditions and the effect of porosity on the sand spill uniformity. All the uniformity tests were performed using the first test unit by weighing the sand spill from different locations over the panel height.

We used the puffback code defined in Section 3.4.3. to specify the puffback test conditions and configuration for each individual case.

6.1. Transducer Data on Puffback Pressure Change.

The original transducer data were taken with the CEC transducer which is a diaphragm type transducer with unknown response time. However, we were able to get some idea about the puffback pressure strength range and the duration time. All CEC data were taken using our first unit. After taking these data, we ordered a more accurate Kistler quartz transducer to meet our special requirements. All the Kistler transducer data were obtained using the second unit and since these data are more complete we will discuss them first.

6.1.1. Puffback Pressure Change Monitored by Kistler Transducer on the Second Unit.

Puffback pressure change at different locations of transparent unit using the chevron louvers were monitored by Kistler transducers. Two configurations of the test unit were studied. Downshot puffback data were taken on the unit with a vertical back plate on the clean side and the puffback pressure was introduced through the top of the clean side space. Side shot puffback data were taken on the unit with the tapered back connected to the clean side and the puffback pressure was introduced through the three way valve. The vertical back plate used in downshot test was removed during the side shot tests.

Typical data on downshot puffback is shown in Figure 6.1.-1. Figure 6.1.-1-a shows the pressure decay in the puffback bottle. Figure 6.1.-1-b shows the pressure increase and decay on the clean side of the panel bed.

The zig-zagged curve is due to the shock bouncing between the top and bottom of the clean side space. The shock strength decreased each time it bounces back until it is diminished to zero strength. The data were taken at the middle point of the panel bed louver area. Data taken at the top and the bottom of the panel bed louver area showed similar curves except for some small difference in the first shock peaks which were higher than the first shock peak at the middle point. However, the shock phenomenon is not really important to the puffback process as discussed in Section 5.1. Figure 6.1.-1-c shows the pressure change in

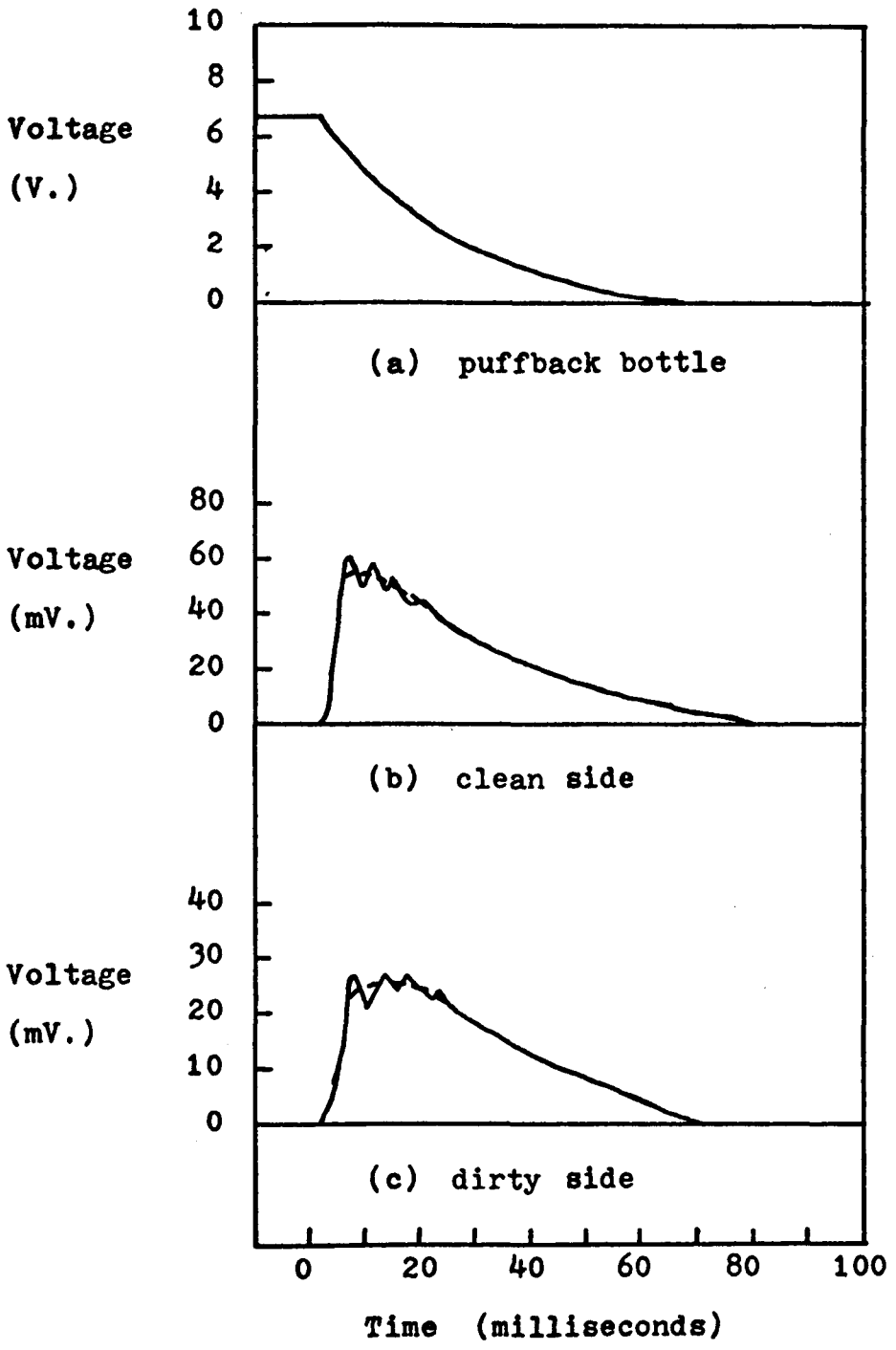

Figure 6.1-1: Typical Downshot Transducer Data

N.B. Dotted line - smoothed curve for data analysis.

the dirty side of the panel. The test point was located between the first and second louvers to prevent any pressure fluctuation and impaction forces due to the falling sand. Because the front side of the dirty side of our unit is open to the atmosphere only through a hole 1 inch in diameter, pressure will build up on the dirty side. We use the smoothed dotted line for data analysis. The signal was monitored electronically by a voltage change and each millivolt corresponds to .63 cm. water pressure.

Typical data on side shot puffback is shown in Figure 6.1.-2. Figure 6.1.-2-a shows the pressure decay in the puffback bottle. Figure 6.1.-2-b shows the pressure rise and decay on the clean side of the panel at the widest portion of the tapered section. Three points, top, middle, and bottom of the panel, were tested and showed no difference. The curves indicate that there was vigorous shock bouncing inside the tapered section. The shock strength decays each time it bounces back. Figure 6.2.-2-c shows the pressure change in the dirty side of the panel bed. Because a portion of the shock wave which hit the clean side transmitted through the bed, the dirty side curve showed an extra-ordinary high first shock peak. We used the smoothed dotted line for data analysis.

The curves shown in Figure 6.1-1-b, c and 6.1-2-b,c are really two superimposed curves. The first is the zig-zagged shock wave bouncing back and forth. The second is the "mountain shaped" bulk air flow, and is the really important portion when talking about puffback. We did one

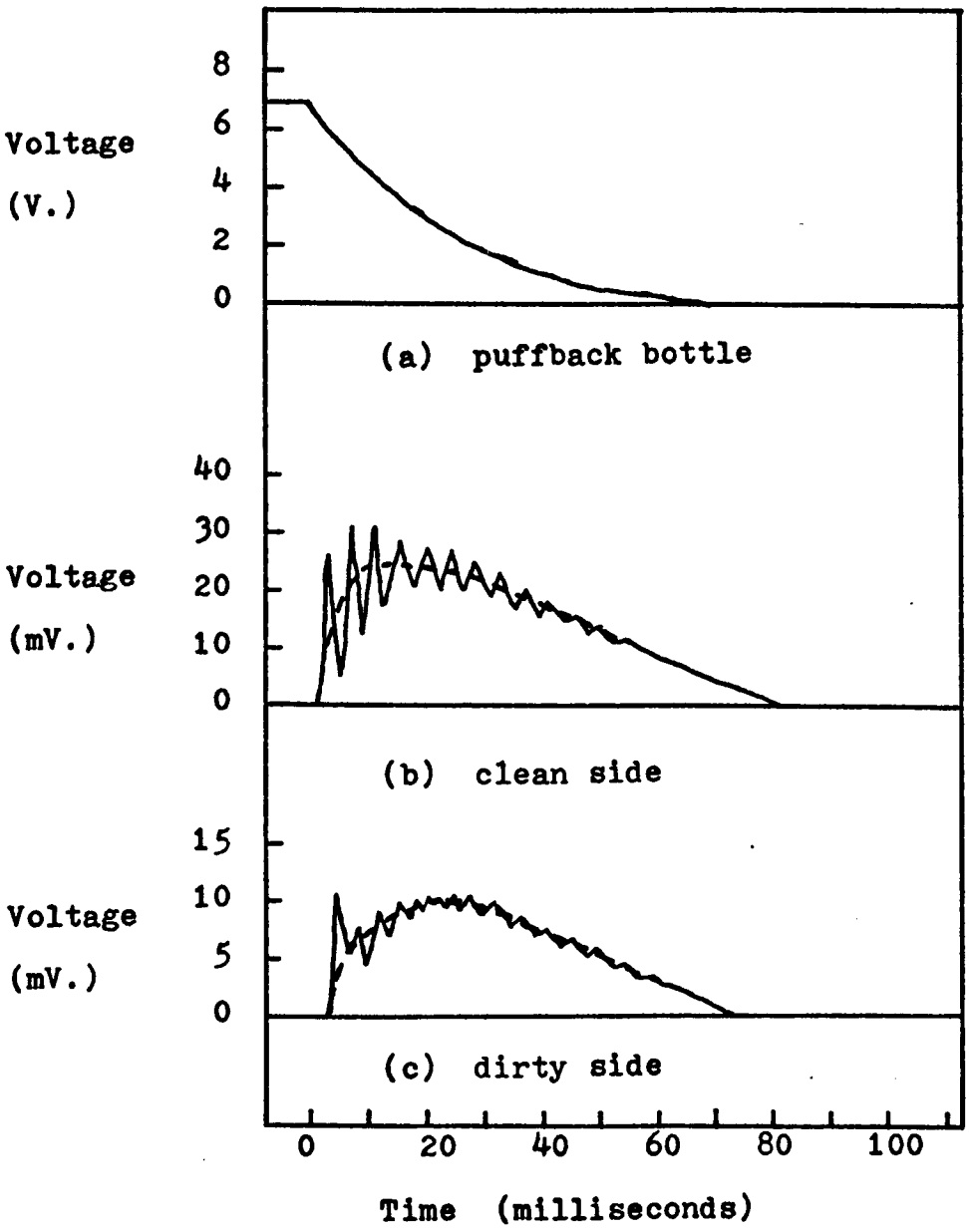

Figure 6.1-2: Typical Sideshot Transducer Data

N.B. Dotted line - smoothed curve for data analysis.

test to show the additive properties of the puffback pressure curves. We know from shock theory that a shock wave can be transmitted through the medium axially independent of the geometry of the container until it hits the boundary. We also know that a non-shock bulk flow will lose its pressure when the flow gets into a big container. In one special test, we left the dirty side transducer quite open to atmosphere so that no static pressure would build up on this side. We got the zig-zag shaped shock wave only. This also explains why in Figure 6.1-2-c the first peak was the highest one in contrary to what is seen in Figure 6.1-2-b where the second peak was the highest one. There was no bulk air pressure in the beginning portion of curve (c) due to the aforementioned pressure loss.

In Figure 6.1-1 and 6.1-2, the smoothed curves show only one hump. There were some cases where the pressure curves showed two humps. These always occurred when the puffback pressure was high or when the bottle volume was very big or when the puffback valve orifice area was small. Figure 6.1-3 shows the smoothed pressure change on the clean side, dirty side and the difference of these two curves (that is, the pressure drop across the bed). This curve represents the data taken at a combination of all the aforementioned conditions, smallest valve orifice (3/16 inch orifice), biggest bottle (No. 5) and high puffback pressure (40 psig). We can see from the figure that there was almost no pressure drop across the bed during the second

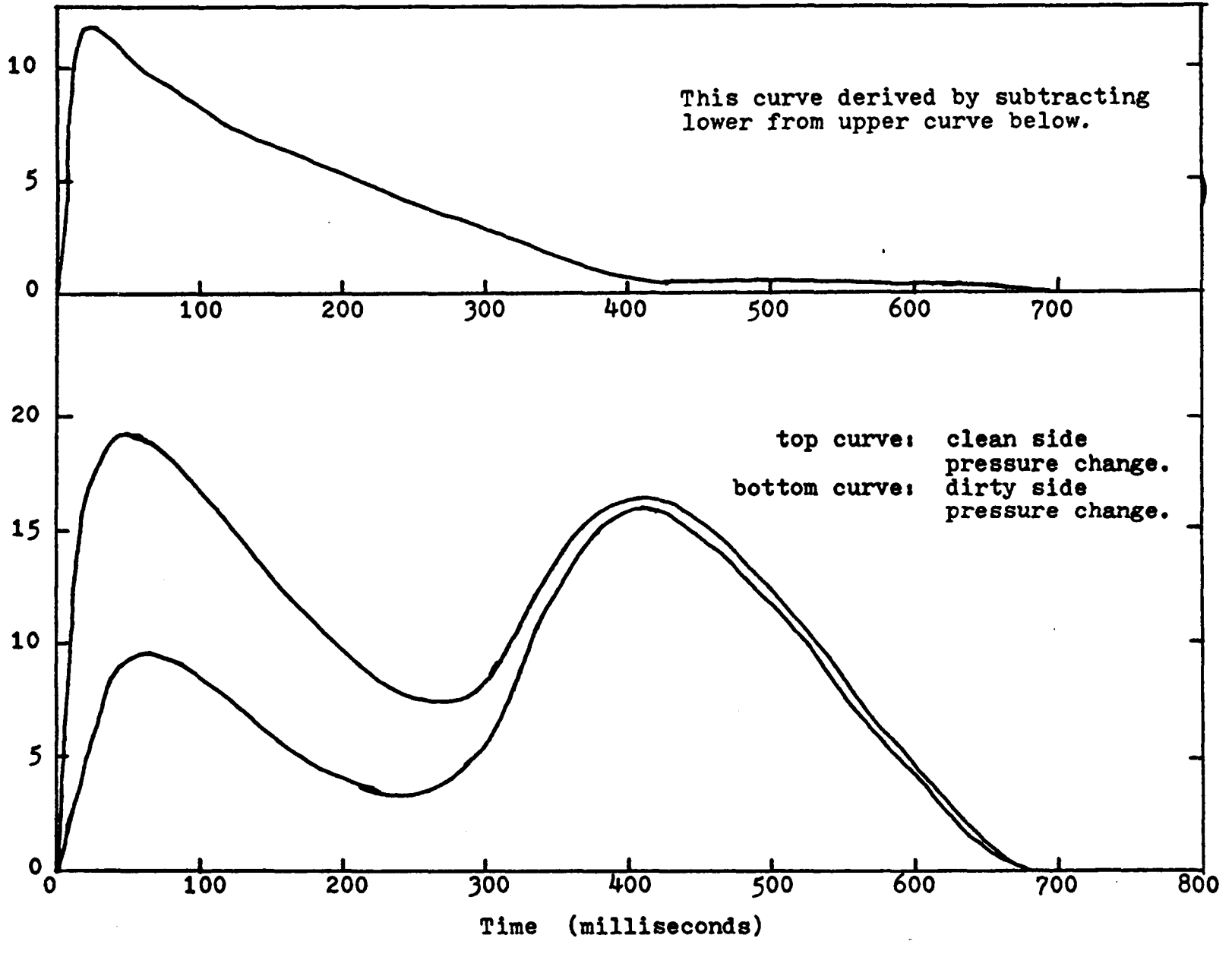

Figure 6.1-3: Two Humps Pressure Change Curves.

hump. It was first suggested that the second rise was due to the rarefaction pressure and the subsequent falling down and falling back of the sand to fill up the separation space as was discussed in Section 5.1. However, we have performed some tests by filling the sand just to the top louver and leaving the top column empty to minimize this effect. Oscilloscope pictures showed no difference and proved this effect is negligible.

The second suggestion was that this two-hump phenomenon is due to the fact that we do not have a large enough vent place at the dirty side of the panel bed since we only have a one inch diameter hole at the bottom of the clean side to let the air escape. We did another test to show this effect. By closing the puffback valve just before the rise of the second hump, that is after about 250 milliseconds, the curve will just decay to zero without the second rise. This showed that the imput flow rate from the puffback bottle was higher than the output flow through the one-inch hole at the bottom of the dirty face side at the last stage. We did another experiment in order to prove this by removing the front cover plate on the dirty side. To our surprise, the transducer data on the clean side still showed the second hump but to a lesser extent. It appears that the output air flow might not only limited by the one inch bottom hole but also be limited by the sand bed.

All the aforementioned three conditions for the second rise in pressure will give rise to a long puffback duration time. Transient compressible fluid flow study might explain

this phenomenon. In our puffback application, however, we are only interested in the low intensity case and short duration times.

The cause of puffback sand spill is due to the pressure drop across the sand bed. Due to our design, there is a pressure build-up at the dirty face side during puffback. We will use the difference of our clean side pressure curve and the dirty side pressure curve to analyse our data. All the data showed in Sections 6.1.1.1 and 6.1.1.2 are based on pressure differences.

6.1.1.1 Kistler Downshot Puffback Data

Figures 6.1-4 to 20 show downshot puffback data in the second unit. The numeral on the curve indicates the puffback pressure in psig. These curves were obtained by calculating the difference of the clean side pressure curve and the dirty side pressure curve. Generally speaking the curves look like triangles except those obtained when the puffback pressure was high. Due to the build up of pressure on the dirty surface side, the pressure drop will be less than that which would be obtained if the dirty side volume was very big. This effect will make the curve concave upward in the tail section and shows a deviation from the triangular shape when the puffback intensity is high. With number 4 or 5 bottle and high pressure, the curves showed two humps like the one shown in Figure 6.1-3. We will not use these double humped curves in our data analysis.

Figures 6.1-4 to 9 show data on 20-30 mesh sand backed

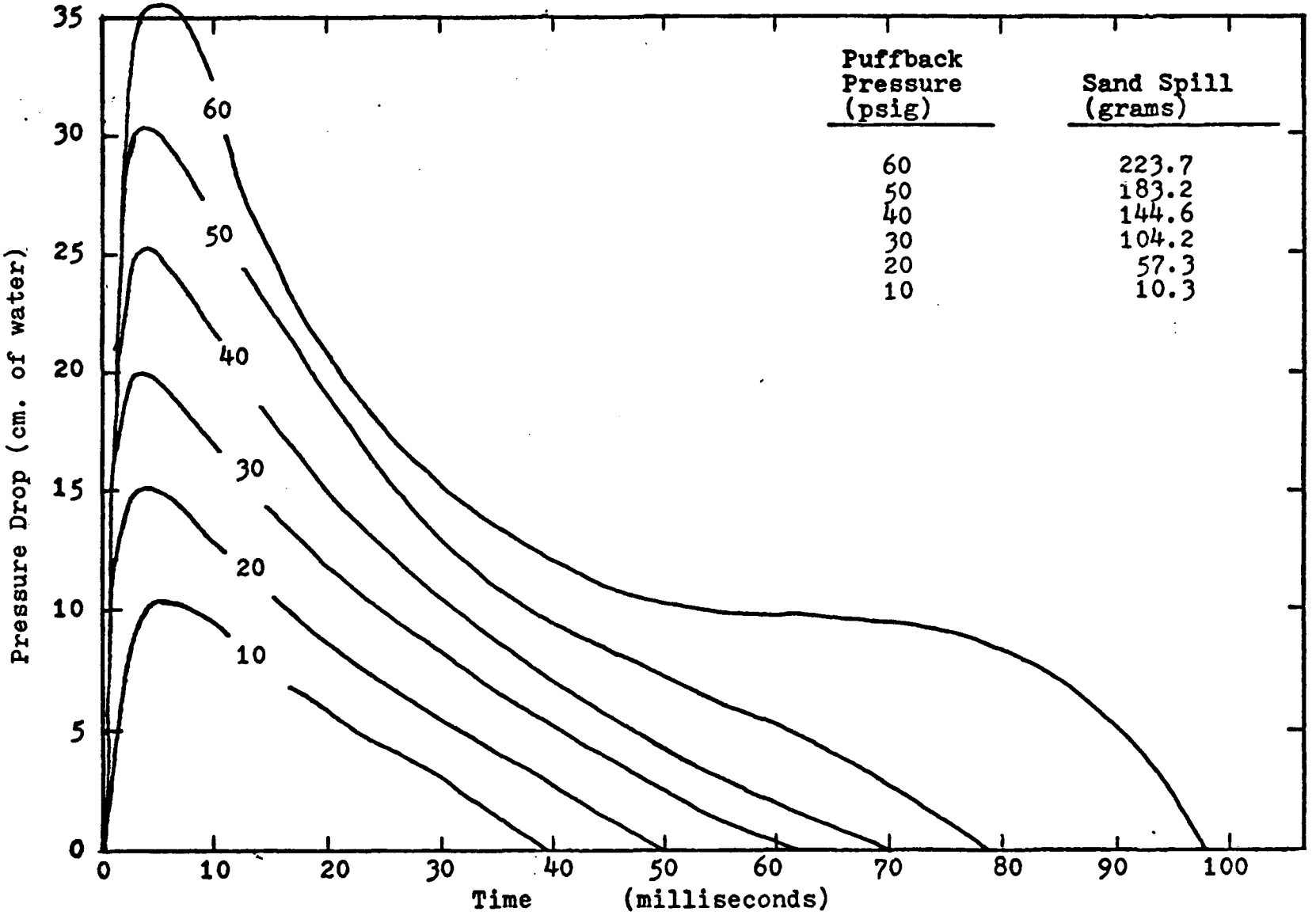

Figure 6.1- 4: Pressure Drop Data of A-3-B-3-x-D Series Runs

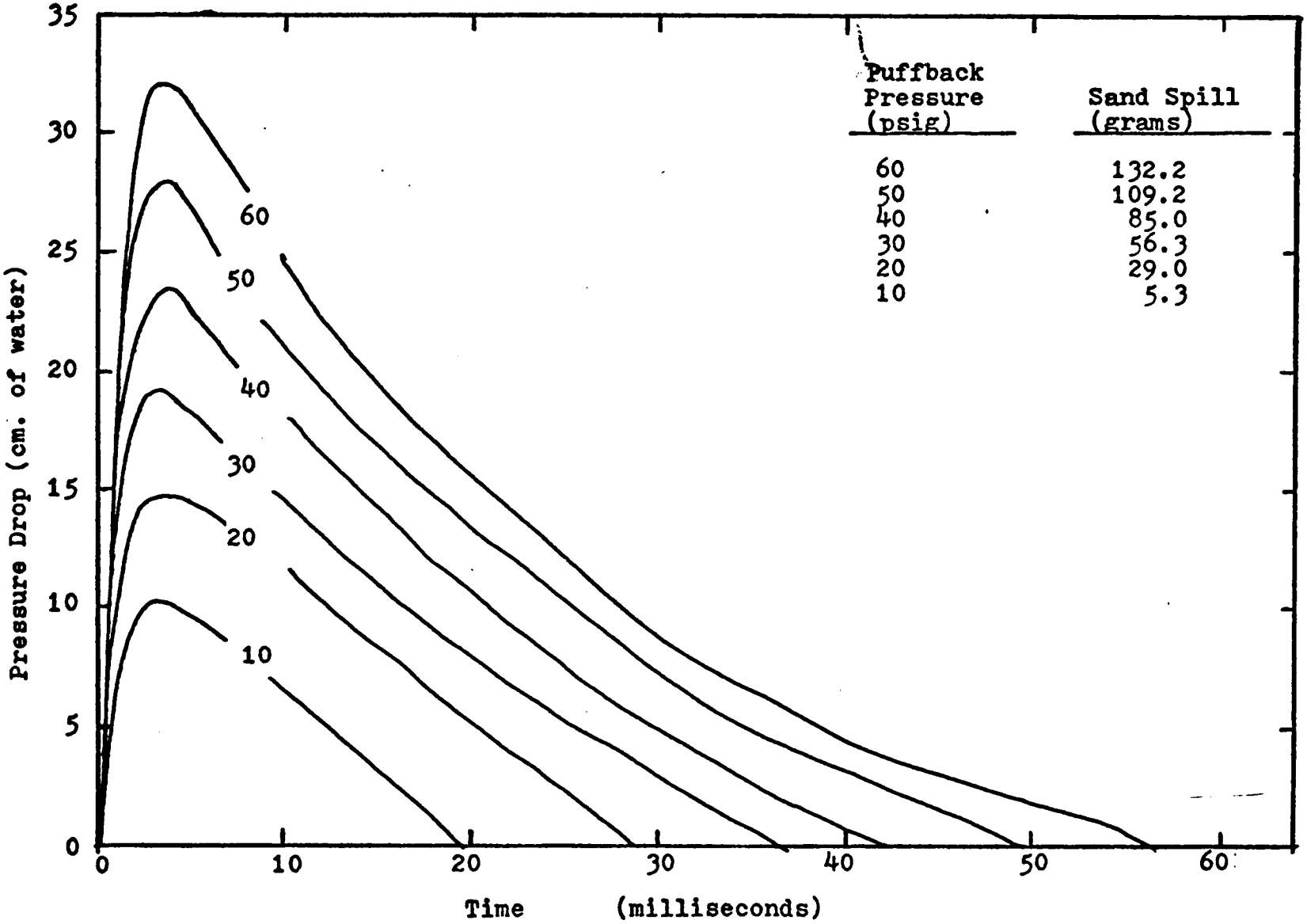

Figure 6.1- 5: Pressure Drop Data of A-3-B-2-x-D Series Runs

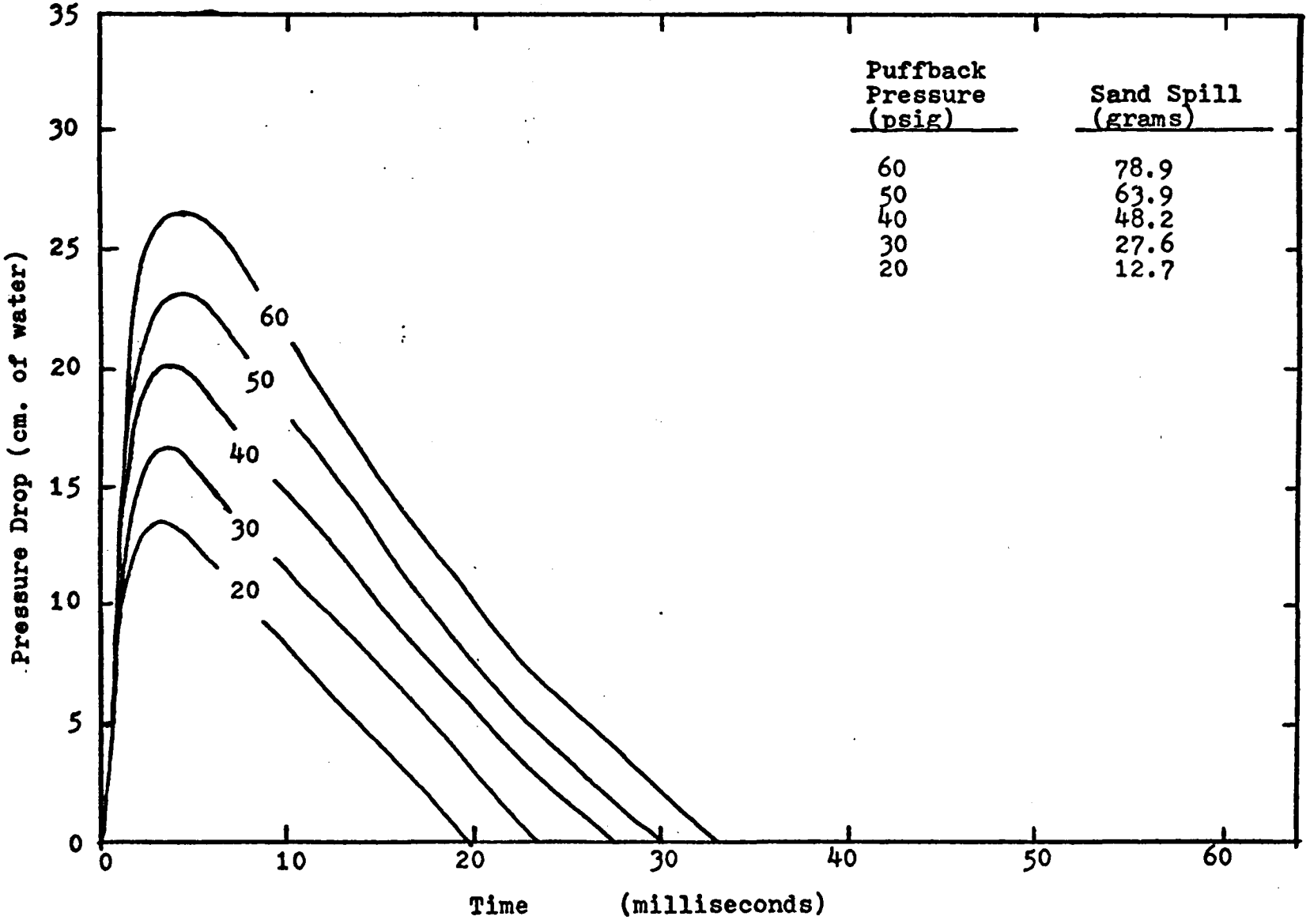

Figure 6.1-6: Pressure Drop Data of A-3-B-1-x-D Series Runs

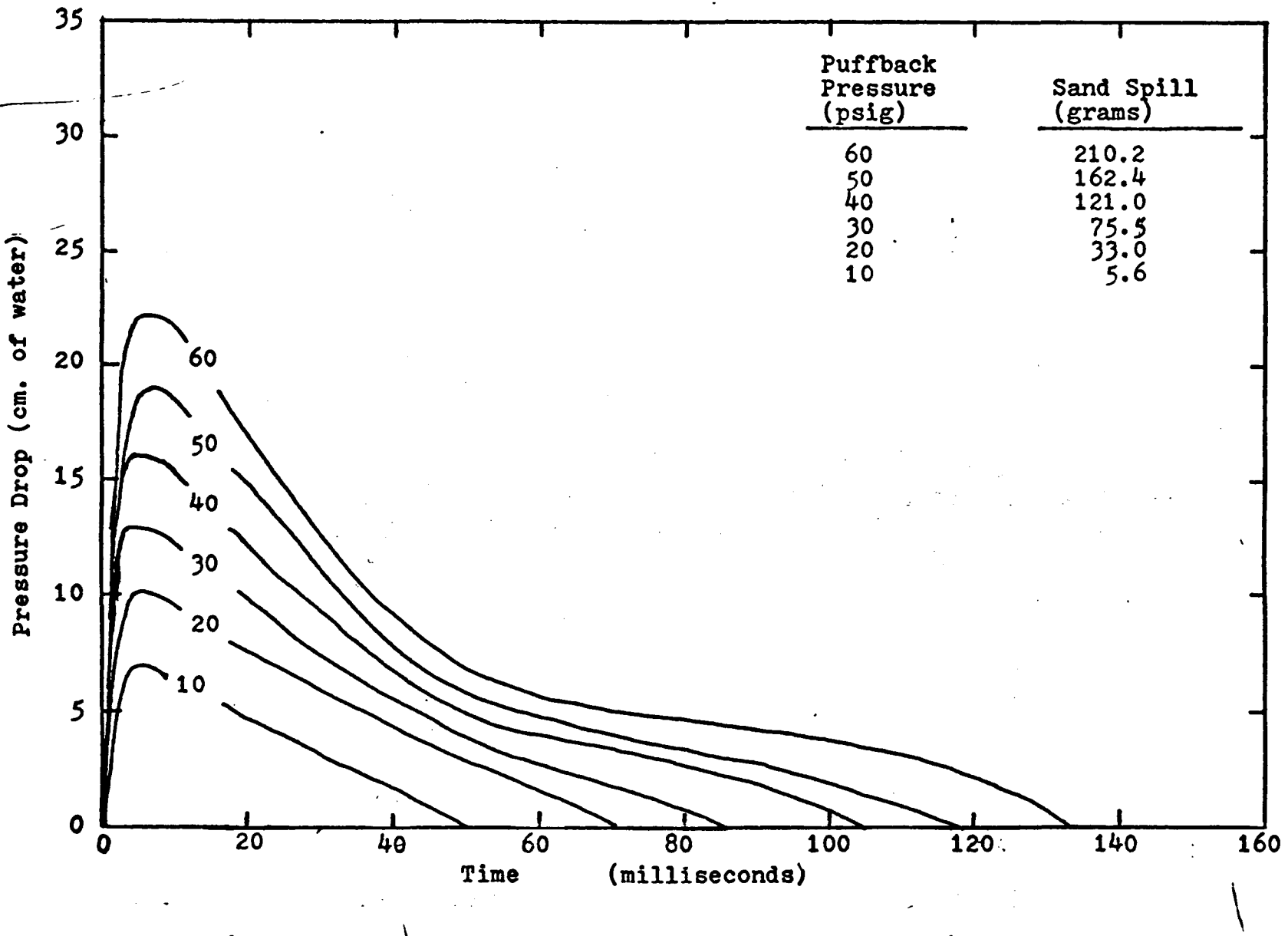

Figure 6.1- 7: Pressure Drop Data of A-3-S-3-x-D Series Runs

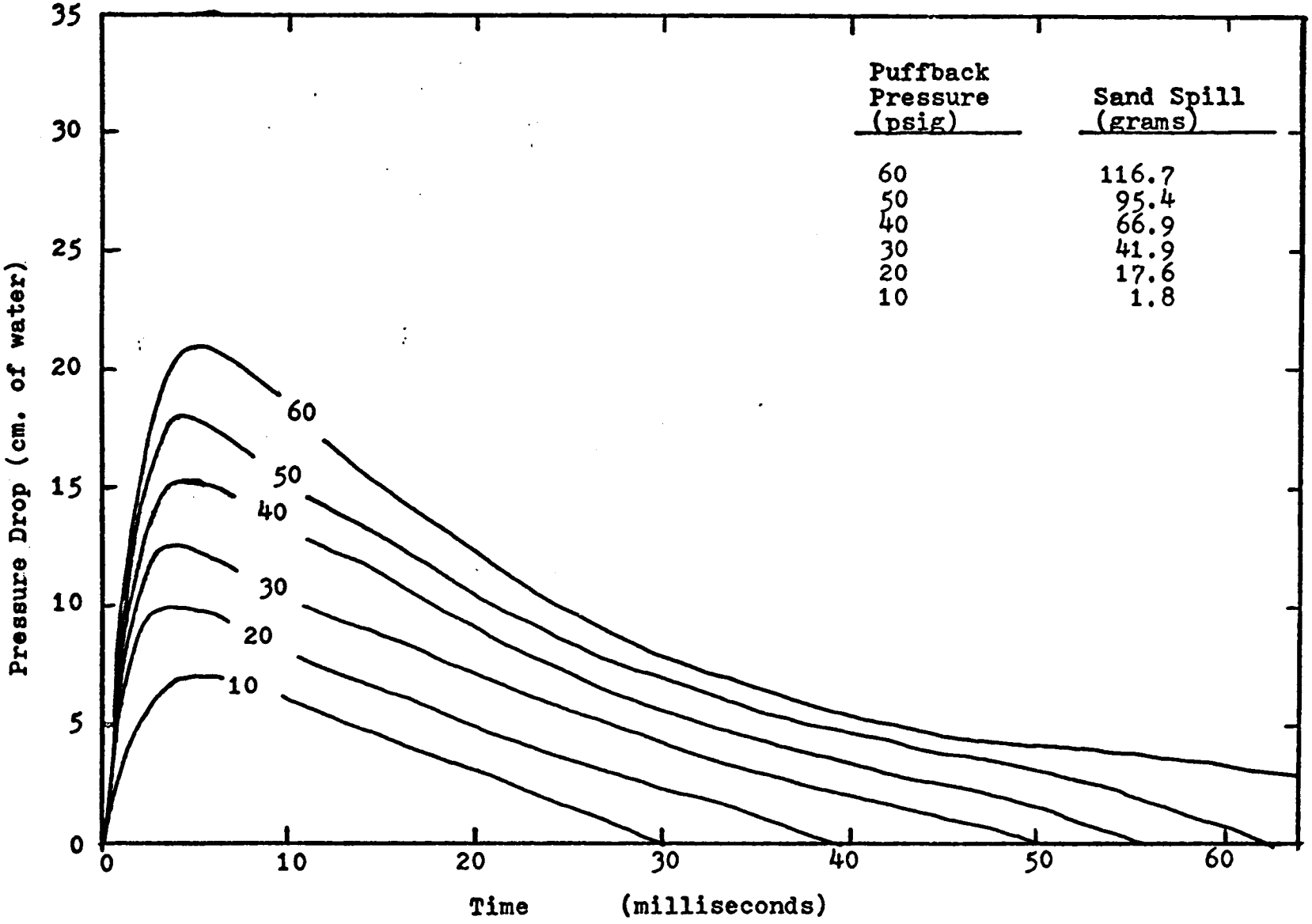

Figure 6.1- 8: Pressure Drop Data of A-3-S-2-x-D Series Runs

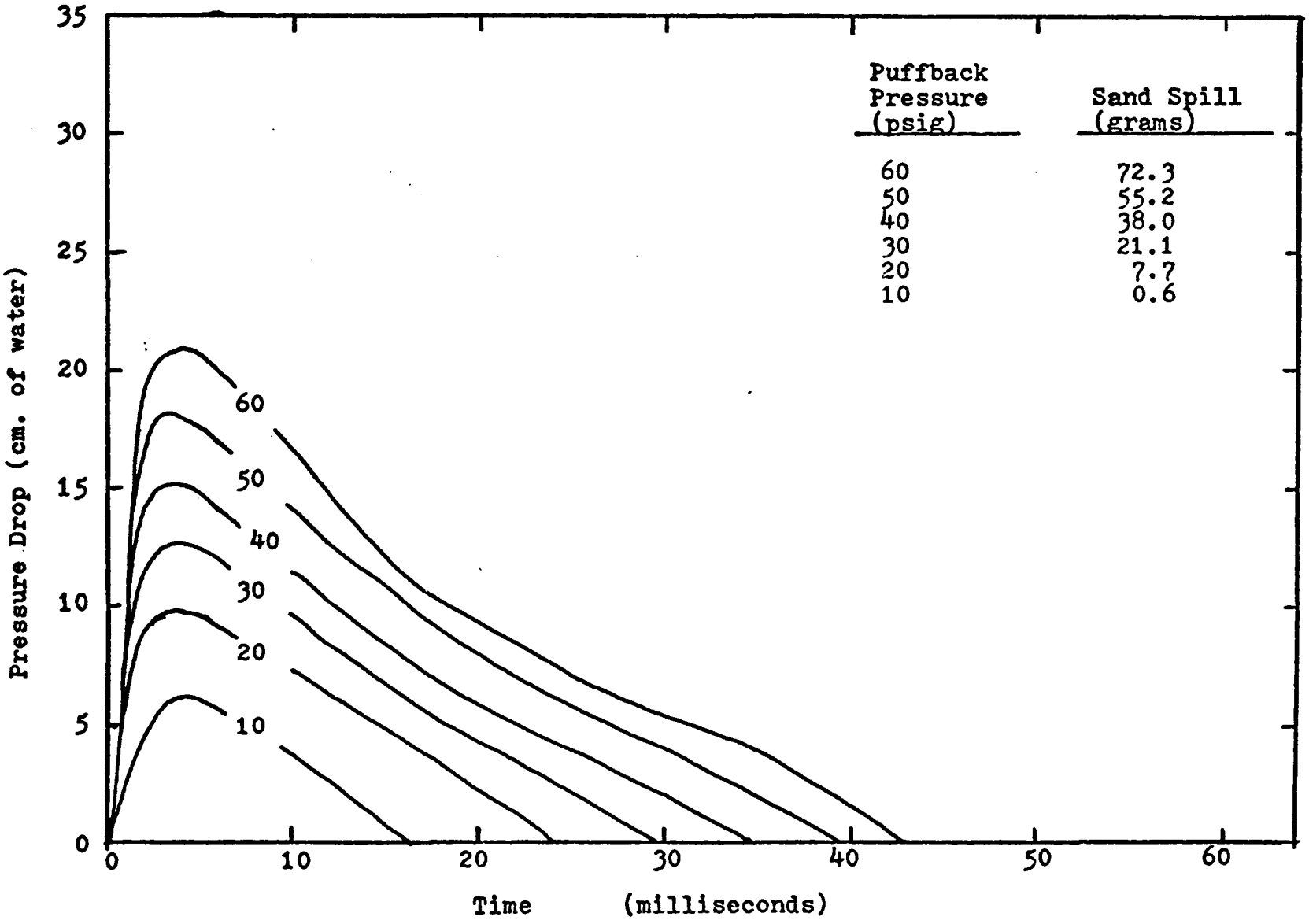

Figure 6.1- 9: Pressure Drop Data of A-3-S-1-x-D Series Runs

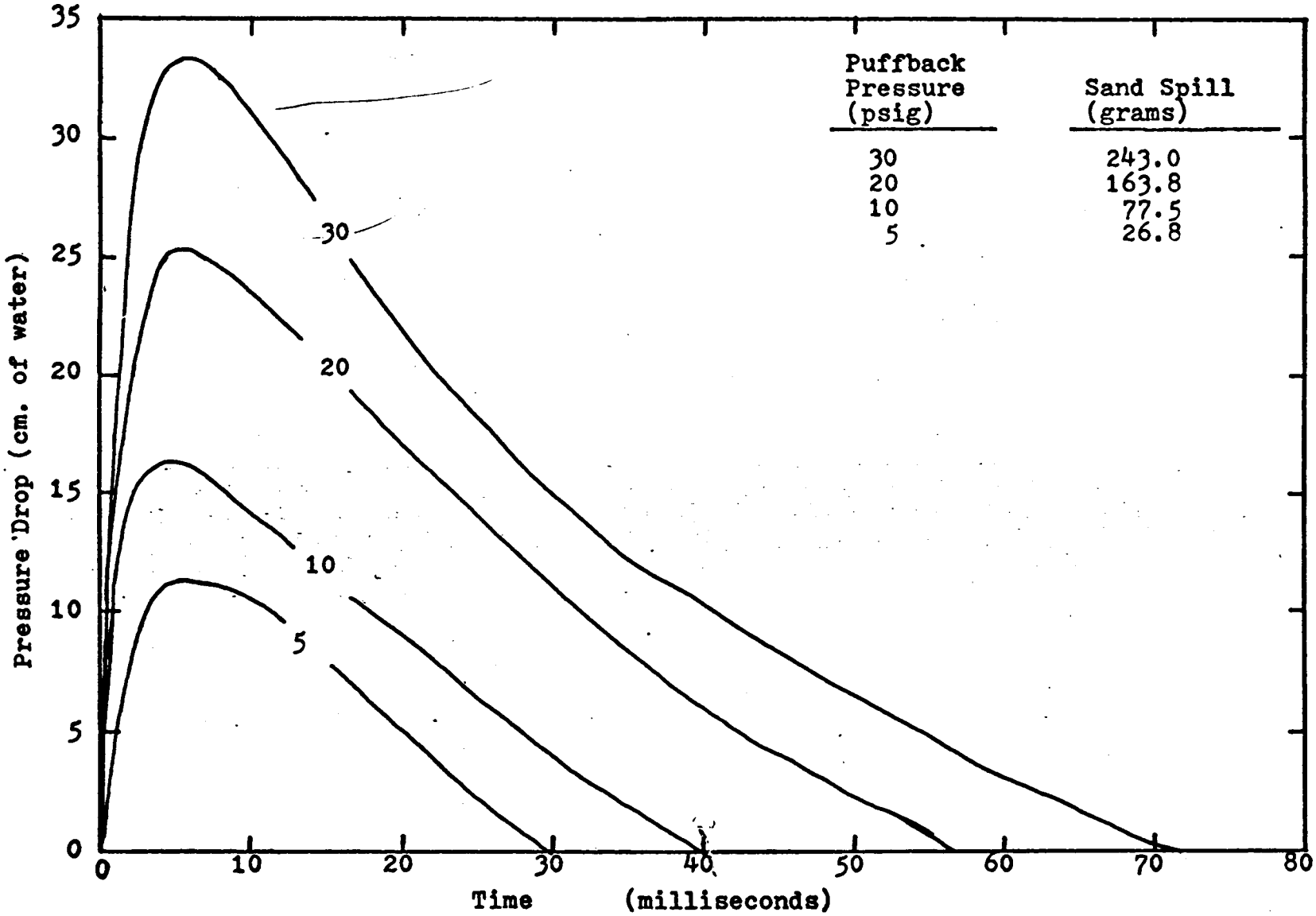

Figure 6.1-10: Pressure Drop Data of C-3-B-3-x-D Series Runs

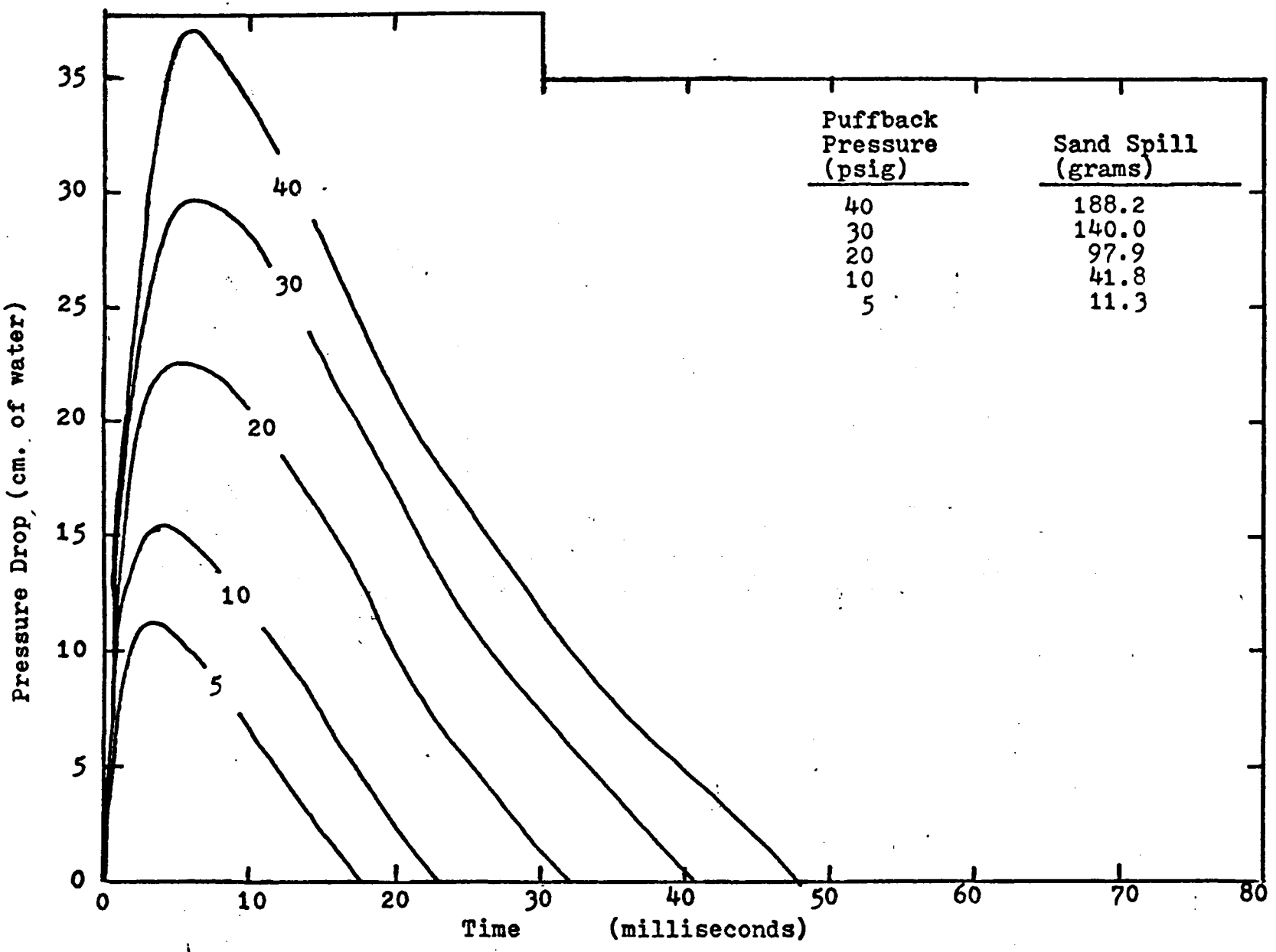

Figure 6.1-11: Pressure Drop Data of C-3-B-2-x-D Series Runs

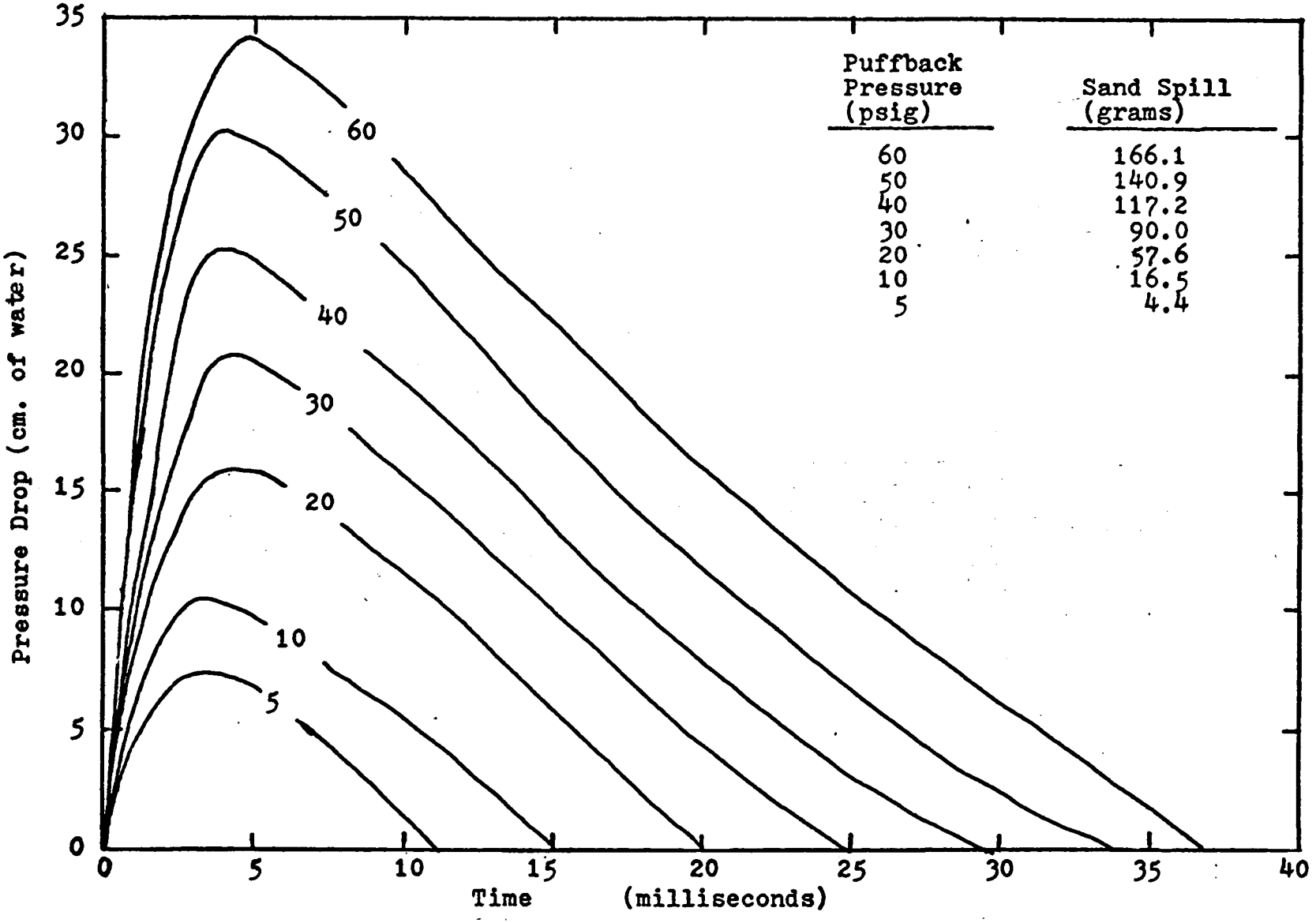

Figure 6.1-12: Pressure Drop Data of C-3-B-1-x-D Series Runs

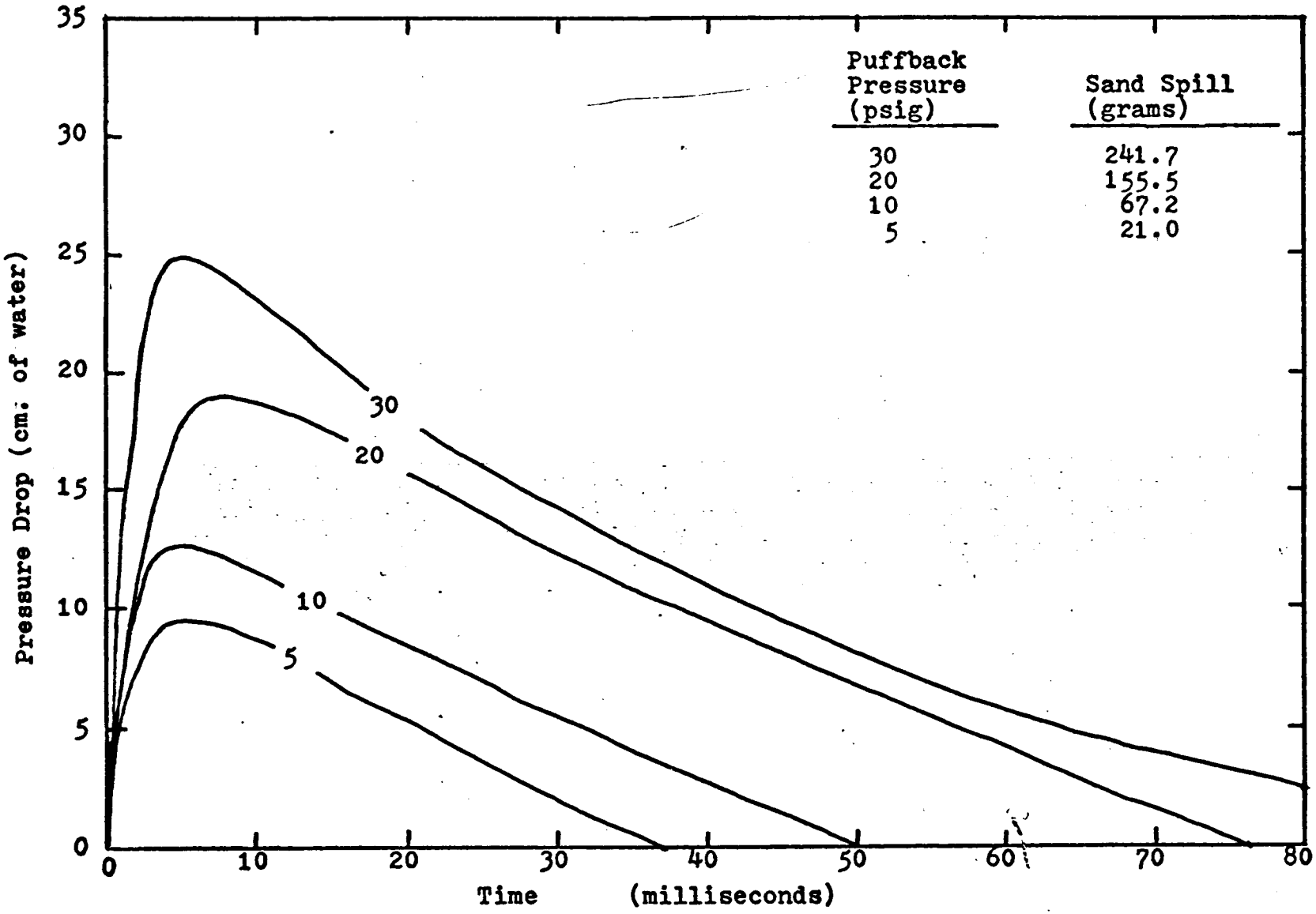

Figure 6.1-13: Pressure Drop Data of C-3-S-3-x-D Series Runs

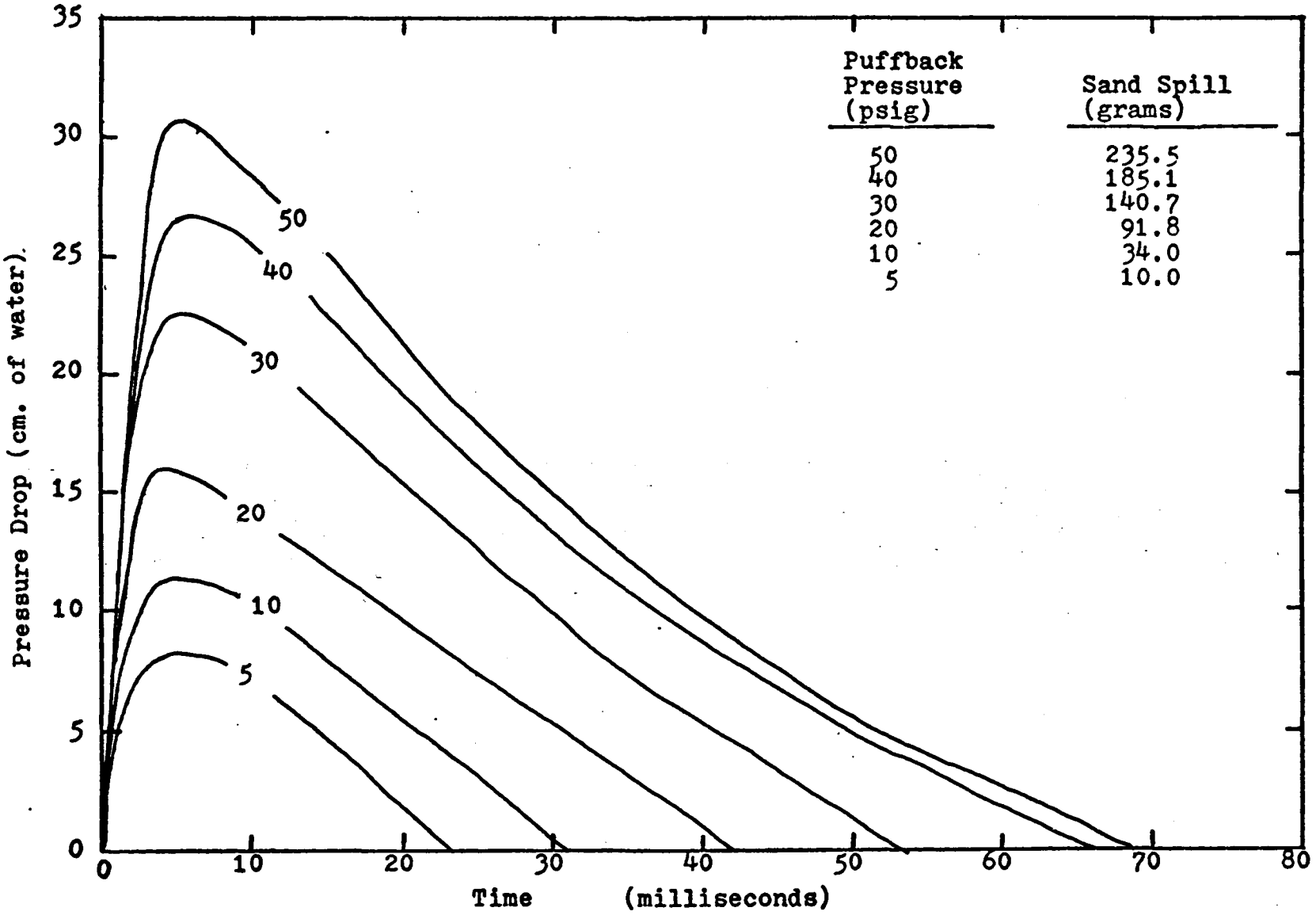

Figure 6.1-14: Pressure Drop Data of C-3-S-2-x-D Series Runs

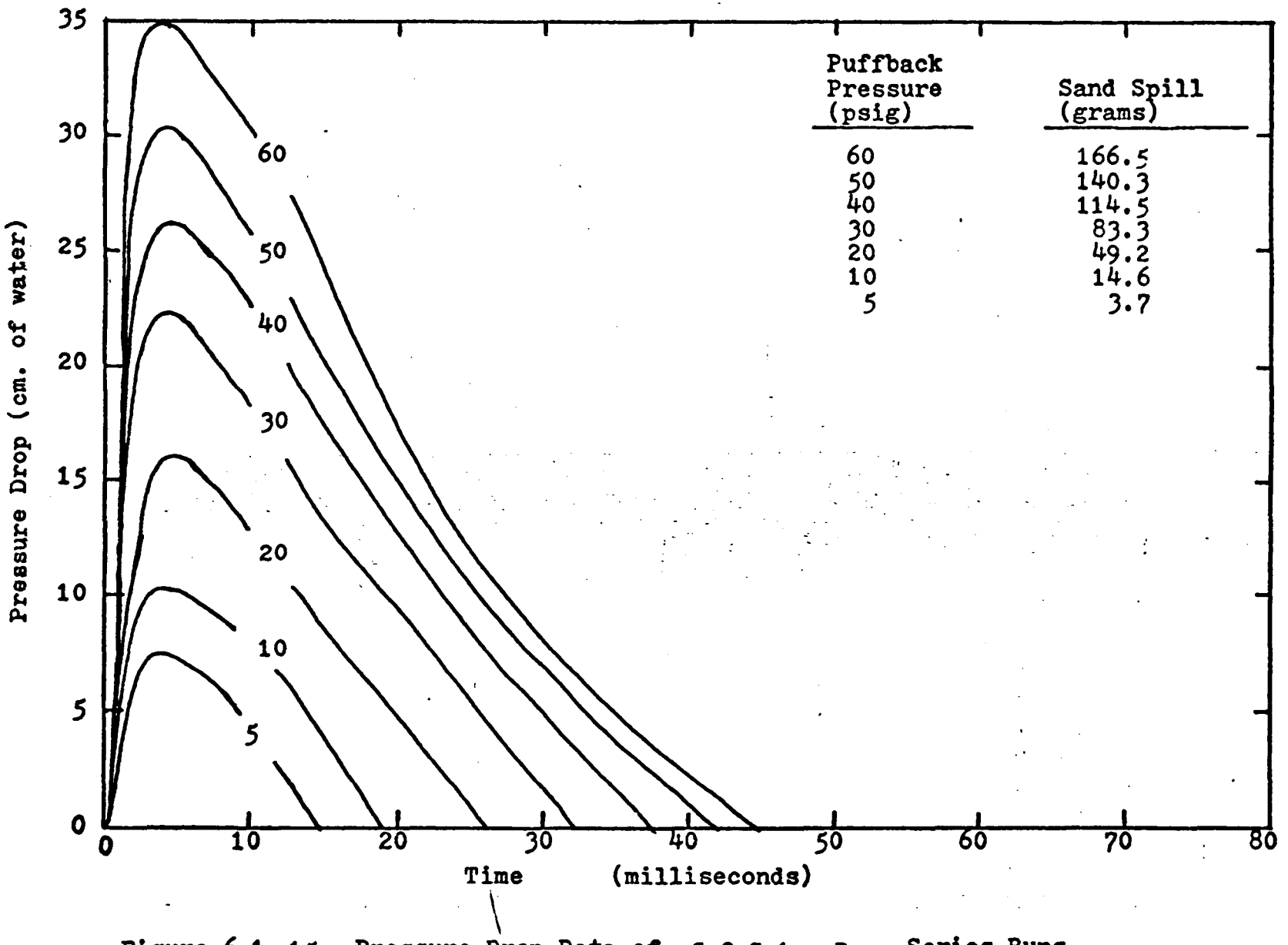

Figure 6.1-15: Pressure Drop Data of C-3-S-1-x-D Series Runs

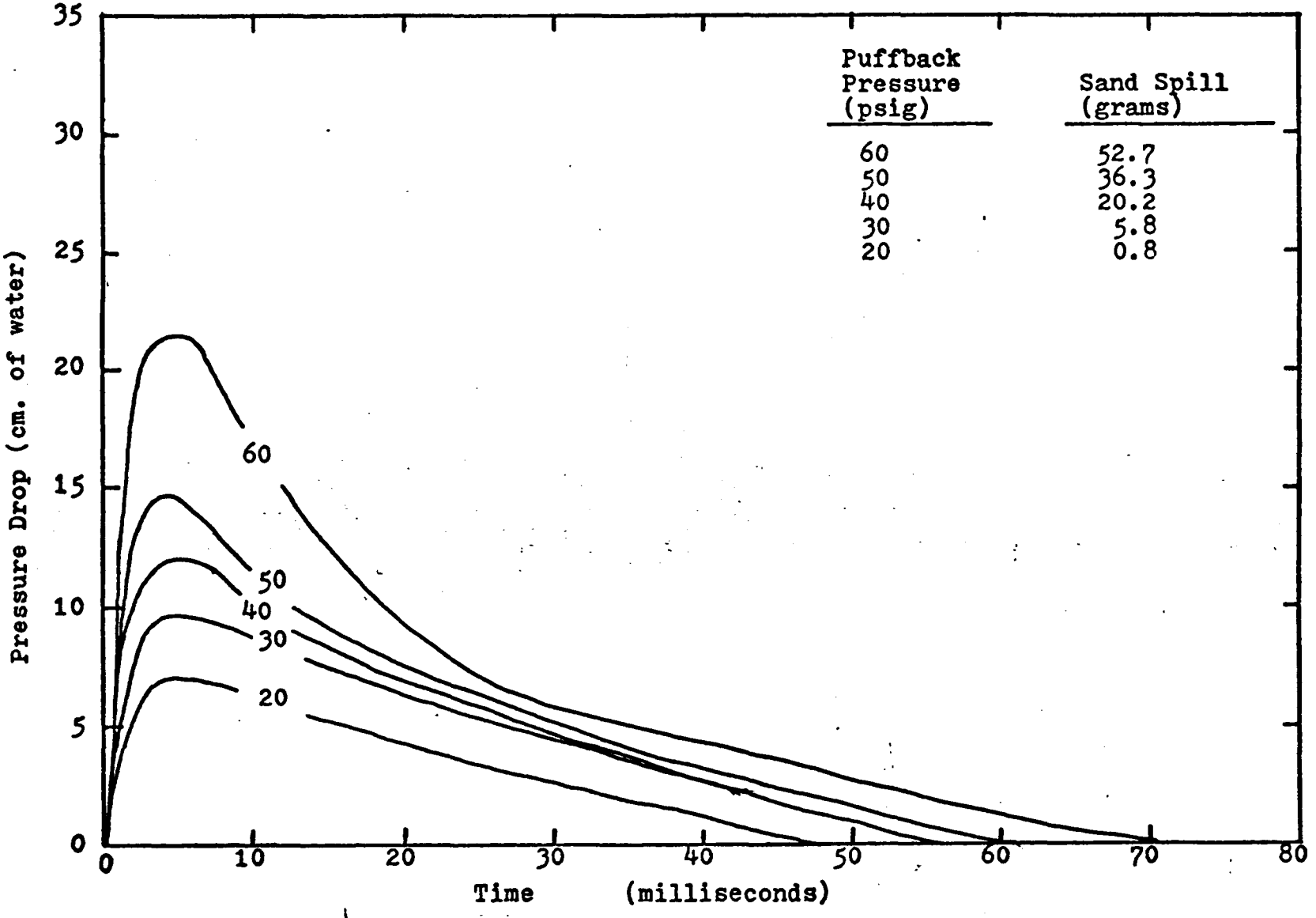

Figure 6.1-16: Pressure Drop Data of D-3-B-3-x-D Series Runs

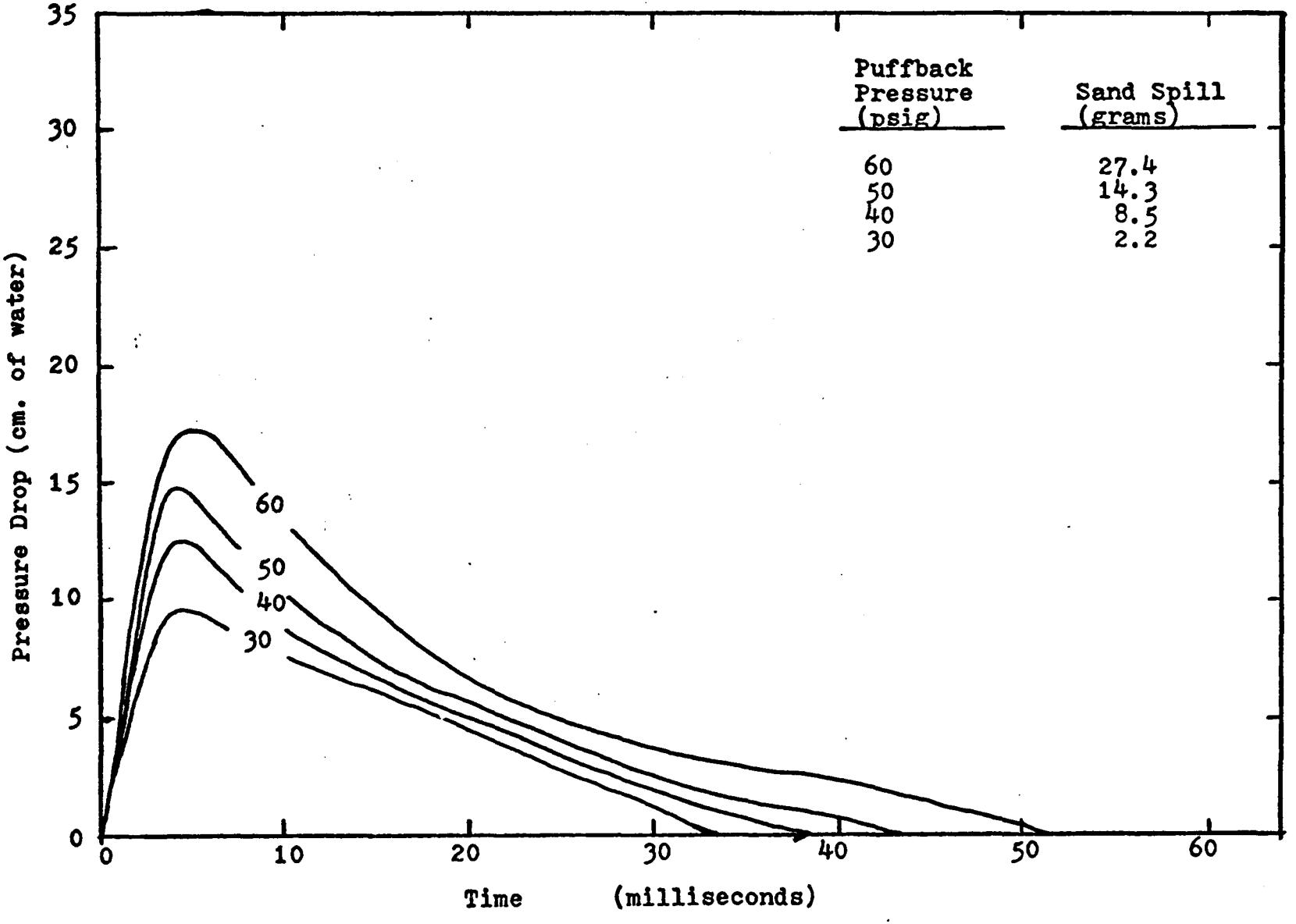

Figure 6.1-17: Pressure Drop Data of D-3-B-2-x-D Series Runs

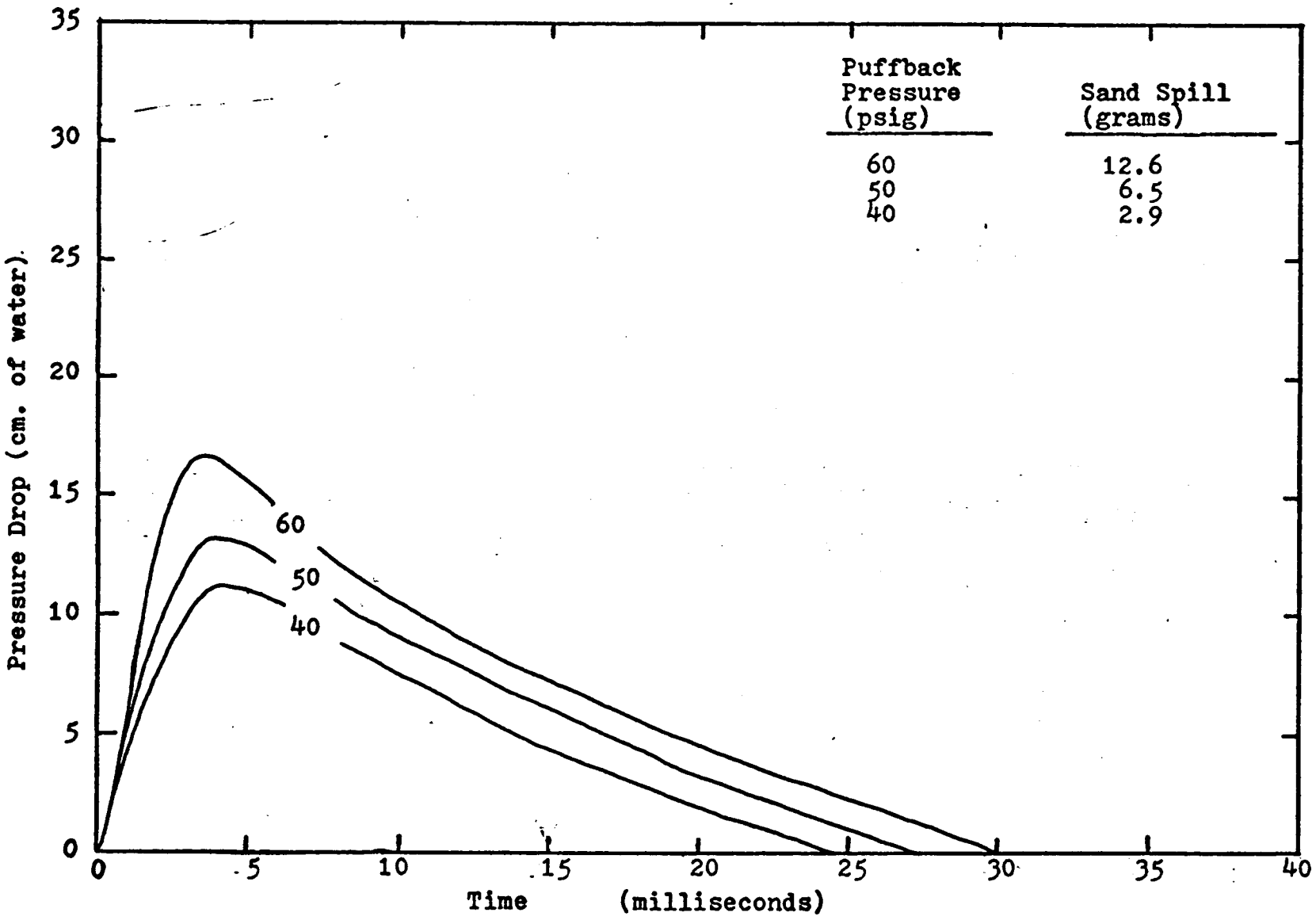

Figure 6.1-18: Pressure Drop Data of D-3-B-1-x-D Series Runs

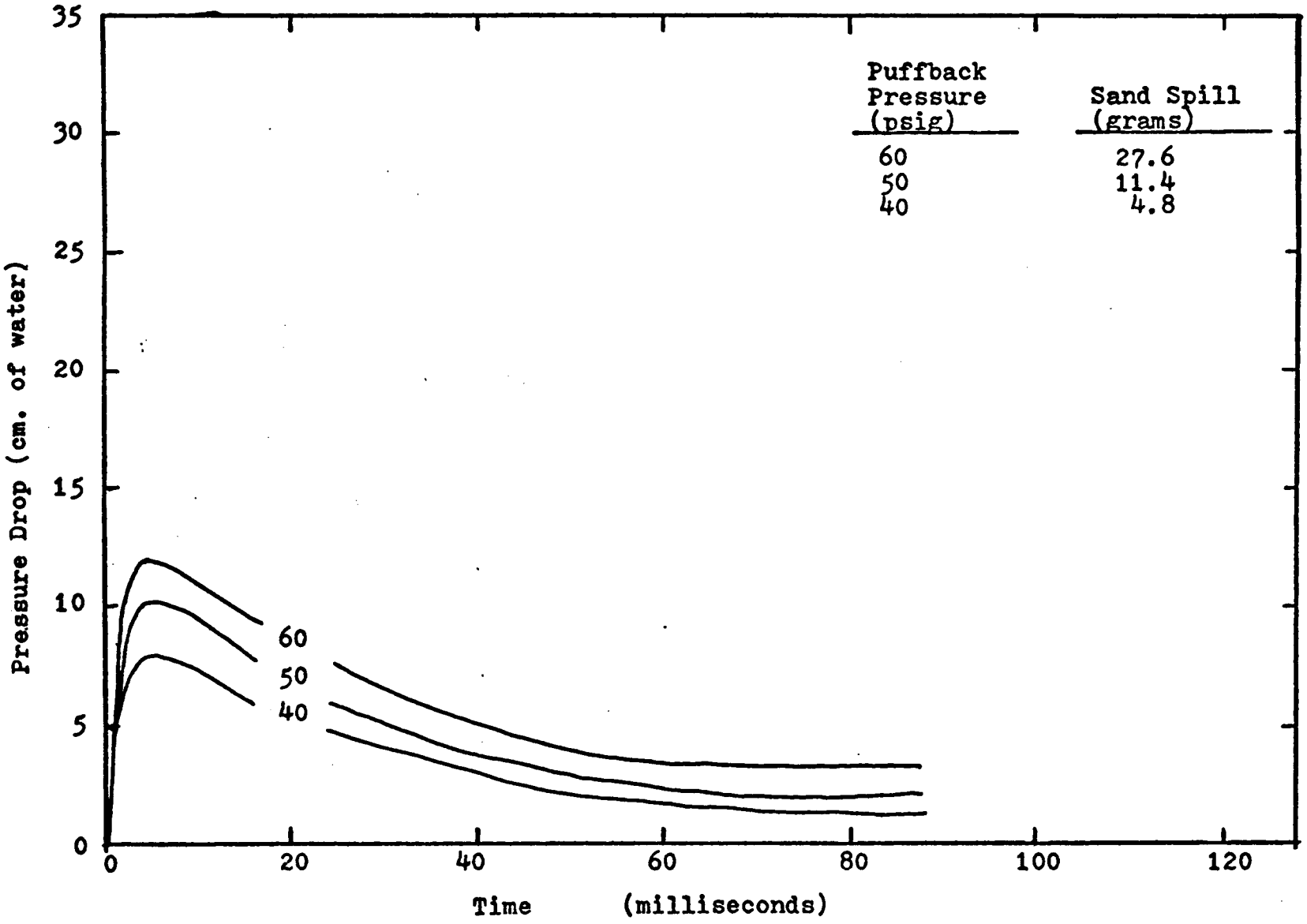

Figure 6.1-19: Pressure Drop Data of D-3-S-3-x-D Series Runs

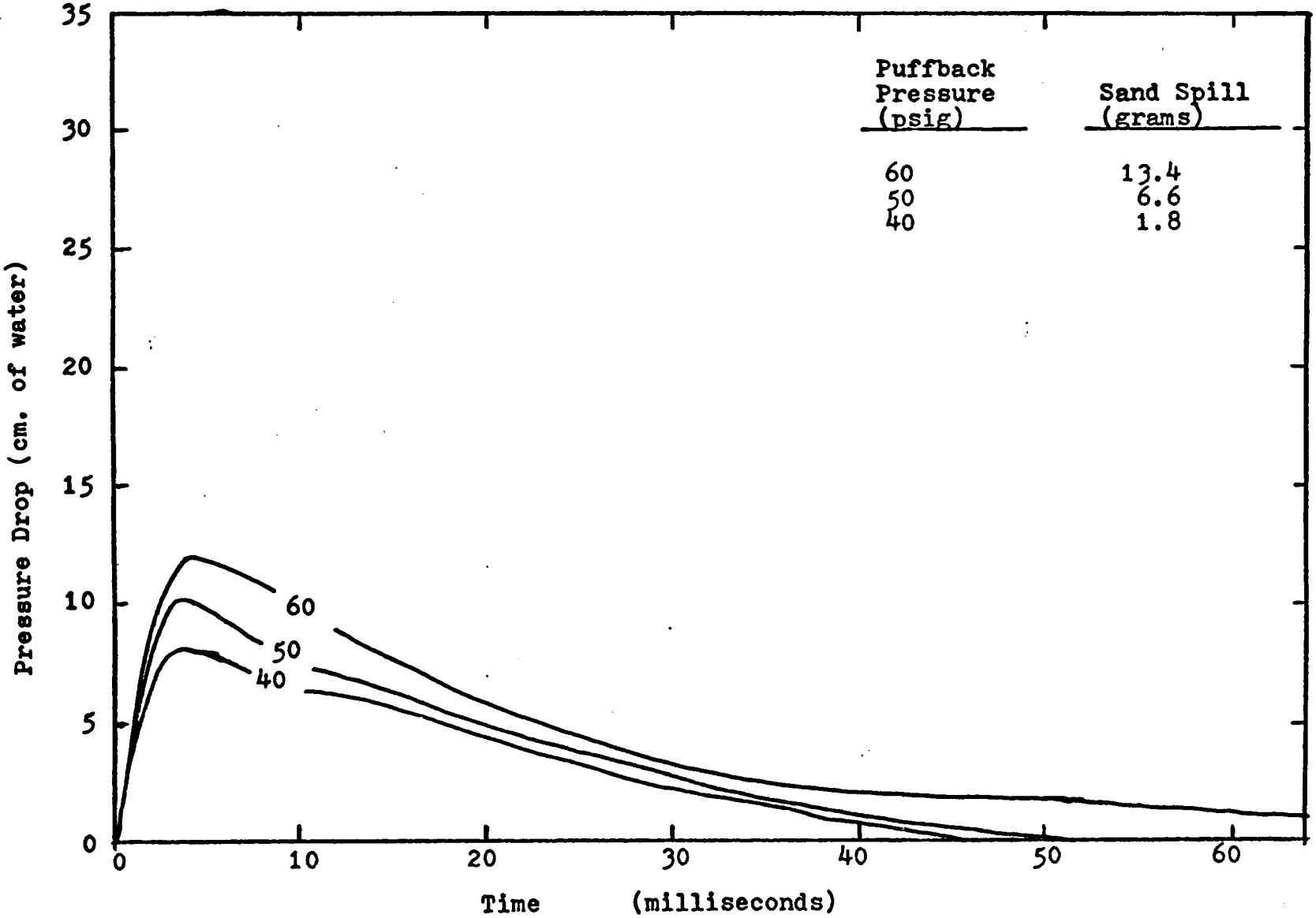

Figure 6.1-20: Pressure Drop Data of D-3-S-2-x-D Series Runs

by 10-14 mesh sand. Figures 6.1-16 to 20 show data on 10-14 mesh sand backed by 10-14 mesh sand. Because of the higher permeability of 10-14 mesh sand, the absolute pressure on the clean side and the dirty side were about the same. There was an additional error in calculating the pressure difference over and above the error introduced by smoothing the curves. The data for 10-14 mesh sand were the least accurate. Figure 6.1-19 showed a horizontal tail which we believe to be due to the limiting flow rate effect of the small bottom hole on the dirty side.

6.1.1.2. Kistler Sideshot Puffback Data.

Figures 6.1-21 to 37 show sideshot or horizontal shot data using our second unit. The numeral on the curve indicates puffback pressure in psig. Because of the big volume of the tapered section, the peak pressure drop was much less than that of the downshot puffback. The duration time of the puffback pressure was longer than that of downshot puffback. Because the big volume of the tapered section acted to dampen the pressure rise, the rise time to peak pressure was also longer. The pressure drop curves for the 3/16 inch valve (S) and the 5/16 inch valve (B) generally had a triangular shape. Curves for 1 inch valve (G) where the big volume effect was balanced by the big valve orifice area, were concave upward at high puffback pressure just like those observed for the downshot puffback curves.

As shown in Figure 6.1-2, there was vigorous shock

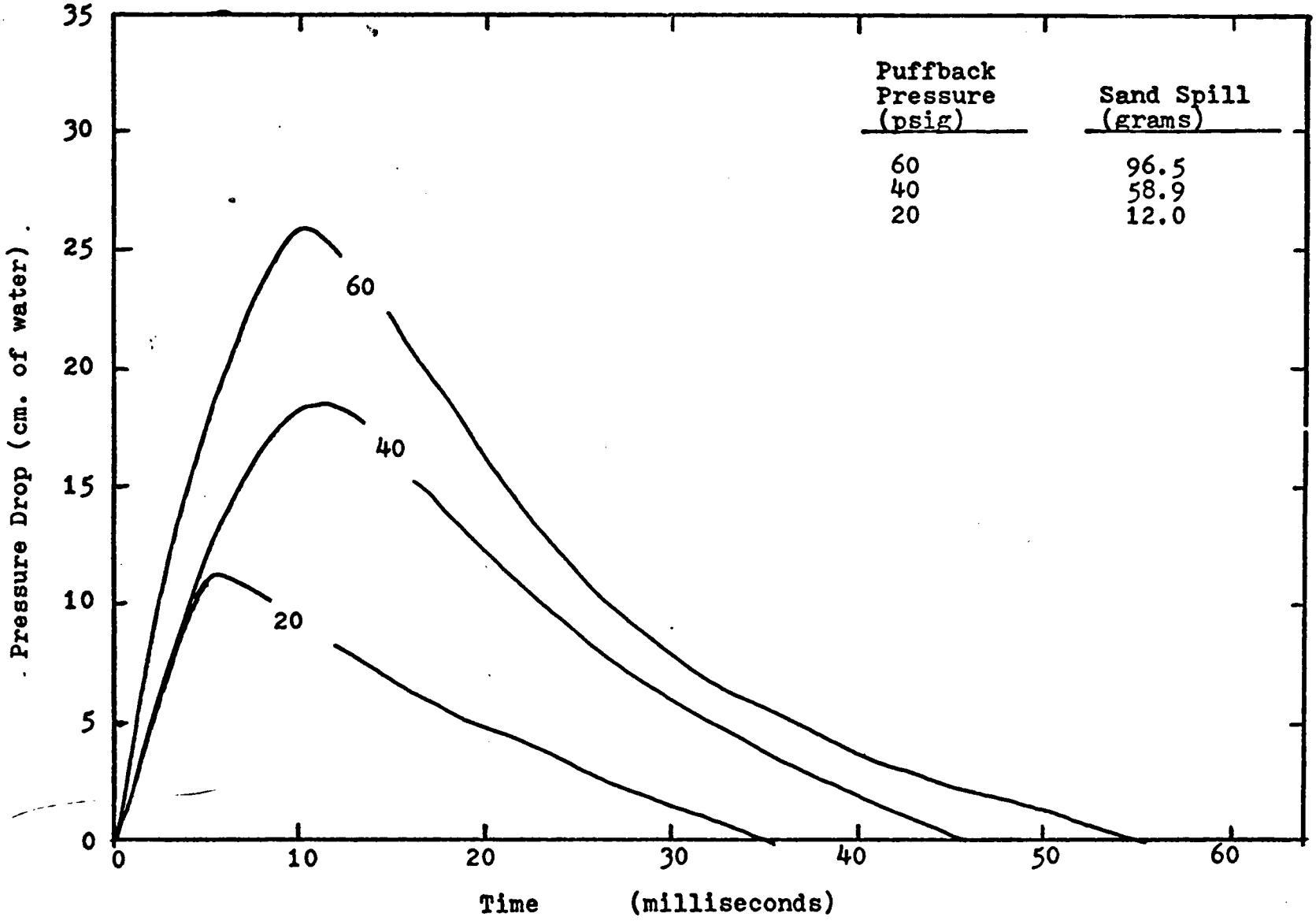

Figure 6.1-21: Pressure Drop Data of A-3-G-2-x-H Series Runs

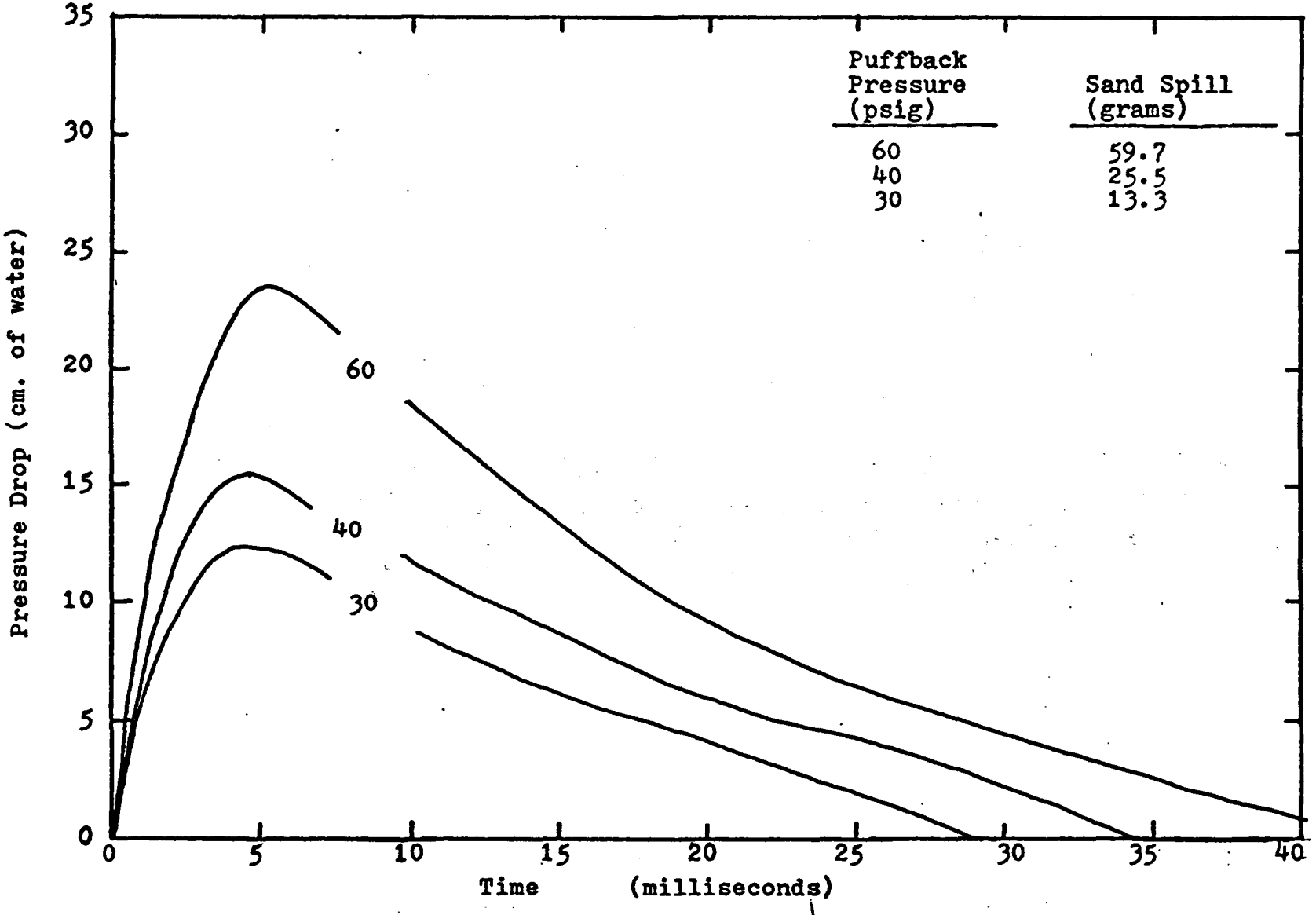

Figure 6.1-22: Pressure Drop Data of A-3-G-1-x-H Series Runs

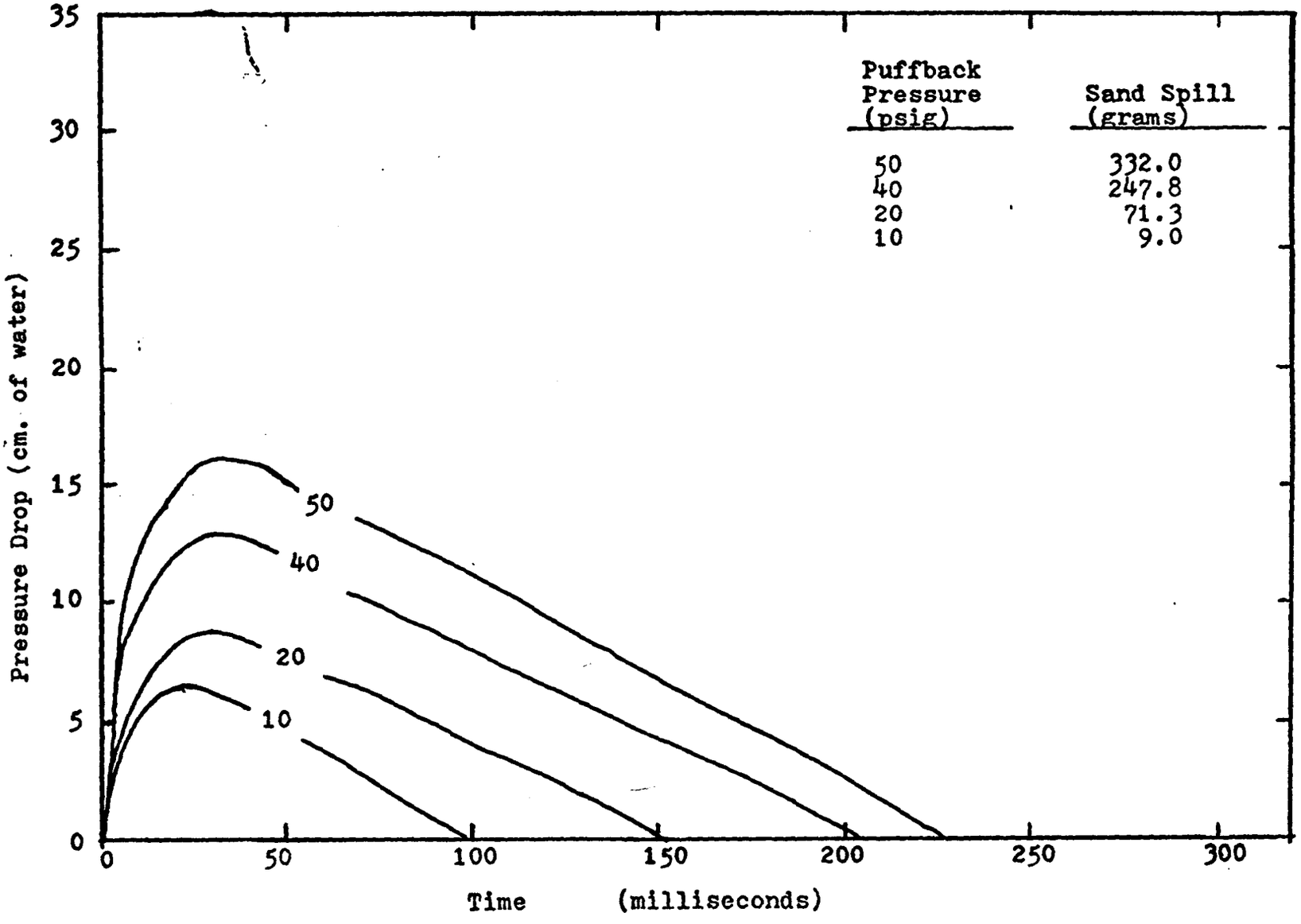

Figure 6.1-23: Pressure Drop Data of A-3-B-4-x-H Series Runs

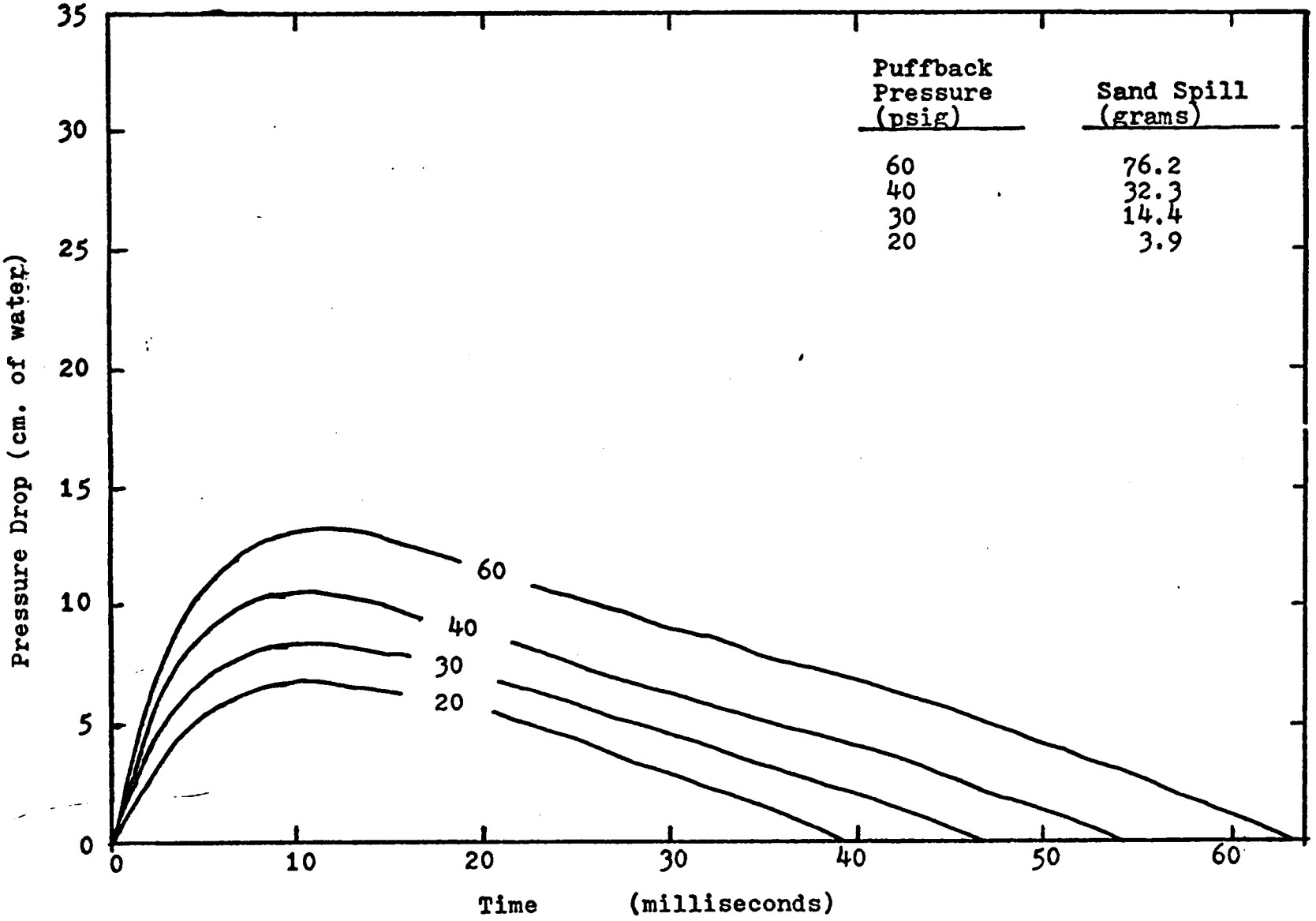

Figure 6.1-24: Pressure Drop Data of A-3-B-2-x-H Series Runs

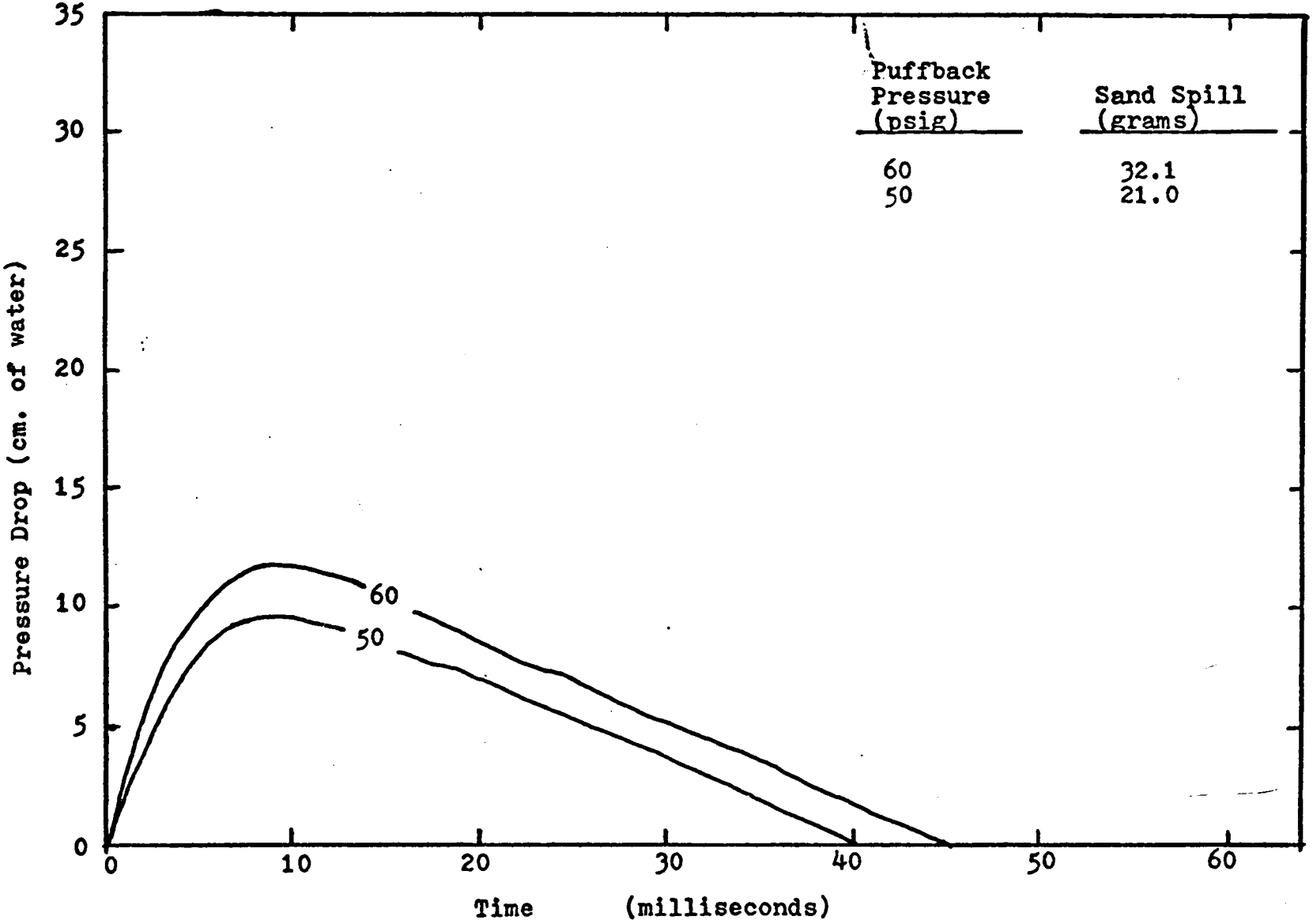

Figure 6.1-25: Pressure Drop Data of A-3-B-1-X-H Series Runs

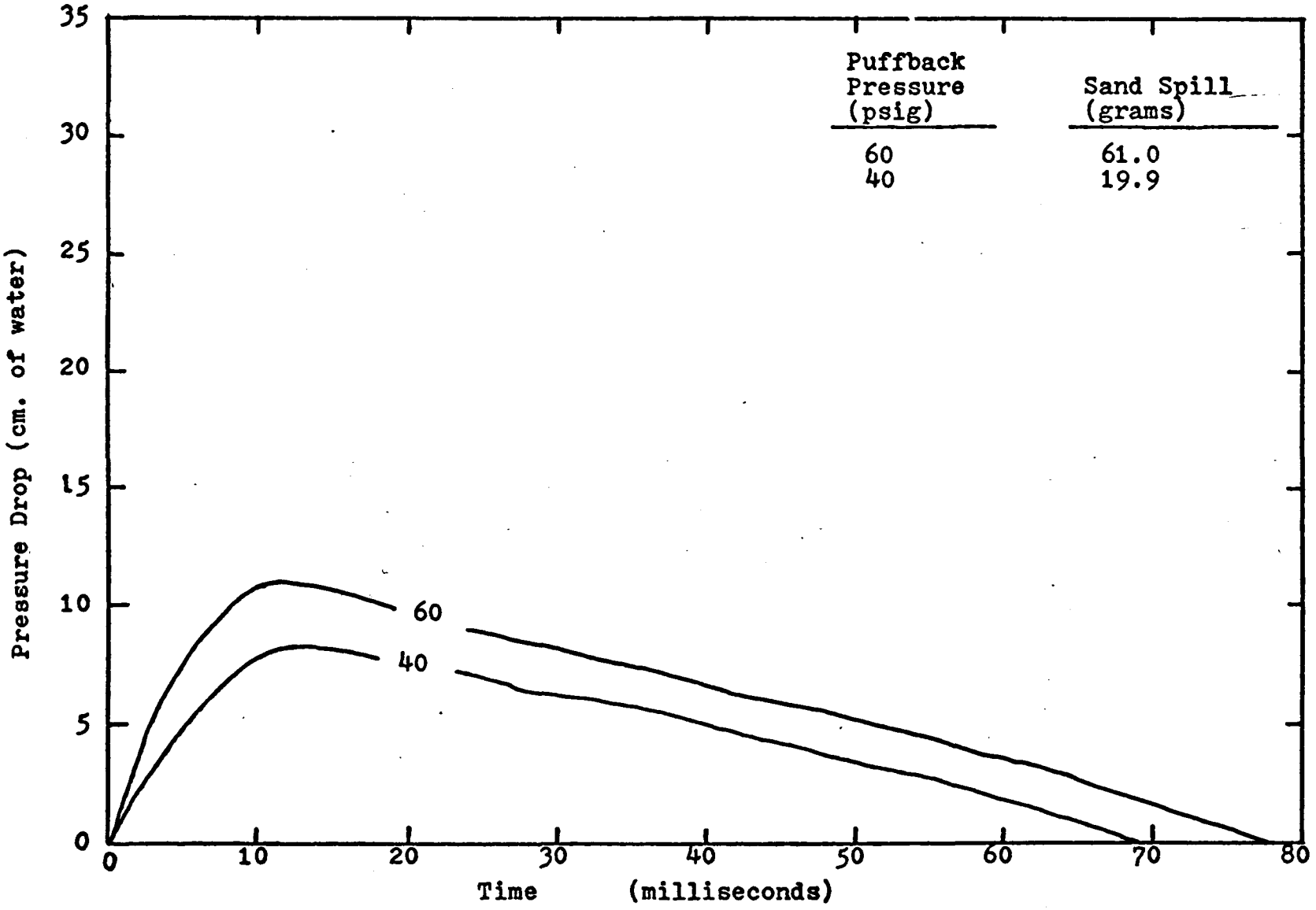

Figure 6.1-26: Pressure Drop Data of A-3-S-2-x-H Series Runs

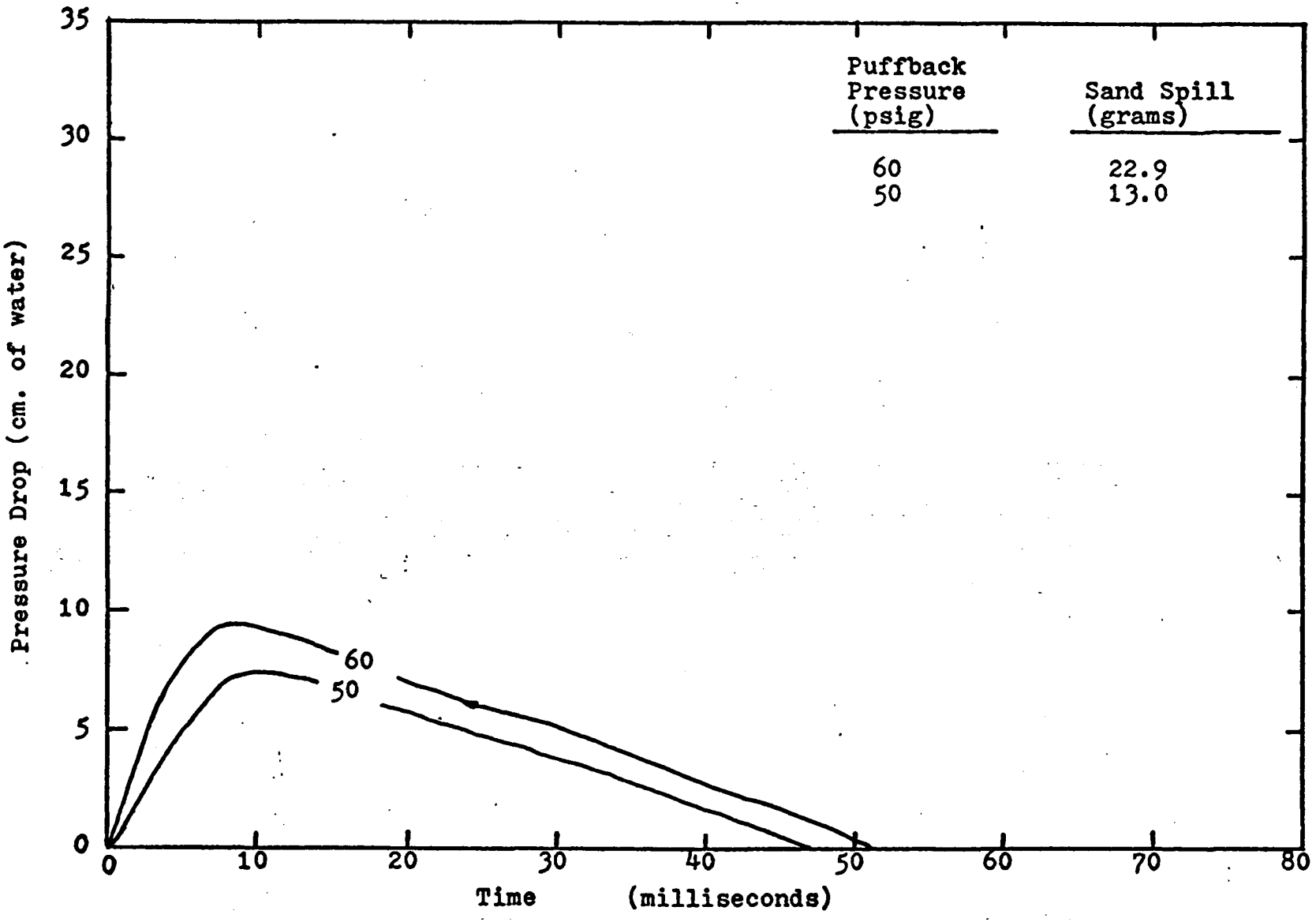

Figure 6.1-27: Pressure Drop Data of A-3-S-1-x-H Series Runs

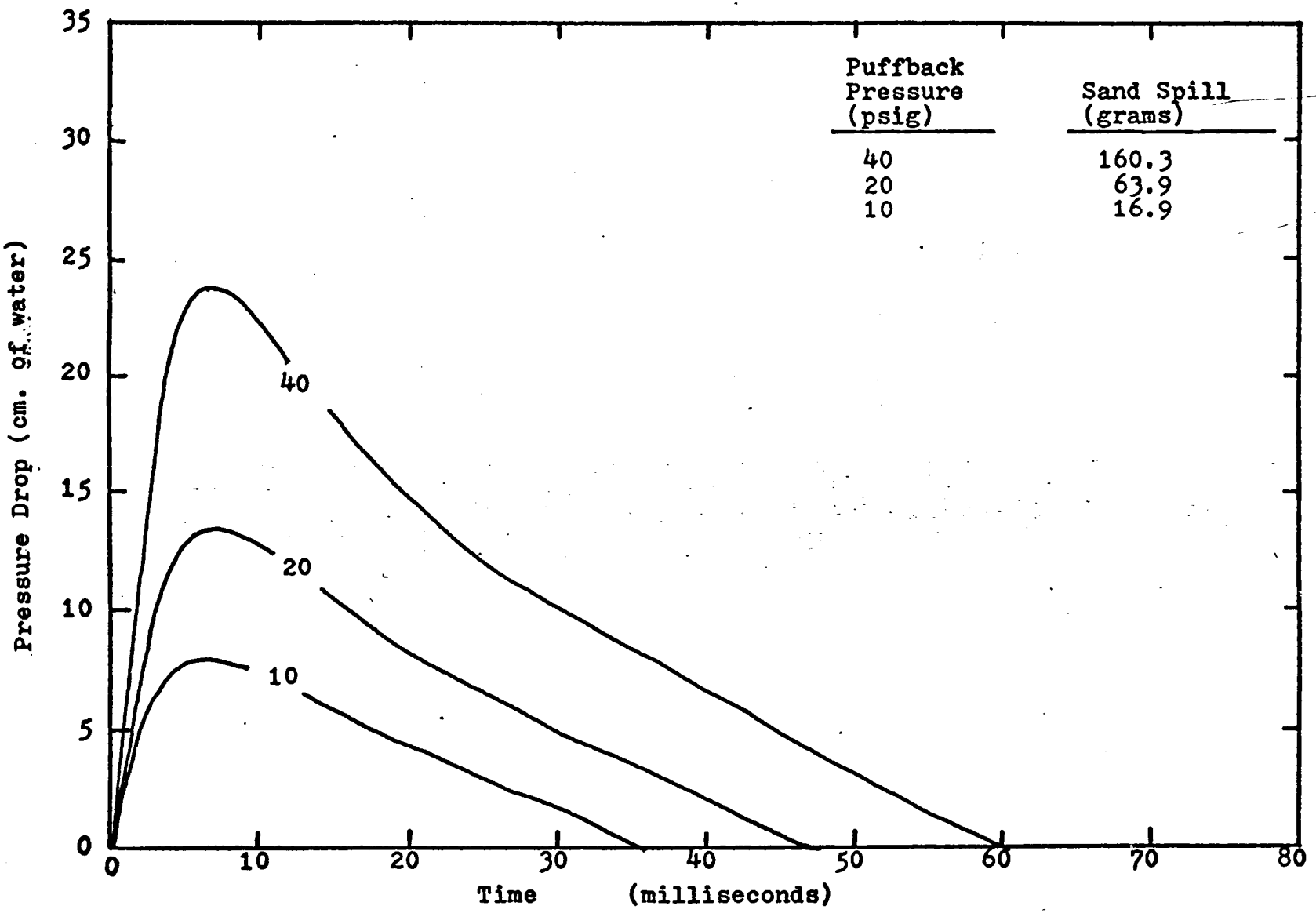

Figure 6.1-28 Pressure Drop Data of C-3-G-2-x-H Series Runs

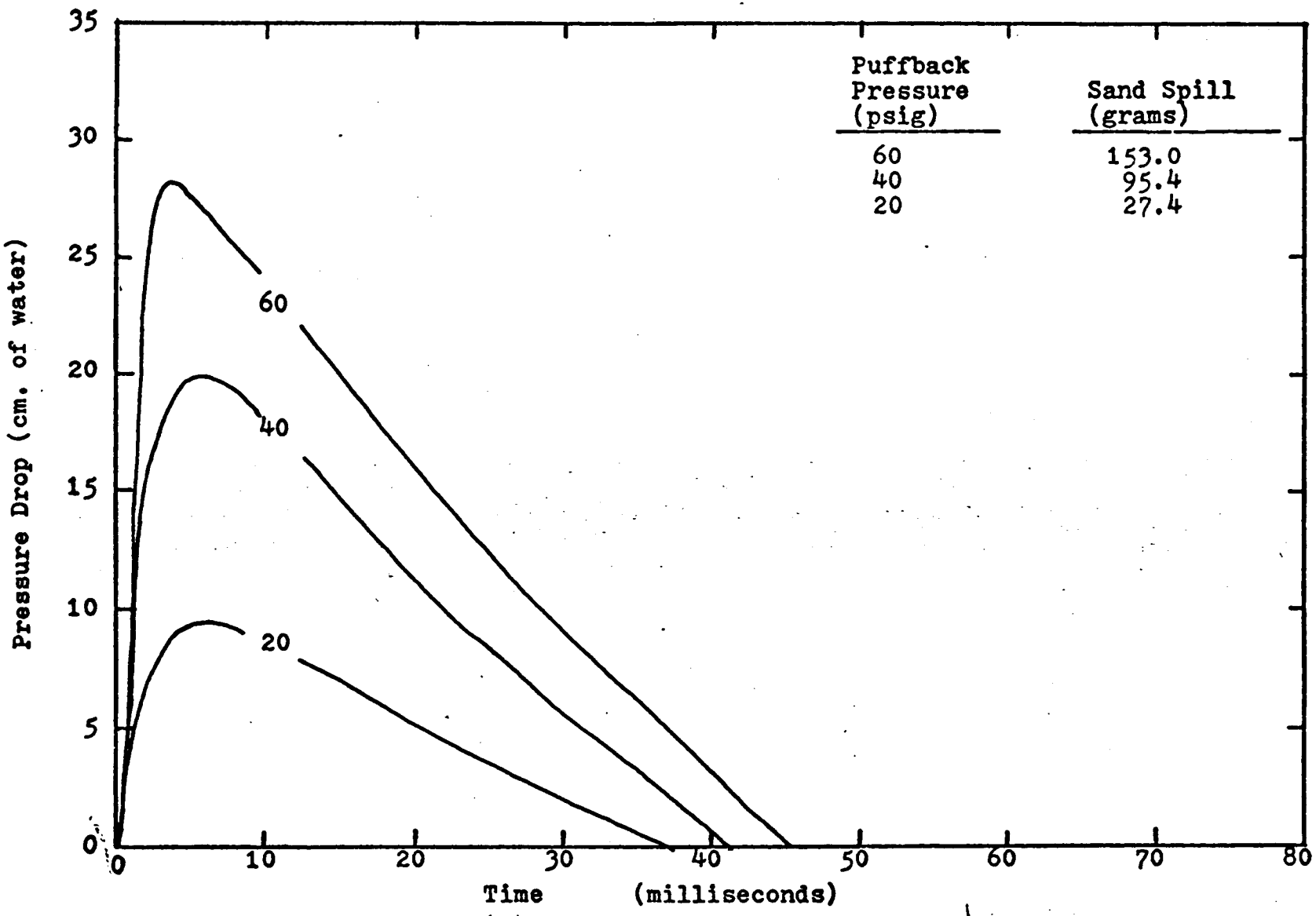

Figure 6.1-29: Pressure Drop Data of C-3-G-1-x-H Series Runs

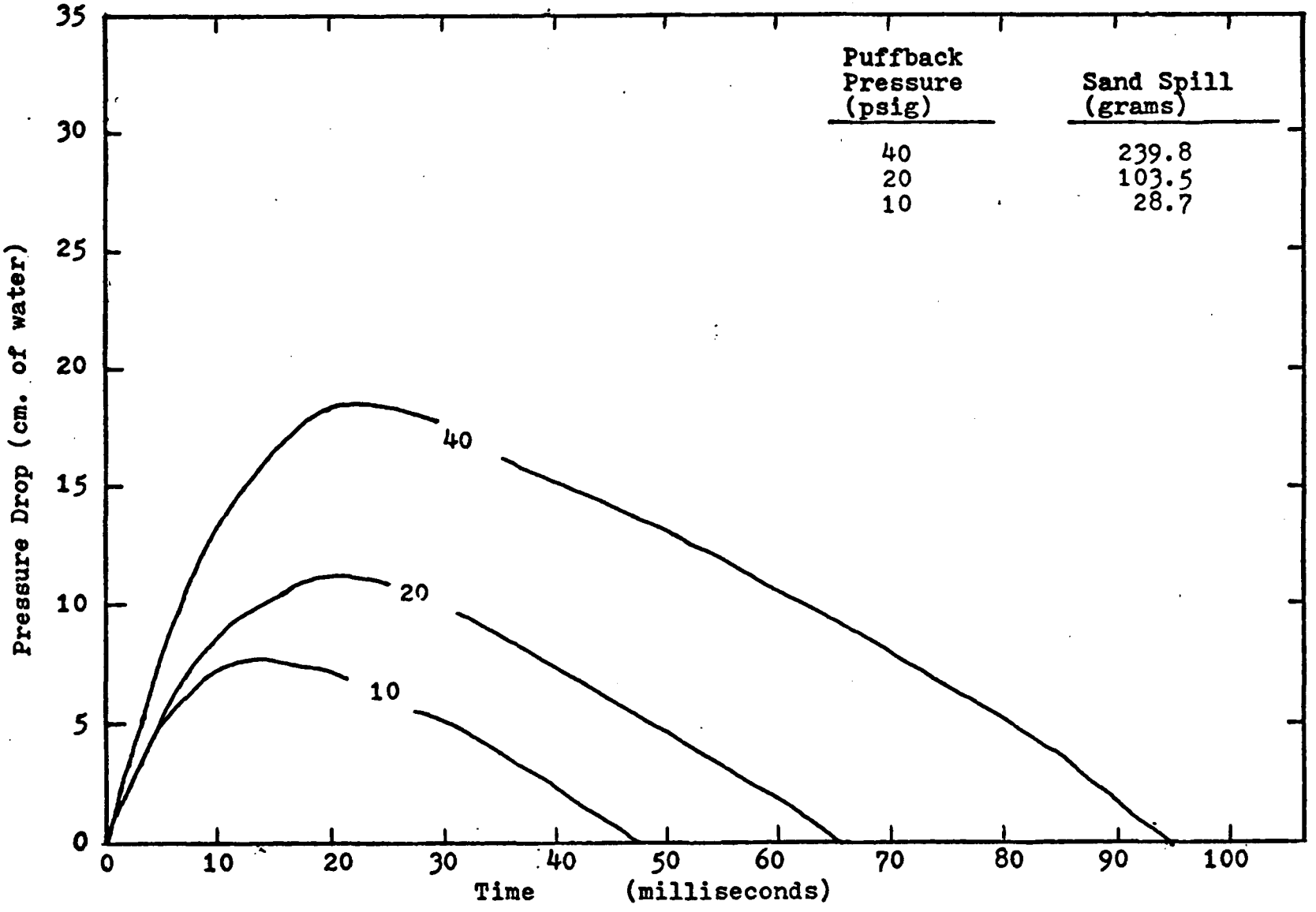

Figure 6.1- 30: Pressure Drop Data of C-3-B-3-x-H Series Runs

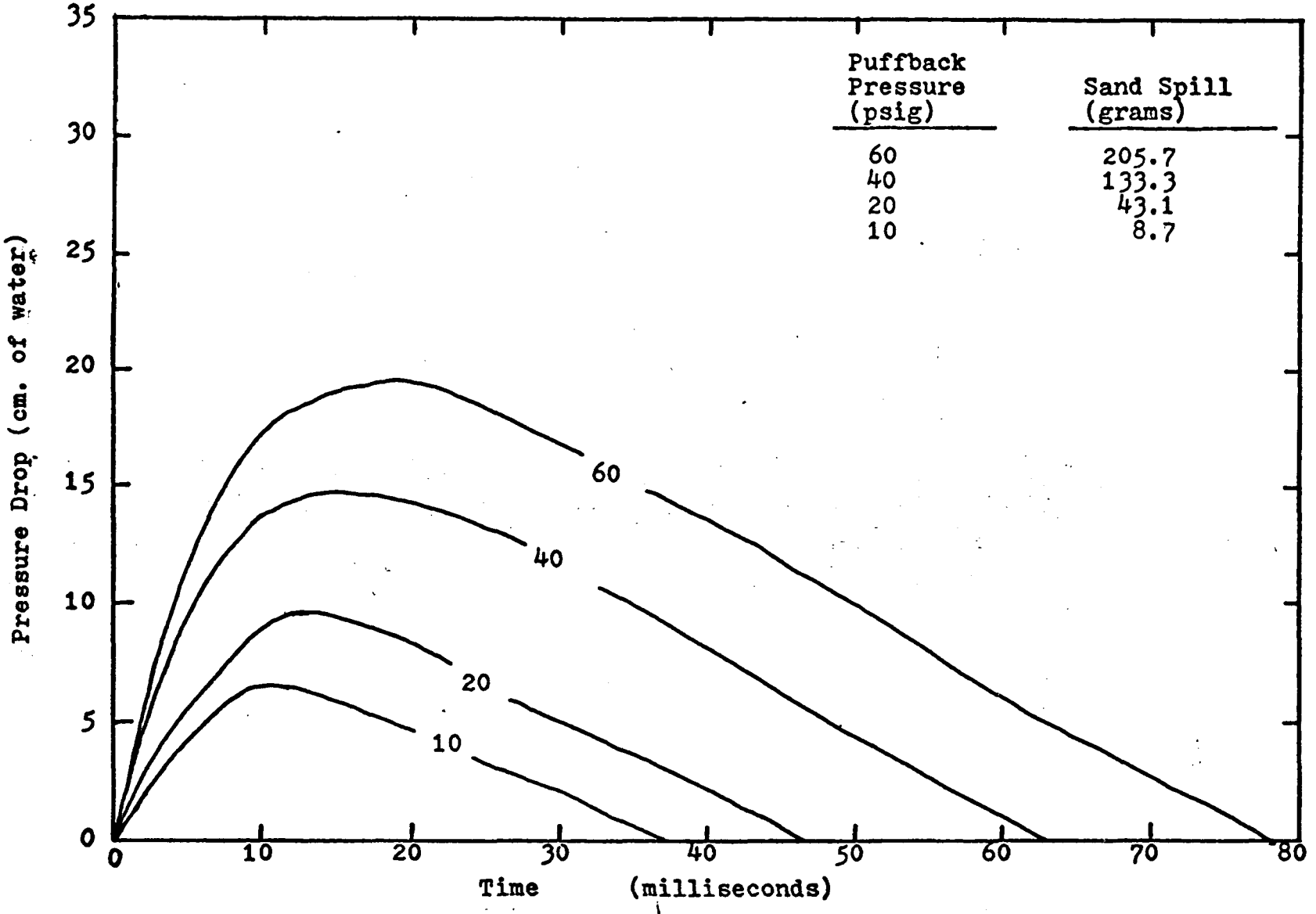

Figure 6.1-31: Pressure Drop Data of C-3-B-2-x-H Series Runs

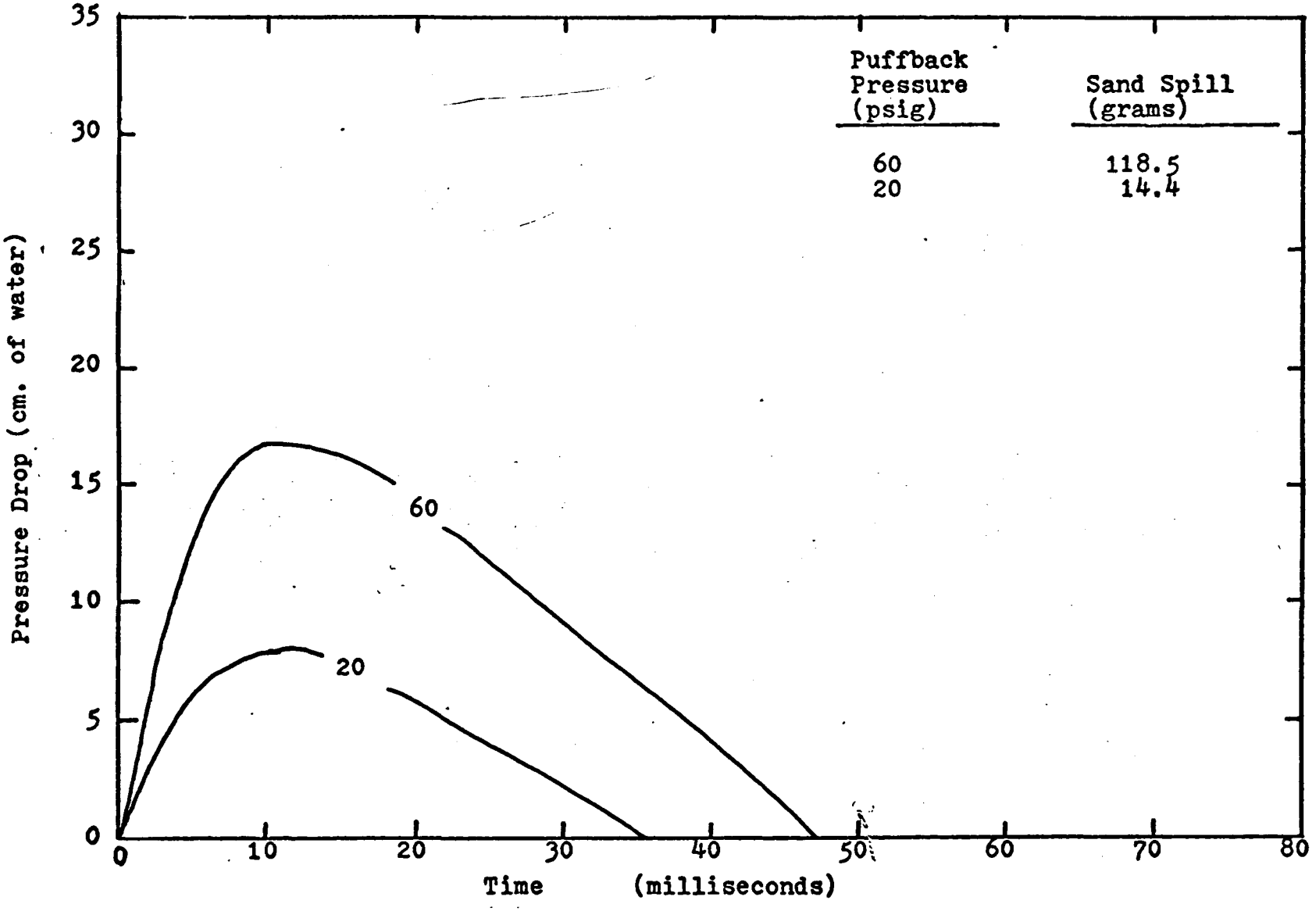

Figure 6.1- 32: Pressure Drop Data of C-3-B-1-x-H Series Runs

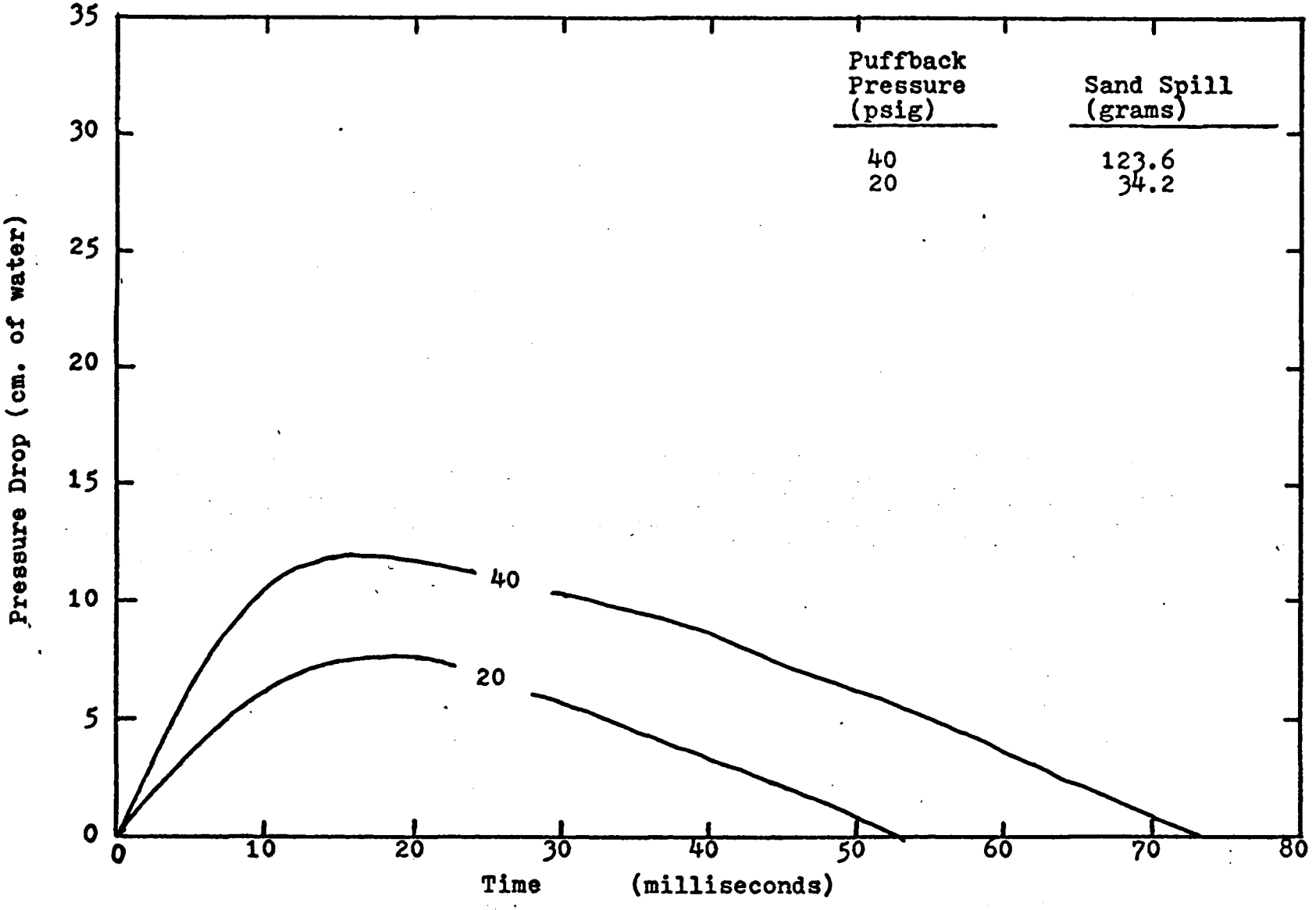

Figure 6.1-33: Pressure Drop Data of C-3-S-2-x-H Series Runs

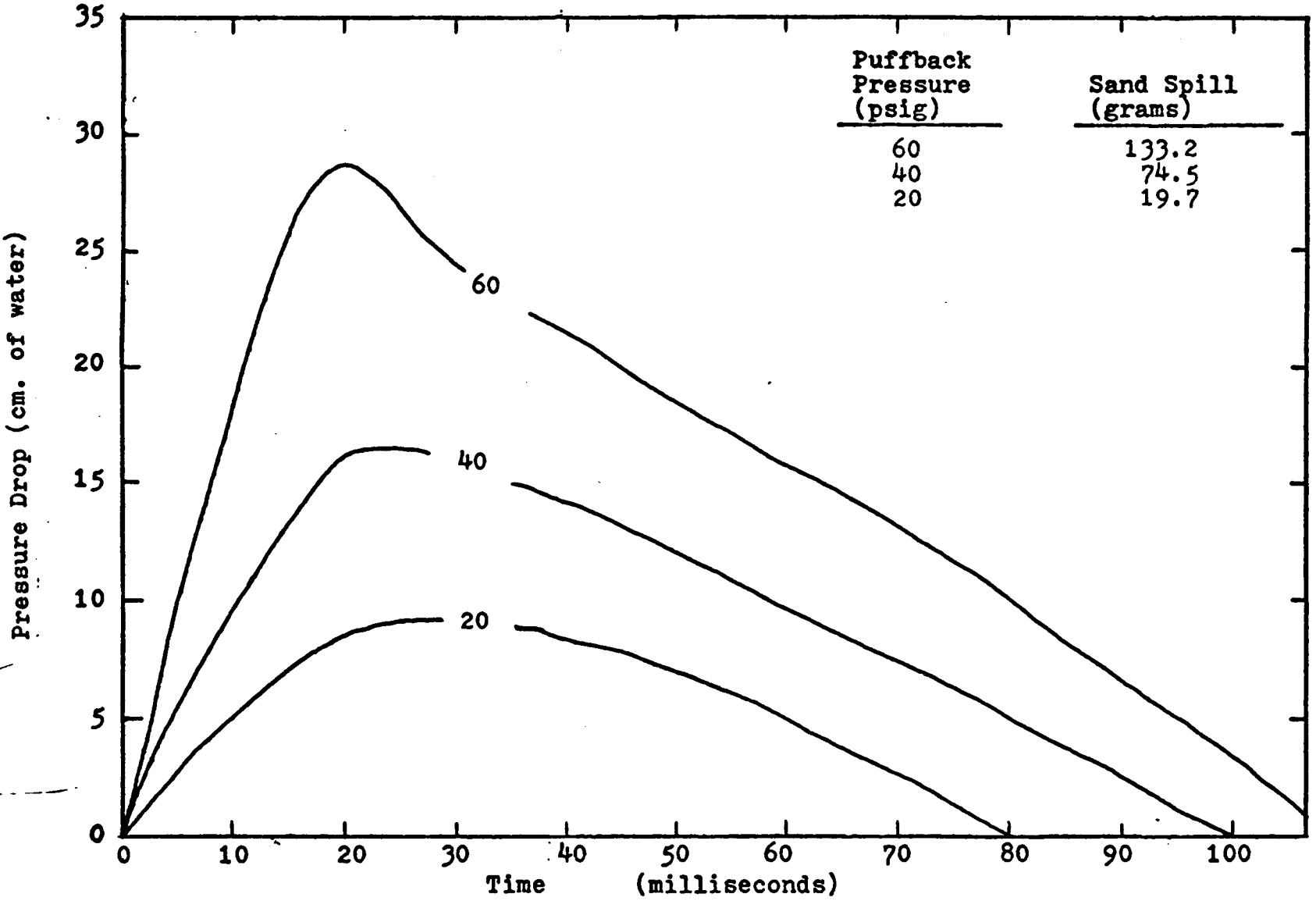

Figure 6.1-34: Pressure Drop Data of D-3-G-4-x-H Series Runs

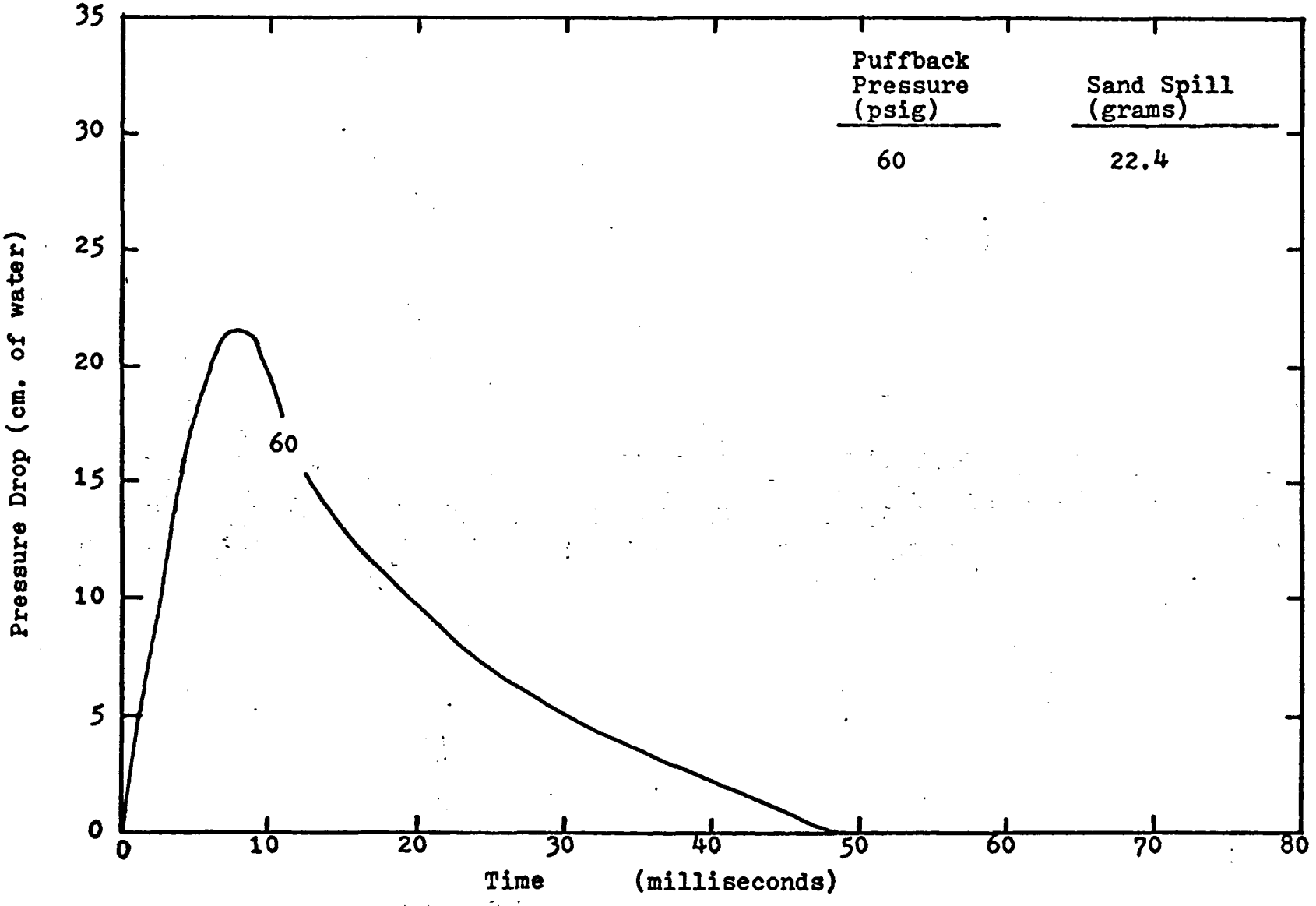

Figure 6.1-35: Pressure Drop Data of D-3-G-2-x-H Series Runs

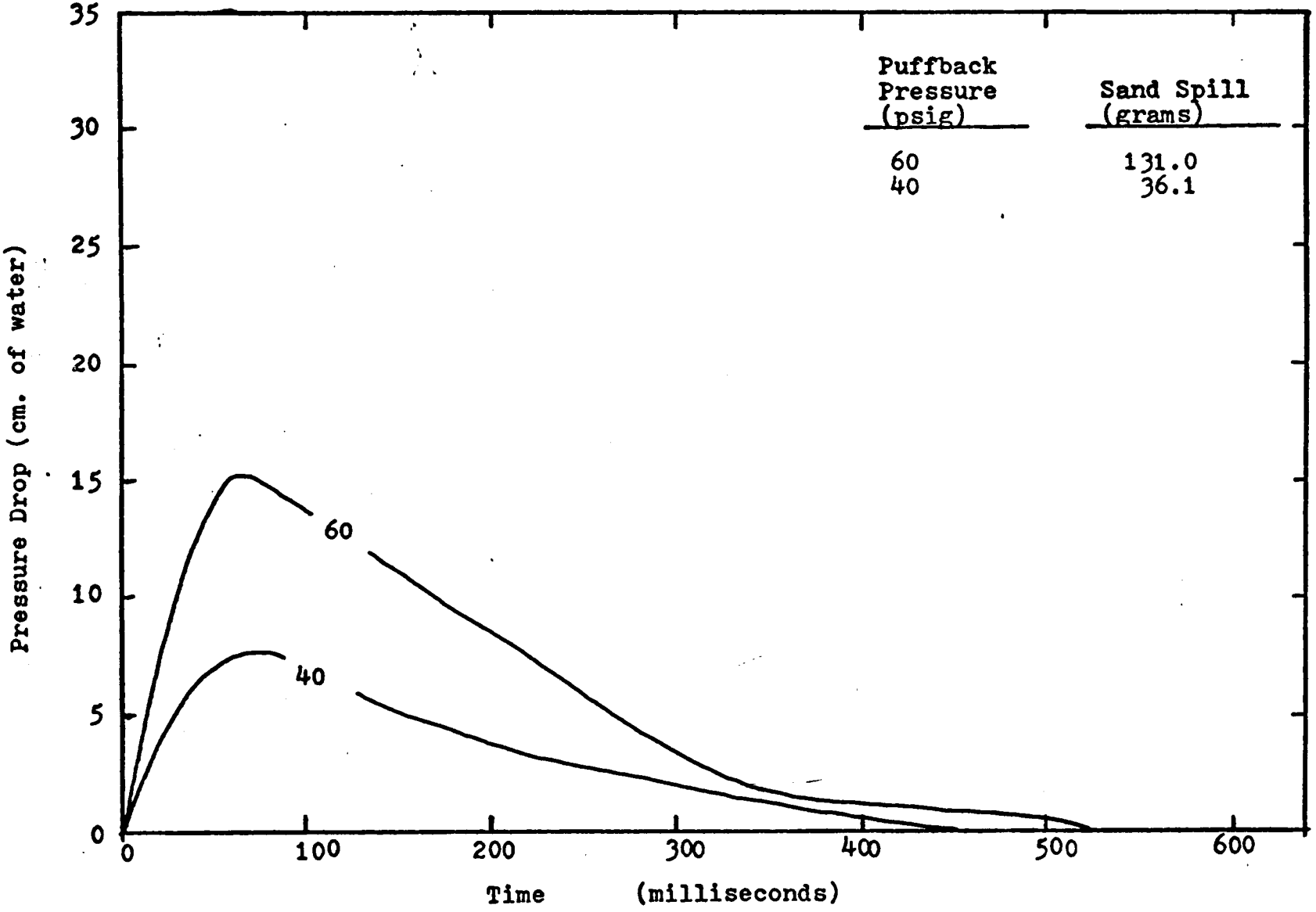

Figure 6.1-36: Pressure Drop Data of D-3-B-5-x-H Series Runs

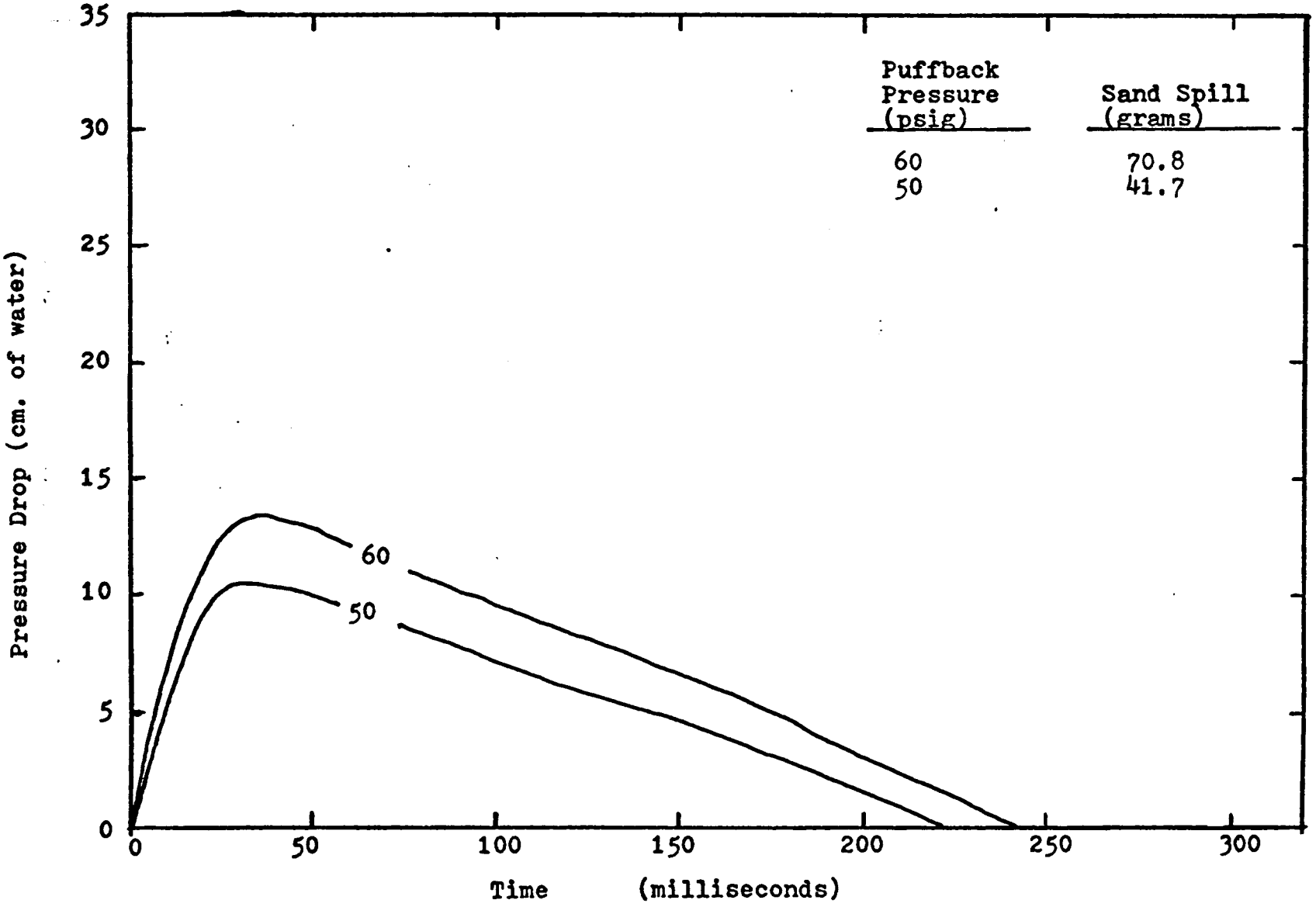

Figure 6.1-37: Pressure Drop Data of D-3-B-4-x-H Series Runs

bouncing inside the tapered section and we used a smoothed curve for data analysis. There were serious errors in smoothing the clean side curves and the dirty side curves. Hence the data for sideshot are not as good as for downshot data.

Figures 6.1-21 to 27 show data on 20-30 mesh sand backed by 10-14 mesh sand. Figures 6.1-28 to 33 show data on 40-50 mesh sand backed by 10-14 mesh sand. Figures 6.1-34 to 37 show data on 10-14 mesh sand backed by 10-14 mesh sand. For the same reason cited in Section 6.1.1.1, the 10-14 mesh sand data were poor. All data for the 1 inch orifice valve were also poor because the shock bouncing was more pronounced resulting in a larger curve smoothing error.

6.2. Puffback Uniformity Test and the Effect of Bed Porosity on Uniformity.

Tests have been conducted for the chevron louvers in the first unit to determine the distribution of spill of sand from various heights of the panel and the effect of puffback strength to the distribution of sand spill. These tests were conducted without filtration. All tests used the 3/16 inch valve (S).

Results for 30-40 mesh sand are given in Table 6.2-1.

In tests at puffback pressure of 15 psig in the No. 2 bottle, after two non-typical puffbacks, the third through eighth puffback afforded a substantially uniform spill of about 1.1 grams of sand per louver. The pressure drop across the panel before the test began was 6.22 cm. of

Table 6.2-1: Sand Spill Distribution over the Panel Height for 30-40 Mesh Sand

Puffback pressure = 15 psig.

Initial pressure drop = 6.22 cm. of water.

Puff No.	1	2	3	4	5	6	7	8
Louver No.*	Sand Spill per Louver Space (grams)**							
- 1	0.03	1.8	0.9	2.3	1.0	2.1	1.0	2.1
2 - 3	0.3	0.9	0.8	1.1	0.95	1.15	0.9	1.1
4 - 12	0.43	0.87	0.98	1.1	1.02	1.05	0.96	1.04
13 - 20	0.21	0.72	0.98	1.15	1.o9	1.14	1.o5	1.11

Puffback pressure = 20 psig.

Initial pressure drop = 7.57 cm. of water.

Puff No.	1	2	3	4	5	6	7	8
Louver No.	Sand Spill per Louver Space (grams)							
- 1	1.8	3.5	3.2	3.4	3.0	3.3	3.0	3.1
2 - 3	2.2	2.7	2.3	2.35	2.3	2.5	2.4	2.4
4 - 12	2.64	2.44	2.25	2.25	2.16	2.29	2.2	2.2
13 - 20	2.17	2.15	2.16	2.19	2.0	2.12	2.07	2.06

Puffback pressure = 25 psig.

Initial pressure drop = 7.01 cm. of water.

Puff No.	1	2	3	4	5	6	7	8
Louver No.	Sand Spill per Louver Space (grams)							
- 1	4.2	4.5	4.6	4.5	4.5	4.1	4.3	4.5
2 - 3	3.95	3.6	3.55	3.65	3.65	3.45	3.41	3.45
4 - 12	4.19	3.61	3.62	3.53	3.47	3.42	3.41	3.45
13 - 20	3.69	3.39	3.36	3.31	3.24	3.2	3.17	3.19

Table 6.2-1: (continued)

Puffback pressure = 15 psig.

Initial pressure drop = 7.08 cm. of water.

Puff No.	1	2	3	4	5	6	7	8
Louver No.	Sand Spill per Louver Space (grams)							
- 1						1.6	1.4	1.6
2 - 3						1.05	1.15	1.15
4 - 12						1.08	1.08	1.14
13 - 20						1.13	1.14	1.16

Final pressure drop = 7.57 cm. water.

* Louver number counted from top to bottom.

** Sand spill per louver space is the average value over the louver number shown.

water at 21 cm./sec. One thing that should be understood is that the initial pressure drop is not a unique value. This pressure drop depends upon how sand is charged to the panel bed filter. A fast dumping of sand will result in a higher porosity, hence, lower pressure drop. That is because the sand grains do not have time to adjust to a stable position. A slow charging of sand will result in a lower porosity, hence higher pressure drop. After the eighth puffback, the pressure drop was 7.57 cm. of water which indicated a decrease in porosity by applying puffback. This is always the case when the puffback intensity is low; the pressure drop across the sand bed is not enough to cause body failure (Section 5.1) and just serves to force the sand bed into a more dense and more stable packing. The sand spill is basically due to local failure. This is similar to the inital stage of porosity change of the sand when undergoing a strain as discussed in Section 2.3.4.3.

For any given puffback condition, the first one or two puffbacks are often non-typical. They serve to move the sand surface from the configuration shown in Figure 6.2-1-a to the configuration shown in Figure 6.2-1-b and change the sand porosity to that appropriate for the given puffback intensity. Thus, the first puffback at 15 psig spilled roughly one-quarter as much sand as the spill observed after the third puffback, and the distribution of the spill on the first puffback was poor.

The spill from the top louver is also non-typical.

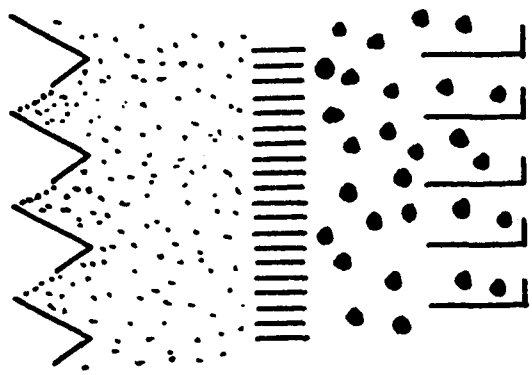

(a) sand surfaces before puffback.

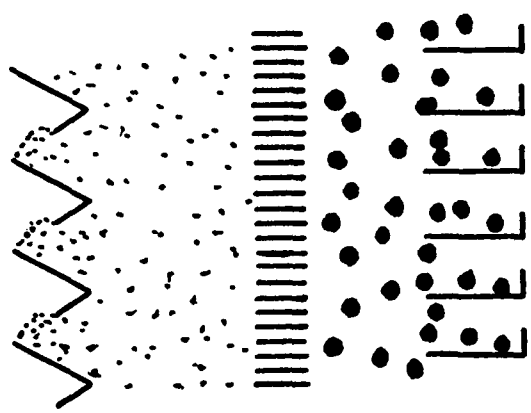

(b) sand surfaces after puffback.

Figure 6.2-1: Change in Sand Surfaces by Puffback.

during the tests at 15 psig, the spill from this louver alternated between roughly the average spill of about 1 gram and a much higher spill, a little over 2 grams. This top effect will be discussed later.

After the tests at 15 psig, a series of eight puffbacks at 20 psig resulted in spills varying smoothly from about 2 grams per louver near the bottom to about 2.3 grams near the top. The pressure drop at 21 cm./sec. fell from the aforementioned 7.57 cm. to 7.01 cm. of water. This decrease in pressure showed an increase in sand porosity. Higher puffback intensity tends to change the sand bed porosity to the ultimate porosity discussed in Sections 2.3.4.2. and 2.3.4.3.

A series of eight puffbacks at 25 psig resulted in a spill of about 3.2 grams near the bottom rising to about 3.5 grams near the top. The pressure drop at 21 cm./sec. was 7.08 cm. of water, substantially unchanged from the drop after the tests at 20 psig.

A repeat series of tests at 15 psig was conducted after the tests at 25 psig. The spills were substantially the same as observed earlier at 15 psig, and the pressure drop was restored to 7.57 cm. of water at 21 cm./sec.

Puffback test of 20-30 mesh sand with the chevron louvers are given in Table 6.2-2. Initial tests at a puffback pressure of 25 psig and using the No.2 bottle produced spills about 50 per cent greater at the top. The amount of sand spill increased gradually from the first puffback to the sixth puffback (Figure 6.2-2) and

Table 6.2-2: Sand Spill Distribution over the Panel Height for 20-30 Mesh Sand

Puffback pressure = 20 psig.

Initial pressure drop = 3.71 cm. of water.

Puff No.	1	2	3	4	5	6	7	8
Louver No.	Sand Spill per Louver Space (grams)							
- 1	.18	.42	.4	.7	.6	.7	.5	
2 - 3	.06	.14	.3	.4	.5	.6	.65	
4 - 12	.05	.11	.19	.31	.39	.44	.49	
13 - 20	.02	.07	.11	.15	.19	.21	.3	

Puffback pressure = 40 psig.

Initial pressure drop = 3.63 cm. of water.

Puff No.	1	2	3	4	5	6	7
Louver No.	Sand Spill per Louver Space (grams)						
- 1	2.9	3.0	3.2	4.2	4.1	3.5	3.7
2 - 3	3.1	3.0	3.2	3.8	3.7	3.25	4.1
4 - 12	3.6	3.6	3.6	3.9	3.7	3.5	3.8
13 - 20	2.5	2.8	2.9	3.0	3.1	2.9	3.1

Puffback pressure = 20 psig.

Initial pressure drop = 3.30 cm. of water.

Puff No.	1	2	3	4	5	6	7
Louver No.	Sand Spill per Louver Space (grams)						
- 1	.1	.6	.4				
2 - 3	.5	.55	.4				
4 - 12	.55	.5	.5				
13 - 20	.5	.5	.5				

Final pressure drop = 3.30 cm. of water.

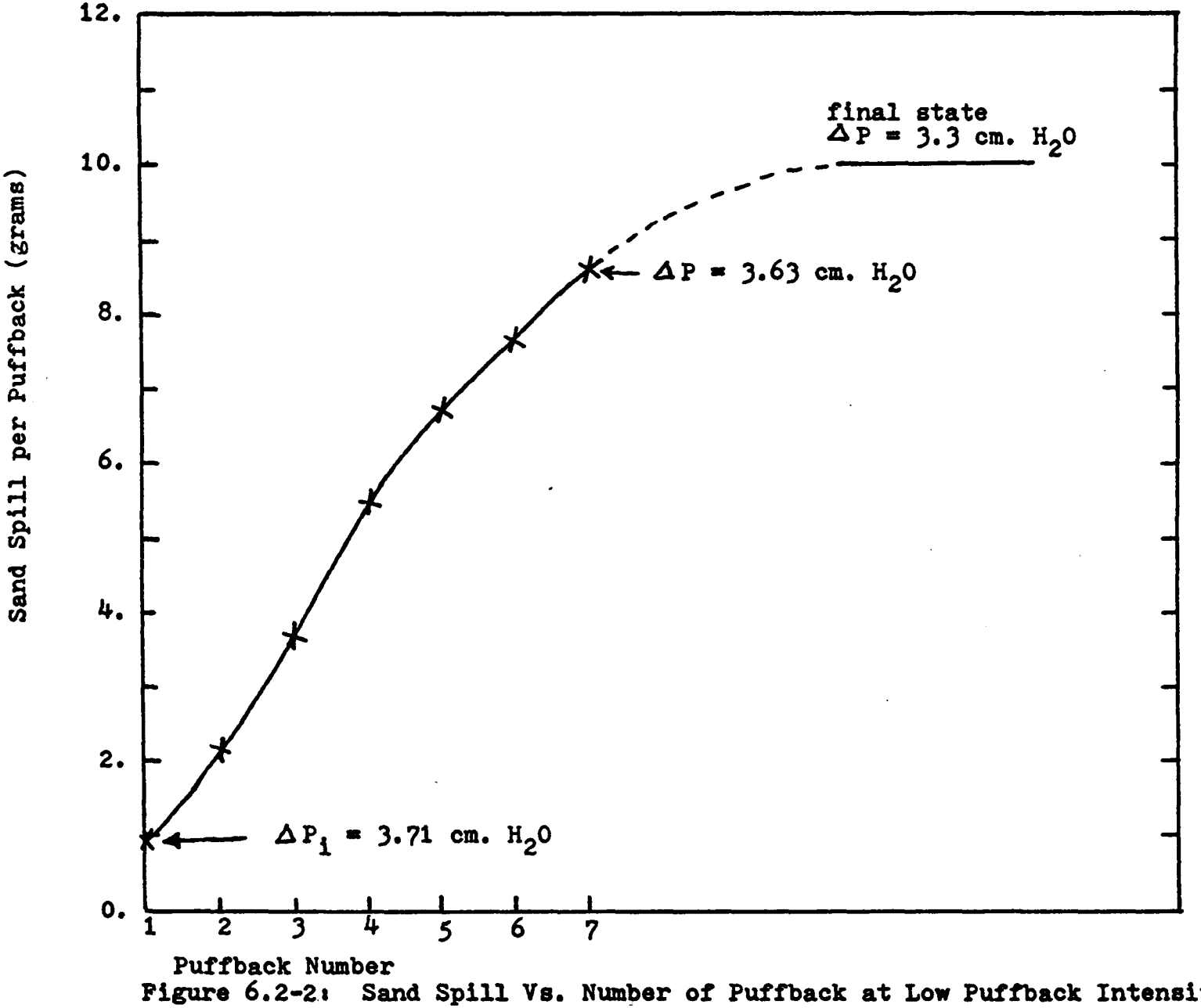

Figure 6.2-2: Sand Spill Vs. Number of Puffback at Low Puffback Intensity.

the pressure drop changed from 3.71 cm. of water to 3.63 cm. of water at 21 cm./sec. apparently still not reaching steady state after six puffbacks.

A series of seven puffbacks at 40 psig were then applied. These resulted in a spill of about 3.0 grams at the bottom rising to about 3.7 grams near the top. The pressure drop decreased further to 3.30 cm. of water.

After this test, a series of puffbacks at 20 psig showed a uniform spill of about 0.5 grams per louver and the same pressure drop (3.30 cm. of water) which was measured at 40 psig puffback pressure, thus indicating that the final steady state packing configuration had been reached.

Puffback tests for 40-50 mesh sand with the chevron louvers produced data similar to that shown in Tables 6.2-1 and 6.2-2.

From the above data, we draw the conclusion that at low puffback strength it is difficult to reach the final state configuration whereas this condition can be accelerated by several intense puffbacks. In other words, going from low puffback pressure to higher puffback pressure takes a long time to reach a steady state. But, going from high puffback intensity to low puffback intensity produces a steady state rapidly. Figure 6.2-2 shows the slow progress to steady state using the chevron louvers for 20-30 mesh sand at low puffback intensity. Another way of accelerating the porosity change process to the final steady state is by opening the bottom plug of the fine sand column and

dumping some of the sand. This will loosen up the sand bed and is similar to loosening the sand bed by a high intensity puffback.

All the above phenomena can be explained by considering the local change in sand porosity within the sand bed. After puffback sand spill, the sand in the bed will move down by gravity to fill up the vacancy left by the sand spill. This downward motion will be largest near the top louvers with almost no downward motion near the bottom louver spaces. This fast downward motion is similar to that of fast dumping the sand into the container and will loosen up the sand packing if the puffback intensity is high enough. The change in sand bed volume during puffback is much more complicated than the volume change produced by shear force alone (See Section 2.3.4.3.), since there is also air flowing within the pores and the pressure drop across the bed is a cummulative effect of the drag force acted on each individual grain of sand by the air flow. The shear forces at different depts of sand bed will thus be different. Generally, the change in porosity after puffback settling can be understood qualitatively as depicked in Figure 6.2-3.

The loosening up of the sand packing by puffback sand spill when the puffback strength is high enough to produce body failure was indicated by the pressure drop change discussed above. Also, the porosity change could be seen in our transparent unit. From soil mechanics, we know that the sand motion is governed by the plane of

failure. Below this plane of failure sand will remain stationary. We can see this plane of failure at the bottom of the panel bed filter as shown in Figure 6.2-4 at an angle of about 68° from the horizontal. This line was marked by two regions of different porosity. Below this line the sand packed at the original density and was stationary. Above this line the sand packed at the looser density produced by puffback failure.

From Section 2.3.4.2 we know that lower initial porosity will have higher soil strength and vice versa. This explains the slow progress in puffback when starting from low puffback intensity and the fast progress in puffback when starting from high puffback intensity. After the sand bed has been loosened by a high intensity puffback the soil strength decreased and the porosity increased. This made the sand bed much easier to achieve its final configuration for low intensity puffback.

Another thing we learned from the above uniformity test is that at relatively low puffback intensity we can get a very uniform sand spill distribution except from the topmost louver space. At high puffback intensity we always obtained slightly more sand spill near the top than at the bottom. This can be also explained by the porosity change during puffback before the sand bed settled down. From transducer data we know that higher puffback intensity is always accompanied with a longer tail or longer duration time. Hence, the time period for body failure to occur

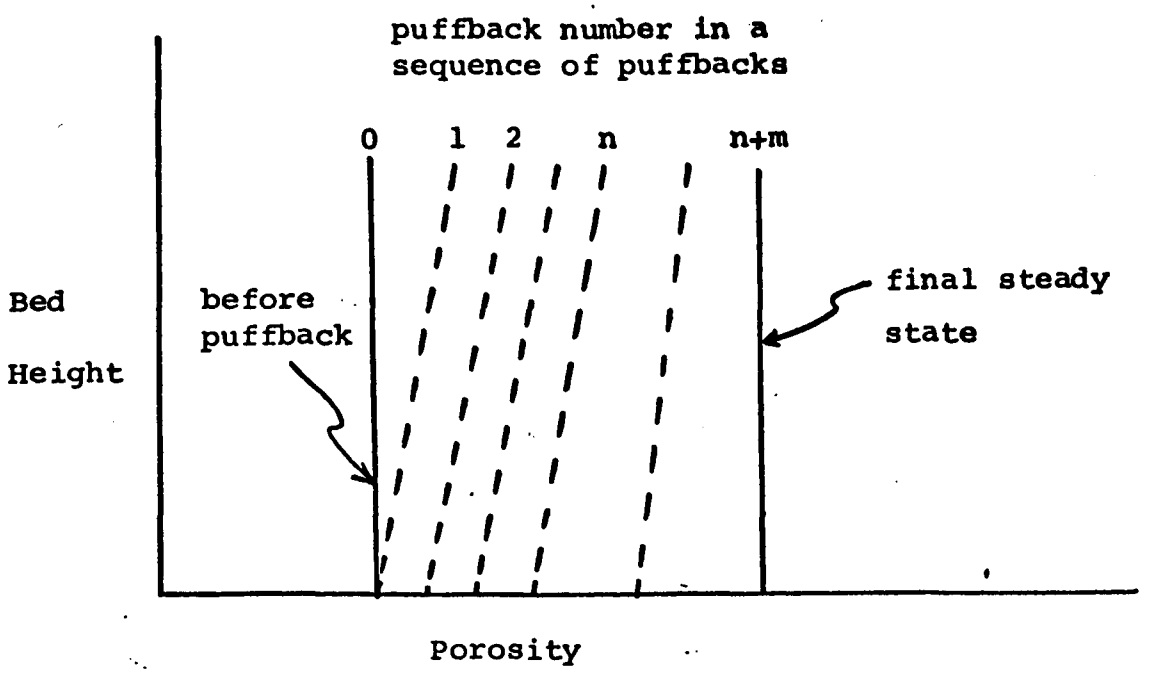

Figure 6.2-3: Porosity Change after Puffback Settling.

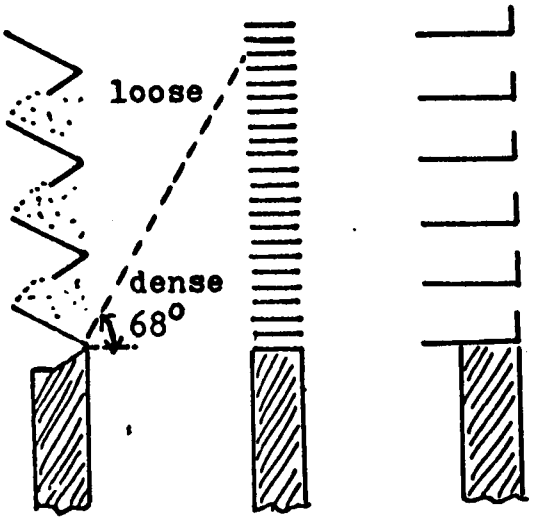

Figure 6.2-4: Observed Porosity Change Due to Puffback.

will be longer too. The period will be so long that the later portion of body failure will progress at a different porosity at different portions of the sand bed as shown in Figure 6.2-5. This will result in slightly more spill from the top since the top of the bed has a lower porosity before the bed can settle down. For panel bed filtration puffback, we are interested in the low puffback intensity range, so that the body failure should occur within 15 milliseconds, say. If higher puffback intensity is required as in a solid-gas reactor, this difference can be corrected by suitable design of the dirty side louvers.

There are two reasons for the special case of the topmost louver space. First, as discussed above, the porosity during puffback will be the loosest at the topmost louver space. This will result in more spill at the topmost louver space. The second reason is due to the design of the louver system as shown in Figure 6.2-6. We put all the louvers at the same height without considering the relative position of each individual louver space. As shown in the Figure, the topmost space will receive twice more air flow than the rest of louvers. This is probably the major reason for the difference in sand spill for the topmost louver space. We tried to put in a hood inside the front louvers to add more resistance to the air flow at top. This arrangement did decrease the amount of sand spill at the topmost space. By adjusting the depth of the hood plate into the topmost louver space, we could control the resistance

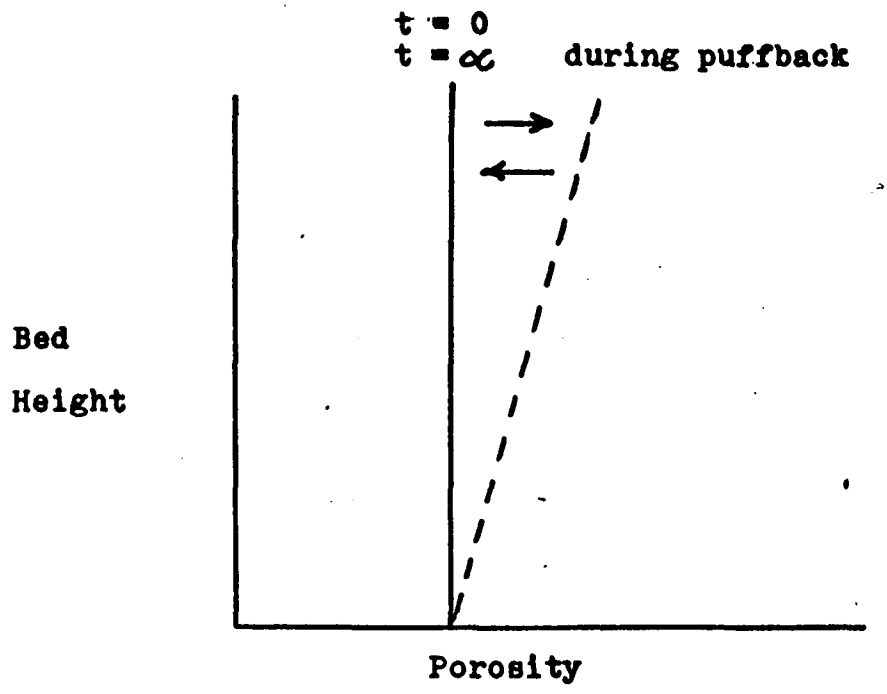

Figure 6.2-5: Porosity Change During Puffback.

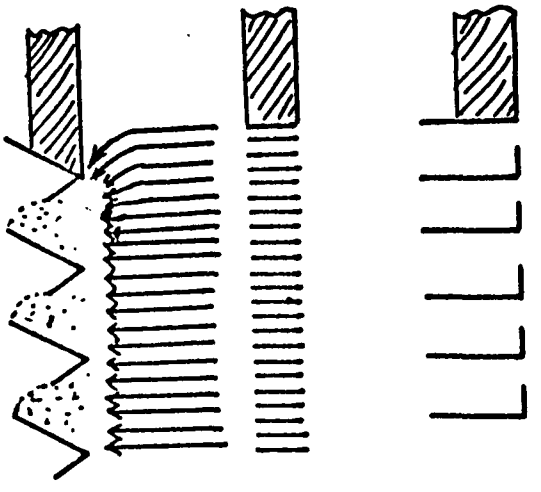

Figure 6.2-6: Top Effect Due to Wrong Design.

at the top and adjust the amount of sand spill at the topmost space. A better way to accomplish this, of course, would be by adjusting the relative height of the louvers.

Chapter 7: Miscellaneous Experiments

This chapter presents further information on filtration and puffback in the panel bed filter. Section 7.1 to 7.3 presents the equipment and data for a horizontal sand bed study. These include aerosol penetration studies and some filter aid studies. Section 7.4 shows failure tests by steady blow back which are important in order to understand how puffback works. Section 7.5 shows the sand level propagation time within the panel bed filter.

7.1. Equipment and Procedures for Aerosol Penetration Test.

Yu (53) extended Paretsky's (34,35) light aerosol penetration test through clean sand in a horizontal bed. Yu's data will be discussed in detail in Section 7.2. We also made additional aerosol penetration tests through different filter cakes which will be discussed in detail in Section 7.3. In this section, we will discuss the apparatus and procedures for the aerosol penetration tests.

Figure 7.1-1 illustrates the sand bed holder adopted for our work. We call it a horizontal bed because of its horizontal free sand surface. Tapered entrace and exit sections precede and follow the sand bed, which is retained on a 100-mesh wire screen. The internal angle of each tapered section is 6^{o}. These tapered sections were designed to avoid loss of the test aerosol in entrance and the exit to the bed. For all the tests the sand bed height was 7.5 cm. (3 inches).

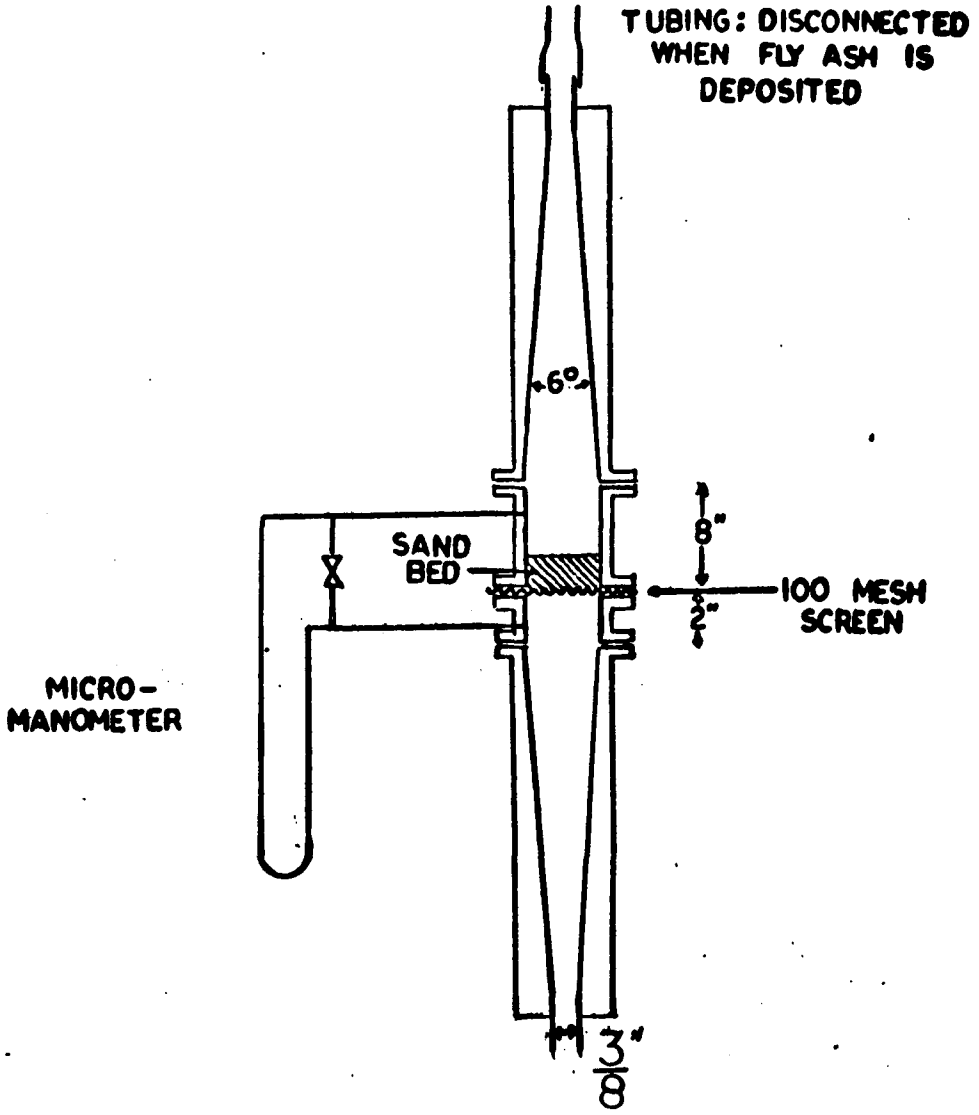

Figure 7.1-1: Horizontal sand bed test section.

Two horizontal sand beds were used, one having a test section diameter of one inch and the other two inches. For the clean sand penetration test studies, we used both the one inch and the two inch tapered sand bed. For the filter cake penetration studies, we used the two inch tapered sand bed only.

Figure 7.1-2 is a schematic diagram of the experimental setup. A filter removes oil, water, and dust from compressed air; a bed of molecular sieves dries the air to a dewpoint below -100^{0}F. A 100 mμ millipore filter following a pressure regulator removes any remaining dust particles.

An AEC-MRL aerosol generator produces an aerosol of 1.1μ polystyrene microspheres. In this generator, air at high pressure is forced through four 1/64 in. holes at the bottom of a metal tube immersed in a suspension of polystyrene micorspheres supplied by the Dow Chemcials Company. The aerosol mist leaving the flask is mixed with a dry "bypass" air stream to vaporize droplets of water. The excess aerosol stream was discharged and the flow rate was monitored by a rotameter. The inlet aerosol concentration was of the order 10^{-5} grams/m.^{3} (about 50 particles / cm.^{3}).

The aerosol concentration was monitored with a Royco Model 220-4 sensor with a Model 263 digital display manufactured by Royco Instrument Co., Menlo Park, California. Since the pump on the Royco operated at only one flow rate (about 3 liter per minute), it was necessary to divide the bed or bypass effluent stream into two portions in order to investigate higher flow rates.

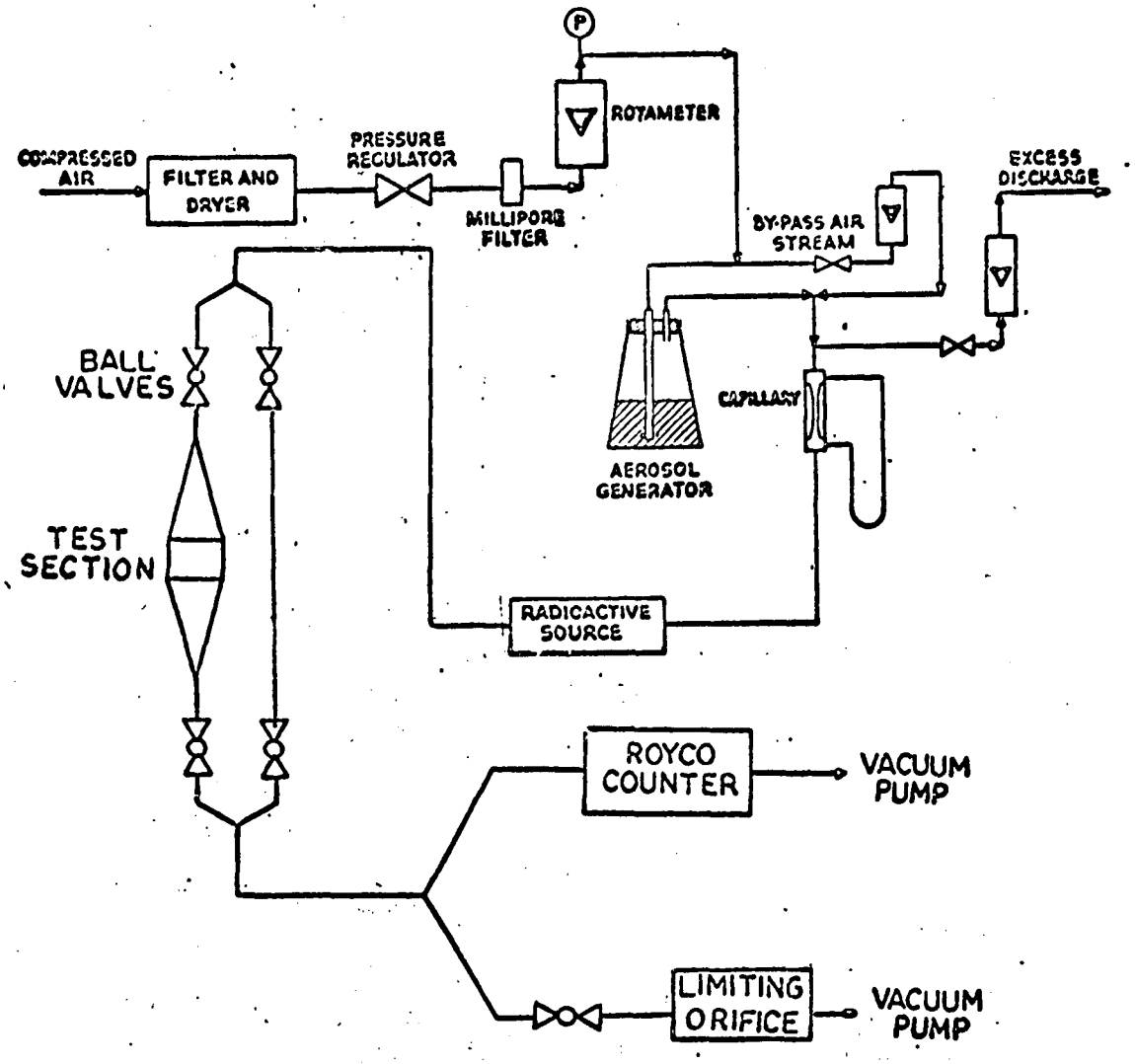

Figure 7.1-2: Schematic of Horizontal Bed Experimental Apparatus.

A 50 microcurie foil of Am^{241} was installed as shown to remove electrostatic charges from the aerosol. Leaving the radioactive source, the aerosol flows through 3/8 in. ID Tygon tubing to the sand bed test section. At approximately 5-10 minute intervals (larger intervals were used at lower velocities) we switched the aerosol from the test section to the bypass of Tygon tubing. Comparison of Royco reading through the test section and through the bypass gives the penetration through the sand bed and/or filter cake, after a correction for the loss observed earlier in a "blank" test section with no sand bed present.

In the clean sand penetration tests, the air flow rate was monitored at high flow rates by a rotameter, and at low flow rates by measuring the pressure drop across a 3/32 in. capillary. At very high velocities, the air velocity in the test section and that in the bypass section are quite different due to the big pressure loss in the sand bed. In order to have the same air velocity during the penetration tests and during the blank tests the bypass tube was removed at high velocities. The blank tests were sampled directly from the upstream of the test section before the air entered the tapered section.

In order to study the mechanics governing the formation and retention of a filter cake on a free surface of a granular solid, e.g. sand, we ran some preliminary experiments, whereby a layer of fly ash or another powder was deposited on a horizontal surface of a sand bed. We used a dilute

1.1 micron monodisperse aerosol of polystyrene microspheres as a probe to explore the nature of a deposit of filter cake at different thickness upon free surface of sand. Fly ash and other powders were deposited onto the sand surface of 20.3 $cm.^2$ (the two inch ID bed) in small increments through the top of the tapered section. After each incremental addition of fly ash or other powder, the pressure drop across the unit and the penetration of the test aerosol of the 1.1 micron monodisperse polystyrene microspheres through the filter cake and sand bed were measured. The inlet aerosol concentration was of the order of 10^{-5} grams per cubic meter or 50 particles per cubic centimeter. The aerosol concentration was monitored by the Royco Particle Counter.

In order to deposit dust onto the sand surface at the same air velocity as the test velocity, we used a different method to control and measure the air velocity than that described above. A 0.45 micron Millipore filter placed in a limiting orifice was installed and followed by a vacumn pump as indicated in Figure 7.1-2. The limiting orifice was also manufactured by the Millipore Co. This was a simple way to maintain a constant flow rate through the horizontal test section and obtain the overall fly ash collection efficiency of the sand bed.

Fly ash or other powders were passed through a 100 mesh wire screen which was placed on top of the tapered section when depositing the powder and was removed afterwards. The use of the wire screen produced a finer and more dispersed

deposit. The fly ash and other powders were allowed to fall onto the sand surface through the top of the tapered section about 65 cm. from the sand surface with the assistance of an electric vibrator and with the assistance of room air that was passed through the bed at a flow rate equal to the flow rate at which pressure loss and aerosol penetration measurements were to be performed. The air flow rate was controlled by the limiting orifice and the vacumn pump as described before. The filter cake will crack by any back pressure produced inside the test section and by a relatively strong shock impaction. Hence, we must be very careful in opening and closing the valves.

Several powders were used in the filter cake penetration test as described below:

Fly ash: Donated by Consolidated Edison Company of New York. This is the same material we used in our panel bed filtration tests except the ash has been sieved by a 120 mesh screen.

Perlite: Donated by Dicalite Division, Grefco Inc., Los Angeles, California. Two grades were used: Perlite 426 with average size of 4.2 microns and Perlite 4156 with average size of 15.0 microns.

Teflon: Donated by Liquid Nitrogen Processing Corp., Malvern, Pennsylvania. One grade was used: TL-102 which has a particle size range of 3 to 8 microns.

Fly ash was deposited onto the sand surface in increments of 0.25 grams. This is equivalent to a weight

of ash deposited per unit area of sand bed of 0.018 grams/cm.^{2} Perlite and Teflon powder was deposited onto the sand surface in increments of 0.15 gram or 0.007 gram/cm.^{2}

7.2. Dilute Aerosols Filtration Tests by Sand Bed.

Yu (53) repeated Paretsky's experiment on the filtration of dilute aerosols by a horizontal sand bed (Section 2.1.4.1.) and extended the veolicty range to 300 cm./sec. in order to study the granular bed filtration phenomena at high velocities. The test sand bed height was 8.2 cm. for all the tests and three sand sizes were used, 10-14 mesh, 30-40 mesh and 40-50 mesh. Both washed and unwashed 40-50 mesh sand were studied. The flow direction of aerosols was downshot with face velocities between 5 cm./sec. to 10 cm./sec. in a two inch diameter bed and with 10 cm./sec. to 300 cm./sec. in a one inch diameter bed.

The penetration of aerosol was plotted against velocity in Figures 7.2-1,2, and 3 for the three sands respectively. The existence of a velocity of maximum penetration observed by Thomas and Yoder (47) and Paretsky (34), is clearly illustrated by these figures.

The aerosol penetration dropped sharply after the maximum point and showed a minimum penetration at high velocities. For washed 30-40 mesh sand and at a vleocity of about 190 cm./sec., there were no counts on the Royco Counter for 10 minutes. Hence, we were not able to determine the penetration, and this velocity range is indicated by

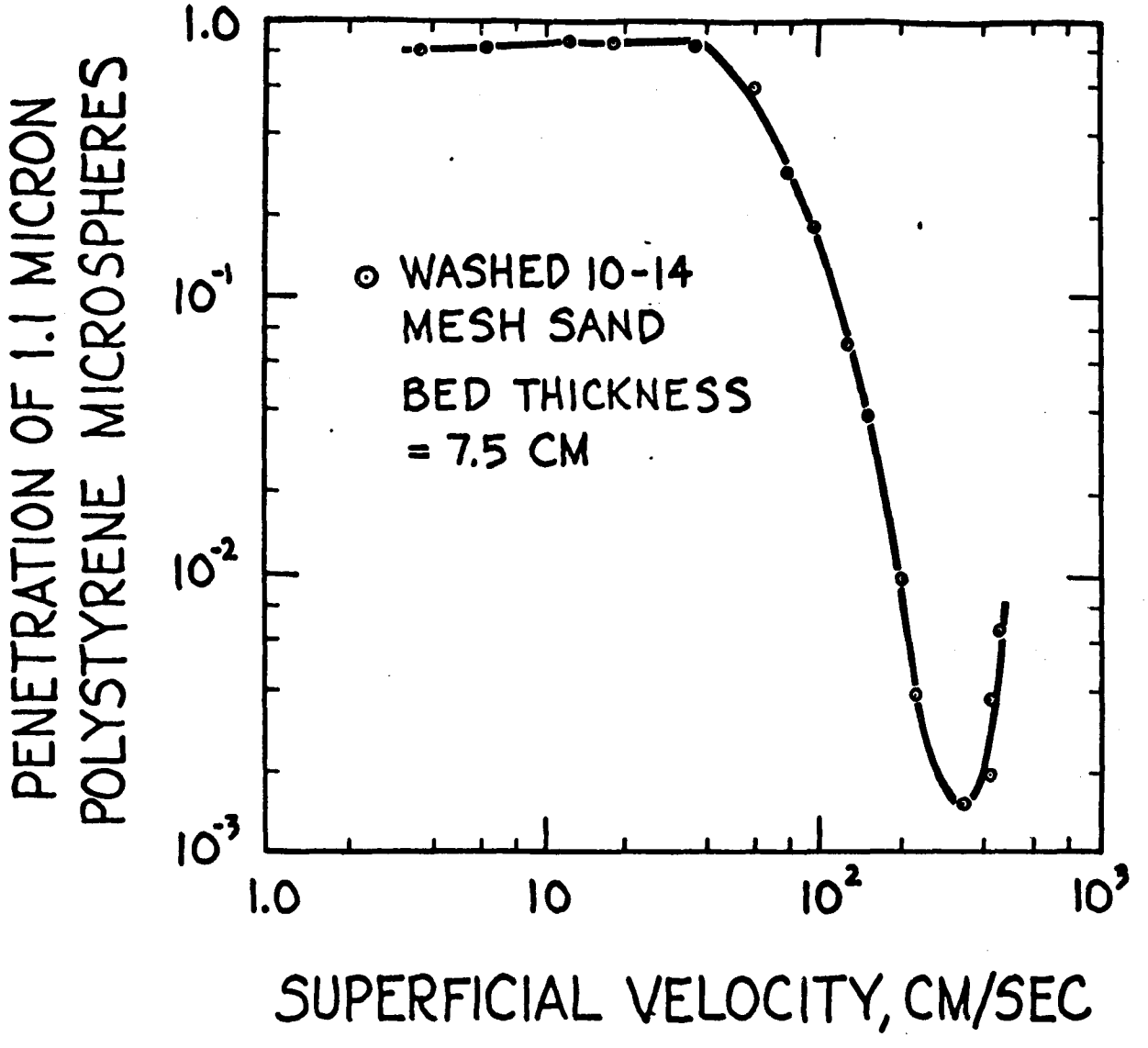

Figure 7.2-1: Penetration of Monodisperse Aerosol by 10-14 Mesh Sand.

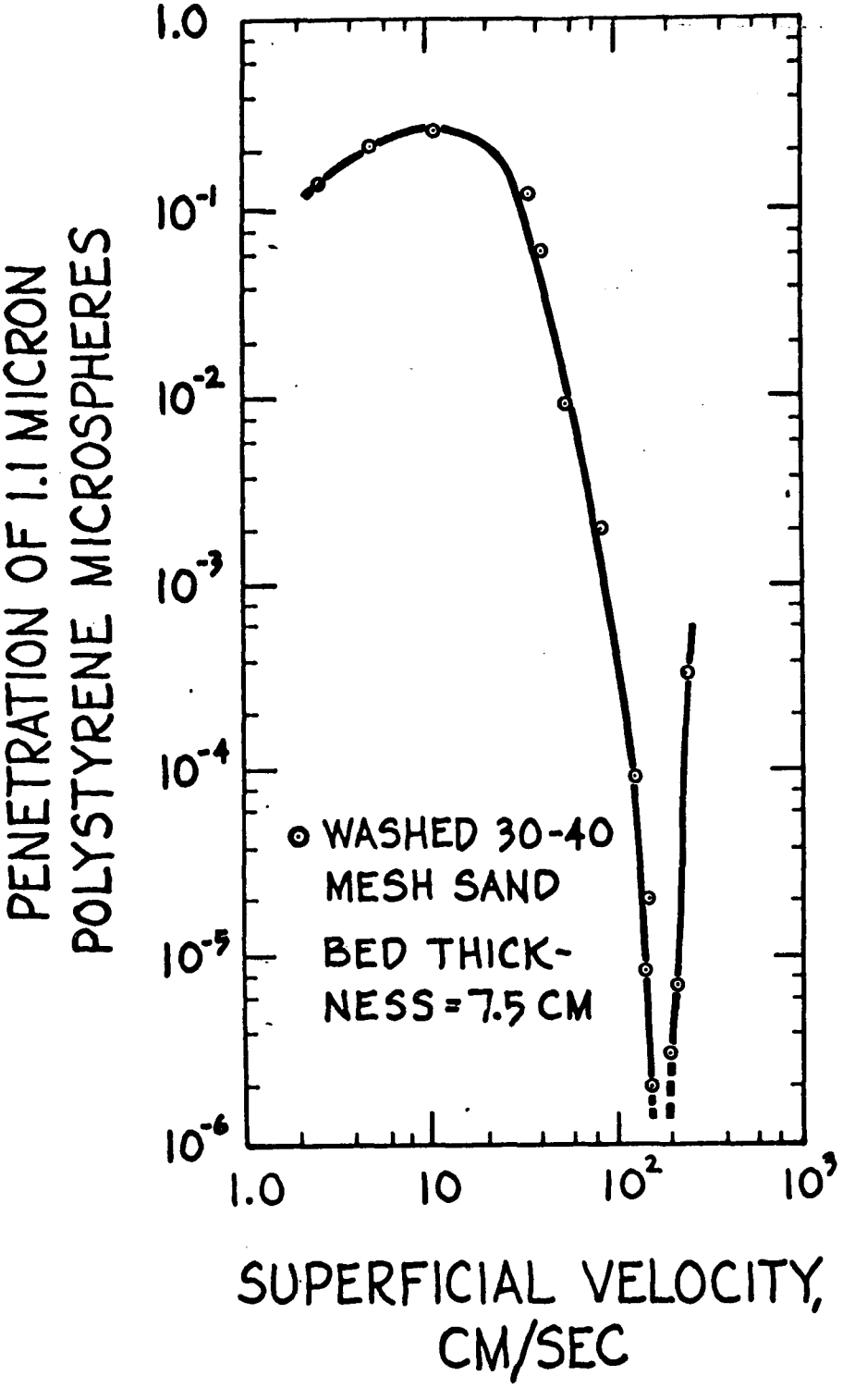

Figure 7.2-2: Penetration of Monodisperse Aerosol by 30-40 Mesh Sand.

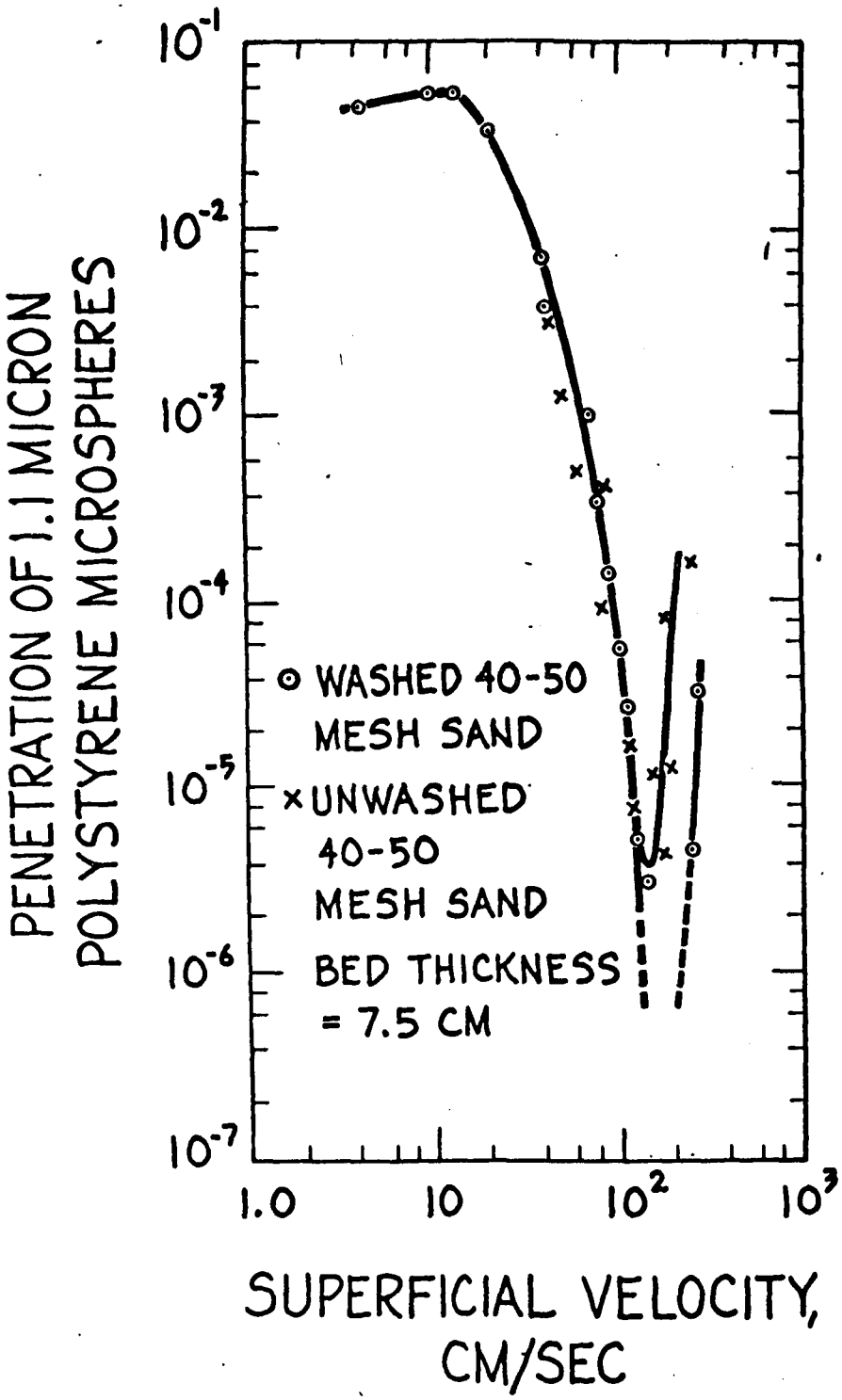

Figure 7.2-3: Penetration of Monodisperse Aerosol by 40-50 Mesh Sand.

the dotted line in Figure 7.2-2. The same phenomenon was observed for 40-50 mesh sand and at velocities between 150 cm./sec. to 240 cm./sec. This range is also indicated by the dotted line in Figure 7.2-3.

The penetration started to rise at velocities somewhat beyond the velocity for minimum penetration. The minimum penetration was markedly higher for unwashed sand than for the washed sand (Figure 7.2-3).

The maximum efficiency or the minimum penetration observed at high velocity is consistant with the observations of Annis (1) and Whitby (50) (See Section 2.1.1.) who explained their results as due to particle bouncing. The kinetic energy of some of the aerosol particles was so large that these particles were no longer being captured when they hit the filtration medium. The results also indicate the importance of the adhesion and autohesion of aerosol particles in the filtration process. An explanation for the higher minimum penetration for unwashed sand is that fine dust particles were re-entrained from the surface of the sand through collisions by aerosol particles or by aerodynamic lifting forces.

It may be remarked that the pressure drops were high in Yu's experiments at velocities beyond about 500 cm./sec., typically attaining levels as high as 13 to 15 psi at the highest velocity used for a given sand.

7.3. Dilute Serosols Filtration Tests by Filter Cake Formed on a Horizontal Sand Surface.

The equipments and procedures for this test were

described in Section 7.1. In this section we will present and discuss data only.

Figure 7.3-1 shows the penetration of the 1.1 micron aerosol through a filter cake of fly ash resting upon various grades of sand. Because of the better filter cake formed on the finer (40-50 mesh) sand, we found a very low penetration of the 1.1 micron aerosol. Actually, the last point we measured showed no counts on the Royco Counter for ten minutes! This filter cake-sand combination can be regarded as an absolute filter.

For the 10-14 mesh sand bed, the space between grains of sand is so large that a very poor filter cake was formed, full of big holes which allowed passage of the test aerosol particles. The efficiency did not change much with increasing amount of fly ash. On the 20-30 mesh sand, a much better filter cake was observed, but it still had a few pin-holes. These pin-holes tended to produce a leveling off of the filtration efficiency at thicker cakes. Due to the change in the number of pin-holes, different curves were observed for higher pressure drop or thicker filter cake. The formation of holes might be due to the fact that the autohesive force of the fly ash filter cake on the coarser sand was not strong enough to support the filter cake over a surface having a large pore size.

Figure 7.3-2 shows the pressure drop through the filter cake (total pressure drop minus clean bed pressure

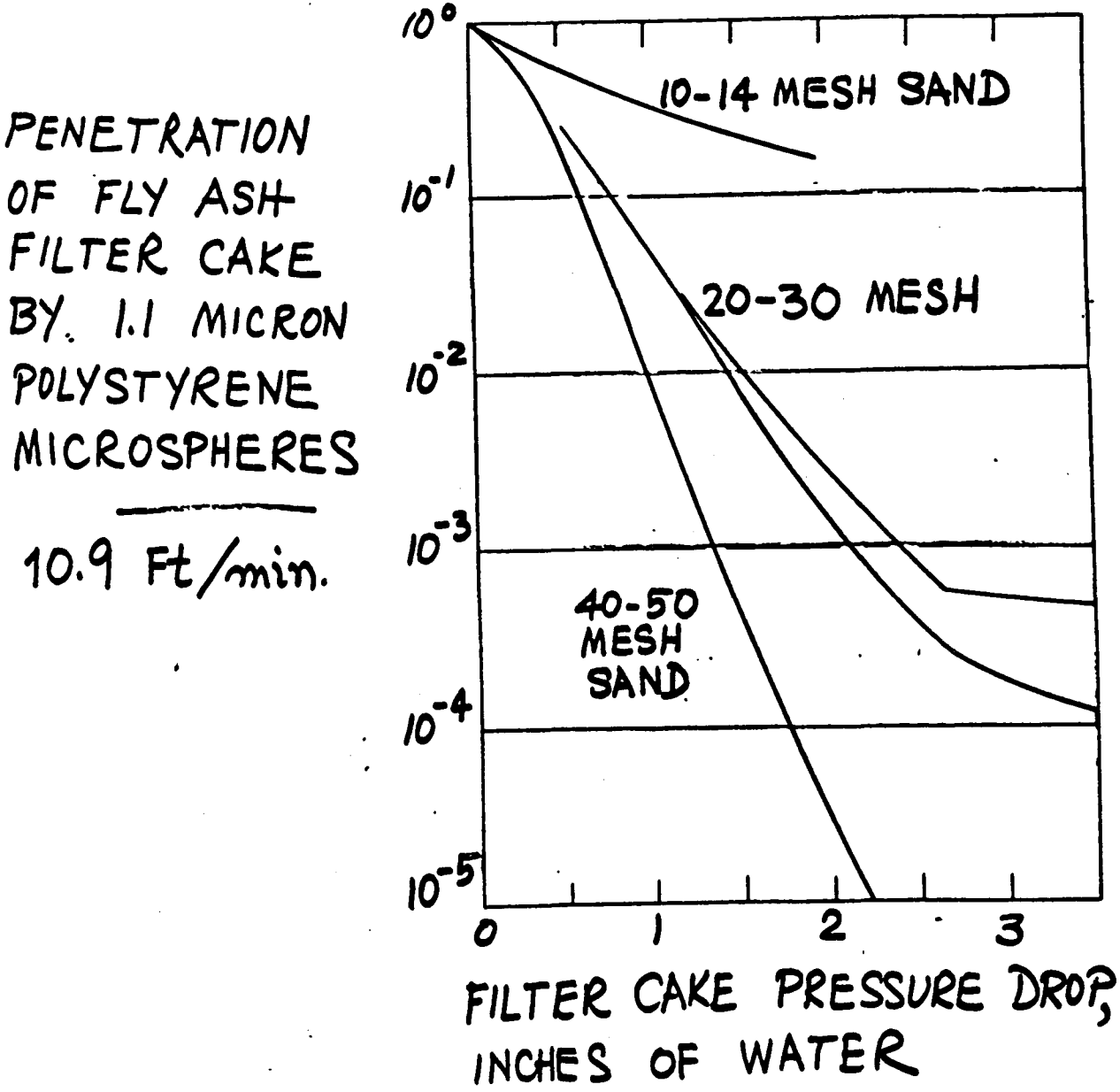

Figure 7.3-1: Penetration of monodisperse aerosol by a filter cake of fly ash filter resting upon a horizontal sand surface

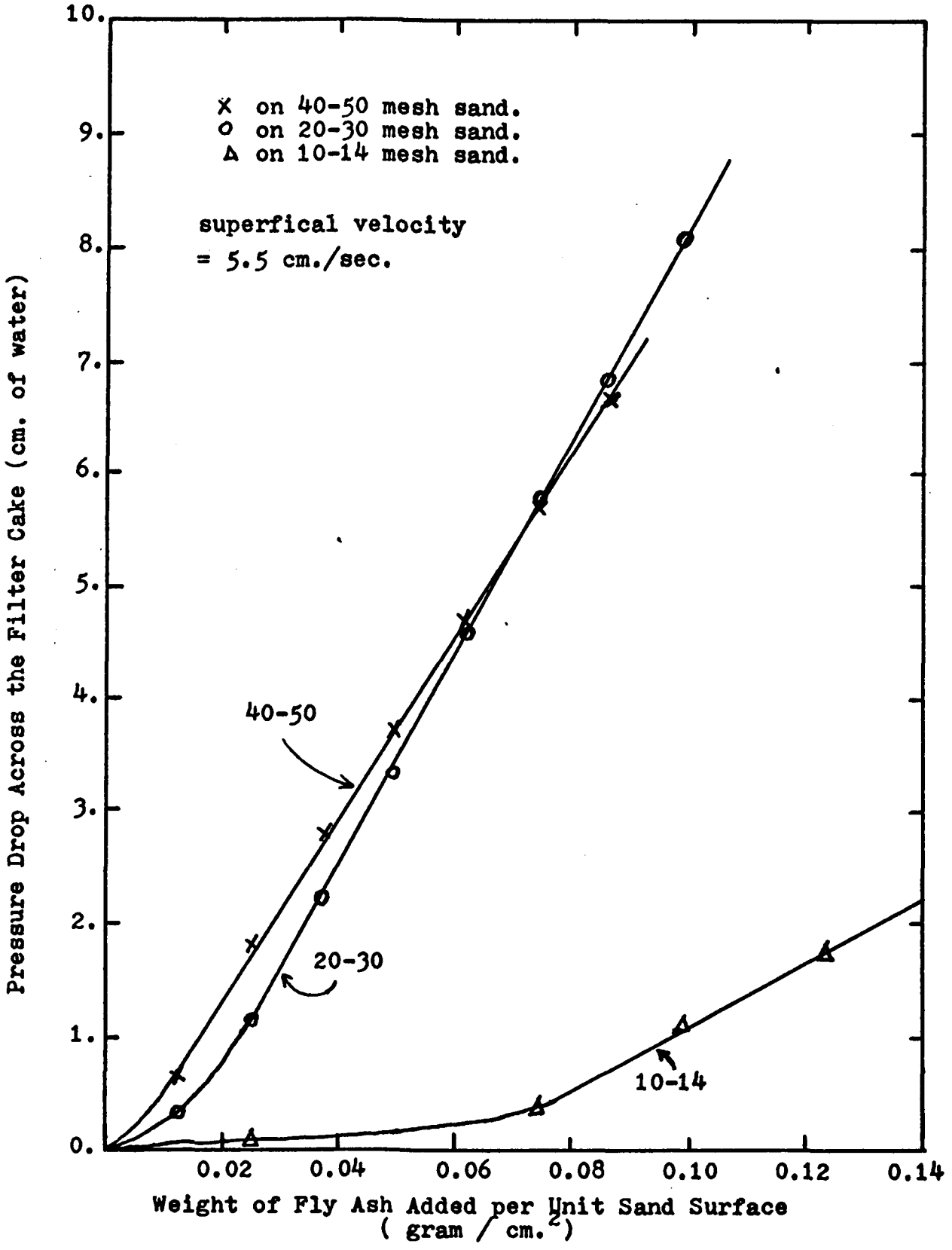

Figure 7.3-2: The Building up of Pressure Drop of Filter Cake.

drop) versus the weight of fly ash deposited per unit area for runs shown in Figure 7.3-1. Basically the filter cake pressure drop was proportional to the amount of fly ash deposited except for the initial stage. There was a smaller pressure increase (for 40-50 mesh sand and 20-30 mesh sand) and almost no pressure increase (for 10-14 mesh sand) during the inital stage. This was because most of the fly ash penetrates into the sand bed and coated the outside of the sand grains and the permeability of the sand bed was not changed much. During this stage, the fly ash acted to build a foundation for the formation of a surface filter cake. The filtration process was in the primary process as discussed in Section 2.1.3. In the panel bed filtration operation we always avoid this stage to get high efficiency. Later on, there was a steady build up of filter cake and the filter cake pressure drop was proportional to the filter cake thickness. The filtration process at this stage should be in the secondary process discussed in Section 2.1.3.

Other tests were run using Teflon powder (3-8 microns) and perlite powders (4.2 microns and 15 microns) (Figure 7.3-3) on 20-30 mesh sand. Teflon powder, due to its lack of adhesive and/or autohesive forces resulted in a very high penetration of the 1.1 micron aerosol. Thus adhesive and autohesive characteristics of a dust are very important to the effectiveness of its filtration in the panel bed filter. Because of its lack of adhesive and/or autohesive forces, the Teflon filter cake on 20-30 mesh sand looked much like

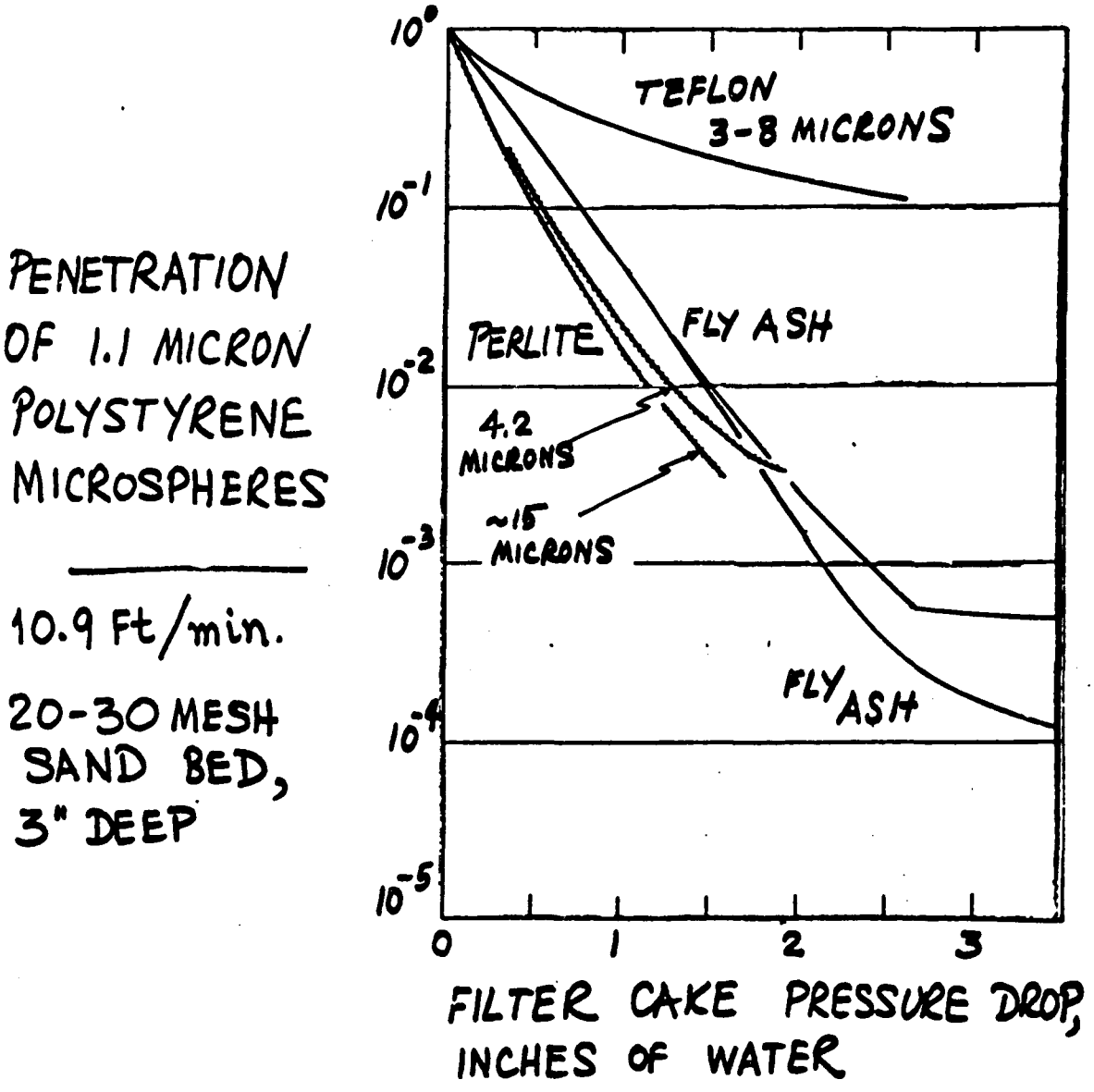

Figure 7.3-3: Filtration of monodisperse aerosol by a deposit of a fine dust resting upon a horizontal sand surface

fly ash on 10-14 mesh sand and was full of pin-holes which acted as passage to the test aerosol particles.

These results indicate that a combination of sand bed and fly ash filter cake can act as an extremely efficient filter for the 1.1 micron polystrene microspheres, which normally are difficult to filter. These extraordinary results may be applicable to filtering small particles such as the alkali fume present in the offgas from a coal combustion process.

7.4. Failure Test by Steady Blowback.

As stated in Squires and Pfeffer's first paper on the panel bed filter (44), a steady blowback air flow through the filter would merely remove sand from the topmost louver surface. Increasing the air velocity will just cause the top two or three louver surfaces to spill sand. A steady blowback air flow will cause a sand spill concentrated at the top portion only (Figure 7.4-1). They used the classical 60^{o} louvers, and the lower portion of the dirty sand on the top louver was drawn down by gravity to supply the spill from the second louver.

The failure phenomena of this steady blowback were studied in detail by using our transparent filtration unit (the second unit) with the tapered back and the chevron louvers. The three way valve shown in Figure 3.2-3 was replaced by an air supply hose. We increased the flow rate from zero until the sand bed failed and all the sand at the top was blown out. Three grades of sand (20-30 mesh,

40-50 mesh, and 10-14 mesh) were used in the front column. All the tests used 10-14 mesh sand as the backing sand.

The tests were conducted under two conditions -- initially dense and initially loose. The initially dense sample refers to a fresh filled sand bed without undergoing any other disturbance. From the soil mechanics point of view, what we call initially dense samples here were actually at a loose packing condition. But, the bed was packed at a relatively denser condition than that of a bed undergoing a strong puffback sand spill as discussed in Section 6.2. Hence, we will call this fresh filled bed an initially dense sample. By initially loose sample, we mean the bed has been loosened by dumping some sand from the botton hole of the fine sand column. The performance for these two kinds of samples was quite different and will be discussed in detail below.

For an initially dense sample, the sand will start to be blown out from the topmost louver space when the velocity increases to a certain point. At this critical velocity, only sand near the inner top surface would move out as shown in Figure 7.4-2-a. This is the weakest point within one louver space. When the velocity is increased further, the bottom portion of the topmost louver space will start to move gradually and the top portion of the sand in the second space will be blown too. In the mean time the sand will move down along the angle of failure plane of the topmost louver as shown in Figure 7.4-2-b.

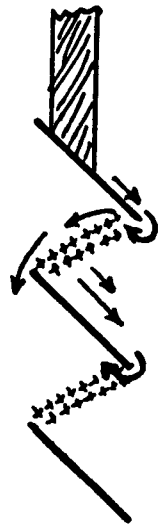

Figure 7.4-1: Steady Blow Back Sand Motion for 60° Louvers.

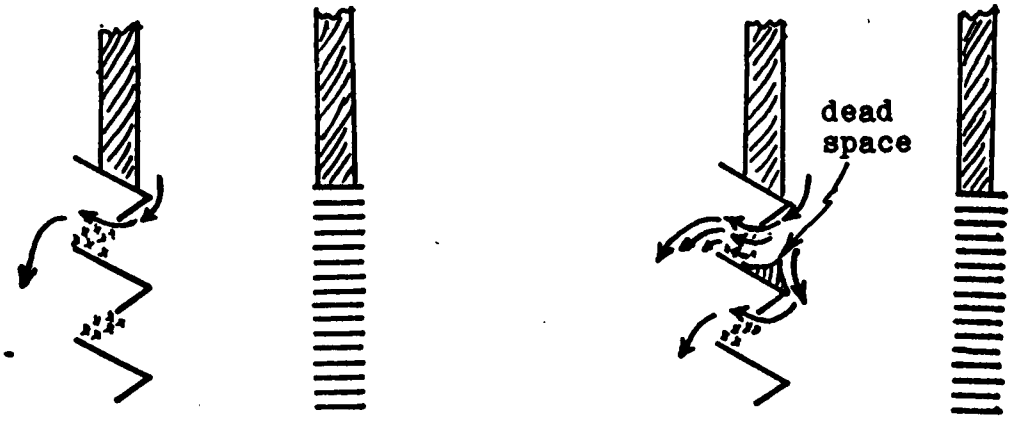

(a) failure start.

(b) increase air velocity.

Figure 7.4-2: Steady Blow Back Sand Motion for Chevron Louvers.

There is a dead space in the shape of a triangle. This process will continue to propagate down as the velocity is increased further. As observed by Squires and Pfeffer on 60° louvers, the sand spill will concentrate at the top portion only.

For an initially loose sample, the performance was different every time. Sand spill would start from any place, unpredictably -- top, middle, or bottom. Generally speaking, no matter where the sand spill started, it always ends up with the most sand flowing from the top first louver space. We discussed in Section 2.3.2. the nature of soil strain. The motion within the sand bed is a very complex process when considering individual sand grains. At any instant during the deformation process different mechanisms, friction resistance or interlocking, may be acting in different parts of an element. At the same location the mechanism will change with time too. For an initially loose sand bed, the porosity is about the same all over and the soil strength will be about the same too. There are no locations especially strong or especially weak. A location which has the weakest strength would start to spill sand first. There were occasions that after failure started sand would move to a new configuration of greater strength, and the sand spill would stop suddenly, although the air velocity did not change. There were also some cases where the bed was stable at a certain velocity for a period time, but due

to a slight movement in some part of the bed, the sand would start to spill suddenly. This spill might continue or might stop suddenly depending on the individual case.

Because of problems in louver construction, the dimensions for each louver space cannot be made the same. Some of the louver spaces have a larger surface angle and are closer to the true angle of repose of the sand. This will produce another type of weak point. Hence, most of the time but not all the time, the sand spill started from the top first or fourth space or the last space or the fifth from the last space, which were the weakest points from the point of view of construction.

When performing a steady blowback test, the flow rate should increase very slowly and without any abrupt change. Any fast change in flow rate will cause a temporary sand spill resembling puffback.

Data on steady blowback tests are shown in Figures 7.4-3, 4, and 5. It was observed that the starting of a continuous sand spill always happened at about a constant pressure drop. This pressure drop was called the "failure pressure." For an initially loose bed, the porosity is higher, hence, the pressure drop will be lower at the same velocity as compared with the dense bed. The sand spill will then occur at higher velocities as shown in the Figures. The actual failure pressure for the loose bed was about the same or slightly less than that of the dense bed.

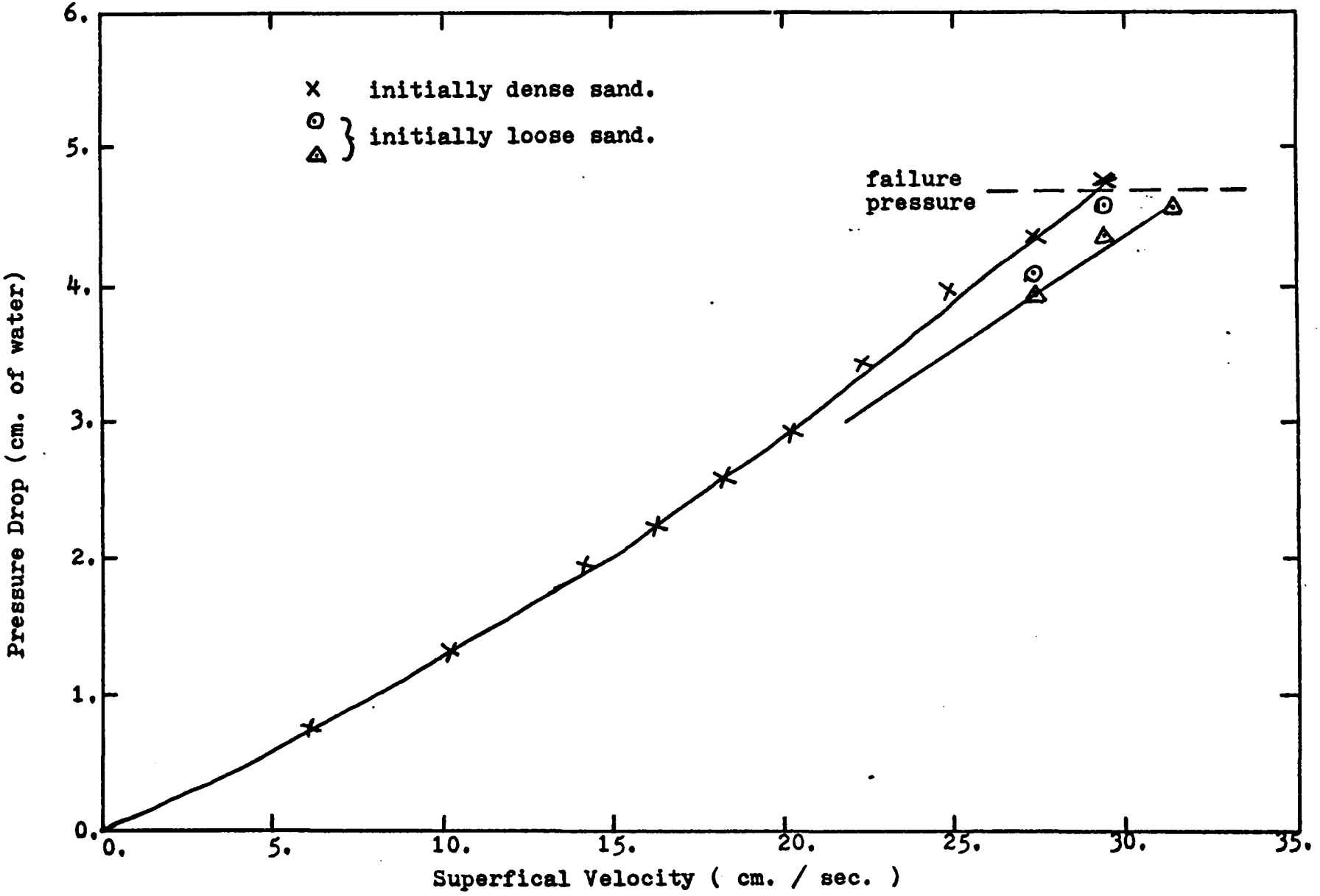

Figure 7.4-3: Failure by Steady Blow Back for 20-30 Mesh Sand.

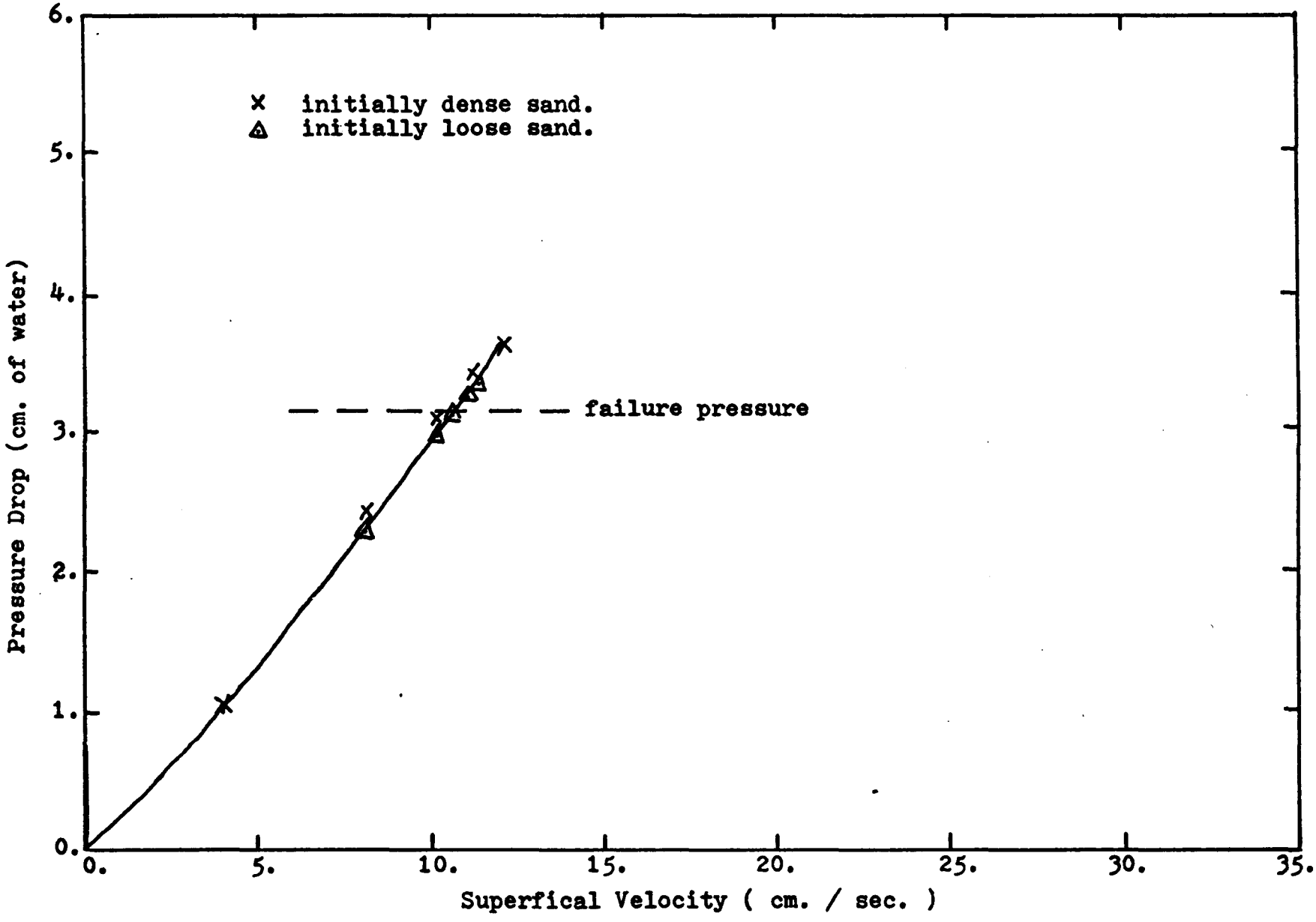

Figure 7.4-4: Failure by Steady Blow Back for 40-50 Mesh Sand.

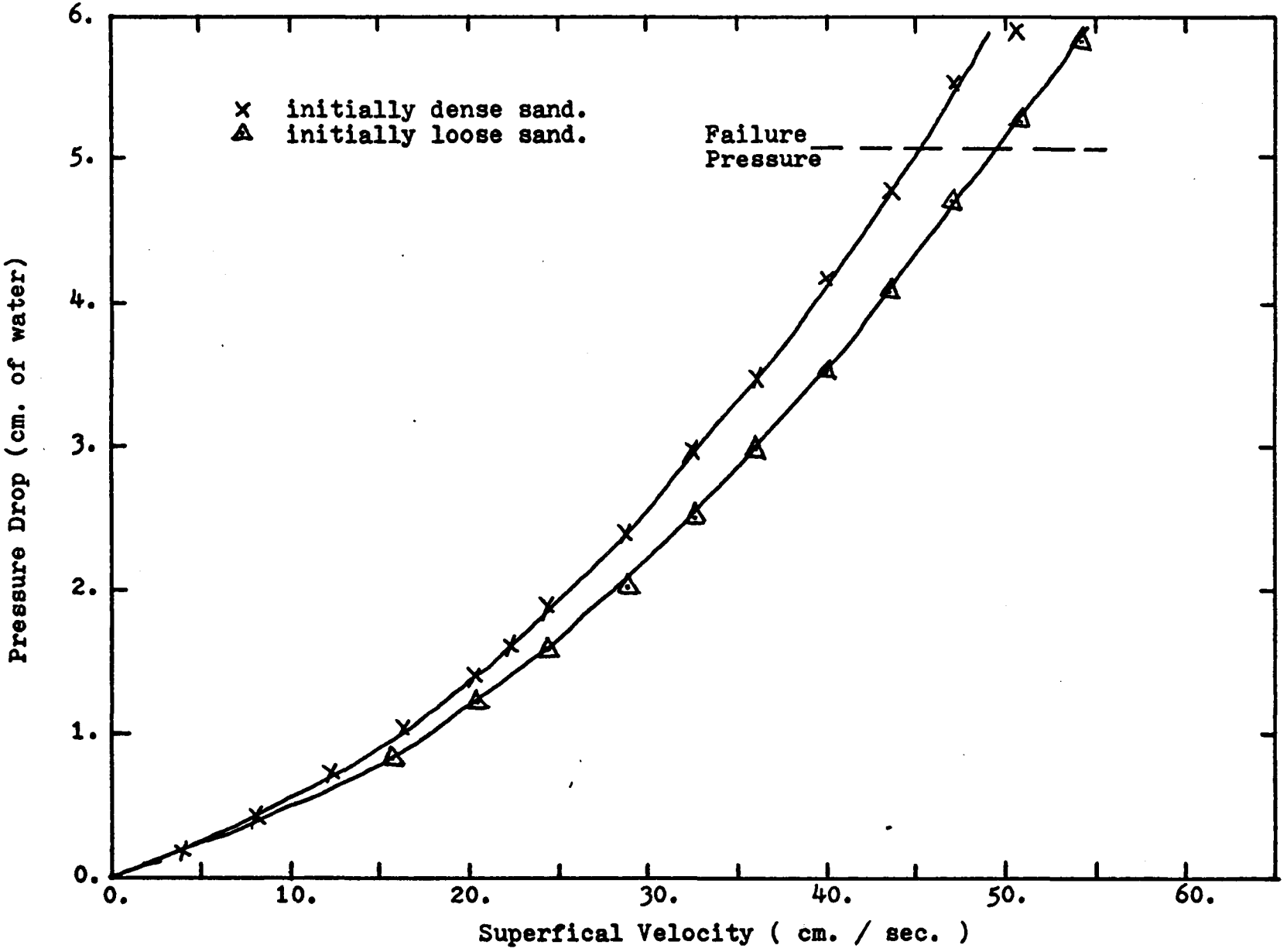

Figure 7.4-5: Failure by Steady Blow Back for 10-14 Mesh Sand.

The difference was very little. The failure pressure for 20-30 mesh sand backed by 10-14 mesh sand is about 4.6 cm. of water. The failure pressure for 40-50 mesh sand backed by 10-14 mesh sand is about 3.3 cm. of water. The failure pressure for 10-14 mesh sand backed by 10-14 mesh sand is about 5.3 cm. of water.

If we neglect end effects and use Equation 2.2-6, we can get the pressure drop velocity relation by curve fitting as given below:

20-30 mesh/10-14 mesh,

$$P = 0.07\ v + 5.66 \times 10^{-3}\ v^2 \qquad (7.4\text{-}1)$$

40-50 mesh/10-14 mesh,

$$P = 0.14\ v + 0.016\ v^2 \qquad (7.4\text{-}2)$$

10-14 mesh/10-14 mesh,

$$P = 0.02\ v + 3.86 \times 10^{-3}\ v^2 \qquad (7.4\text{-}3)$$

where P is pressure drop in cm. of water and v is superfical velocity in cm./sec.

From these steady blowback failure tests, we can draw the conclusion that steady blowback fails to do the job of cleaning the dirty sand surface, because the air flow has time to find the weakest point in the bed, and the flow concentrates at that point. On the other hand, in puffback the pressure reaches the failure pressure so quickly that it will cause failure throughout the bed. The air flow at a given point does not have time to know what is happening elsewhere, or to find the weakest point of the bed.

7.5. Sand Level Propagation Time Test.

In Section 6.2. we talked about the importance of a porosity change during the puffback sand failure. In a puffback of long duration, the transient porosity can cause non-uniform sand spill, with a greater spill at the top. Hence, it will be important to know how long it will take for the sand bed to settle down to the stable state at ultimate packing condition after puffback. The time required from one level where the sand grains have just reached a stable position to another upper level when the sand grains reach a stable position will be named the sand level propagation time or the propagation time for that distance. Special tests have been designed to measure this time.

From Newton's conservation of momentum law,

$$f \cdot t = m\, v_2 - m\, v_1 \qquad (7.5\text{-}1)$$

we know that there will be an impaction force "f" when the motion of one body with mass "m" is stopped suddenly ($v_1 = 0$) from a velocity of "v_2". At a level where the sand grains have just reached a stable position, there will be an impaction force due to falling sand grains hitting the just-stabilized sand surface. This impaction force can be monitored by a transducer and we can measure the propagation time by taking the difference of two transducer measurements.

Four transducer holes were drilled along the side wall of the front column sand as shown in Figure 7.5-1.

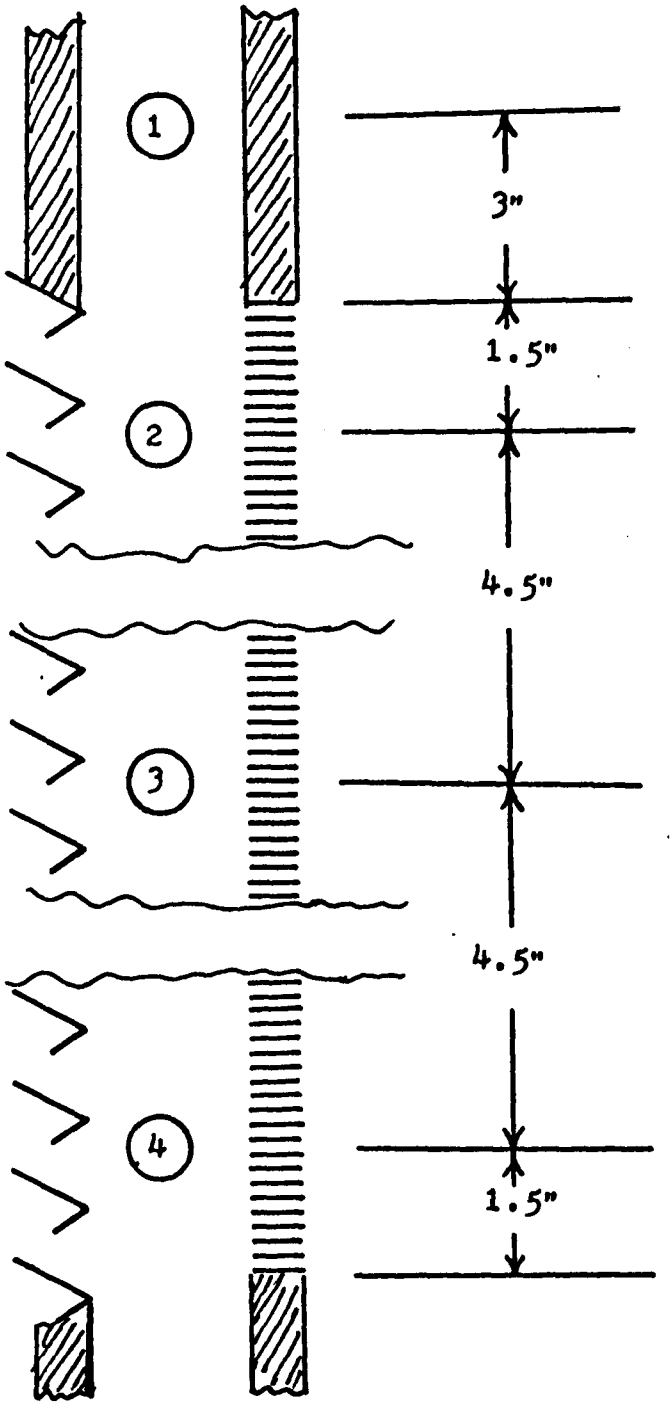

Figure 7.5-1: Propagation Time Transducer Test Points

Number 1 hole was 3 inches above the louver area, where there would be downward gravity settling motion only. The other three holes were in the louver area as shown. The distance between two adjacent holes wea 4.5 inches or 11.43 cm.

Figure 7.5-2 shows typical transducer data at each position. The initial mountain like curve was due to puffback pressure change. The little peak at the end is believed to be due to the impaction forces of sand grains. The vertical lines represent the disturbance measured by the transducer by the falling sand grains. Figure 7.5-2-2 shows data taked at the No. 1 test point, which was 3 inches above the louver area. As mentioned before, there was no forward motion at this point. The curve always showed two little impaction peaks which we do not understand. Figures 7.5-2-b, c, and d were taken at test points No.2, 3, and 4, respectively. The curve taken at point 4 showed no impaction peak, perhaps due to very little downward motion at the bottom.

Table 7.5-1 summarizes the propagation time measured in milliseconds. It seems from the data that the propagation time is inversely proportional to the sand spill per unit area. Hence, we will define the propagation time constant as the time required in msec. for the sand level to propagate 1 cm. upward when the sand spill is 1 gram/cm.^{2} based on the projected louver area.

From the table we can observe the general trend

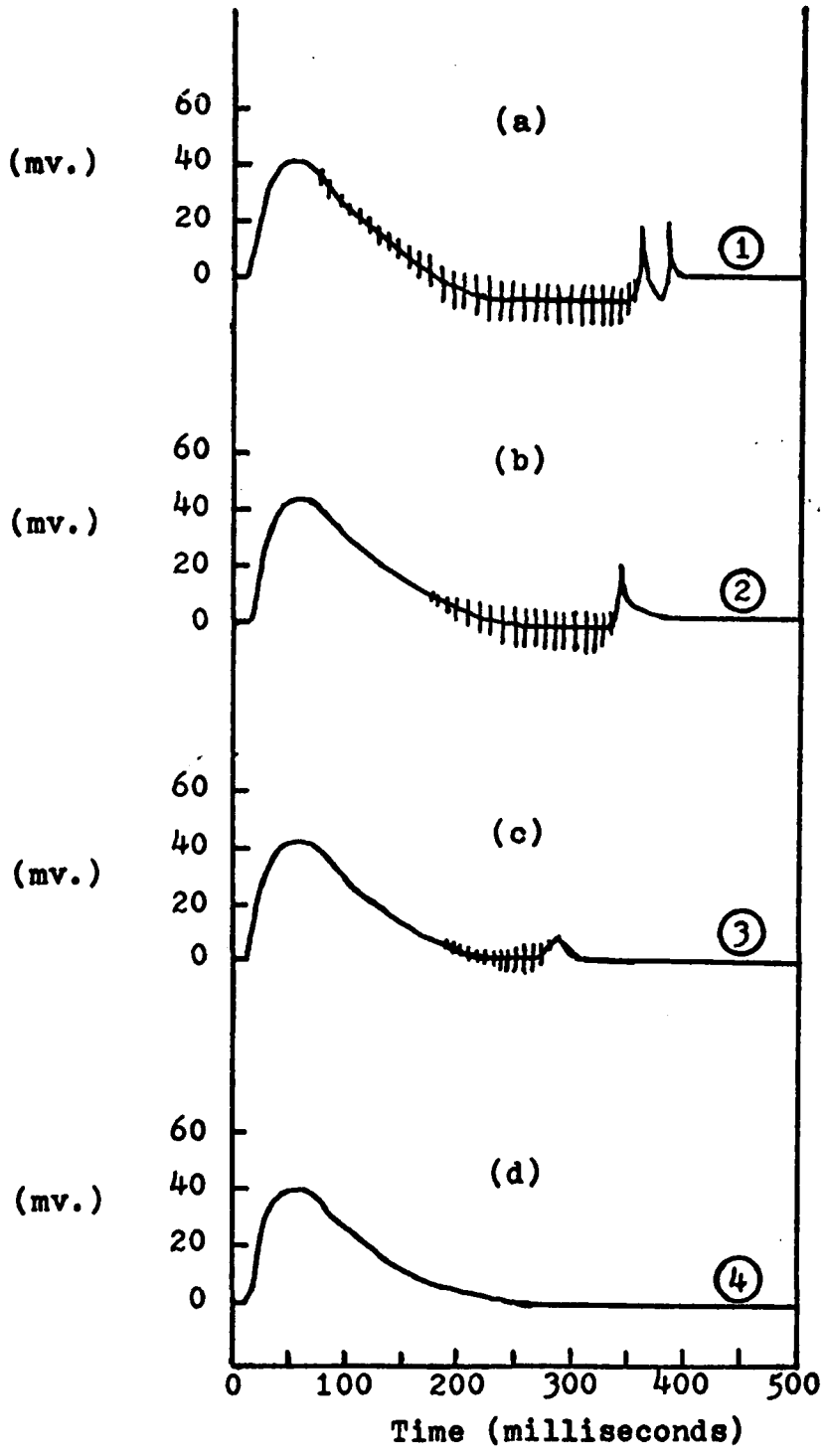

Figure 7.5-2: Typical Propagation Time Test Curves.

Table 7.5-1: Sand Level Propagation Time Test Data

Puffback Code (refer to Sec. 3.4.3.)	Sand Spill ($gm./cm.^2$)	Propagation Time (msec)		Propagation Time Constant $msec./(gm./cm.^2)/cm.$
		Δt_{1-3}	Δt_{2-3}	
A-3-B-1-60-H	.135	18.4		5.95
			6.5	4.2
A-3-B-2-60-H	.312	29.5		4.14
			15.	4.2
A-3-B-2-40-H	.135	14.5		4.7
A-3-B-4-50-H	1.43	81.5		2.51
			57.	3.5
A-3-G-5-30-H	1.79	128.5		3.14
A-3-G-5-10-H	.505	41.2		3.56
A-3-G-5- 5-H	.187	15.8		3.70
A-3-G-2-60-H	.422	36.		3.73
A-3-G-2-40-H	.256	27.4		4.68
A-3-G-1-60-H	.249	23.7		4.17
A-3-G-1-40-H	.112	16.8		6.56

that at a combination of conditions of large valve, small puffback volume or low pressure, which are the conditions for a short pressure tail, there results a large time constant. On the other hand, a combination of small valve, large puffback volume or high pressure, which are the conditions for a long pressure tail, there results a small time constant. This can be understood if we look at Figure 7.5-2 and review Section 5.1 -- the high speed movies study. We learned from the high speed movies that puffback can be divided into two important stages (neglecting the first shock jump stage which is not important in talking about puffback). At the body failure stage, the motion will basically move forward and at the local tail failure stage the motion will be basically downward. The transition between these two stages is gradual. Figures 7.5-2-b and c also showed no sand falling disturbance during the initial stage and then showed a large disturbance until the sand bed reached a stable position shown by the impaction peak. These curves indicate the existence of these two stages too. With the condition of long pressure tail, the transition time between these two stages will be longer too. Hence, sand started settling down while there was still some sand spilling due to body motion and the measured propagation time will be shorter.

From Table 7.5-1, it seems a time constant of about 4 msec. per (grams/cm.^{2}) per cm. can be used for design

purpose. A typical puffback will remove about 0.15 gram/cm.^{2} sand. Hence, a filter unit of 30 ft. (9.14 m.) height would require

$$4 \times 0.15 \times 914 = 548.6 \text{ msec.}$$

for the sand bed to return to a stable position after puffback sand spill or after the body failure.

Chapter 8: Filtration Analysis.

This chapter will discuss various filtration processes in granular bed filtration and the variables which will affect granular bed filtration as applied to panel bed filtration with puffback cleaning.

8.1. Model for Granular Bed Filtration.

We discussed fibrous filtration phenomena in Section 2.1.3 and we showed that there were two types of filtration processes -- primary filtration or clean filter filtration and secondary filtration or filter cake filtration. The filtration efficiency of the secondary process may be improved 100 times or more over the primary process. In the primary process, the major filtration mechanism will be adhesion. In the secondary process, the major filtration mechanism will be straining.

In the horizontal bed filter cake study, we also observed two types of filter cake performance. In Figure 7.3-1 penetration of an monodisperse aerosol by a filter cake of fly ash showed an initial curved region and then a straight line region that persisted until the penetration leveled off. Figure 7.3-2 showed a similar behavior in respect to the incremental pressure drop caused by a filter cake. Up to about 0.7 cm. of water, the pressure drop versus weight of fly ash was curved. After about 0.7 cm., the line was straight, and we can call this the

the Darcy's law region.

Because the granular bed filter usually is much thicker than a fibrous filter we would like to classify the granular bed filtration processes into three types -- the clean bed filtration, the rooting-cake filtration, and the surface-cake filtration, as shown in Figure 8.1-1. In granular bed filtration, the primary process of fibrous filtration can be best separated into two processes, as shown in Figure 8.1-1-a and b. Clean bed filtration is the stage where the granules are basically clean, or have some dust particles adhering on their surface, but the dust is not heavy enough to form a thick layer over the surface, i.e., the dust does not fill up the front and rear space of the granules. In the clean bed filtration process, the efficiency will be very poor.

As discussed in Section 2.1.2.5. (Figure 2.1-2), dust particles tend to be accumulated in the front and rear of the granules. This was also observed by Taub (45). Figure 2.1-3 showed that dust adhered to the back of the granules will be very difficult to be detached by the air flow. In a bed of granules, dust laden air goes through a three-dimensional, zig-zagged channels of non-uniform diameter. Section 2.1.5. showed there will be turbulent deposition on the wall of a tube and in this case on the side of the zig-zagged channels. In this way the dust will build up a filter cake within the sand bed near the surface. For 40-50 mesh sand and fly ash this surface layer was observed to be about 1/10 inch at a superfical

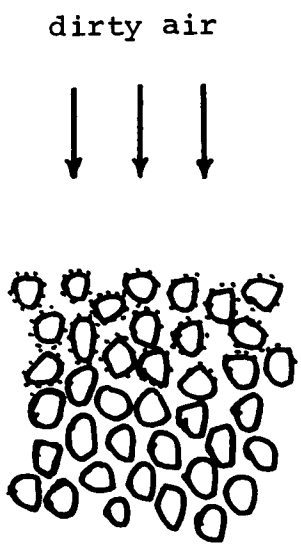

(a) clean bed filtration

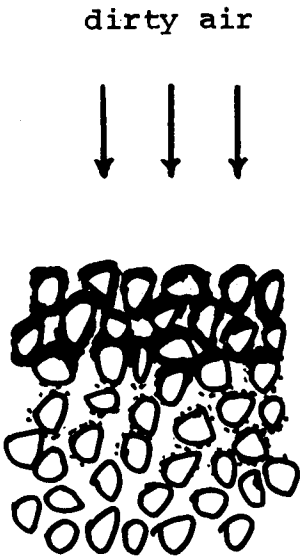

(b) rooting-cake filtration

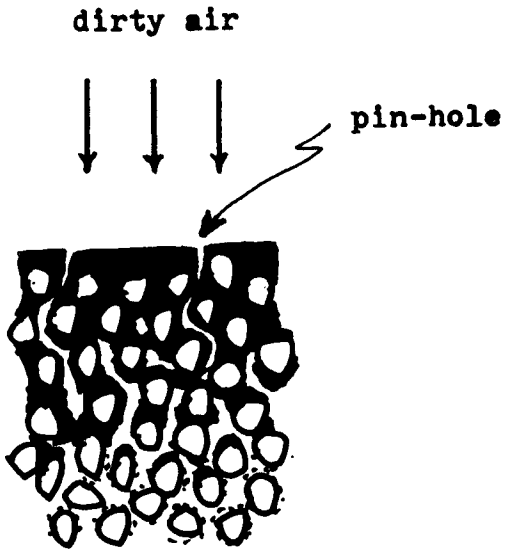

(c) surface-cake filtration

Figure 8.1-1: Model for Gravel Bed Filtration.

velocity of about 20 cm./sec. For 20-30 mesh sand and fly ash this surface layer was observed to be about 1/4 inch at a superfical velosity of about 20 cm./sec. We call this stage the rooting-cake filtration because it forms the foundation or the roots for the formation of the surface filter cake.

In the rooting-cake filtration process, the front and rear of the granules will be filled with dust and the dust tends to form a continuous phase with the granules. The efficiency will increase remarkedly, yet the pressure drop will not change much, as seen at the curved region of the curves in Figures 7.3-1 and 7.3-2.

After the rooting-cake is formed, the filter cake tends to grow as shown in Figure 2.1-6. The efficiency will increase to such an extent that most of the dust will be stopped at the granular bed surface and form a surface filter cake. At this point begins what we call the surface-cake filtration process, which is represented by the straight line region in Figures 7.3-1 and 7.3-2. This stage is similar to the secondary filtration discussed in fibrous filtration. The filtration efficiency will be proportional to the thickness of the filter cake.

The characteristics of surface filter cakes are quite different for those formed at high velocities from formed at low velocities. The filter cakes formed at high velocities will be more dense, tending toward a higher pressure drop and higher efficiency. But, due to

the stronger aerodynamic force, there will be many pin-holes formed over the pores of the granular surface. The overall permeability of the filter cake will tend to be lower, so that the pressure drop and efficiency will also tend to be lower. So, the net result of the combination of a dense filter cake and many pin-holes in the cake is difficult to determine. Filter cakes formed at low velocities will be more porous but with fewer and smaller pin-holes. The result of the combination of these two conditions is also difficult to determine. In considering filtration efficiency, we have to consider other variables such as Brownian diffusion and inertial impaction (Section 2.1.1.). To predict the efficiency of a granular bed filter is not a simple procedure.

8.2. Model for Panel Bed Filtration.

As discussed in the last section, for a clean bed filtration process the efficiency will be very poor. In the panel bed filter operation, we try to avoid this mode. We even avoided the rooting-cake filtration mode and always operated in the surface-cake filtration mode. This was achieved by controlling the puffback intensity so that we just removed the surface filter cake and a little of the rooting-cake. This is important in order to get the best continuous operation of granular bed filter and we will discuss this further later. For best practice, puffback cleaning will leave most of the rooting-cake in the surface sand. This rooting-cake will act as a

foundation for the build-up of a surface filter cake for the next cycle. Hence, in the steady state operation of panel bed filter each cycle started from Figure 8.1-1-b (after puffback) and ended at Figure 8.1-1-c (before puffback).

The first cycle of the panel bed operation always resulted in poor efficiency (See Tables 4.2-1, 4.3-1, and 4.4-1, Figure 4.3-1) because we started the process for clean sand filtration. After the first puffback there is some fly ash resting in the surface sand as rooting cake, but not enough for surface filtration to commence at the beginning of the next cycle. The initial pressure drop will increase a little due to this rooting cake. The fly ash will continue to accumulate near the sand surface to form a rooting cake until it reaches steady state after four to five cycles. The filtration efficiency and initial pressure drop will both increase until the fourth or fifth cycle. After that, the panel bed filter will operate in the surface-cake filtration mode only and will be able to achieve very high efficiency with little further increase in the initial pressure drop (See Table 4.2-1).

We discussed in Section 8.1 that the efficiency of surface-cake filtration depends on the porosity of the filter cake, the number and size of pin-holes, the velocity of the air, and the adhesion and autohesion of the dust. Data presented in Chapter 4 told us that the panel bed

filter using finer sand gave a higher efficiency. This is because a better filter cake with less and smaller pin-holes was formed over the smaller pores of fine sand.

Taub's study (See Section 2.1.4.2.) with big granules and high air flow rates showed a saturation phenomenon. The filtration efficiency decreased with time and reached zero when the granular bed was saturated with fly ash. Although he did not observe this saturation phenomenon for his 30 cm./sec. data and for his finer (0.47 mm.) glass sphere bed runs, his observation tells us that fly ash tends to keep on penetrating into the bed. This penetration process might be slower at lower velocities and for finer particles, but we cannot say that there will be no penetration at all. This may be because the deposition of particles carried along by the flow and the detachment of previously adhering particles take place simultaneously. Taub's observations imply that we have to keep on suppling fresh granules, either continuously or intermittently, in order to avoid an accumulation of dust and to avoid a continuous increase in pressure drop. So, the puffback intensity should be at least strong enough to remove one layer of surface granules in addition to removing the surface filter cake. After steady state for a particular puffback intensity is reached, the initial pressure drop of each filtration cycle will be a function of puffback intensity, which

will govern the amount of rooting-cake dust within the sand bed. Table 4.2-1 showed that for a puffback pressure of 25 psig, the initial pressure drop will be 1.5 inches of water; for a puffback pressure of 35 psig, the initial pressure drop will be 1.3 inches of water.

8.3. The Role of Adhesion and Autohesion in Panel Bed Filtration.

In Section 2.1.2.3. we discussed adhesion of powder upon striking a target; in Section 7.2. we discussed particle bouncing; and in Section 2.1.3. and Section 8.1. we discussed the formation of a filter cake. All these phenomena indicate the importance of adhesion and autohesion to the capture of dust. The capture of the first layer of dust around the granules depends on the adhesion of the dust on the granules. The first layer of dust is difficult to detach (10,11,12). The subsequent formation of filter cake will depend on the autohesion of the dust. Hence, the successful operation of a panel bed filter depends strongly on the adhesion and autohesion properties of the dust to be filtered.

We observed that for the first cycle, dirty sand worked better than clean sand (Section 4.1.). We believe that this occurred because the autohesive force of fly ash is greater than the adhesive force of fly ash to sand and that the dust was therefore more readily captured and a filter cake formed easier on the dirty sand.

The experience with the Teflon filter cake (Section 7.3.)

also showed that dust with weak adhesive and/or autohesive forces cannot form a good filter cake, which is necessary to obtain a high efficiency with a granular bed filter.

From the above discussion we can predict that the panel bed filter efficiency can always be improved by either surface treatment of the granular bed or by surface treatment of the dust to increase the adhesion and/or autohesion properties of the system. Alternatively this can be done by increasing the humidity or by introducing static electrical charges on the dust (Section 2.1.2.1. and 2.1.2.2.).

We will talk a little about the relative importance of adhesion and autohesion. We discussed in Section 2.1.3. that two processes, the detachment of previously adhering particles and the deposition of particles carried along by the flow, should take place simultaneously. In Section 2.1.2.4., we discussed two types of dust layer detachment -- erosion and denudation. In erosion type detachment, dust layers will be removed gradually and slowly. This helps in the building-up of a good filter cake. In denudation type detachment, the dust layers will be removed all at once in a short time, and this means that the dust tends to penetrate through the granular bed easily. Hence, in panel bed filtration, the adhesive force between the dust and the granules should not be much less than the autohesive force between the dust particles. A strong autohesive force will be required to

form a good filter cake and a strong adhesive force will be required to form a stable filter cake.

Our technique of dispersing fly ash through a critical orifice is subject to the criticism that fly ash particles dispersed in this way will become charged as fly ash agglomerates are torn apart. Charged fly ash particles will have stronger adhesive and autohesive forces due to the additional Coulomb forces, and this will result in both a better filter cake and a stronger filter cake. Further studies concerning the general effects of adhesion and autohesion of the dust and filter medium should be performed. These include effects of surface tension force, effects of electrostatic force, effects of Van der Waal's force, and effects of surface treatment.

Chapter 9. Puffback Analysis

9.1. Experiment Results for Puffback Failure.

In this section, we will analyze the data presented in Chapter 6. Section 9.1.1. will show the measured minimum failure pressure under puffback condition for different sand sizes and different configurations -- sideshot and downshot. It is interesting to note that the minimum failure pressure is almost independent of the sand size but dependent on the puffback configuration. We have the most complete data for 20-30 mesh sand using downshot puffback. Hence, for most of the analysis we will use this set of data.

Section 9.1.2. will present an empirical correlation of sand spill and puffback intensity. We found the puffback intensity can be represented by an "active time" which is the period of time the pressure drop is strong enough to cause body failure of the sand bed. We will show the importance of the louver construction on the amount of sand spill.

9.1.1. Minimum Pressure Drop Required to Cause Sand Spill.

Figure 9.1-1 shows two typical curves of puffback sand spill versus peack puffback pressure drop. From these curves we were able to obtain the minimum pressure drop required to cause any sand spill, that is the failure pressure. The solid line showed actual experiment results. The curves basically are straight lines except when the

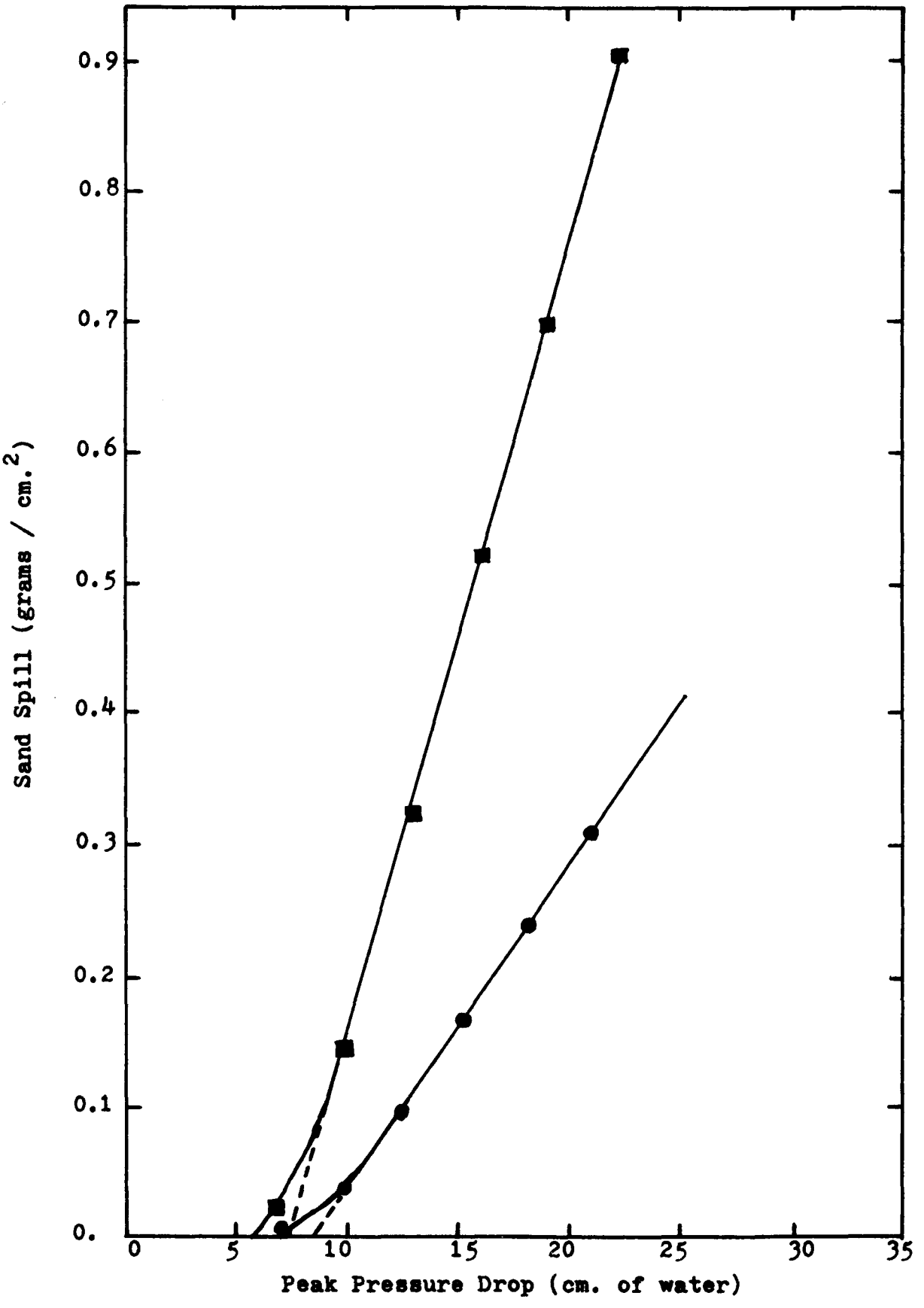

Figure 9.1-1: Typical Sand Spill Vs. Peak Pressure Drop Curves.

amount of sand spill was small. The dotted lines are extrapolations of the straight line portions. All the data for sand spill per unit area were calculated based on the total projected louver area (0.25 ft.^{2} or 232.3 cm.^{2}), and were not based on the actual sand surface.

We discussed in Section 5.1 that the high speed movies showed that there are two types of failures -- local failure which happens at the surface region only and body failure which removes most of the sand during the puffback. Also, when the puffback intensity is low, only local failure will occur. The curved portion in Figure 9.1-1 is believed to be due to that local failure mechanism. Since the sand spill due to local failure normally consists of only a small portion of the total sand spill, we will neglect this effect and consider body failure only. In other words, we will use the extrapolated straight line to find the minimum failure pressure, "$\Delta P_{min.}$"

The triangle shaped puffback pressure drop curves shown in Chapter 6 can be best described by two parameters, the peak pressure drop "ΔP_{peak}" and the parameter "m" which is defined as the duration time divided by the peak pressure. The duration time is defined as the time required for the puffback pressure to drop off to zero. These two parameters specify the puffback intensity. As we will show later, the puffback intensity can be well represented by the product $(\Delta P_{peak} - \Delta P_{min.}) \cdot m$; this has the dimension of time, and we will call the

product "active time".

If all the puffback variables are kept the same in a series of runs except the puffback pressure, we will find that the value of m for the series will be about the same. Figure 9.1-2 shows the data for the duration time versus peak pressure drop from the data of Figures 6.1-4 to 9. These curves were drawn for downshot puffback data on 20-30 mesh sand backed by 10-14 mesh sand. Each curve was an approximately straight line, indicating that "m" was nearly constant. We will use the average value of the slope "m" as the characteristic parameter for each combination of puffback variables (bottle size and valve opening). The values of m tend to decrease slightly as we increase the puffback pressure for any specific puffback arrangement (bottle size and valve area), since the curves in Figure 9.1-2 are somewhat concave downward.

Figure 9.1-3 shows downshot puffback sand spill in grams per square centimeter of projected louver area versus peak puffback pressure drop in centimeters of water for 20-30 mesh sand backed by 10-14 mesh sand. The intersection of each straight line with the abscissa indicates the minimum pressure drop (the failure pressure) required to cause any sand spill for that specific puffback arrangement. The "m" value for that specific puffback arrangement is also indicated on the curves. From Figure 9.1-3 we can see the minimum pressure drop for the same grade of sand was not a unique number, and

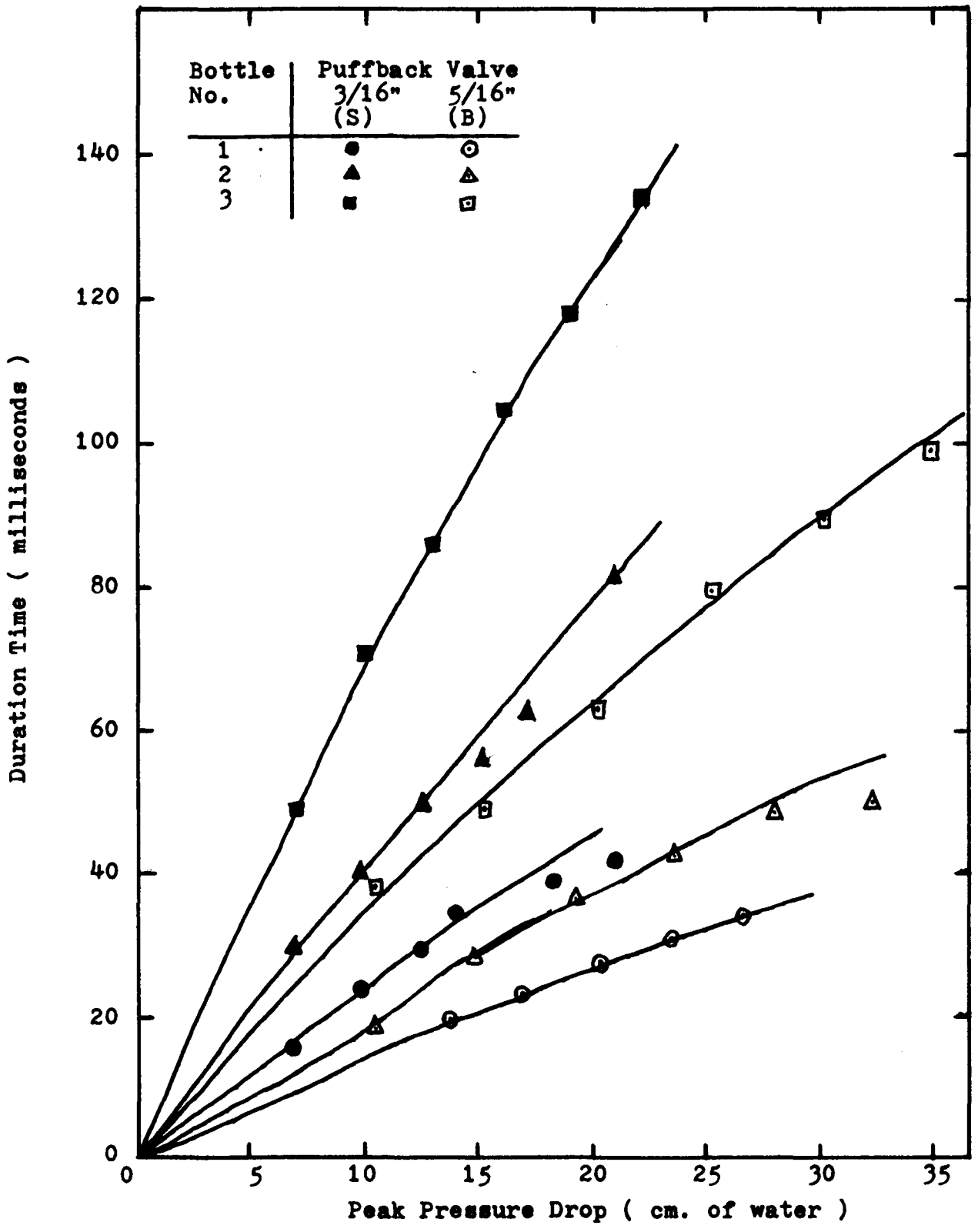

Figure 9.1-2: "m" Value for 20-30 Mesh Sand, Downshot Puffback Runs.

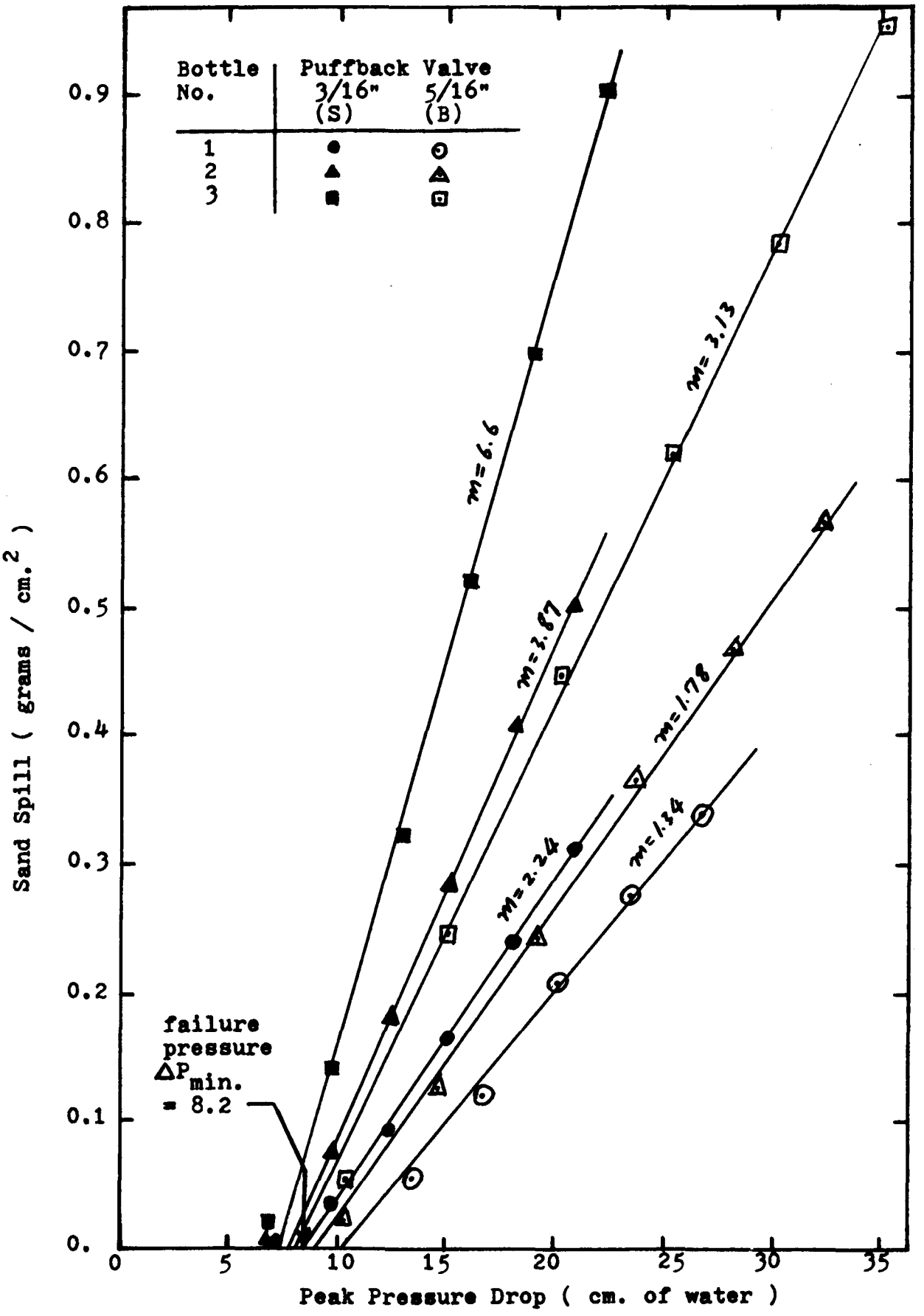

Figure 9.1-3: Failure Pressure for 20-30 Mesh Sand and Downshot Puffback.

seems to increase slightly with decreasing m-value. A larger m-value will result in a lower minimum failure pressure drop and vice versa. This difference in "$\Delta P_{min.}$" can be explained by the transient failure phenomenon discussed below.

In Section 2.3.4.3., we said that for a granular material undergoing straining there will be a decrease in volume; the material will shrink a little during the initial stage even if the specimen was originally in a dense condition (Figure 2.3-7 curve A) or in a loose condition (Figure 2.3-7 curve B and Figure 2.3-9). This indicates that the sand spill will not occur immediately after the pressure reaches the minimum value. From the evidence and results shown in Section 6.2 and the soil mechanics test, we know that normally the sand packing in the panel bed filter is in a very loose condition. Hence, it will shrink more during the initial stage of puffback and a longer time will be required before sand starts to spill than for a densely packed bed.

In Section 2.3.4.4. we discussed some transient sand failure phenomena. Whitman's (51,52) work on fast loading on the sand showed that for the initial stage, strain results primarily from elastic deformation of the individual grains. With further loading grains start to slide relative to one another and resistance to straining decreases. Hence, putting all of the stress on suddenly

will make it more difficult for the soil to strain in the initial stage. This also indicates that puffback sand spill cannot happen immediately for a fast loading. We will also call the puffback failure pressure " $\Delta P_{min.}$ " the dynamic failure pressure.

If we define the failure pressure under steady blow back condition " ΔP_f" (Section 7.4) as the static failure pressure, we can calculate the failure time at the minimum puffback failure pressure in the following manner: We assume the pressure drop curve has a triangular shape as shown in Figure 9.1-4, reaching a maximum defined by $\Delta P_{min.}$.

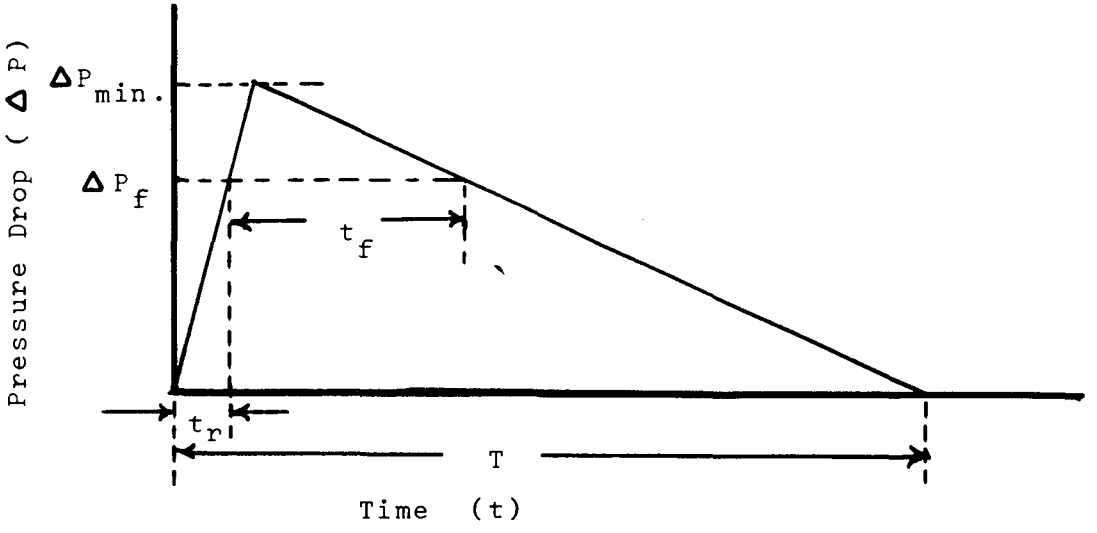

Figure 9.1-4: Calculation of Failure Time.

ΔP_f : Steady blowback failure pressure from Section 7.4.

$\Delta P_{min.}$: Puffback failure pressure from Figure 9.1-3 which is the intersection of the straight line and the peak pressure axis.

T : Total duration time of the puffback pressure.

t_r : Rise time until ΔP_f is reached.

t_f : The failure time which is the time required to cause sand spill after the pressure drop rises to ΔP_f and at the condition that the peak pressure drop will reach the minimum value "$\Delta P_{min.}$".

From the definition on "m", we get:

$$m = \frac{T}{\Delta P_{min.}} \qquad (9.1\text{-}1)$$

By similar triangles,

$$\frac{t_f}{\Delta P_{min.} - \Delta P_f} = \frac{T}{\Delta P_{min.}} = m \qquad (9.1\text{-}2)$$

$$t_f = m \cdot (\Delta P_{min.} - \Delta P_f) \qquad (9.1\text{-}3)$$

ΔP_f = 4.6 cm. of water for 20-30 mesh sand backed by 10-14 mesh sand, and is constant for each specific puffback arrangement.

Table 9.1-1 sumarizes the failure time calculated for each puffback combination.

From this table (See next page), we conclude that a larger "m" or longer tail in pressure drop curve will require a smaller minimum pressure drop to cause sand spill, but results in a longer failure time. The average failure time is about 10 milliseconds after the pressure drop rises to ΔP_f. These calculated times agree fairly well with the observed data from the high speed movies (Table 5.2-1).

Table 9.1-1: Puffback failure time from Equation 9.1-3.

Puffback Code*	m (msec./cm. H_2O)	$\Delta P_{min.}$ (cm. H_2O)	t_f (msec.)
A-3-S-3-x-D	6.6	7.17	16.3
A-3-S-2-x-D	3.87	7.87	12.3
A-3-B-3-x-D	3.13	8.25	11.1
A-3-S-1-x-D	2.24	9.08	9.8
A-3-B-2-x-D	1.78	9.52	8.6
A-3-B-1-x-D	1.34	10.28	7.5

* Refer to Section 3.4.3. for the definition of the code. For 20-30 mesh sand and sideshot puffback it will take about 20 msec. for body failure to start. The rise time for sideshot is about 10 msec. Hence, the failure time for 20-30 mesh sand is about 10 msec. from the high speed movies. We should remember, however, that the puffback process is a transient process and is more complicated than we have described above.

The above analysis explains why the minimum pressure drop required to cause sand spill is slightly different even for the same grade of sand. However, it is fairly constant and we will use an average value.

Figure 9.1-5 shows the minimum pressure drop required for 40-50 mesh sand backed by 10-14 mesh sand from the data in Figures 6.1-10 to 15. Figure 9.1-6 shows the minimum pressure drop required for 10-14 mesh sand backed by 10-14 mesh sand from the data in Figures 6.1-16 to 20.

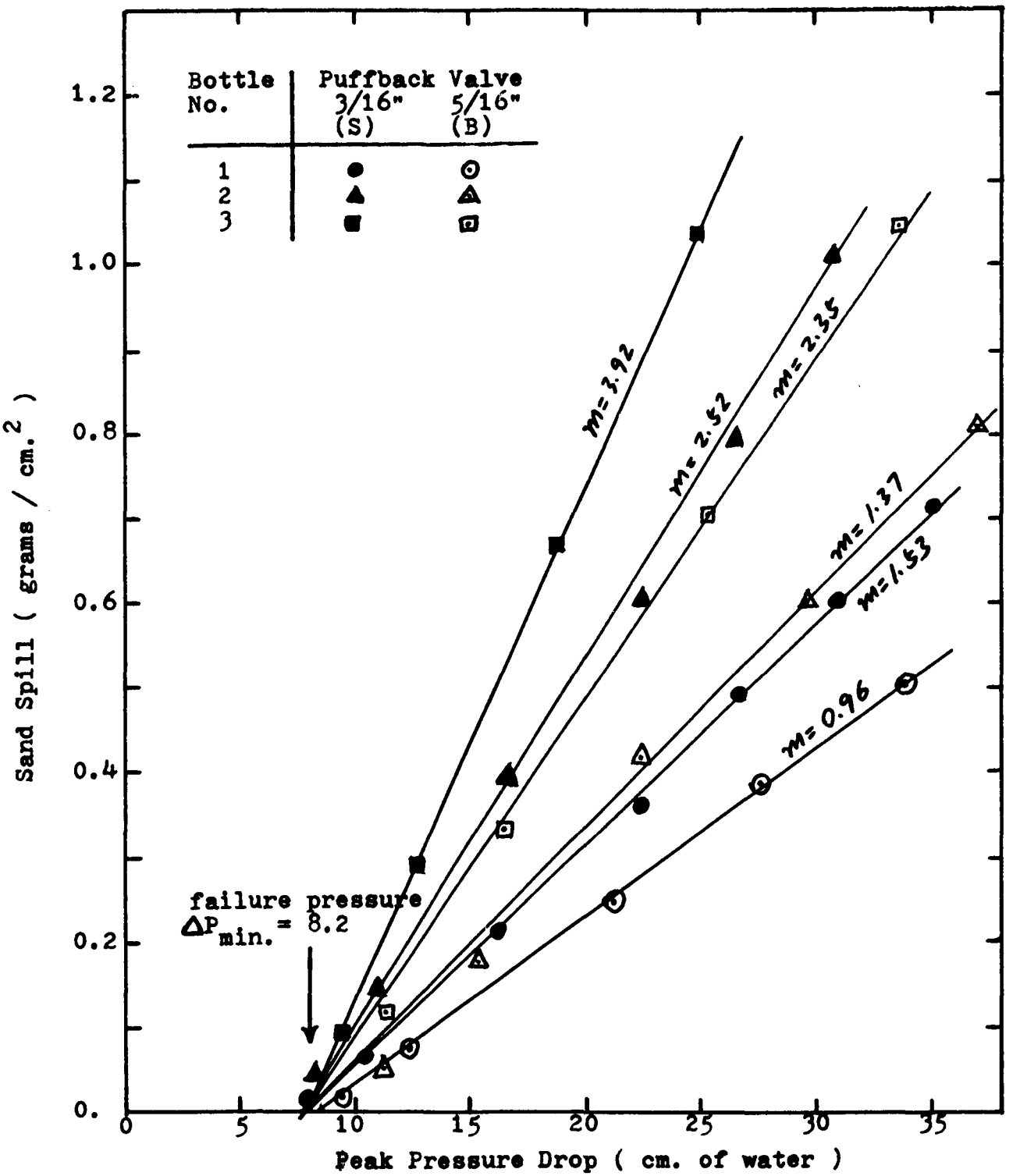

Figure 9.1-5: Failure Pressure for 40-50 Mesh Sand and Downshot Puffback.

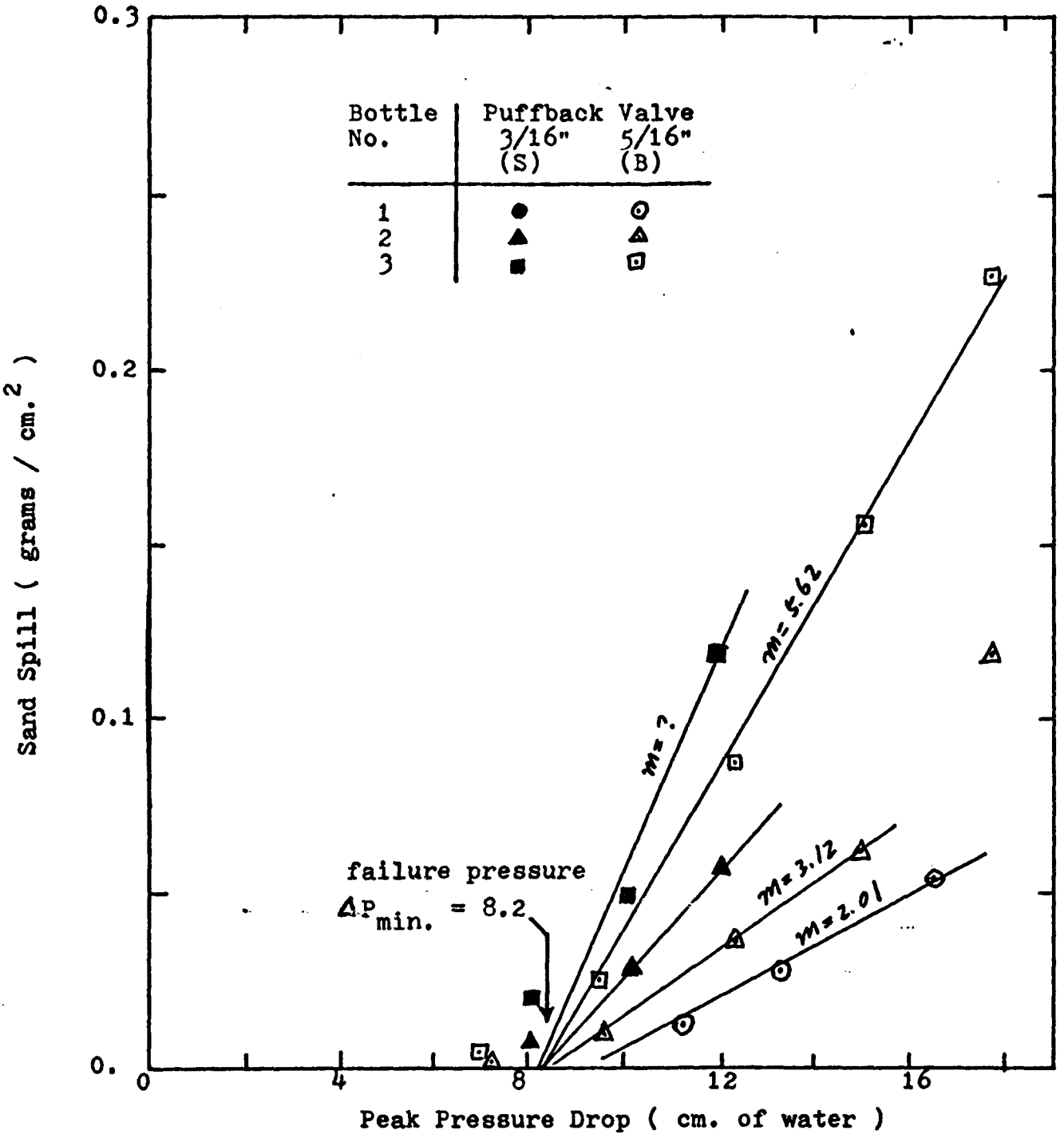

Figure 9.1-6: Failure Pressure for 10-14 Mesh Sand and Downshot Puffback.

We have mentioned in Section 6.1.1.1., that the data for 10-14 mesh sand were not very good, and the data points in Figure 9.1-6 showed some scatter. But the general trend is for all of the straight lines to converge to a single point. It is interesting to find that the minimum failure pressure for downshot puffback has about the same value for different grades of sand and is equal to:

$$\Delta P_{min.} = 8.2 \text{ cm. of water} \qquad (9.1\text{-}4)$$

Figure 9.1-7 shows sideshot puffback minimum failure pressure drop for 20-30 mesh sand backed by 10-14 mesh sand from data in Figures 6.1-21 to 27. Figure 9.1-8 shows sideshot failure pressure for 40-50 mesh sand backed by 10-14 mesh sand from data in Figures 6.1-26 to 33. Figure 9.1-9 shows sideshot failure pressure for 10-14 mesh sand backed by 10-14 mesh sand from data in Figures 6.1-34 to 37. As we observed for downshot puffback, the failure pressure for sideshot puffback was approximately the same independent of sand size and is equal to:

$$\Delta P_{min.} = 5.7 \text{ cm. of water} \qquad (9.1\text{-}5)$$

Table 9.1-2 summarizes the failure pressures for steady blowback tests (Section 7.4) and puffback tests. From this table we conclude that the failure pressure is almost independent of sand sizes under transient puffback condition while the failure pressure for steady blowback test showed some variation.

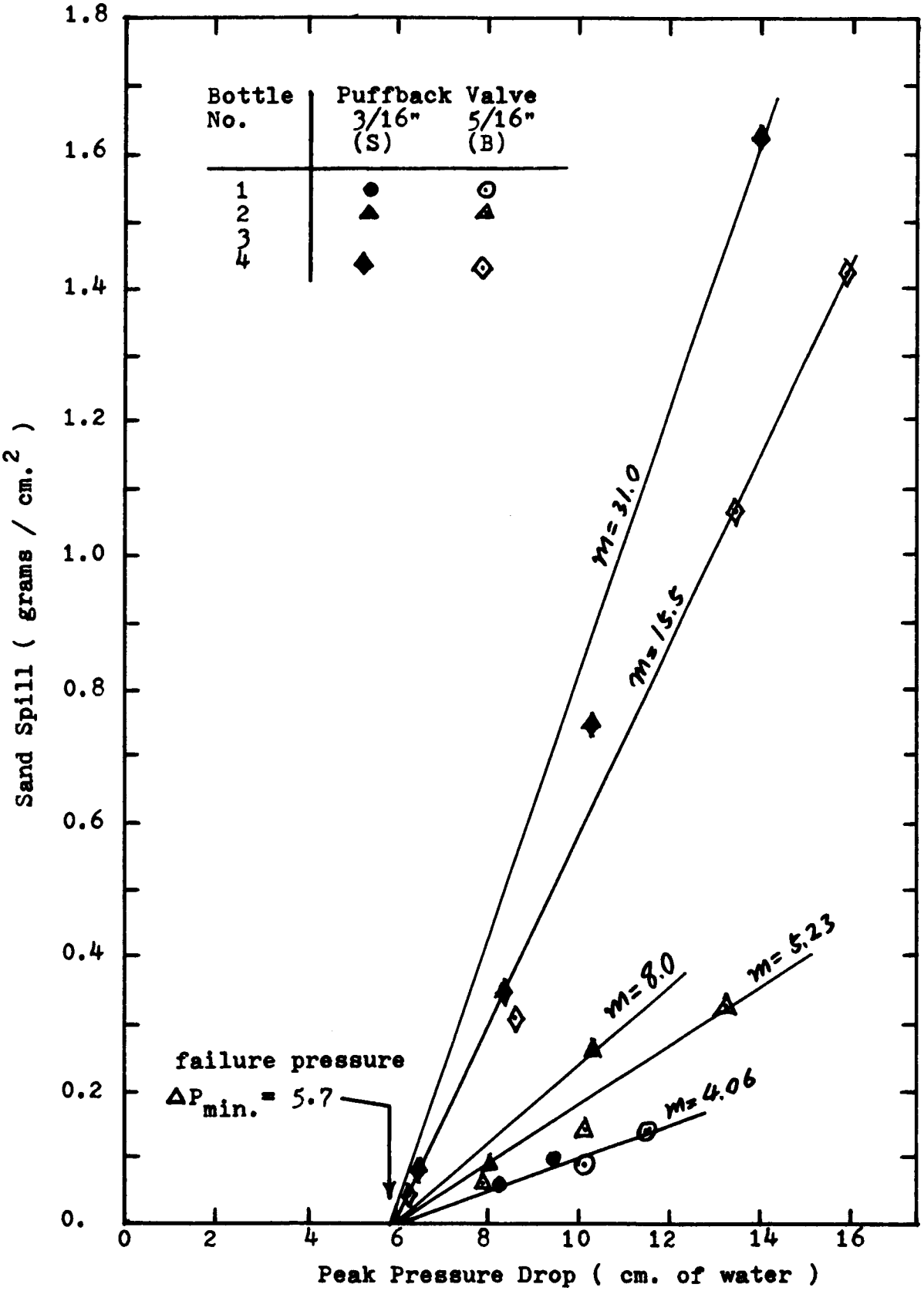

Figure 9.1-7: Failure Pressure for 20-30 Mesh Sand and Sideshot Puffback.

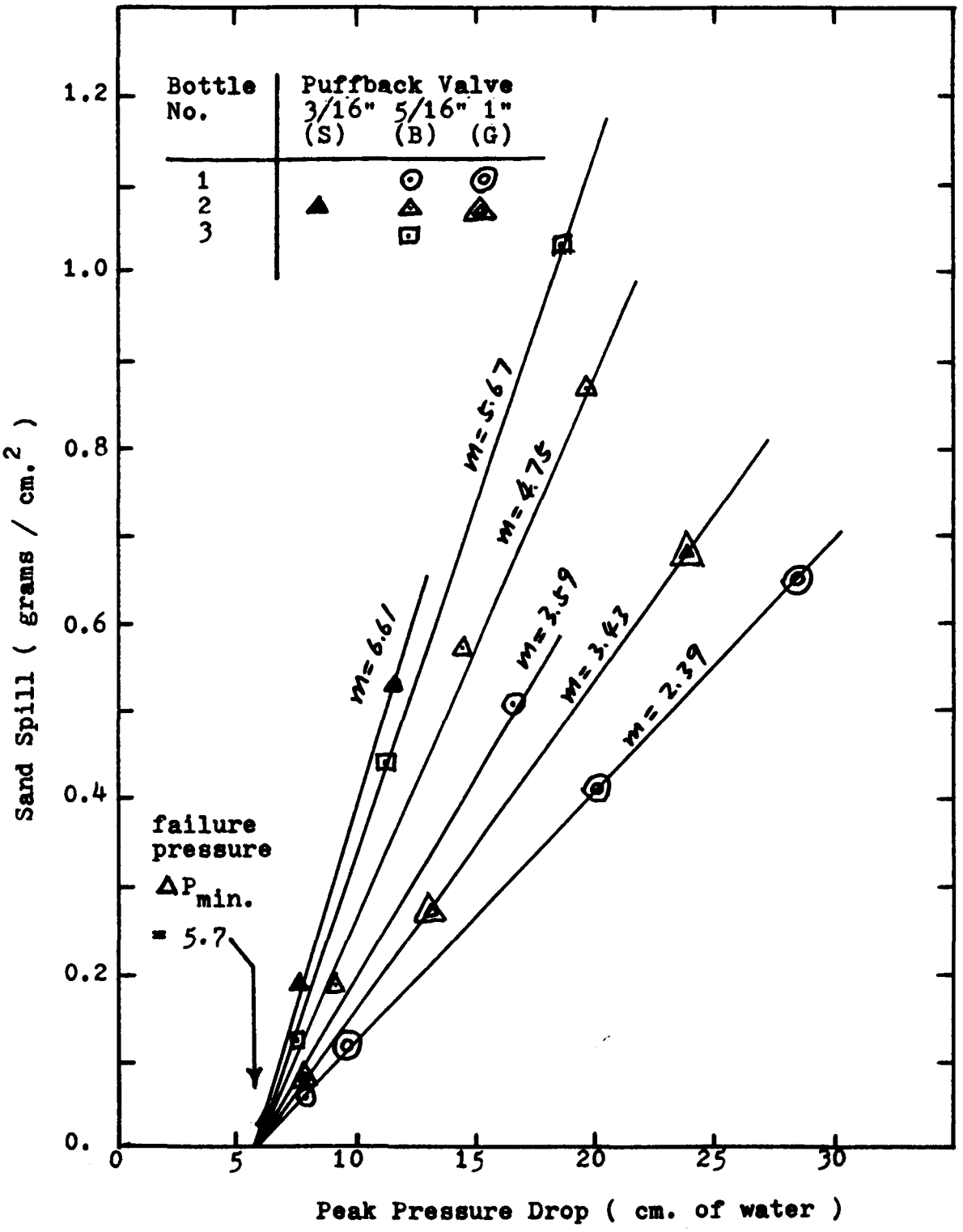

Figure 9.1-8: Failure Pressure for 40-50 Mesh Sand and Sideshot Puffback.

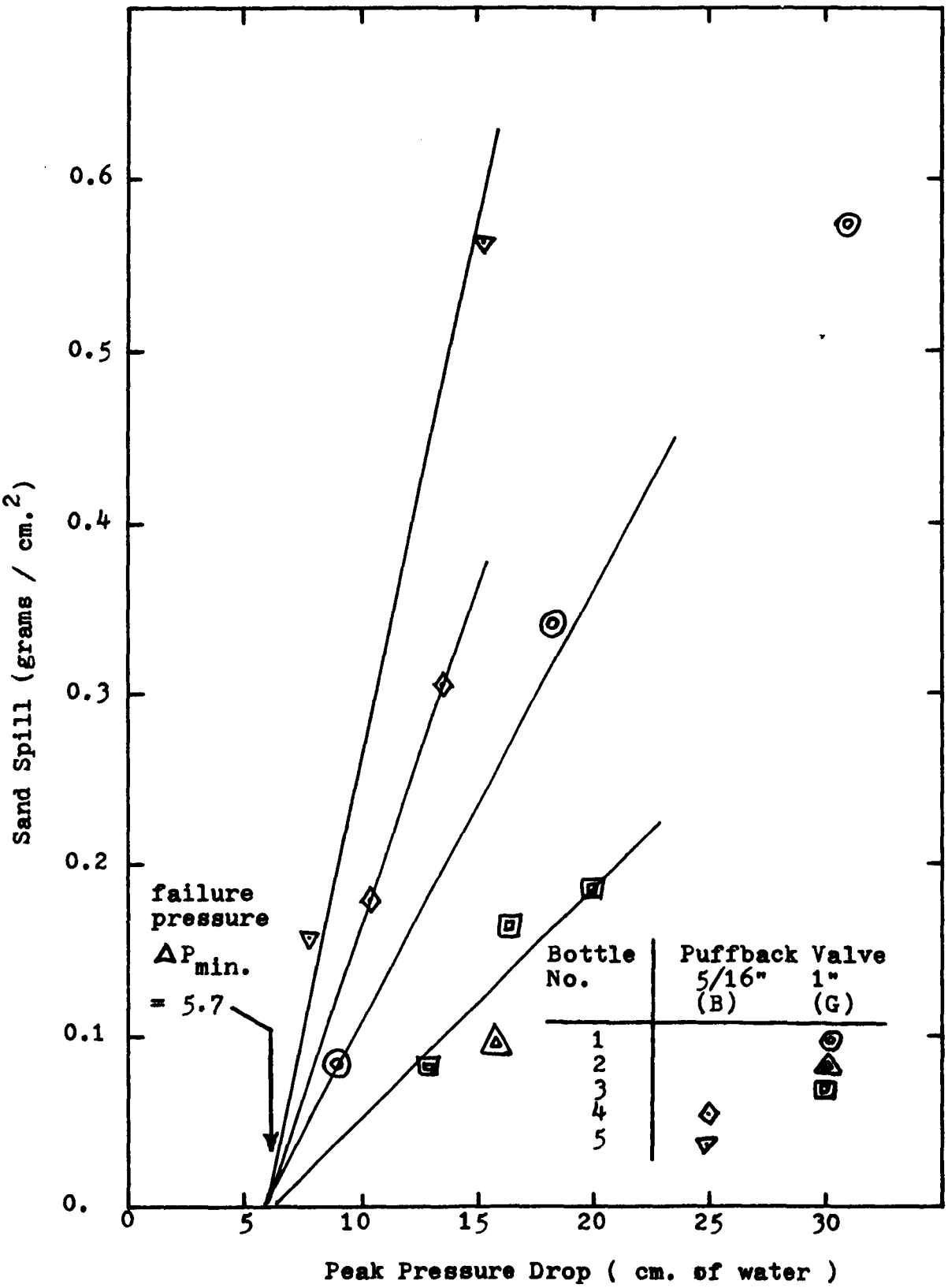

Figure 9.1-9: Failure Pressure for 10-14 Mesh Sand and Sideshot Puffback.

Table 9.1-2: Failure Pressure Under Different Conditions.

Sand Grade (mesh)	Steady Blowback (cm. of water)	Sideshot Puffback (cm. of water)	Downshot Puffback (cm. of water)
10-14	5.3	5.7	8.2
20-30	4.6	5.7	8.2
40-50	3.3	5.7	8.2

The failure pressure for steady blowback was determined as the point where there was some sand spill from one of the louver spaces. We never obtained a uniform spill or even obtained sand spill from all of the louver spaces. As discussed in Section 7.4, there is a tendency for the flow to concentrate to the weakest point during a steady blowback test. The over-all pressure drop measured might not be enough to represent the local aerodynamic force which causes the local sand spill. Also, the resistance of the louvers to the sand spill should be different for a steady sand flow and a transient sand flow.

The higher failure pressure for sideshot puffback than that for steady blowback and the still higher value for downshot puffback than that of the sideshot can be understood by considering the difference in rise time of the pressure curves. Section 2.3.4.4. showed

Whitman's (51, 52) work on fast loading on dry sand. Their work showed that the effect of increasing the rate of stress was to increase the elastic or plastic deformation. Putting all of the stress on suddenly will make it more difficult for the soil to fail. From data in Section 6.2., we know that the rise time for sideshot is about 10 msec. and the rise time for downshot is about 5 msec. This difference in rise time is believed to be due to the big tapered section volume of the sideshot puffback test set-up. The big volume will damp the rise in peak pressure. This explains why downshot puffback requires a higher failure pressure. The higher failure pressure for fast rise time does not necessarily mean that this condition should be avoided. There are other variables to be considered and this will be discussed in detail in Section 9.2.

9.1.2. Empirical Relation Between Sand Spill and Puffback Intensity.

In this section, we will show empirical correlations between the amount of sand spill and puffback intensity. We said before that the puffback intensity can be represented by two parameters -- the peak pressure drop " ΔP_{peak}" and the parameter "m". We can further simplify this by using one number, the active time, to represent the puffback intensity.

By assuming the puffback pressure drop curve has a triangular shape as in Figure 9,1-10, we can get the

following relation:

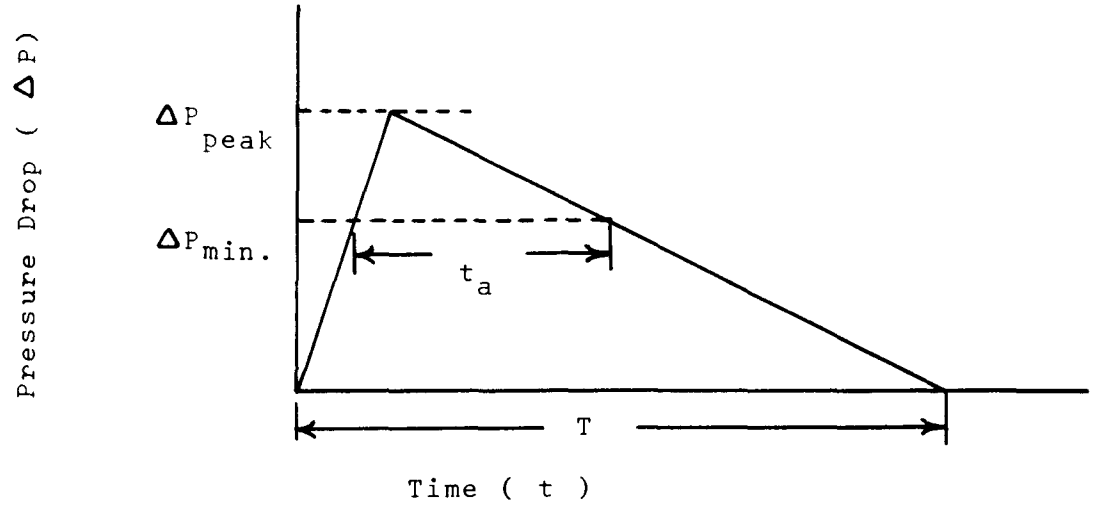

Figure 9.1-10: Triangular Shape Pressure Drop Curve.

$$\frac{t_a}{\Delta P_{peak} - \Delta P_{min.}} = \frac{T}{\Delta P_{peak}} \qquad (9.1\text{-}6)$$

By definition,

$$m = \frac{T}{\Delta P_{peak}} \qquad (9.1\text{-}7)$$

Substitute m into Equation 9.1-6,

$$t_a = m \cdot (\Delta P_{peak} - \Delta P_{min.}) \qquad (9.1\text{-}8)$$

We will call "t_a" the active puffback time or the active time which is the time period the pressure drop across the sand bed is greater than the minimum pressure drop required to cause sand spill. Or, we can think of this

as the time period during which body failure (Section 5.1) occurs.

If we plot sand spill per unit projected louver area versus $m \cdot (\Delta P_{peak} - \Delta P_{min.})$ or t_a, we obtain a good correlation. Figures 9.1-11 to 15 show this correlation for 20-30 mesh sand, 40-50 mesh sand, and 10-14 mesh sand for both downshot puffback and sideshot puffback. All of these sands were backed by 10-14 mesh sand. There were only a few data points for sideshot puffback on 10-14 mesh sand, and no correlation was obtained for this combination.

If we take w as the sand spill per unit area in grams per $cm.^2$ and t_a as the active time in msec., we obtain the following correlation equations:

20-30 mesh sand backed by 10-14 mesh sand, downshot puffback,

$$w = 11.36 \times 10^{-3} \cdot t_a \qquad (9.1\text{-}9)$$

20-30 mesh sand backed by 10-14 mesh sand, sideshot puffback,

$$w = 5.74 \times 10^{-3} \cdot t_a \qquad (9.1\text{-}10)$$

40-50 mesh sand backed by 10-14 mesh sand, downshot puffback,

$$w = 18.3 \times 10^{-3} \cdot t_a \qquad (9.1\text{-}11)$$

40-50 mesh sand backed by 10-14 mesh sand, sideshot puffback,

$$w = 13.0 \times 10^{-3} \cdot t_a \qquad (9.1\text{-}12)$$

10-14 mesh sand backed by 10-14 mesh sand, downshot puffback,

$$w = 3.87 \times 10^{-3} \cdot t_a \qquad (9.1\text{-}13)$$

The above equations can be expressed by a general form,

$$w = a \cdot t_a$$

$$= a \cdot m \cdot (\Delta P_{peak} - \Delta P_{min.}) \qquad (9.1\text{-}14)$$

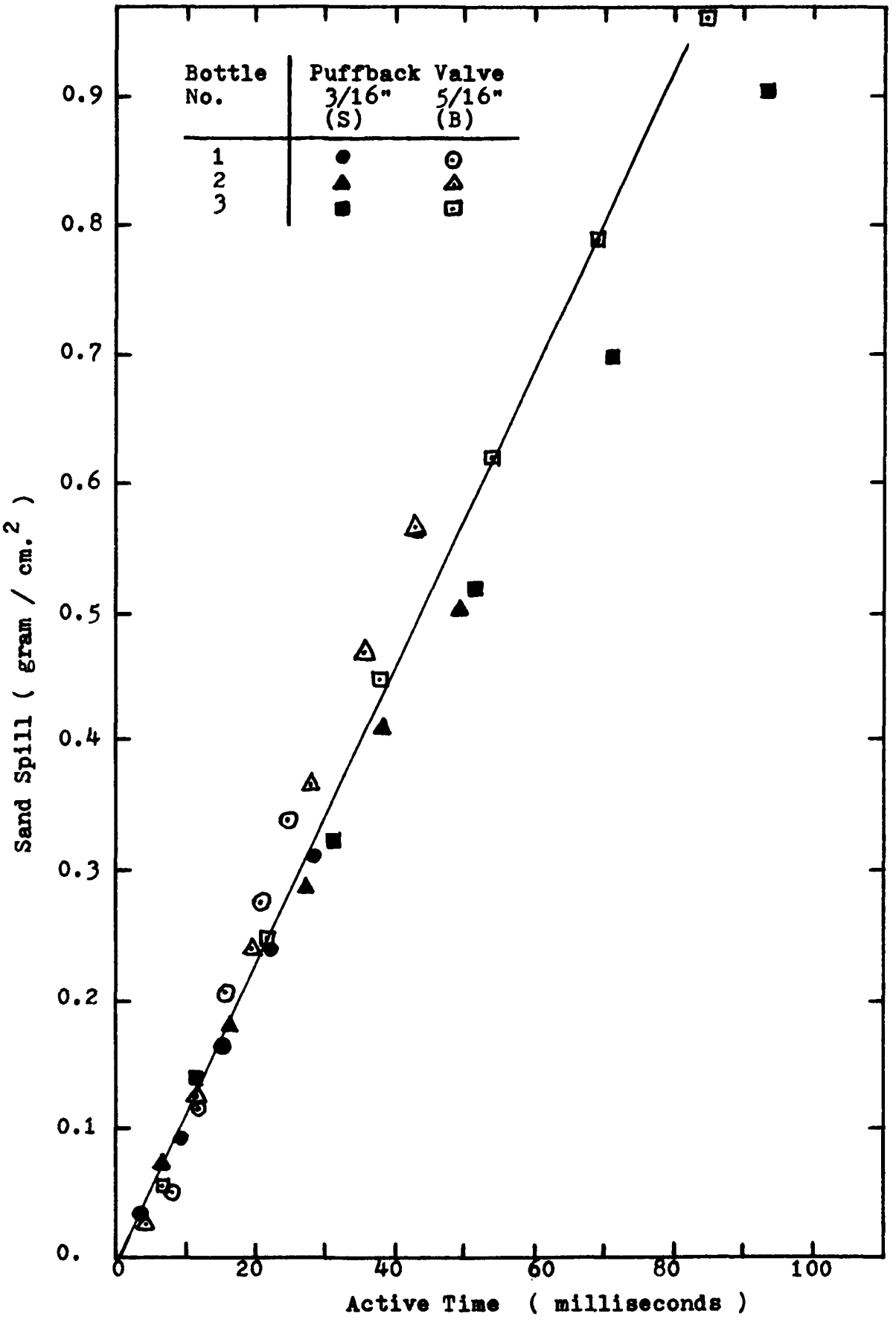

Figure 9.1-11: Sand Spill and Puffback Intensity Correlation for 20-30 Mesh Sand, Downshot Puffback.

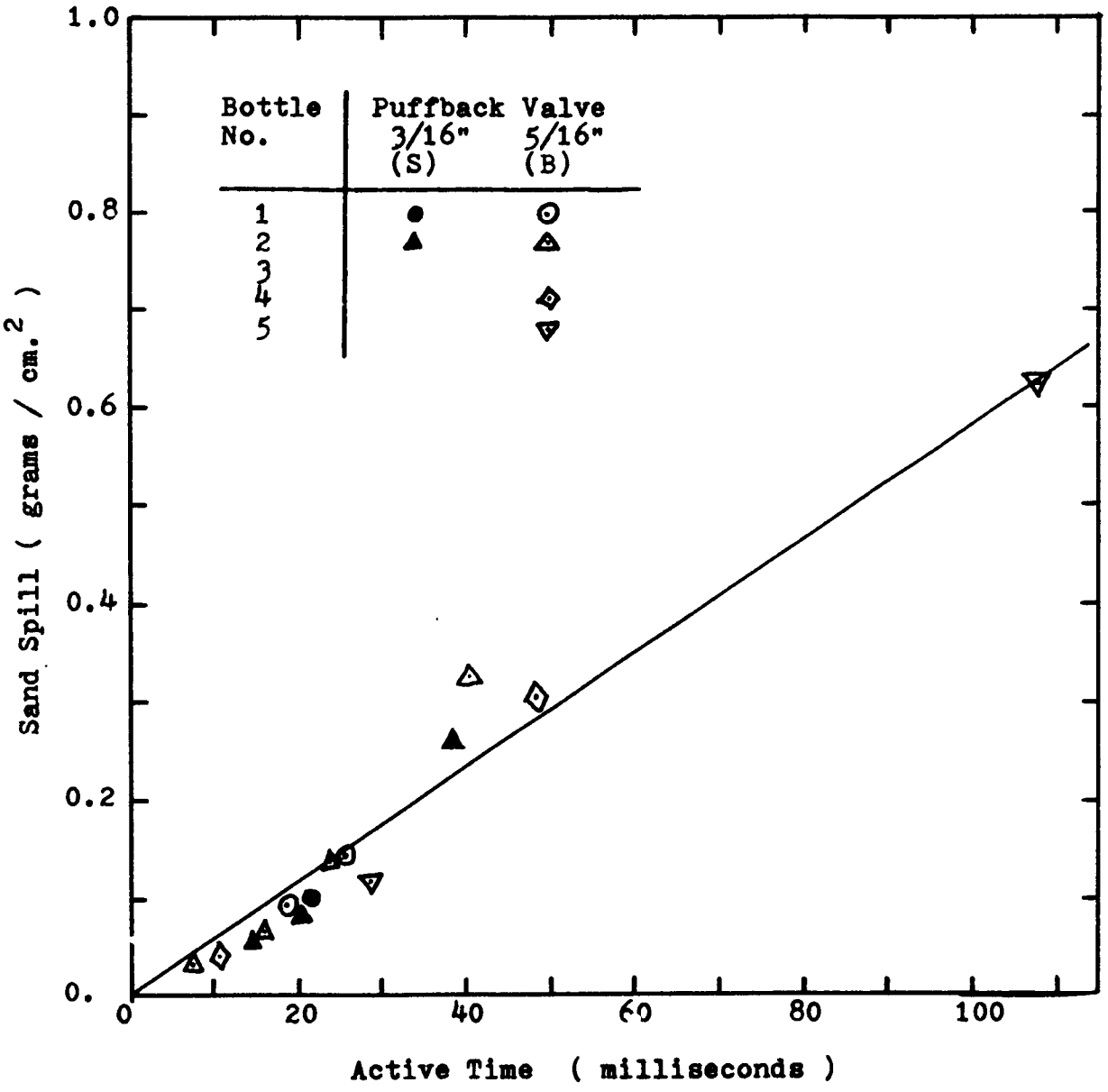

Figure 9.1-12: Sand Spill and Puffback Intensity Correlation for 20-30 Mesh Sand, Sideshot Puffback.

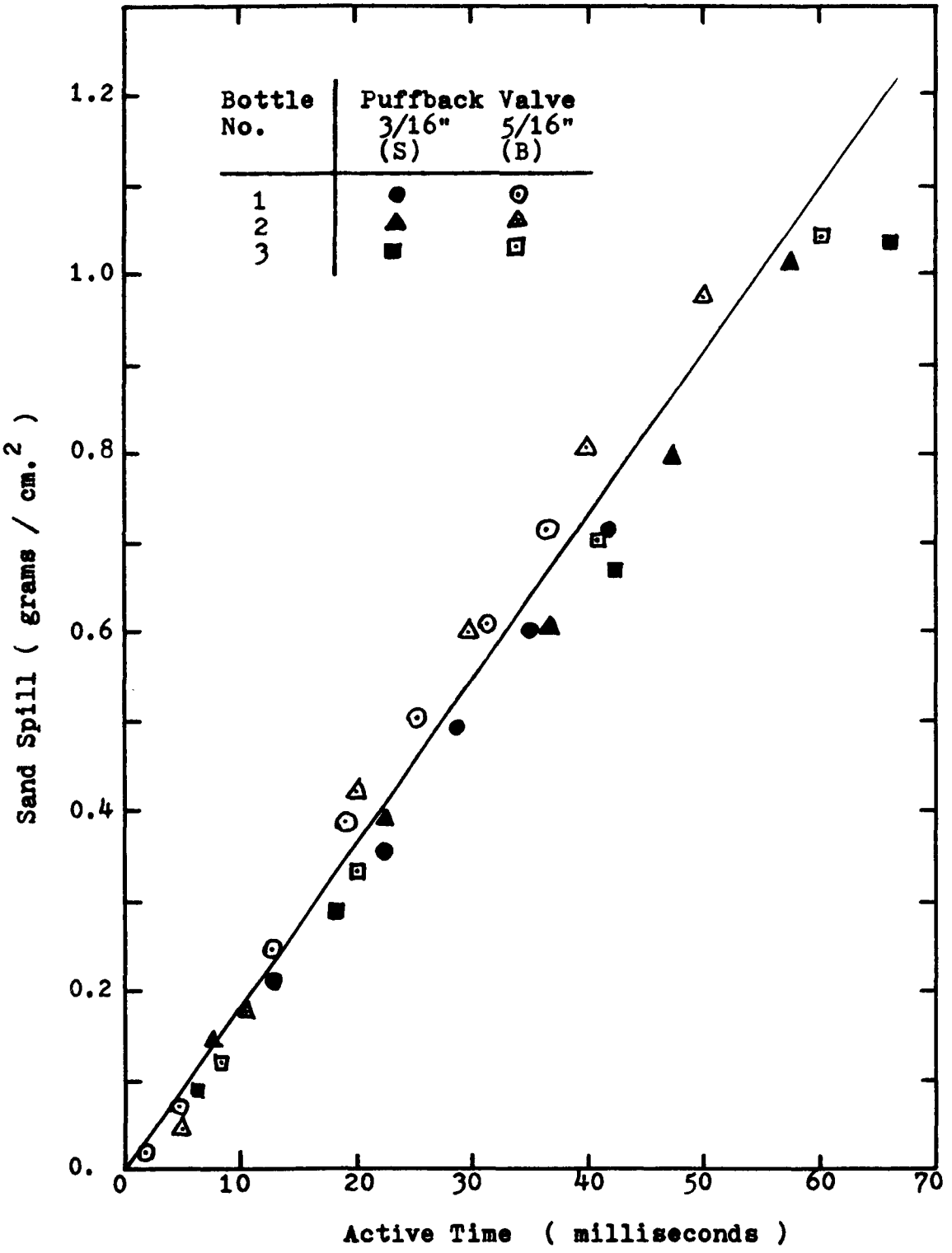

Figure 9.1-13: Sand Spill and Puffback Intensity Correlation for 40-50 Mesh Sand, Downshot Puffback.

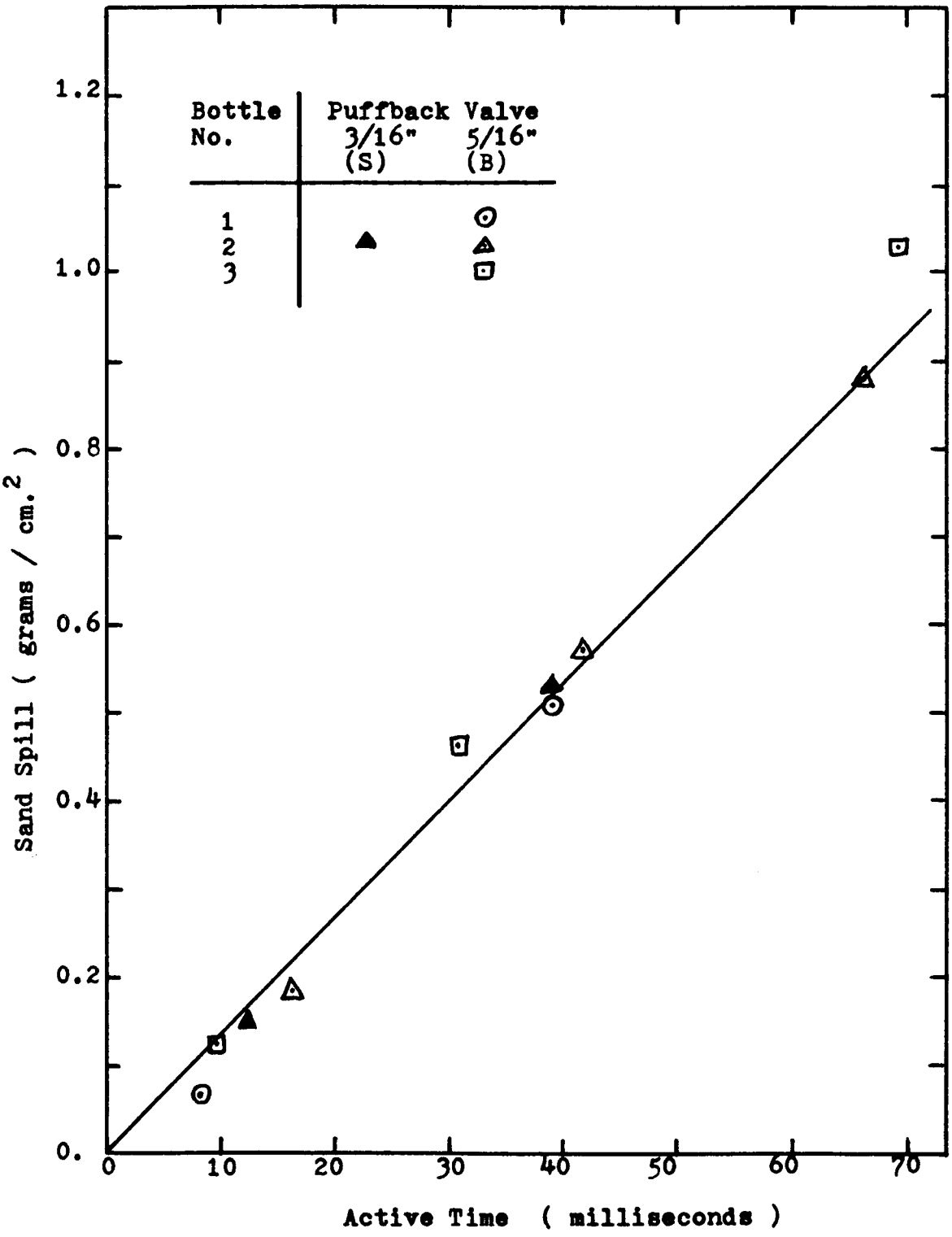

Figure 9.1-14: Sand Spill and Puffback Intensity Correlation for 40-50 Mesh Sand, Sideshot Puffback.

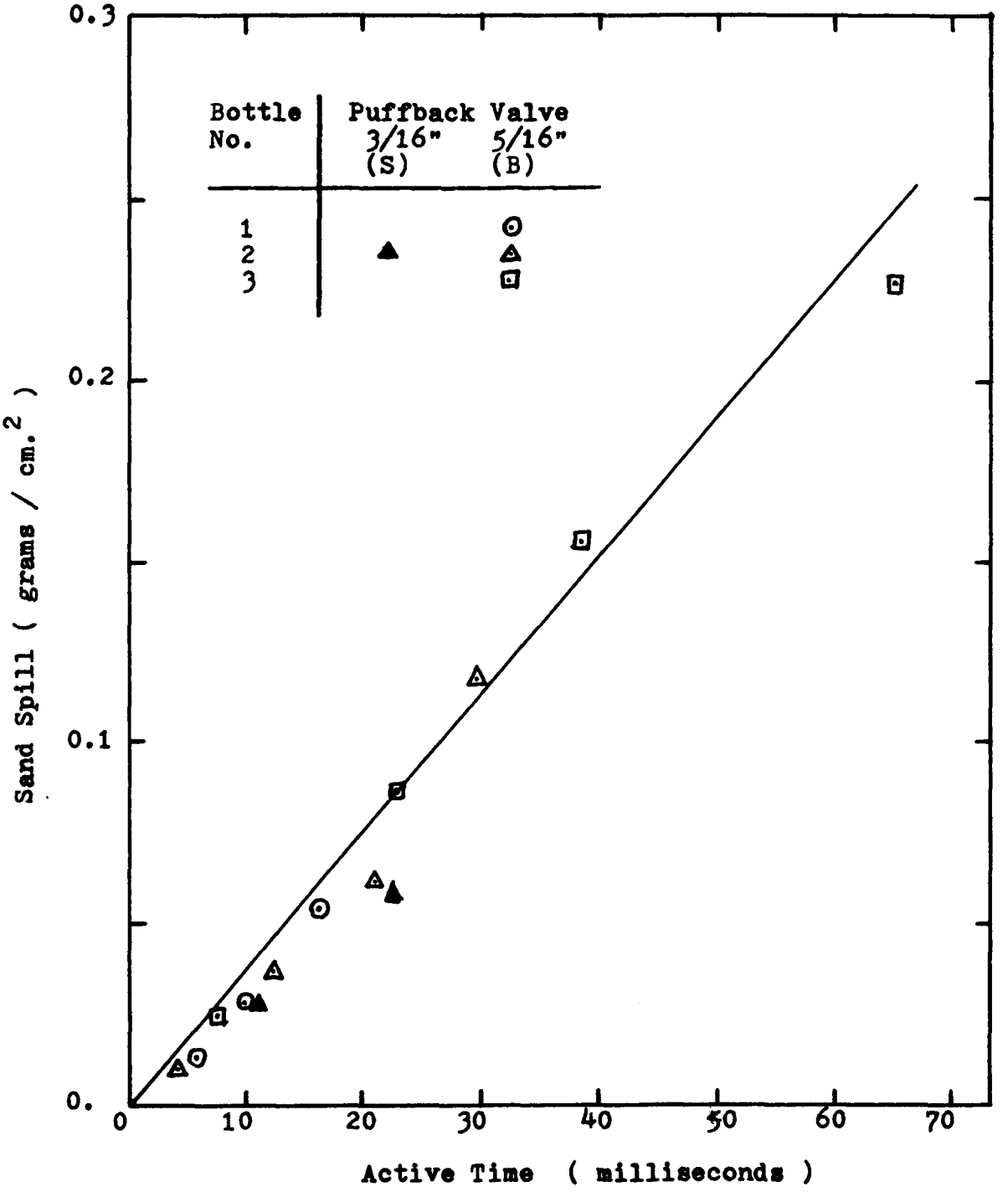

Figure 9.1-15: Sand Spill and Puffback Intensity Correlation for 10-14 Mesh sand, Downshot Puffback.

where "a" is a constant.

These equations indicate that the amount of sand spill is proportional to the active time only and is independent of the peak pressure drop.

Correlation of sand spill from CEC transducer using the first unit gave similar results. But comparison of the sand spill with the same puffback arrangement showed twice as much sand was removed from the first unit as that removed from the second unit. We believe that the difference is in the louver construction. This difference was discussed in Section 3.2.2. The opening of the chevron louvers used in the first unit is slightly wider than that of the chevron louvers used in the second unit. Also, there is much more wall resistance for the louvers used in the second unit because of the special requirement to get a good side view of the process. This means that we can lower the puffback intensity required to half of the value by slightly changing the structure of the louvers, although the general shape of the louvers remained the same.

9.2. Calculation of Pressure Drop and Design Consideration.

From the previous discussion we learned that the puffback sand spill is basically governed by the pressure drop across the bed. A steady blow air flow cannot build up a pressure drop much higher than the failure pressure. At the failure pressue the air will try to find the weakest point of the sand bed and cause sand to spill at that point. There will not be enough time to increase

the pressure drop before all the sand stocked in the top reservior will flow out, mostly from the topmost louver space. For the condition of puffback we build up a pressure drop across the sand bed in a very short time. The rise time is so short that the air has no time to find the weakest point of the sand bed. Hence, a uniform sand spill will result. Also, the pressure rise in the clean surface side is so fast that there is not enough time to let all the puffback air escape through the sand bed and we can build a much higher pressure drop than the failure pressure. From the data analysis in Section 9.1. we showed that we were able to correlate our data by considering the pressure drop only. It will be important to be able to predict the pressure rise on the clean surface side. This information can be obtained by considering a material balance across the system.

We consider a system consisting of the clean side space between the puffback valve and the sand bed. We assume the dirty side surface has a very large space so that the pressure on this side is constant and equal to zero pressure. Then, the pressure on the clean side will be equal to the pressure drop through the bed. A material balance will consist of the following terms.

$$\text{Input} = - \frac{dm_T}{dt} \qquad (9.2\text{-}1)$$

$$\text{Accumulation} = \frac{dm_c}{dt} \qquad (9.2\text{-}2)$$

$$\text{Output} = v_e \cdot A \cdot \rho \qquad (9.2\text{-}3)$$

where,

m_T = Mass of air in the puffback tank.

m_c = Mass of air in the clean side space.

v_e = Superfical escape velocity through the sand bed.

A = Projected panel bed louver area.

ρ = Air density.

From the transducer data in Section 6.1., we know that the pressure change across the bed is of the order of a few inches of water. We can assume the whole process is isothermal and from the ideal gas law,

$$m_T = \left(28.8 \frac{V_T}{R\ T}\right) \cdot P_T \qquad (9.2\text{-}4)$$

$$m_c = \left(28.8 \frac{V_c}{R\ T}\right) \cdot P_c \qquad (9.2\text{-}5)$$

where V_T is the volume of puffback tank and V_c is the volume of the clean side space. The material balance equation is:

$$\left(28.8 \frac{V_c}{R\ T}\right) \frac{dP_c}{dt} = -\left(28.8 \frac{V_T}{R\ T}\right) \frac{dP_T}{dt} - v_e \cdot A \cdot \rho \qquad (9.2\text{-}7)$$

Since the pressure change across the bed is only about 10 to 30 cm. of water, we can assume the puffback air is essentially incompressible. We discussed in Section 2.2.5. that Emanuel and Jones' (15) work showed that we can assume the gas is incompressible if

M_3 is less than 0.239. The escape velocity calculated from Equation 9.2-7 and transducer measurements of P_c and P_T showed that M_3 for our case is less than 0.05. For an incompressible fluid we can use Equation 2.2-6 to correlate P_c and v_e for a steady flow. In a transient condition like puffback, we can assume a quasi-steady exists at each instant and Equation 2.2-6 will still be applicable. Within the initial 20 msec. or so, we believe this equation will not be applicable since the initial portion of the pressure curve is basically due to a shock wave. It will also take some time to build up a pressure gradient for the quasi-steady state assumption to hold. Or, the dynamic pressure change cannot be too fast for the quasi-steady state to hold since Equation 2.2-6 is obtained for steady flow. Hence, for the initial 20 msec., we will have to take into consideration the shock wave and the transient air flow through porous media. The end effects will also have to be considered. If we neglect the initial portion and the end effect, then we can write Equation 2.2-6 in difference form.

$$-\frac{\Delta P}{\Delta x} = \frac{P_c}{b}$$

$$= \frac{\mu}{k} v_e + \frac{c\,\rho}{k^{\frac{1}{2}}} v_e^2 \qquad (9.2\text{-}8)$$

where b is the thickness of the sand bed. Solving for v_e from Equation 9.2-8,

$$v_e = \frac{-\frac{\mu}{k} + \sqrt{\left(\frac{\mu}{k}\right)^2 + \frac{4c\rho P_c}{k^{\frac{1}{2}} b}}}{2\frac{c\rho}{k^{\frac{1}{2}}}} \qquad (9.2\text{-}9)$$

If we neglect the second term in Equation 9.2-8, we obtain Darcy's law:

$$v_e = \frac{k P_c}{\mu b} \qquad (9.2\text{-}10)$$

Substituting into Equation 9.2-7,

$$\frac{dP_c}{dt} = \frac{V_T}{V_c}\frac{dP_T}{dt} - \frac{R T k A \rho}{28.8 V_c \mu b} \cdot P_c \qquad (9.2\text{-}11)$$

$$\frac{dP_c}{dt} = -\alpha\frac{dP_T}{dt} - \beta \cdot k \cdot P_c \qquad (9.2\text{-}12)$$

where,

$$\alpha = \frac{V_T}{V_c} \qquad (9.2\text{-}13)$$

$$\beta = \frac{R T A \rho}{28.8 V_c \mu b} \qquad (9.2\text{-}14)$$

α and β are constants depends on the configuration of the filter design and on the air properties.

From Figure 6.1-1-a and Figure 6.1-2-a, we see that the pressure decay in the puffback tank can be written in a general form as:

$$P_T = P_{T,o} \cdot e^{-\delta t} \qquad (9.2\text{-}15)$$

where $P_{T,o}$ is the initial pressure in the puffback tank and δ is a constant depending upon the puffback tank volume

and the flow parameters between the puffback tank and the clean side space, such as valve orifice area, valve opening time, and all of the piping and fittings between these two points. The general characteristics of Equation 9.2-14 are shown in Figure 9.2-1. δ is actually a measure of the decay rate of the puffback tank air pressure or a measure of the input flow rate of puffback air to the filter. A large value of δ indicates a fast decay in puffback pressure or a rapid air flow across the filter.

Differentiating Equation 9.2-15 with respect to t gives,

$$\frac{dP_T}{dt} = - P_{T,o} \cdot \delta \cdot e^{-\delta t} \qquad (9.2\text{-}16)$$

Substituting this into Equation 9.2-12, gives,

$$\frac{dP_c}{dt} + \beta k P_c = \alpha P_{T,o} \delta e^{-\delta t} \qquad (9.2\text{-}17)$$

Multiplying by $e^{\beta k t}$ and integrating gives:

$$e^{\beta k t} P_c = \int \alpha P_{T,o} \delta e^{-\delta t} e^{\beta k t} dt + C \qquad (9.2\text{-}18)$$

$$P_c = \frac{\alpha P_{T,o} \delta}{\beta k - \delta} e^{-\delta t} + C e^{-\beta k t} \qquad (9.2\text{-}19)$$

At $t = 0$, $P_c = 0$ and

$$C = - \frac{\alpha P_{T,o} \delta}{\beta k - \delta} \qquad (9.2\text{-}20)$$

so that,

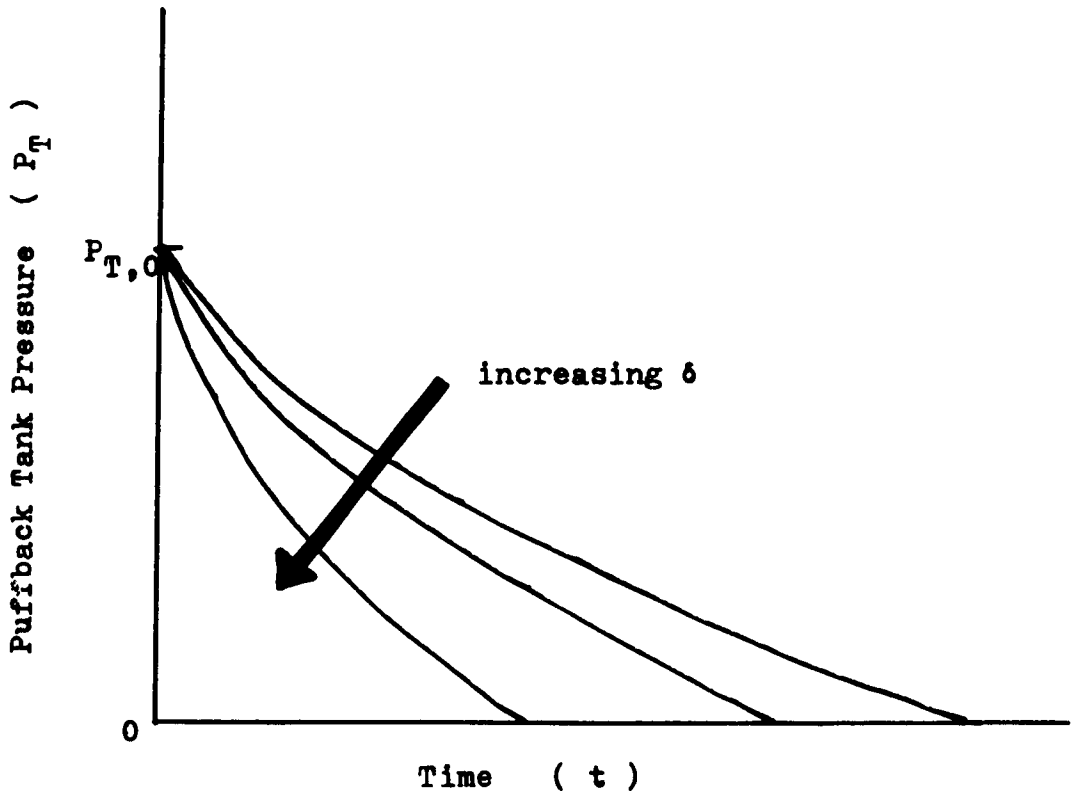

Figure 9.2-1: Pressure Decay in the Puffback Tank.

$$P_c = \frac{\alpha P_{T,o} \delta}{\beta k - \delta} (e^{-\delta t} - e^{-\beta k t}) \qquad (9.2\text{-}21)$$

which shows the pressure change within the clean side space.

In order to find the peak value of P_c or ΔP_{peak} we differentiate P_c with respect to t and set it to zero.

$$\frac{dP_c}{dt} = \frac{\alpha P_{T,o} \delta}{\beta k - \delta} (-\delta e^{-\delta t} + k e^{-\beta k t})$$

$$= 0. \qquad (9.2\text{-}22)$$

$$-\delta e^{-\delta t} + \beta k e^{-\beta k t} = 0. \qquad (9.2\text{-}23)$$

$$e^{(\beta k - \delta) t} = \frac{\beta k}{\delta} \qquad (9.2\text{-}24)$$

Therefore, t_{peak}, the time required to reach the peak pressure is,

$$t_{peak} = \frac{1}{\beta k - \delta} \ln \left(\frac{\beta k}{\delta}\right) \qquad (9.2\text{-}25)$$

The peak pressure drop will be,

$$\Delta P_{peak} = \frac{\alpha P_{T,o} \delta}{\beta k - \delta} (e^{-\delta t_{peak}} - e^{-\beta k t_{peak}}) \qquad (9.2\text{-}26)$$

or,

$$\Delta P_{peak} = \frac{\alpha P_{T,o} \delta}{\beta k - \delta} \left(e^{\frac{\delta}{\beta k - \delta} \ln\left(\frac{\beta k}{\delta}\right)} - e^{\frac{-\beta k}{\beta k - \delta} \ln\left(\frac{\beta k}{\delta}\right)}\right) \qquad (9.2\text{-}27)$$

Since $t \geqq 0$, we note that $0 \leqq e^{-\delta t} \leqq 1$, and $0 \leqq e^{-kt} \leqq 1$, Equation 9.2-26 shows that the peak pressure value is

basically determined by $\frac{\alpha P_{T,o} \delta}{\beta k - \delta}$. In Section 9.1. we learned that the puffback sand spill is proportional to the active time, t_a. For the same value of m, the active time is proportional to the peak pressure. Hence, increasing the peak pressure will increase puffback intensity. The m-value will be basically determined by δ. Equation 9.2-26 showed certain ways to increase the peak pressure drop.

1. Increase α, that is increase the puffback tank volume V_T or decrease the clean side space V_c.

2. Increase $P_{T,o}$ the initial puffback tank pressure.

3. Increase δ, the input flow rate to the clean side space. This can be done by increasing the puffback valve orifice area, increasing the valve opening rate, or decreasing all the flow resistance between the puffback tank and the filter.

4. Decrease k which is the permeability of the sand. Equation 2.2-3 showed this can be done by decreaseing the porosity or using fine sand.

Equation 9.2-21 showed that for a given test set-up and given puffback tank pressure, $P_{T,o}$, the pressure drop history will depend on the permeability of sand bed only. For a media composed of relatively uniform-size particles, the permeability of the media can be predicted from Equation 2.2-3. The ultimate packing of the sand bed (fine sand) in the panel bed filter

after undergoing puffback should be similar to that of a sand bed which has been deposited by flood water (Section 2.3.4.2.). The ultimate packing of the panel bed should have a porosity of about $\epsilon = 0.50$. Equation 2.2-3 thus becomes:

$$k = 1.50 \times 10^{-3} d^2 \ (cm.^2) \qquad (9.2\text{-}28)$$

For 20-30 mesh sand, the average sand diameter is 0.0715 cm. and the predicted permeability from Equation 9.2-28 is,

$$k = 7.69 \times 10^{-6} \ (cm.^2) \qquad (9.2\text{-}29)$$

The measured permeability can be obtained from Equation 2.2-6 using pressure drop data. Comparison of Equation 2.2-6 and Equation 7.4-1 gives,

$$0.07 = \frac{\mu \Delta x}{g k} \qquad (9.2\text{-}30)$$

where g is the acceleration of gravity and Δx is the thickness of the sand bed. If we neglect the back-up 10-14 mesh sand, Δx will equal b, the thickness of the fine sand and

$$k = \frac{\mu b}{0.07 g} = 6.78 \times 10^{-6} \ cm.^2 \qquad (9.2\text{-}31)$$

This shows that Equation 9.2-28 gives a very good prediction.

With a known pressure decay rate in the puffback tank or a known input signal to the clean side space as expressed by Equation 9.2-15, we can calculate the pressure buildup on the clean side space with Equation 9.2-21.

The pressure decay rate in the puffback tank is expressed by the decay rate constant, δ, which depends on all the puffback equipment used. Figure 9.2-2-a shows one experimental pressure decay curve (the dotted line) in the puffback tank and one curve calculated from Equation 9.2-15 with the same puffback tank pressure, $P_{T,o}$, for both curves. The value of δ used in Equation 9.2-15 was calculated by arbitrarily picking up a point from the experimental curve and fitting into the equation.

Figure 9.2-2-b shows the measured pressure drop curve and the calculated pressure drop curve using Equation 9.2-21. The puffback code for this calculation was A-3-S-2-60-D. The following values of the variables were used in the calculation.

Panel Bed: $V_T = 2.06 \times 10^2$ cm.^{3}

$V_c = 7.13 \times 10^2$ cm.^{3}

$A = 232.3$ cm.^{2}

$b = 2.6$ cm.

Sand: $k = 6.78 \times 10^{-6}$ cm.^{2}

Air: $T = 298^o$ K

$R = 8.478 \times 10^4$

$\rho = 1.123 \times 10^{-3}$ g/cm.^{3}

$\mu = 1.79 \times 10^{-4}$ poise

Puffback: $P_{T,o} = 60$ psig. $= 4.22 \times 10^3$ g/cm.^{2}

$\delta = 32.3$

$\alpha = 0.289$, and $\beta = 6.76 \times 10^8$

The calculated pressure drop was about half the value of that measured experimentally. We should

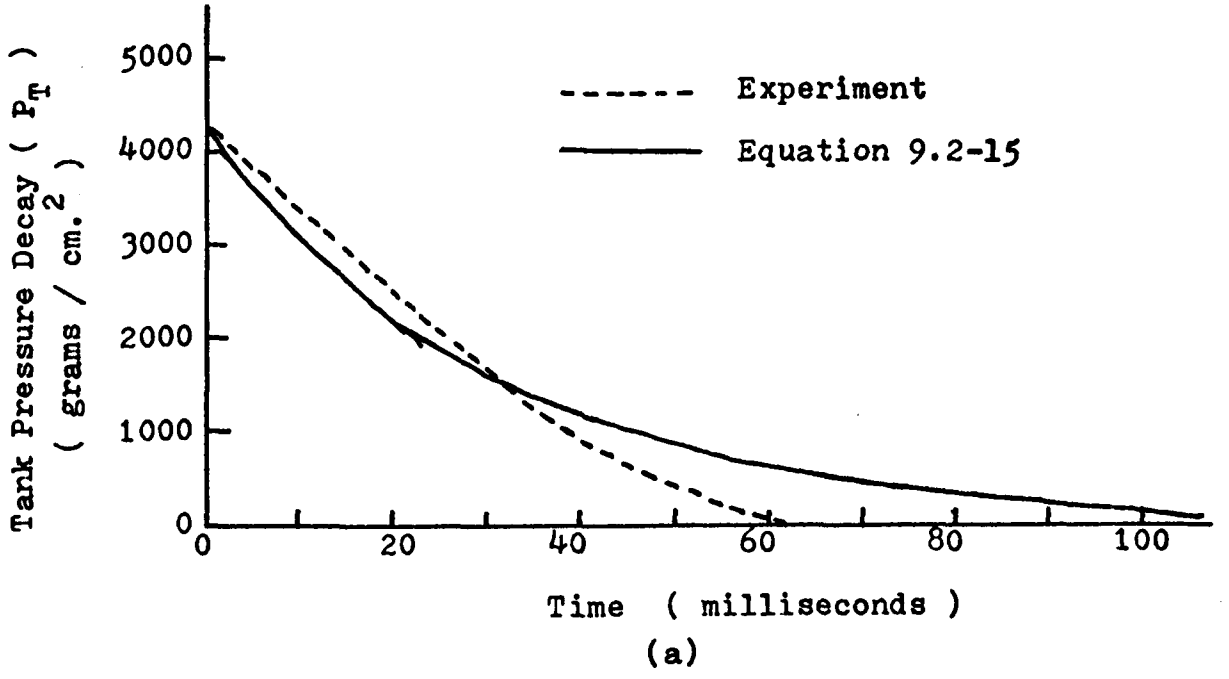

(a)

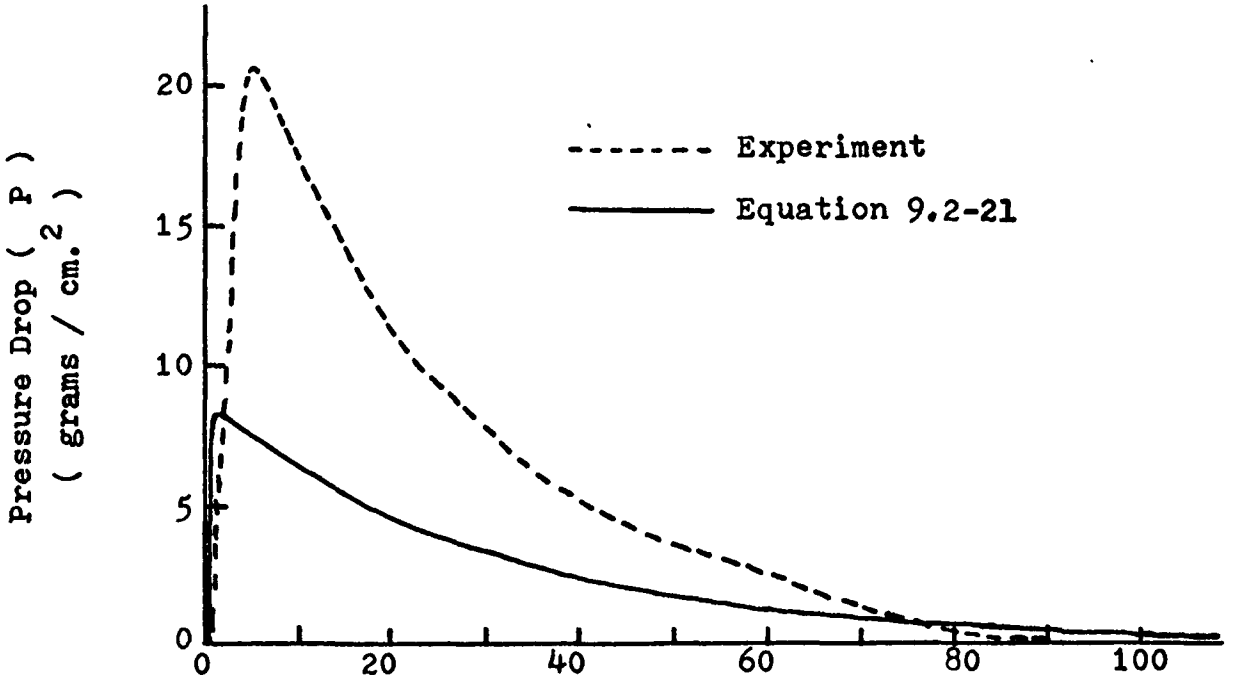

(b)

Figure 9.2-2: Calculated Tank Pressure Decay and Panel Bed Pressure Drop

remember that in the theoretical analysis we neglected the initial shock wave, the end effect, the louver resistance, and the transient air flow phenomena. We also neglected the second term in the modified Darcy's law. We did not consider the porosity change during the puffback process. The decrease in porosity will decrease the soil strength from the soil mechanics point of view, which will cause more sand spill. But, the decrease in porosity will increase the permeability which in turn will decrease the aerodynamical drag force from the aerodynamics point of view. The interaction of these two effects should be studied further, especially for a tall panel bed.

9.3. Effects of Fly Ash Deposit on Puffback.

Puffback with the deposit of fly ash at the surface sand is the actual condition which we deal with. The effect of fly ash deposit should be considered both from soil mechanics and aerodynamics.

In Section 2.3.3. we showed that there are three sources of soil strength -- the friction resistance, the interlocking, and the true cohesion. During the filtration process, the fly ash deposited on and within the surface sand grains formed agglomerates and adhered to the sand grain surfaces. The fly ash deposit tends to bind the sand grains together due to the adhesion and the cohesion. Hence, the soil strength will increase and decrease the sand spill. We will have to increase the puffback intensity to remove the same amount of sand.

Equation 9.2-21 and 27 showed that for a given test set-up, the puffback intensity will depend on the permeability of the sand bed. Decreasing the permeability will increase the peak pressure for the same puffback arrangement. The deposit of filter cake in the surface sand grains will serve to decrease the local permeability. This effect will tend to increase the puffback intensity and cause more sand spill. Hence, less puffback pressure or a smaller puffback tank volume will be required. Or, we can consider that for high permeability most of the puffback air leaks through the pores of the sand bed and its energy is wasted and is not used to cause any sand spill. A decrease in permeability will utilize a portion of this originally wasted energy. Like the porosity effects discussed in last section, soil mechanics and aerodynamics will have an opposite effect on puffback. Actual puffback tests during the filtration study showed both these effects. The final result of these opposing effects depends on which effect is stronger.

For 10-14 mesh sand, when the amount of dust deposited was not too great, most of the dust penetrated into the sand bed and coated the sand grains near the surface. There was almost not change in permeability (See Section 7.3. for pressure drop change). Hence, the soil mechanics effect governed and a higher puffback intensity was required. When the fly ash deposit was thick, the filter cake started to form at the sand surface and the permeability

decreased. In this case, aerodynamics effect governed and a lower puffback intensity was required.

For 20-30 mesh sand, the pores were small enough to allow a filter cake to be formed on the surface easily, yet the pores were large enough to let a portion of the puffback air go through freely without fully utilizing its energy. We always observed that a lower puffback intensity was required than for a clean sand bed. It seemed that the aerodynamics effect overcame the soil mechanics effect very quickly for 20-30 mesh sand. We believe that when the dust deposit on the sand surface is very thin, there might be instances when slightly less sand will be dislodged due to the soil mechanics effect.

In the filtration studies on 40-50 mesh sand, it seemed that we will always need to increase the puffback pressure as the number of cycles increased. The penetration of fly ash into the sand is always less than 0.1 inch. The permeability was already very low for 40-50 mesh sand. Due to this low permeability, very little amount of puffback air was required. It seems than any additional reduction in permeability at the sand surface has almost no effect on the puffback intensity. Or, we can say that the puffback air has been used near its maximum efficiency in removing the sand due to the already low permeability. An additional decrease in permeability will not help. On the contrary, the fly ash deposit

formed a very good filter cake near the surface grains and bound the surface sand grains together. Hence, we will require a higher puffback intensity than for a bed of clean sand only.

Chapter 10: Conclusions.

The conclusions will be classified into three categories.

General conclusions:

1. We developed a fly ash feeder which can feed fly ash in small amounts into a high pressure air stream at either high flow rate or low flow rate. This was accomplished by balancing the pressure between the feeder and the high pressure line and using two variable motor drives. One criticism of the fly ash feeder is that the redispersed fly ash will become electrically charged.

2. Two test units were built. All filtration data presented in this thesis were taken in the first unit. Most of the puffback tests used the second unit, which had a transparent side wall for visual observation.

3. A series of louvers of different shapes were tested with the conclusion that the chevron louver is believed to be the best. The angle of repose and the angle of failure are the two most important factors to be considered in the louver design.

Conclusions of filtration studies:

4. We developed isokinetic sampling systems for collecting dust directly on filter paper. We believe our technique gave us reliable filtration efficiency data.

5. For the first few cycles, the penetration of fly

ash was about five times lower for dirty sand than for washed clean sand. We believe the reason for this is that fly ash sticks to itself better than to sand.

6. The panel bed filter operates better at higher velocities, about 30-40 ft./min. than at about 10-15 ft./min. The panel bed filter also operates well at very low velocities, around 5 ft./min., because of the formation of a better filter cake and an increased Brownian diffusion effect. But, for practical purposes we prefer higher velocities for high capacity operation.

7. We obtained super-high efficiencies with 40-50 mesh sand. Because the efficiency was so high we were able to use the Royco particle counter to obtain some qualitative data on the performance of panel bed filtration of micron-size particulates.

8. Poor efficiencies were observed on 10-14 mesh sand. At high velocities (30 ft./min. or higher), fly ash penetrates deep into the sand bed and tends to saturate the sand bed.

9. Yu's work on penetration of 1.1 micron polystyrene aerosols by a horizontal sand bed showed a two-fold rise and fall in penetration with increase in velocity. The second rise in penetration was believed to be due to particle bouncing and re-entrainment.

10. The penetration of 1.1 micron monodisperse aerosols by different filter cakes were studied. Fly ash can form a good filter cake over fine sand and the fly

ash filter cake can be used as an absolute filter. Teflon powder formed a very poor filter cake and gave poor efficiency. Difference in adhesion and/or autohesion of the powders is believed to be the reason.

11. Three models for granular bed filtration were suggested. Clean bed filtration gives poor efficiency. Rooting-cake filtration forms the foundation of a surface filter cake. Surface-cake filtration gives very high efficiency.

12. The panel bed filter operation with properly regulated puffback cleaning avoids clean bed filtration and rooting-cake filtration and always operates at surface-cake filtration after the first few cycles.

13. The efficiency of the panel bed filter depends strongly on the integrity of the filter cake. Filter cakes formed at low velocities (10 ft./min. or lower) contain fewer and smaller pin-holes resulting in a higher efficiency, but the filter cake will be more porous tending to reduce the efficiency. Filter cakes formed at high velocities (20 ft./min. or higher) contain many pin-holes resulting in a lower efficiency, but the filter cake will be more dense tending to raise the efficiency.

14. The integrity of the filter cake depends strongly on the adhesion and autohesion properties of the dust to be filtered. Adhesion is important to form a filter cake with a strong base which is more stable. Autohesion is important to catch additional dust and to form a good

filter cake for subsequent high filtration efficiency.

15. We believe that panel bed filtration efficiency can be improved by improving the adhesion and autohesion of the system. This could be done by surface treatment of the dust and/or the granules, increasing the humidity, and increasing electrical charge.

Conclusions of puffback studies:

16. A steady backflow of gas does not remove a uniform layer of dust and sand from all free surfaces over the height of a panel bed, whereas puffback air flow can result in a uniform sand spill.

17. For an initially dense sand bed, steady blowback flow always leads to a local surface failure of the bed causing a spill of solid from the inner edge (the weakest point within one louver space) of the top gas-entry surface. The top gas-entry surface is the weakest point over the panel height because the porosity is lowest at this point. For an initially loose sand bed, steady blowback flow will cause a sand spill to start from any point where the soil strength is weak. This is followed by large sand flow from the topmost surface, which becomes the weakest point once the sand bed is in motion.

18. We believe puffback sand spill is a transient soil mechanics failure phenomenon caused by a transient aerodynamic drag force.

19. The puffback air flow rate has to rise rapidly to build pressure on the clean side of the panel bed to

a value beyond a critical minimum pressure in order to cause a body movement failure of the sand bed, and thereby to cause a uniform sand spill. The rise time should be fast enough so that the sand failure will start at substantially the same time everywhere in the panel bed. The rise time should also be fast enough so that the porosity of the bed will not be affected unequally in different parts of the bed by the sand motion, such as would result in a major soil strength decrease. For this reason, the puffback duration time must not be too long.

20. High speed movies showed that there are three stages of puffback failure. In the first stage, sand grains jump up from the inner edge of the gas-entry surface. This is a local failure that we believe is caused by the shock wave, and gives negligible sand spill. In the second stage the sand moves forward in a plug flow with a slightly downward motion. We call this body failure. In the third stage, a small amount of sand falls from the outer edge of the gas-entry surface while the bulk of the sand is moving downward by gravity. This is also a local failure, and may merely reflect the relatively slow adjustment of the newly formed free surface to a stable configuration.

21. Sand failure does not appear to occur immediately after the pressure pulse reaches the minimum critical pressure. There is a time delay of about 10 milliseconds.

22. Two types of transducers were used to measure the pressure pulse. CEC transducers, which are diaphragm type, were used for initial tests on the first unit. Kistler transducer data from the second unit are more reliable.

23. Two puffback configurations were tested -- sideshot and downshot, the volume of the space between puffback valve and the clean side of the panel bed being larger for the sideshot configuration. Sideshot puffback gave a rise time in the pressure difference of about 10 milliseconds and downshot puffback gave a rise time of about 5 milliseconds.

24. Comparison of puffback data for the first unit and the second unit showed that the louver surface angle has a strong effect on the sand spill. A smaller angle results in less sand spill even though the pressure curve was about the same.

25. Sand spill uniformity tests showed that the height of the front louver relative to the middle and rear louvers has a strong effect. Initial sand bed porosity is also a critical factor. Non-uniform initial sand bed porosity results in non-uniform soil strength and hence non-uniform sand spill.

26. A sand level propagation time constant of about 4 msec. per (grams/cm.^{2}) per cm. was measured. This constant is defined as the time required in msec. for the sand level to propagate 1 cm. upward when the sand spill is 1 gram/cm.^{2} based on the projected louver area.

27. ($\Delta P_{min.}$), defined as the minimum pressure drop required to cause a body movement sand spill, of 8.2 cm. of water was obtained for downshot puffback and a value of 5.7 cm. of water was obtained for sideshot puffback. This value appears to be independent of sand size.

28. The difference in $\Delta P_{min.}$ of the two different puffback configurations is believed to be due to the difference in the rise time of the pressure curve. A fast rise time will result in more soil resistance due to the elastic and plastic deformation of the sand, and a higher $\Delta P_{min.}$ will be required.

29. We found that active time (t_a) can be used to represent the puffback intensity. This is the time period the pressure drop across the sand bed is greater than the minimum pressure drop required to cause a body movement sand spill.

30. Empirical relations showed that puffback sand spill is proportional to the active time and is almost independent of the peak pressure drop.

31. Peak pressure drop seemed to have no direct effect on sand spill. We believe this is because any additional peak pressure drop is balanced by an increase in the soil friction force due to the confining effect of the louver plates.

32. Under real operating conditions, $\Delta P_{min.}$ will not be a constant due to the porosity change during the puffback sand spill and other factors. A complete stress analysis

will have to consider transient aerodynamics coupled with transient soil mechanics.

33. The pressure build up on the clean side can be fairly well predicted by considering the air input and Darcy's law for air output through sand bed.

34. In order to obtain a more uniform sand spill, the pressure rise time on the clean side should be as fast as possible, as discussed in conclusion 19. A fast rise time normally results in higher value of minimum failure pressure, $\Delta P_{min.}$. But, we will get longer active time, t_a, since the pressure decay rate on the clean side will be limited by the permeability of the granular bed and more sand will be removed.

35. The design of puffback systems should preferably tend toward making the air inlet rate as fast as reasonably possible. This can be done by increasing the puffback valve orifice area, increasing the valve opening rate, and decreasing the flow resistance between the puffback tank and filter. We should use higher puffback pressure and keep the clean side space as small as possible. However, the large difference in clean side volume for our sideshot and downshot puffback arrangements, and the difference in the pressure rise time for the two arrangements, provides assurance that there is a considerable latitude available to the design of a puffback system in respect to the aforementioned variables.

36. A fly ash deposit on the sand surface will decrease

the permeability of the sand bed. Hence, we can build up a higher pressure on the clean side. This means that for the same puffback set-up, we will get a higher puffback intensity (higher active time).

37. Further study should be addressed toward a detailed stress analysis within the louver area, so that we can design a better louver keeping the louver resistance as small as possible.

38. In order for the panel bed filter to be properly operated at high temperatures we should understand the soil mechanics of granular beds at high tmeperature. We should also know more about the autohesivity and adhesivity of dusts and powders at high temperatures.

APPENDIX I: Comparison of Ground Area of a Panel Bed Filter and an Electrostatic Precipitator of 99% Efficiency

In a commercial design for a panel bed filter, we might for example arrange a series of panel bed filter elements in parallel as shown in Figure I. Each panel bed is taken to be 4 inches across in the direction of the gas flow. Suppose the panel beds operate at 30 ft./min. superficial velocity across the beds. Suppose their height is 30 feet. Each gas-entry surface of a panel bed will treat 30 x 30 x 1= 900ft.^{3}/min. of dirty air per foot of bed in the horizontal direction (i.e., in the direction perpendicular to the drwaing in Figure I). Each aisle between two dirty faces will then receive 1,800ft.^{3}/min. of dirty air for treatment by the two opposing panel beds. A reasonable velocity of the dirty air as it enters the aisle, for example flowing upward into the aisle as shown in Figure I, would be about 30 ft./sec., or 1,800 ft./min. At this velocity, the width of a dirty aisle will be 1 foot. For the same velocity of clean air leaving a clean aisle between two clean faces, the width of the clean aisle will also be 1 foot. The ground area occupied by one panel bed element will then be (16/12) x 1 = 1.33 ft.^{2} per foot of bed in the horizontal direction (perpendicular to the drawing). Hence, the capacity per unit ground area will be (900/1.33) = 677 ft.^{3}/min. per ft.^{2} of ground area.

An electrostatic precipitator of 99+% efficiency generally has a capacity of about 150 ft.^{3}/min per ft.^{2} of ground area.

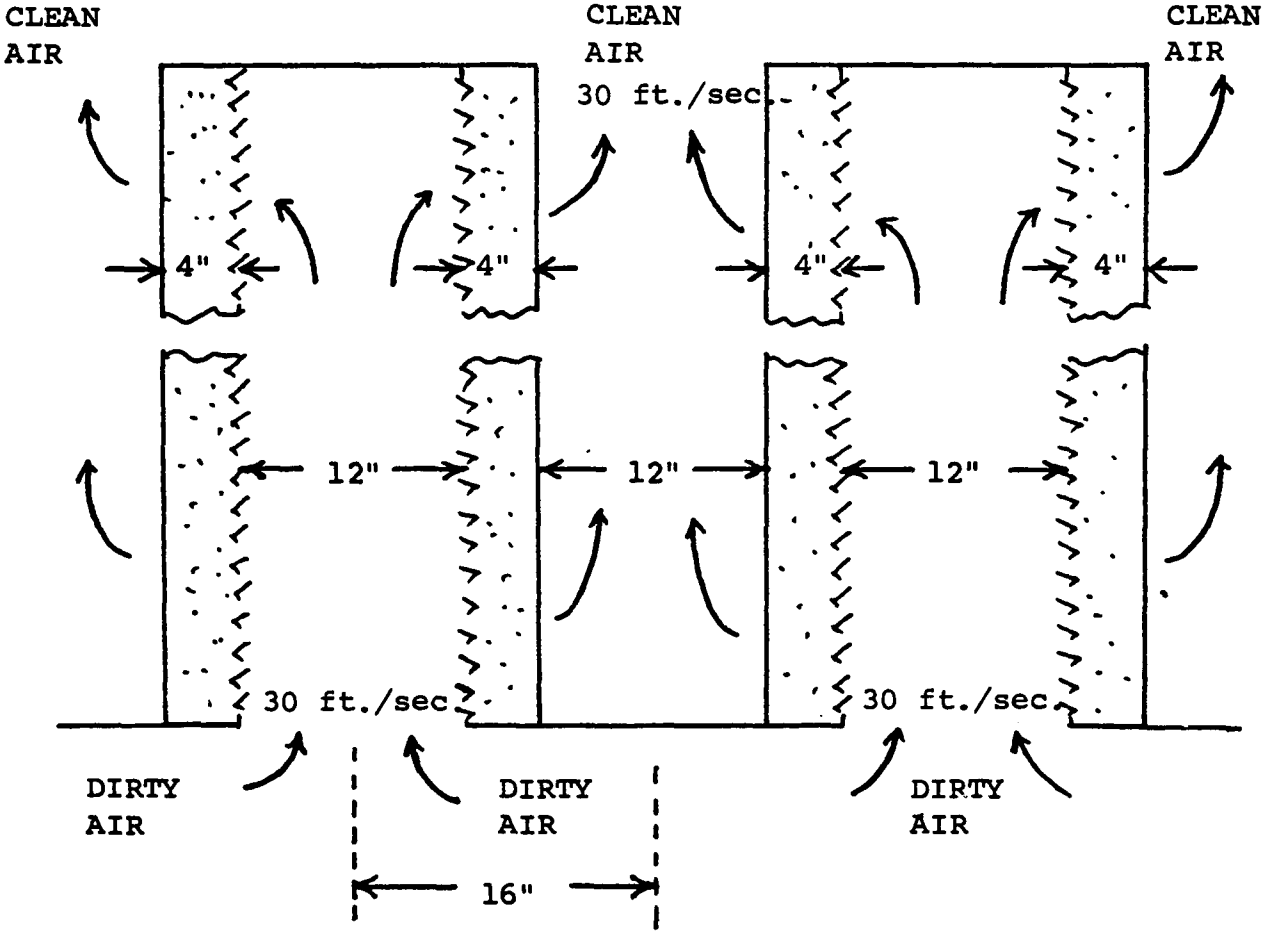

Figure I: Conceptual Design of a Commercial Panel Bed Filter Assembly.

Taking into consideration structural members and auxiliary equipment, we see that a panel bed filter assembly should occupy roughly one-quarter of the ground area required for an electrostatic precipitator.

APPENDIX II: Empirical Correlations of Sand Spill with Puffback Tank Pressure, Puffback Tank Volume, and Puffback Orifice Area for the First Experimental Unit.

40-50 Mesh Sand:

$$W = 7.80 \times 10^{-4} P_T V_T - 8.33 \times 10^{-4} \frac{V_T^{0.5}}{A}$$

20-30 Mesh Sand:

$$W = 3.99 \times 10^{-4} P_T V_T - 6.33 \times 10^{-4} \frac{V_T^{0.7}}{A}$$

10-14 Mesh Sand:

$$W = 1.23 \times 10^{-4} P_T V_T - 5.82 \times 10^{-4} \frac{V_T^{0.84}}{A}$$

where,

W = Total amount of sand dislodged (lbs.)

P_T = Puffback tank pressure (psig.)

V_T = Puffback tank volume ($in.^3$)

A = Puffback valve orifice area ($in.^2$)

Valve opening time $\approx$ 15 milliseconds.

Superficial louver area = 0.25 $ft.^2$

BIBLIOGRAPHY

1. Annis, J.C., "Particle Bounce and Air Filtration Theory", Presented at the 63rd Annual Meeting of the APCA, St. Louis, Mo., June 1970.

2. Aranafsky, J.S. and Jenkins, R., "Unsteady Flow of Gas Through Porous Media, One-dimensional Case", First U.S. National Congress, Applied Mechanics, P763-771, 1952.

3. Beavers, G.S. and Sparrow, E.M., "Non-Darcy Flow Through Fibrous Porous Media", J. of Applied Mechanics, P711-714, Dec. 1969.

4. Beavers, G.S. and Sparrow, E.M., "Compressible Gas Flow Through a Porous Material", International Journal of Heat and Mass Transfer, Vol. 14, No. 11, P1855-1859, Nov. 1971.

5. Beavers, G.C. and Matta, R.K., "Reflection of Weak Shock Waves from Permeable Materials", AIAA J. 10, No. 7, P959-961, 1972.

6. Brandt, H., "The Possibilities of Further Developments in Dust Removal Techniques", Staub Reinhaltung der Luft (in England), 25, P23, 1965.

7. Casagrande, A., "Characteristics of Cohesionless Soils Affecting the Stability of Slopes and Earth Fills", Contributions to Soils Mechanics, Boston Society of Civil Engineers, 1925-1940.

8. Chen, C.Y., "Filtration of Aerosols by Fibrous Media", Chemical Reviews, 55, P595-623, 1955.

9. Collins, R.E., Flow of Fluids Through Porous Materials, Reinhold, New York, 1961.

10. Corn, M., "The Adhesion of Solid Particles to Solid Surfaces, I -- A Review", J. of the Air Pollution Control Association,11, P523-528, 1961.

11. Corn, M., "The Adhesion of Solid Particles to Solid Surfaces, II", J. of the Air Pollution Control Association 11, P566-575, 1961.

12. Corn, M. and Silverman, L., "Removal of Solid Particles from a Solid Surface by a Turbulent Air Stream", American Industrial Hygience Association J., 22, P377, 1961.

13. De Wiest, R.J.M., Flow Through Porous Media, Academic Press, New York, 1969.

14. Emanuel, G. and Jones, J.P., "Compressible Gas Flow Through a Porous Plate", International J. of Heat and Mass Transfer, 11, No. 5, P827, May, 1968.

15. First, M.W. and Silverman, L., "Predicting Performance of Cleanable Industrial Fabric Filters", J. of the Air Pollution Control Association, 13, P581-586, 1963.

16. Friedlander, S.K. and Johnstone, H.F., "Deposition of Suspended Particles from Turbulent Gas Streams", I & EC, 49, P1151, 1957.

17. Fuchs, N.A., The Mechanics of Aerosols, Pergamon Press, London, 1964.

18. Gillespie, T., "On the Adhesion of Drops and Particles on Impaction at Solid Surfaces, I.", J. of Colloid Sciences, 10, P266, 1955.

19. Gillespie, T. and Sir Eric Rideal, F.R.S., "On the Adhesion of Drops and Particles on Impact at Solid Surfaces, II.", J. of Colloid Science, 10, P281, 1955.

20. Green, H.S. and Lane, W.R., Particulate Clouds: Dust, Smokes, and Mists, 2nd Ed., Spon, Ltd., London, 1958.

21. Herne, H., "The Classical Computations of the Aerodynamic Capture of Particles", E.G. Richardson, Editor, Pergamon Press, 1960.

22. Holtz, W.G. and Gibbs, H.J., "Shear Strength of Pervious Gravelly Soils", Proc. ASCE., Paper No. 867, 1956.

23. Hough, B.K., Basic Soils Engineering, The Ronald Press Co., New York, 1957.

24. Hoy, H.R. and Stantan, J.E., "Fluidized Combustion Under Pressure", Amer. Chem. Soc. Div. Fuel Chem., 14(2), P59, May 1970.

25. Jorden, R.M., "Electrophoretic Studies of Filtration on Packed Bed", J. Amer. Water Works Assoc., 55, P771, 1963.

26. Jumikis, A.R., Soil Mechanics, D. Van Nostrand Co., Princeton.

27. Ketchum, M.S., "The Design of Walls, Bins and Grain Elevators", 3rd. Ed., McGraw-Hill, New York, 1919.

28. Lambe, T.W., Soil Testing for Engineers, John Wiley & Sons, New York, 1951.

29. Lambe, T.W. and Whitman, R.V., Soil Mechanics, John Wiley & Sons, New York, 1969.

30. Leslie, D.D., "Large-scale Triaxial Tests on Gravelly Soils", Proc. 2nd. Pan Am. Conf. Soil Mech. Found. Eng. (Brazil), Vol.1, P181.

31. Lunge, G., A Theoretical and Practical Treatise on the Manufacture of Sulphoric Acid and Alkali with the Collateral Branches, 1st Ed., Vol. 3, Jan Van Voorst, London, P248, 1880.

32. McCabe, W.L. and Smith, J.C., Unit Operations of Chemical Engineering, 2nd. Ed., McGraw-Hill, New York, 1967.

33. Muskat, M., The Flow of Homogeneous Fluids Through Porous Media, McGraw-Hill, New York, 1937.

34. Paretsky, L., Theodore, L., Pfeffer, R., and Squires, A.M., "Panel Bed Filters for Simultaneous Removal of Fly Ash and Sulfur Dioxide: II. Filtration of Dilute Aerosols by Sand Beds.", J. Air Pollution Control Association, 21, P204, 1971.

35. Paretsky, L., Ph.D. Dissertation, City College of City University of New York, 1972.

36. Pfeffer, R., "Heat and Mass Transport in Multiparticle Systems", Industrial and Engineering Chemistry Fundamentals, 3, P380, 1964.

37. Ramskill, E.A. and Anderson, W.L., "The Inertial Mechanism in the Mechanical Filtration of Aerosols", J. of Colloid Science, 6, P416, 1951.

38. Reynolds, O., Papers on Mechanical and Physical Subjects, Cambridge University Press, 1900.

39. Rowe, P.W., "The Stress-dilatancy Relation for Static Equilibrium of an Assembly of Particles in Contact", Proc. Roy. Soc., A269, P500, 1962.

40. Schwandiman, L.C. and Postama, A.K., "Turbulent Deposition in Sampling Lines", Seventh A.E.C. Air Cleaning Conference, P127, Oct. 1961.

41. Schwartz, J. and Probstein, R.F., "Experimental Study of Slurry Separators for Use in Desalination", Desalination, 6, P239, 1969.

42. Squires, A.M., U.S. Patent 3,296,775 (Jan. 10, 1967).

43. Squires, A.M., "Clean Power from Coal", Science, 169, P821, 1970.

44. Squires, A.M. and Pfeffer, R., "Panel Bed Filters for Simultaneous Removal of Fly Ash and Sulfur Dioxide; I. Introduction", J. Air Pollution Control Assoc., 20, P534, 1970.

45. Taub, S.I., Ph.D. Dissertation, Carnegie-Mellon University, 1970.

46. Thomas, J.W. and Yorder, R.E., "Aerosol Penetration Through a Lead Shot Column: A Method of Particle Size Estimation", AMA Arch. Ind. Health, 13, P550, 1956.

47. Thomas, J.W. and Yorder, R.E., "Aerosol Size for Maximum Penetration Through Fiberglass and Sand Filters", AMA Arch. Ind. Health, 13, P545, 1956.

49. Ward, J.C., "Turbulent Flow in Porous Media", J. of Hydraulics Division. Proceedings of A.S.C.E., Vol. 90, HY5, P1, 1964.

50. Whitby, K.T., Lundgren, D.A., McFarland, A.R., and Jordon, R.C., "Evaluation of Air Cleaners for Occupied Spaces", J. Air pollution Control Association, 11, P503, 1961.

51. Whitman, R.V. and Healy, K.A., "Shear Strength of Sands During Rapid Loadings", Transactions A.S.C.E., 128, P1553, 1963.

52. Whitman, R.V., Miller, E.T., and Moore, P.J., "Yielding and Locking of Confined Sand", J. of Soil Mechanics and Foundation Division, Proceedings of A.S.C.E., 90, No. SM4, P57, 1964.

53. Yu, E.K., B.S. Chemical Engineering Research, City College of City University of New York, 1972.

54. Zenz, F.A. and Othmer, D., Fluidization and Fluid-particle Systems, Reinhold Publishing Co., New York, 1960.

55. Zimon, A.D., Adhesion of Dust and Powder, Plenum Press, New York, 1969.

VITA

Kun-chieh Lee, son of Huey-chou and Mong-chu Lee, was born on April 24, 1944 in Kunmin, Yunnan, China. He received a Bachelor of Science degree in Chemical Engineering from National Taiwan Univeristy, Taipei, Taiwan, in June 1967 and then served in the Chinese Army as a second Lieutenant for one year. In September 1968, he entered the graduate school of the Univeristy of Missouri at Rolla and received a Master of Science degree in Chemical Engineering in June 1970. In February 1971, he entered the graduate division of The City University of New York to study towards the Ph.D. degree.

On May 30, 1970, he married Miss Shiow Yeh, daughter of Mr and Mrs. Lai-chen Yeh. The Lees have two sons.